UNIVERSITÀ
DEGLI STUDI
DI PADOVA

Sede Amministrativa: Università degli Studi di Padova
Dipartimento: Territorio e Sistemi Agro-Forestali

SCUOLA DI DOTTORATO DI RICERCA IN:
"TERRITORIO, AMBIENTE, RISORSE E SALUTE"
INDIRIZZO:
"IDRONOMIA AMBIENTALE"

CICLO XXIV

DIGITAL TERRAIN ANALYSIS FOR HYDROGEOMORPHIC FEATURE RECOGNITION

Direttore della Scuola: Ch.mo Prof. MARIO ARISTIDE LENZI

Coordinatore d'indirizzo: Ch.mo Prof. MARIO ARISTIDE LENZI

Supervisore: Ch.mo Prof. GIANCARLO DALLA FONTANA

Dottorando: GIULIA SOFIA

RIASSUNTO

Le innovazioni tecnologiche e il potenziamento di hardware e software, l'ampia diffusione di software geografici (GIS), di sensori e strumenti per il remote-sensing e la creazione di reti di scambio di informazioni connesse con l'avvento del web, hanno facilitato la possibilità di collezionare estensivamente (sia nello spazio che nel tempo) dati idrogeomorfologici, ponendo le basi per nuovi progressi in idrologia e geomorfologia, anche attraverso lo sviluppo di sofisticati modelli di simulazione. Tra gli scopi dell'idrologia, oltre a quello di comprendere i processi, vi quello di poterli quantificare e prevedere, nella prospettiva di fornire strumenti sempre più idonei alla prevenzione e mitigazione del rischio idrogeologico. Tale scienza è quindi ad un punto della sua evoluzione per cui le sfide e i problemi emergono nel momento in cui ci si interfaccia con altre discipline scientifiche, e con elementi che riguardano non più semplicemente l'ambito scientifico o di ricerca, ma anche l'ambito politico, scientifico-tecnologico, computazionale e socio-economico. Attualmente nella comunità scientifica è stata posta la necessità di analizzare la risposta idrologica in una prospettiva più ampia, non solo a livello di ricerca, ma anche con l'ottica di trasferire le conoscenze in ambito applicativo e gestionale.

La problematica principale relativa alla possibilità di comprendere e prevedere la risposta idrologica di un bacino è legata alla forte eterogeneità derivante non solo dal regime pluviometrico, ma anche dagli assetti geologico-strutturali, dalla conformazione morfologica, dai caratteri pedologici, dall'uso del suolo e dalla presenza di infrastrutture antropiche. Tale eterogeneità permane a tutte le scale di analisi, e la sua struttura spaziale e l'organizzazione delle sue proprietà e caratteristiche esibiscono un significativo controllo nel condizionare la risposta idrologica di piena al variare delle scale spaziali di indagine. La risposta di ogni sistema deriva dall'interazione tra numerosi processi e dai vari feedbacks tra le varie componenti del sistema stesso, e si mostra allora necessaria una corretta rappresentazione delle complesse dinamiche di interazione presenti alle varie scale di indagine. Nell'idrologia moderna esiste una lunga tradizione che mette in relazione gli elementi morfologici di un bacino con le sue dinamiche idrologiche. Essa si può far risalire alla formulazione della risposta idrologica geomorfologica (Rodriguez-Iturbe et al. 1986) e, più recentemente, è stata investigata in dettaglio grazie alle possibilità offerte dalla grande e sempre più accurata base di dati topografici derivante da rilievo remoto (LiDAR), che consentono una lettura dettagliata del paesaggio e offrono strumenti efficaci per la comprensione dei processi idrologici (Tarolli et al 2009; Tarolli e Dalla Fontana, 2009). Nonostante i progressi ottenuti negli approfondimenti riguardanti l'analisi e la comprensione dei singoli fenomeni idrologici, il processo di comprensione completo dei sistemi pone una serie di interrogativi irrisolti. Nel corso degli anni, parallelamente allo sviluppo di interpretazioni sempre più raffinate delle teorie governanti i singoli processi idrologici non si è visto un parallelo

progresso di strutture che permettano di comprendere il funzionamento dei sistemi idrologici a larga scala, e molto spesso i risultati non consentono il trasferimento delle conoscenze tra vari operatori, su diverse scale spaziali o temporali. Vi è quindi la necessità di identificare e uniformare nuove metodologie per identificare tali processi in maniera oggettiva, automatica e facilmente ripetibile, in modo da superare l'eterogeneità geomorfologica, ma anche sintattica e semantica intrinseca negli operatori, per facilitare ed ottimizzare la gestione delle risorse territoriali. Tale approccio richiede la definizione di indici di somiglianza, e l'identificazione di particolari attributi che caratterizzano il comportamento idrologico dei bacini idrografici. Data l'eterogeneità morfologica e idrologica presente a tutte le scale, questo richiede lo sviluppo di strumenti di classificazione diagnostica che siano in grado di integrare e prendere in considerazione fattori come ad esempio la. Ovviamente questo richiede l'acquisizione ripetuta di informazioni topografiche ad alta risoluzione, e la rapida crescita della disponibilità di modelli digitali del terreno (DTM) come quelli derivati da scansioni laser (LIDAR), ha fornito un modo di guardare al nostro pianeta con livello di dettaglio senza precedenti, spesso consentendo il riconoscimento di caratteristiche morfologiche precedentemente sconosciute (Tarolli et al. 2009). Non vi è alcun dubbio che oggi rispetto al passato, abbiamo una capacità migliore di rappresentare in maniera corretta e realistica i vari sistemi idrologici, e abbiamo una migliore comprensione e capacità predittiva dei fenomeni idrologici, ma rimane comunque la necessità di regole semplici e/o procedure chiare per determinare i processi dominanti che operano in diversi bacini. Lo sviluppo di queste regole e procedure consentirebbe un approccio molto più sistematico e fattibile, anche per il trasferimento di conoscenze a scale diverse. Ogni indagine richiede l'identificazione accurata della scala spaziale di interesse, oltre che della scala temporale del problema in analisi, per consentire la selezione del processo rilevante e delle variabili che lo caratterizzano. La letteratura in questo settore ha mostrato che, in generale, l'idrologia è di fronte alla necessità di andare oltre il concetto di 'modellare tutto', e di muoversi verso l'idea di 'catturare le caratteristiche essenziali', e questo parte dall'identificazione di una corretta scala di analisi. L'Analisi Digitale del Terreno (Digital Terrain Analysis -DTA) applicata a DTM ad alta risoluzione, sviluppata nel lavoro di tesi del dottorato, può essere uno strumento utile in questo contesto, fornendo il quadro di riferimento per la quantificazione della morfologia superficiale e la sua classificazione, puntando sia all'identificazione dei vari processi, con gli obbiettivi futuri anche di simularli correttamente in modo tale da ottenere informazioni sia sulle condizioni attuali, che sui possibili risvolti futuri. Il principio fondamentale della DTA è la possibilità di rappresentare in maniera digitale la morfologia superficiale, a partire dall'abbondanza di informazioni topografiche contenute nei dati di elevazione (modelli digitali del terreno, DTM). Tale morfologia appare con diversi livelli di complessità e deriva dall'interazione di processi geologici e idrologici, le cui componenti principali possono essere lette morfologicamente attraverso l'utilizzo degli attributi topografici. La varietà di forme di rappresentazione incorporate nei DTM, le grandi opportunità di elaborazione in tempo reale, e la facilità di rappresentazione multi-scala, hanno portato l'analisi digitale del terreno ad essere qualcosa che va oltre la ricerca, ma che può essere vista anche come supporto per la creazione di mappe morfologiche e per l'identificazione automatica o semiautomatica di features. L'attività di ricerca ha avuto come come filo conduttore l'esplorazione e l'analisi di quella che può essere chiamata 'firma statistica' di diversi processi idro-geomorfologici sulla morfologia superficiale, analizzando vari elementi su una vasta gamma di scale spaziali, con l'obbiettivo di identificare il processo fisico dominante. In particolare, l'idea è analizzare i dati derivanti da DTM LiDAR ad alta risoluzione con l'obiettivo di estrarre particolari features di interesse geomorfologico/idrogeologico. In combinazione con una formulazione ottimale, questo tipo di approccio permette l'estrazione accurata e automatica di reticoli idrografici o features geomorfiche sia di origine naturale che antropica. Più in particolare, il lavoro di ricerca è risultato nella definizione di metodi oggettivi o semi-automatici per l'identificazione di features, che mirano a risolvere una serie di problemi ben documentati legati alla rappresentazione di tali features in idrologia e geomorfologia. Il lavoro è stato sviluppato considerando due principali ambiti di studio: bacini montani e aree antropiche (in particolare piane alluvionali). In contesti naturali (montani), l'efficienza della topografia LiDAR ad alta risoluzione è già stata testata in diversi lavori in letteratura, ed è stata nuovamente evidenziata durante il triennio di ricerca; un ulteriore obiettivo è stato quello di testare se tale informazione topografica può essere uno strumento di analisi utilizzabile anche per ambienti antropici, dove sono presenti caratteristiche diverse, e le attività umane possono risultare in elementi di disturbo. L'analisi digitale del terreno proposta si basa principalmente sull'uso di indici topografici (alcuni già collaudati in letteratura e alcuni nuovi) valutati a varie scale di analisi per quantificare morfologia del terreno. Dal momento che le proprietà statistiche della morfologia catturata dal DTM dipendono strettamente dalla scala a cui il modello viene analizzato, studiare come esse cambiano al variare della scala può essere uno strumento efficace per identificare la scala ottimale di analisi, sia nel mondo digitale che in quello reale, e quindi nel contesto idrogeomorfico. A questo punto, alcuni interrogativi restano ancora aperti: processi fisici statisticamente diversi, sono fautori di regimi idrologici statisticamente diversi? E' vero che le diverse leggi che regolano i processi lasciano una firma sulle proprietà statistiche della morfologia? Quanto della relazione tra idrologia e morfologia viene catturata da tale firma? Ora che siamo in grado di valutare la morfologia con un elevato livello di dettaglio grazie alla topografia ad alta risoluzione, è possibile rispondere ad alcune di queste domande. Se i processi fisici lasciano firme importanti sulle statistiche dei parametri morfologici, e se siamo in grado di quantificare queste firme in dettaglio, la statistica può essere utilizzata per aiutare la modellazione e la previsione dei vari processi su scale diverse e ambienti diversi. La topografia ad alta risoluzione accoppiata ad un approccio statistico può quindi essere un potente mezzo di inferenza, per definire la scala di analisi ottimale e per individuare soglie di inizio o fine di particolari processi, al fine di facilitare l’approfondimento e il trasferimento delle conoscenze idrogeomorfologiche.

ABSTRACT

Technological innovations and the upgrading of hardware and softwares, the wide distribution of geographical information softwares (GIS), sensors and instruments for remote sensing, and the increasing of networks to transfer information facilitated the ability to collect extensively (both in space and time) hydrogeomorphological data, offering new opportunities for advances in hydrology and geomorphology, also thanks to the development of sophisticated simulation models. However, one of the purposes of hydrology is not only to understand processes, but also to forecast them, in order to prevent risks, and hydrology is therefore, at a point of its development where challenges and problems arise when interfacing with other disciplines and elements that do not involve simply the scientific context, but also the political, technological, computational and socio-economic ones. Recently, the scientific community highlighted the need to analyze hydrological responses in a broader perspective, not only for research purposes, but also with the aim of transferring knowledge in the application and management world.

The main issue concerning the ability to understand and predict the hydrological response of a basin is, however, related to the heterogeneity that derives not only from the different rainfall regimes, but also from the geological structure of a watershed, and its morphology, soil characteristics and land use, and of course, it is influenced by the presence of human infrastructure. This heterogeneity persists at all scales of analysis, and its spatial structure and the organization of its properties and characteristics exhibit a significant influence in controlling the hydrological response at the full range of scales. The hydrological response of each system comes from the interaction between various processes and various feedbaks between the components of the system itself; therefore a correct representation of the complex dynamics of interactions present at different scales is needed. The connection between hydrological dynamics of a basin and its morphological structure is not new, but has deep roots in hydrology. It can be traced back to the formulation of the hydrological-geomorphological response (Rodriguez-Iturbe et al. 1986) and, more recently, it has been deeply investigated thanks to the possibilities offered by the availability of large-scale and highly accurate topographic data derived from remote sensing (LiDAR), that allowed a detailed reading of the landscape and offered effective tools for the understanding of hydrological processes (Tarolli et al 2009; Tarolli and Dalla Fontana, 2009). Despite progress in the analysis and insights on the understanding of individual hydrological phenomena, understanding the process of complete systems raises a number of unanswered questions. Over the years, with the development of increasingly refined interpretations of the theories governing the individual hydrological processes, there has not been a parallel increasing of understanding the hydrological functioning at a large-scale, and very often the results do not allow the transfer of knowledge between different operators

in different spatial and temporal contexts. There is therefore, a deep need of defining new methods to identify these processes in an objective, easily repeatable and automatic or semi-automatic way, in order to overcome the issue of geomorphological heterogeneity, but also the inherent syntactic and semantic heterogeneity that comes from the operators themselves, to facilitate and optimize the land management. This approach requires the definition of indices of similarity, and the identification of specific attributes that can characterize the hydrological behavior of watersheds. Given the morphological and hydrological heterogeneity present at all scales, this requires the development of diagnostic classification tools that are able to integrate and take into account factors such as topography. Obviously, this requires the acquisition of repeated high-resolution topographic information, and the rapid growth in the availability of digital terrain models (DTM) as those derived from laser scanning (LIDAR), has provided a way of looking at our planet with a level of unprecedented detail, often allowing the recognition of morphological features previously unknown (Tarolli et al. 2009). There is no doubt that today we have a greaterability to accurately and realistically represent the various hydrologic systems than in the past, and we have a betterunderstanding and predictive capability about hydrological phenomena. However, there is still the need for simple rules and/or clear procedures to determine the dominant processes operating in different basins. The development of these tools allows a much more systematic and practicable approach to transfer knowledge at different scales. Every investigation requires the accurate identification of the spatial scale of interest, as well as the time scale of the problem in analysis, to allow selection of the relevant process and variables that characterize it. The literature in this area has shown that, in general, the hydrology is facing the need to go beyond the concept of 'model everything', and to move towards the idea of 'capturing the essential features', and this starts from the identification of a correct scale of analysis. The Digital Terrain Analysis (DTA) applied to high-resolution DTM, as proposed in this thesis, can be a useful tool in this context, providing the framework for the quantification of the surface morphology and its classification, aiming to identify the various processes, with the future goals also to simulate them correctly to gather information about their current conditions, but also their possible future implications. The fundamental principle of the DTA is the ability to represent the surface morphology in a digital form, starting from the abundance of information within the topographic elevation data. This morphological surface appears with different levels of complexity, that derive from the interaction of geological and hydrological processes, whose main components can be read morphologically through the use of topographical attributes. The variety of forms of representation embedded in the DTM, their fast real time processing, and easy multi-scale representation, have led the digital analysis to be something that goes beyond research, but that can be also seen as support for the creation of maps and the morphological identification of features through automatic or semiautomatic approaches. The present work has as a main theme, the exploration and analysis of what might be called 'statistical signature' of hydro-geomorphological processes on surface morphology, analyzing various elements that can characterize this morphology over a wide range of spatial scales, to identify the dominant physical process. In particular, the idea is to analyze data from high-resolution LiDAR DTM to recognize the hydrogeomorphic features of interest. In combination with an optimal formulation, this approach allows accurate and automatic extraction of river networks and geomorphic features both with natural or anthropogenic origin. More specifically, the thesis aims to develop objective and semi-automatic methods that aim to solve a series of well documented problems related to the representation of these features in hydrology and geomorphology. The work has been developed considering two main study areas: mountainous basins and anthropogenic areas (flood plains). In natural settings, the effectiveness of high-resolution LiDAR topography has already been tested in several works in literature, and one of the objectives of this thesis is to test whether this information can be a tool to perform topographic analysis also in disturbed environments. The proposed digital terrain analysis is primarily based on the use of terrain attributes (some already known and tested in literature, and some new) evaluated at different scales to quantify terrain morphology. Since statistical properties of the morphology captured and derived by DTMs critically depend on the scale at which the model is analyzed, analyzing how they change at changing scale can be an effective tool to identify the 'characteristic scales' in both the cell and the hydrogeomorphic realms. At this point, some open questions still remain: Are statistically-distinct hydrological regimes the result of physically-distinct processes? Do differences in laws governing processes leave their signature on the statistical properties of landform geometry, and how much of the behavior of the coupled hydrologic/geomorphologic system is reflected in the statistics that we can digitally derive?

Now that we can assess landforms with a high level of detail thanks to high resolution topography, some of these questions can be answered. If physical processes do leave important signatures on the statistics of landscapes, and if we can quantify these signatures in detail, statistics can be used in assisting modeling, prediction and observatory design across scales and across environments. High resolution topography coupled with statistic approaches can thus be a powerful means of inference, to define the optimum scale of analysis, to identify a threshold to label where a process starts, to transfer knowledge across scales.

CONTENTS

The thesis is organized to provide a general introduction (Sect. *I.Introduction*), and on a second section the considered study sites are described (Sect. *II.Study sites*). The section *III.Materials and methods* describes the research context behind the work, and a detailed description of the proposed approaches is presented in Sect. *IV.DTA for feature recognition*.

More in detail, after a first introduction to the importance of scales and similarities in hydrological processes in the hydrogeomorphic and the digital realms (Chapt. 1, Sect. *I.Introduction*), the research context is discussed (Chapt. 2, Sect. *I.Introduction*), providing a literature background for the considered features. The thesis approaches to two different types of environments, a natural landscape and an anthropogenic ones, and the considered study sites are described in detail in the section *II.Study areas*. In the section *III.Materials and methods*, the theoretical basis of, and problems associated with Digital Terrain Analysis (*DTA*) for characterizing surfaces, landforms, and hydrogeomorphic features using high resolution LiDAR-Digital Terrain Models are presented. In the first two chapters of this section, a description of LiDAR technology (Chapt. 1) and derived DTMs (Chapt. 2) is provided. In particular, concerning the DTMs (Chapt. 2), the research is focused on the quality of the models (Chapt. 2.1) and on how to apply them to model continuous surfaces (Chapt. 2.2). Chapter 3 is completely dedicated to the hydrological and morphological characterization of surfaces, and a detailed description of all the topographic parameters used in the thesis is provided. All the proposed Digital Terrain Analyses share the use of statistical operators, and the conceptual background for this framework is described in chapter 4, where the main statistics are addressed (Chapt. 4.1), and their use for the definition of the scale of analysis and for the extraction of features is described (Chapt. 4.2). A thorough analysis of the effect of errors on DTMs on the topographic parameter statistics is also proposed (Chapt. 4.3).

The fourth section of this thesis (*IV.DTA for feature recognition*) contains the detailed description of the different approaches applied for feature recognition. The first two cases (Chapt. 1 and 2) are focused on the mountainous environment, and they address the main hydrogeomorphic features that are generally considered in hydrological analyses. In the first example of feature extraction (Chapt. 1), an a posteriori approach is presented to test different objective statistical operators used to characterize geomorphic features. On the second approach (Chapt. 2), a methodology to objectively extract network features is discussed, and its robustness and limits are assessed through a statistical framework.

However, hydrological processes span outside the mountainous context, therefore Chapt. 3 and 4 present an analysis of the effectiveness of the different topographic parameters as the basis for DTA in engineered landscapes. On the first approach (Chapt. 3), different topographic parameters are tested to extract levees, underlining the limits or the advantages of each one, and identifying the optimal one. Chapt. 4 describes a full DTA approach for the characterization of the drainage network in floodplains, starting from the same topographic parameter highlighted as optimal in Chapt. 4. Chapter 5 presents the final remarks about all the proposed procedures, underlining how high-resolution topography connected with the use of statistics is a powerful tool to gain knowledge about hydrogeological features both in mountainous contexts and engineered landscapes.

A short commentary with summary, conclusions and recommendations is provided at the end of the thesis (Sect. *V.Conclusions and future challenges*).

The whole work has been carried out by integrating a GIS and non-GIS environment, briefly commented in Appendix A.

INDEX

I. INTRODUCTION

1. Scales and similarities in hydrological processes: the hydrogeomorphological and the cell realms

Runoff generation results from the interaction of different hydrological processes, and one demanding aspect in hydrology is the understanding of its spatio-temporal patterns. The investigation of runoff in different contexts is challenged by the specific characteristics of the environments: for alpine catchments, for example, this study is often challenged by inaccessibility of these regions; for engineered landscapes, it is challenged by the extent of the areas, and the continuous disturbance introduced by human activities. Another problem related to this matter is the heterogeneity of the terrain and of its morphometric properties that directly influence hydrologic processes (Gregory and Walling, 1973), and that differs across spatial and temporal scales. In turn, topography is a direct manifestation of the same processes that dynamically and continually shape the surfaces, and transform the terrain with different levels of dissectivity, and with a variety of morphological entities.

Hydrology and geomorphology spatial heterogeneity is scale-dependent (Klemes, 1983; Bloschl and Sivapalan, 1995), since both fields deal by nature with patterns and processes, as well as their interactions and functional implications on a variety of scales (Sivapalan, 2005), and the concept that "scale matters", common ground in environmental sciences, has been underlined by a flourishing literature both in hydrology (e.g. Bloschl and Silvapalan, 1995; Vogel and Roth, 2003; Sivapalan , 2005) and geomorphology (e.g. Evans 1972, 1979, Dodds and Rothman, 2000; Shary et al. 2005). Processes that are important at one scale are not necessarily important at other scales (Sivakumar, 2008), and dominant processes change within changing scales (Grayson and Bloschl, 2001). Processes are influenced by past and present events interactions and thresholds (Dietrich et al. 1993, Grayson and Bloschl, 2001, Montgomery and Dietrich 1992, McDonnell and Woods, 2004), and depending on their intrinsic scale, they are controlled and influenced by different driving forces. Several studies have investigated the influence of different landscape controls on hydrological functioning and behavior of catchments such as topography (Anderson and Burt, 1978a,b; Grabs et al., 2009; Jencso et al.,2009), geology (Uchida et al., 2005; Spence, 2007), soil cover (Carey and Woo, 2001; Kirkby et al., 2002;Laudon et al., 2007; Tetzlaff et al., 2007a) and climate(Devito et al., 2005; Hrachowitz et al., 2009; Troch et al., 2009). These studies have revealed the complex way in which catchment characteristics and forcing factors affect hydrological flow paths, and they demonstrated how different physical factors exert dominant controls in different geomorphic regions that can be addressed at local scale, hillslope scale and catchment scale (Fig. 1).

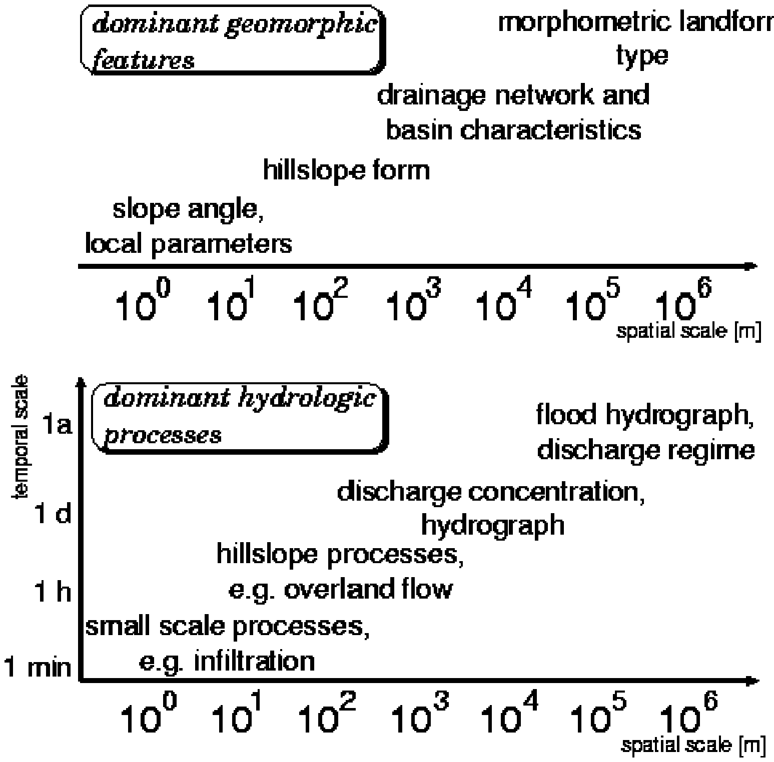

Fig. 1 Scales in hydrology and geomorphology: dominant features of each discipline in a spatial and temporal context (Anderson and Burt, 1978)

Considering hydrological processes on the local scale, the main driving element is the slope: flow path geometries, flow velocities and quantities are influenced directly by the steepness of the landscape. Additionally, geomorphology affects hydrologic processes indirectly through their dependency on several other factors (like soil parameters). When dealing with the hillslope scale, runoff production mechanisms are directly influenced by soil properties (partitioning of overland flow and subsurface flow) and landscape form. On the basin scale, the hydrograph is influenced by basin morphology, which can be expressed, for example, by representative attributes for catchment height distribution (relief indices), length and form of the basin (form indices), or parameters describing the drainage network (Cooke and Doornkamp, 1990; Gregory and Walling, 1973). It is also well known that moving to an even wider scale, mesoscale or macroscale landform types affect hydrologic characteristics significantly. Relations between large-scale drainage basin parameters and hydrologic indices have been investigated in numerous studies. Cooke and Doornkamp (1990) and Gregory and Walling (1973) provide useful discussion of these issues. Other authors underlined the effectiveness on modeling and prediction of quantitative description of basin morphology and land use and the establishment of functional relationships between these parameters and hydrologic catchment characteristics (Gupta et al., 1980; Rodriguez-Iturbe and Valdes, 1979; Acreman and Sinclair, 1986; Sauer et al., 1983).

The structure of a catchment depends to a large extent on the interaction between hillslope and channel processes, and it is widely acknowledged that the hydrologic response bears the signatures of both the structure of the channel network and of the characteristic hillslope lengths defining the drainage density of the basin. The deep interaction between the two processes raises numerous questions, as in which process is mainly responsible for characterizing the catchment response; or what determines the importance of one process over the other, and again, what is the correct scale to use to analyze and represent both processes and their interaction.

The transition from straight or convex hillslopes to concave valley forms is understood to represent a transition in process dominance, but the nature of that transition has been debated. Gilbert (1909) argued that convex-concave forms correspond to a gradual transition in process dominance from creep to wash with increasing distance from a drainage divide. This approach is based on the view that valleys form where flow convergence causes rill or gully excavation by runoff erosion. An alternative view is that valley and channel formation are controlled by geomorphic thresholds. A number of researchers have argued, for example, that hillslope-valley transitions occur where a threshold for runoff erosion is regularly exceeded during large storms (Horton, 1945; Montgomery and Dietrich, 1989; Willgoose et al., 1991a.b). Some authors commented that these two approaches constitute end-member cases, and any given landscape may be both threshold-dominated or instability-dominated, depending on the climate, relief, geology, and stage of evolution (Kirkby, 1988).

A further element that drives the hydrologic response of a basin is its geomorphologic structure: Rodriguez-Iturbe and Valdes (1979), for example, developed a theory for linking the surface hydrologic response to geomorphological settings. They used the classical unit hydrograph concept to describe the hydrologic response and Horton numbers, as well as other parameters, to describe the geomorphologic structure of a watershed. Their pioneering study was followed by several other similar studies on the links between hydrologic processes and basin morphology (e.g., Gupta et al., 1980; Rodriguez-Iturbe et al., 1986; see also Rodriguez-Iturbe and Rinaldo, 1997, chapter VII).

Information on the internal behaviour of catchments is necessary to identify similarities and differences between catchments in terms of their response to natural and anthropogenic disturbance and change (Buttle, 2006). Given the importance of heterogeneity at all scales, process conceptualization requires the development of diagnostic classification tools that consider factors such as topography to develop indices of similarity (Buttle, 2006). Thus, there is a need for simple rules and/or clear procedures to determine the dominant processes operating in different catchments, and how these reflect variations in landscape controls (Buttle, 2006). Clearly, catchment can be viewed as a nested hierarchy, in which the larger landforms are made up of smaller ones, but investigating landforms at different scales typically requires changing the research focus, since the functioning and evolution of large-scale landforms often cannot be understood by simply integrating the behavior of the smaller ones. Such changes in focus occur over the full range of geomorphological interest. Any investigation requires careful identification of the spatial and temporal scale of the problem, to allow selection of the relevant processes and variables.

Digital Terrain Analysis (DTA) can be framed in this context, providing the basis and the tools for landform quantification, segmentation and classification, aiming both at processes recognition and simulation to extrapolate terrain knowledge. In general, DTA allows to handle the complexity of individual processes and patterns as well as some of the difficulties that are encountered in delineating the appropriate spatial and temporal scales (Wilson and Gallant, 2000). Digital Terrain Analysis has been an active study field for years, and it has been consolidated in the scientific literature. Wilson and Gallant (2000) collected a significant amount of work regarding terrain analysis methods and their applications to soils, hydrology and vegetation. Pike (2000) underlined the significance of digital terrain modeling and computerized technology in practical applications, and numerous publications before that have emphasized the role of terrain, and as a consequence DTA, in hydrologic modeling, sediment transport, soil erosion estimation, drainage basin morphology, vegetation, and ecology (Krcho 1991, Parson and Abrahams 1993, Rodriguez-Iturbe and Rinaldo 1997). The main principle of Digital Terrain Analysis is that a continuous landscape surface can be generated from the abundance of topographic information contained within elevation data (geomorphic position, slope, etc.), and various studies underlined how the spatial distribution of topographic attributes can often be used as an indirect measure of the spatial variability of hydrological, geomorphologic and biological processes (i.e. Moore et al., 1991).

In DTA, analysis starts thanks to the availability of Digital Elevation Models (DEMs), that can be used for the extraction of land-surface parameters (Pike, 2000). The variety of representation forms embedded in the DEMs, and their high feasibility of automation and real-time processing, and the easy multi-scale representation, brought Digital Terrain Analysis beyond a research tool, supporting landform mapping and the automatic or semiautomatic identification of landform elements at their specific scale, through the use of topographic attributes (Lashermes et al. 2007; Tarolli and Dalla Fontana, 2009; Passalacqua et al. 2010; Pirotti and Tarolli, 2010; Tarolli et al., 2010; Sofia et al. 2011).

One of the simplest attributes of a terrain is the elevation itself, that carries information about the length, gradient and frequency distribution of surface slopes, the magnitude of relief, the degree of incision of drainage channels, etc. of any given point in a landscape. This information can be used to describe and characterize most of the hydrological processes. The advantage of considering and analyzing topography, compared to other information such as soil parameters or biomass production estimates, is based on the relatively simple and fast techniques available to model it in large areas, that allows the description of the complex spatial patterns of environmental systems as seen by Moore et al. (1993). Terrain can be characterized by features and landform elements that can be observed at a different scale, and that carry information about the underlining hydro-geomorphological processes. Landform entities, of course, differ from one another in terms of characteristics and scale of analysis, and they differ in terms of the physical processes that were involved in their formation, and that continue to operate within them at the moment. Recognizing and characterizing such features from terrain data, therefore, is a key element, for any hydro-geomorphological analysis. Dikau (1989) differentiates these elements with homogeneous plan and profile curvature from facets having homogeneous gradient, aspect and curvature. Shary et al. (2002) proposed an objective, local, scale-specific classification of elemental landform features based entirely on consideration of signs of curvatures. MacMillan et al. (2000) described the three major problems for an automated landform classification algorithm for identifying various types of landscapes at different scales as connected *i)* to the selection and computation of an appropriate suite of terrain derivatives; *ii)* to the identification of meaningful landforms at different scales and their salient or defining characteristics; and *iii)* to the selection and application of classification procedures capable of using the available terrain derivatives to represent correctly the landform types at the desired scale.

The concept of scale and scaling in terms of hydrology and geomorphology has already been underlined. Most land-surface parameters and objects vary with spatial scale, but when observing and classifying terrain it is necessary to rely on a combination of the intrinsic scale of the process itself, and a scale imposed by the level of detail of the displayed surface, as controlled by resolution of the data used to represent it. In the digital realm, the scale at which we are able to represent a landform is therefore understood as a function of cell size or grid resolution (Wilson and Gallant, 2000). The dependence of land-surface parameters on grid resolution has been described by Evans (1972) as '*a basic problem in geomorphometry*'. The horizontal and vertical resolution of the elevation data used to portray a terrain surface has a significant influence on the level of detail and the accuracy of the portrayal of surface features, and on the values of land surface parameters that are directly computed from a digital representation of surfaces. Numerous authors have examined the effects of the grid resolution on the value accuracy of land-surface parameters and objects derived from elevation data sets of differing resolutions (Florinsky, 1998; Wilson and Gallant 2000). Shary et al. (2002) provided a theoretical examination of the effects of grid resolution on land surface parameters and objects. They demonstrated that the local variables of slope gradient, aspect and curvatures are very sensitive to DEM resolutions, exemplifying how second derivatives (curvature) are more sensitive than first derivatives (slope). Arrell et al. (2007) examined the scale dependency of morphometric classes. They found that the relative importance of landform classes varies with DEM resolution. Some authors underlined that it is possible to identify characteristic dimensions over which specific landforms may occur (Evans, 2003) and (either implicitly or explicitly) it is possible to recognize a hierarchy with different types and sizes of landforms occurring at different scales. However, in the absence of scale optimization techniques, the geomorphometric analysis is conducted at rather arbitrary scales, which rely on the user's experience.

Recent advances in data collection technology such as airborne and terrestrial laser scanning have enabled rapid, accurate, and effective acquisition of geographic information (Ackermann 1999, Kraus and Pfeifer 2001, Briese 2004, Slatton et al. 2007, Tarolli et al. 2009) and this enabled advances in the analysis of landform morphometry through the availability of high resolution data. A new generation of high resolution (~ 1m) Digital Elevation Models (in the form of Digital Terrain Models –DTM-, or Digital Surface Models –DSM-) is nowadays widely available, offering new opportunities for the scientific community to use detailed representations of surfaces. The rapid growth in the availability of this type of DEMs, provided a way to look at our planet with an unprecedented detail, often allowing the recognition of previously unknown features and the establishment of their spatial relationships (Tarolli et al. 2009). The challenge is now focused on their application for understanding earth and surfaces processes at different scales and for different contexts (Tarolli et al. 2009; Tarolli and Dalla Fontana, 2009). Originally, terrain-related analyses were limited by the coarse spatial resolution of available DEMs, applying the concept of scale just as a function of the grid resolution. Nowadays, Increasing availability of high resolution topography anyway, is leading to a paradigm shift regarding the scale issues, and it has been recognized that analyses should not be driven by the finest available grain size, but that it might be appropriate to consider a coarser resolution, more relevant to particular research objectives (Wood, 1996; Pirotti and Tarolli, 2010, Tarolli et al. 2010, Sofia et al. 2011). Scale dependency of land-surface parameters and land-surface objects has been underlined by a number of studies (Wood, 1996; Florinsky and Kuryakova, 2000; Evans, 2003; MacMillan et al., 2003; Schmidt et al. 2003; Hengl, 2006; Arrell et al., 2007; Pirotti and Tarolli, 2010; Tarolli et al. 2010; Sofia et al. 2011). There is not a single or fixed value for local land-surface parameters at a point, but rather a whole range of values that are dependent both on DEM resolution, and scale of analysis (windows size) used to compute the parameters. Consequently, there is not a single best resolution for analysis, but the selected resolution needs to be appropriate for capturing and describing not only the surface, but also the features of interests for a particular application. Consequently, the importance of scaling methods has grown significantly, and different methods to account for scale have been proposed. In particular, techniques such as filtering and resampling are frequently applied to high resolution grids to smooth out noise that may lead to erroneous results (MacMillan et al., 2000; Lashermes et al. 2007, Passalacqua et al. 2010a,b; Pirotti and Tarolli, 2010, Tarolli et al. 2010, Sofia et al. 2011). In his thesis, Wood (1996) clearly showed the scale dependency of land-surface parameters by computing and analyzing them over a range of spatial scales. As a major outcome he introduced the open-source software package, LandSerf, that is currently one of few products capable of performing 'multi-scale surface characterization'.

The mentioned literature underlined that decisions on an appropriate resolution involve compromise between noise reduction and generalization. A similar conclusion was drawn by Hengl (2006), who suggested a number of intermediate values between the finest available and coarsest legible resolutions to be an appropriate scale for a specific problem. Schmidt and Andrew (2005) introduced a spatially adaptive scale detection technique, exemplified for curvatures, in order to recognize dominant scale ranges of landforms and to study local landform variability across scales. Pirotti and Tarolli (2010) tested different filtering techniques on the LiDAR raw data for the characterization of landform curvature, and a filtering approach based on the Wood (1996) moving windows to produce curvature maps for channel network identification. The same generalization procedure has been applied by Tarolli et al. 2010 for the characterization of geomorphic features.

As Olaya (2009) pointed out '*combining ideas from image analysis and geomorphometry can be a fruitful way of…gaining a better understanding of the information contained in the DEM'*, and methods originally developed in image analysis, offer the potential for dealing with scale in DEM analysis (Li, 2005). Lashermes et al. 2007 introduced the use of wavelet to locally filter DTMs in order to bring out the meaningful signal connected to channel network and mask noises related to localized surface morphologies. Passalacqua et al. 2010a introduced a filtering approach based on a non linear adaptative filter, tested in comparison with the work of Lashermes et al. 2007 in the paper produced 2010b. In one of the approached proposed in this thesis, some concept of filtering derived from image segmentation processing have been tested for the recognition of anthropogenic features in agrarian contexts. In Sofia et al. (2011), combining both image analysis filtering techniques and tools, an approach is proposed to determine automatically the optimum scale of analysis.

All these research topics have the common thread of exploring space-time statistical signatures over a range of scales and relating them to the underlying physical processes. The newest approaches aim at analyzing high-resolution digital elevation data towards the goal of extracting features of geomorphologic/hydrologic interest. Combined with optimization formulation, they allow the accurate and automatic extraction of channels and channel networks, as well as locations and length scales of channel interruptions, or the localization of geomorphic or anthropogenic features.

At this point, some open questions still remain: Are statistically-distinct hydrological regimes the result of physically-distinct processes? Do differences in laws governing processes leave their signature on the statistical properties of landform geometry, and how much of the behavior of the coupled hydrologic/geomorphologic system is reflected in the statistics that we can digitally derive?

Now that we can assess landforms with a high level of detail thanks to high resolution topography, some of these questions can be answered. If physical processes do leave important signatures on the statistics of landscapes, and if we can quantify these signatures in detail, statistics can be used in assisting modeling, prediction and observatory design across scales and across environments. High resolution topography coupled with statistic approaches can thus be a powerful means of inference, to define the optimum scale of analysis, to identify a threshold to label where a process starts, and to assess the quality of the considered model, in order to transfer knowledge across scales.

2. Hydrogeomorphic features

2.1 Features in mountainous environments

Mountainous environments are very complex due to the interaction of tectonic, geomorphological, ecological, and climatic agents (Walsh et al., 1997). Consequently, there is a need to monitor and understand complex processes and interactions, as well as characterize and map complex spatial patterns. Many problems cannot be solved without remote-sensing information science, and technology, since topographic data are required to account for the spatial and temporal scale dependencies associated with phenomena and processes (Goodchild and Quattrochi, 1997). New sensor systems with improved spatial resolution offered opportunities to assist scientists, but as a consequence, new information extraction challenges emerged, questioning the effectiveness of some classic methodologies based on lower resolution data. Despite the technological advances, results are anyway dependent upon the complexity of the terrain, data quality, measurement scale, integration of multi-source data, spatial analysis approaches, and pattern recognition algorithms. Consequently, for this type of environment, it is important to develop and empirically test automatic or semi-automatic algorithms that: *i)* handle data with any measurement scale; *ii)* are used to integrate multi-resolution, multi-temporal, and other forms of spatial data; *iii)* do not require data to exhibit homogeneity of variance; and *iv)* recognize complex non-linear patterns.

The Digital Terrain Analyses assessed in this work, concerning mountainous environment, can be framed in this context. Two main features are addressed, in order to obtain information also about the underlying processes: geomorphic features (in particular landslides and bank erosion) and hydrological features (channel network). In the following section, the background context for both is presented.

a. Geomorphic features: landslides crowns and bank erosion

Landslides and erosional processes are a major problem in mountainous regions (Alexander 2008). Shallow landsliding phenomena are critical since in steep, soil-mantled landscapes, they can also contribute to the generation of debris flows that scour low-order channels, deposit large quantities of sediment in higher-order channels, and pose a significant hazard (Borga et al. 2002).

From earth observation data, landslides and erosional features studies can be summarized in three application domains: 1) mapping (inventory), 2) characterization, and 3) spatial and temporal monitoring (Metternicht et al. 2005). In a more wide context, these applications convey in the process of landslide hazards assessment, generally carried out through: 1) field analysis to recognize areas susceptible to landslides; 2) projection of future patterns of instability through analyses of landslide inventories (DeGraff 1985); 3) statistical quantitative approach for medium-scale surveys or inventory-based method (the multivariate or bivariate statistical analysis) (Carrara 1983; Carrara et al. 1991, 1995; Clerici et al. 2002); 4) stability ranking based on criteria such as slope, lithology, land form, or geologic structure (Hollingsworth and Kovacs 1981; Montgomery et al. 1991); 5) physically based or process-based approach for failure probability analysis (Hammond et al. 1992; Montgomery and Dietrich, 1994; Pack et al. 1998; Borga et al. 2002; Crosta and Frattini 2003; Tarolli and Tarboton 2006), and the issue of modeling the propagation of landslide phenomena such as falls and flows/avalanches to predict the potentially affected areas (Wieczorek et al. 1999; Iovine et al. 2003).

All these applications starts from the capability to actually detect landslides on the surfaces, and this requires fine and up-to-date spatial information to provide correct assessments. One of the greatest limiting factors in predicting and mapping landslide activity is the lack of understanding of scale-dependent processes. The literature on this topic is predominantly theoretical, although several uses of remote sensing and statistics to describe scale and morphometric parameters have been proposed (Bishop et al., 1998, 2003; Bonk, 2002; Wallace et al., 2004). Topographic data with a resolution relevant to the scale of morphological features are necessary to understand the space- and time-dependent processes, and previous studies based on the availability of high-res data have linked landslide processes with morphology and slide components (Smith, 2001; Korup, 2004; McKean and Roering, 2004). In practical application, however, visual photo-interpretation techniques combined to ground survey remains the most used method to locate and characterize landslides (Mantovani et al. 1996), allowing the identification of precursor signs, characteristic forms, and predisposition factors. They also allow to locate and map past events, but this technique is complex to apply over large areas, and it is time-consuming. Moreover, it requires an expert knowledge on the hazard, and therefore, it remains very subjective (McKean and Roering 2004). The generation of high spatial resolution images offered new opportunities to provide detailed information on landslides, moving towards methods considering objected oriented image analysis (Geneletti et al. 2003; Harayama et al. 2004). However, in the presence of vegetation covers, these images result still not feasible for applications.

Numerical analyses of topography, on the other hand, can provide preliminary insight into landslide-scale mechanics and surface deformation (McKean and Roering, 2004). For example, relationships between topographic data and the surface expression of processes may provide insight into landslide activity, age, and material type. Advances in topographic surveys and the development of LiDAR techniques offered new opportunities to gather detailed information about topography, allowing to provide this information also over areas with vegetation cover, due to LiDAR’s pulse penetration and multi-echo recording capability. Identification of potential or actual erosional/landslide hazard can now be possible even with vegetation cover. The use of LiDAR for these types of quantitative analyses is relatively new; however, previous studies have used DEM-based geomorphometry for landslide delineation and risk (Gritzner et al., 2001), discriminating zones of superficial processes in mountainous terrain (Bishop et al., 2003), and mapping landforms for structural interpretations (Ganas et al., 2005) or regional analysis (Bolongaro-Crevenna et al., 2004). These analyses typically included first- and second order derivatives of elevation such as slope angle, slope aspect, profile curvature, tangential curvature, etc. A few studies have used statistical measures such as semivariograms and spatial autocorrelation for geomorphometry, which can provide information about topographic variability and surface roughness (Bishop et al., 1998, 2003; Walsh et al., 2003; Miska and Hjort, 2005, Trevisani et al. 2009). Looking at the last few years we can mention the use of high resolution topography for characterization and differentiation of landslide morphology and for the determination of the location and distribution of landslide activity (Chigira et al. 2004; McKean and Roering 2004; Glenn et al. 2006; Ardizzone et al. 2007; Booth et al. 2009), for geomorphological mapping of glacial landforms (Smith et al. 2006) and for recognition of depositional features on alluvial fans (Staley et al. 2006; Frankel and Dolan 2007). In Trevisani et al. (2009) a LiDAR-derived DTM is analyzed using variogram maps to characterize and compare different morphological features, showing that geostatistical approach on a local search window can efficiently synthesize the spatial variability of topography representing suitable “fingerprints” of surface morphology. Other authors discussed about the critical issues and limits of high resolution DTMs for the numerical modeling of shallow landslides (Tarolli and Tarboton 2006; Tarolli and Dalla Fontana 2008).

Finding methodologies to automatically recognize geomorphic features really represent a challenge, and a useful tool for natural hazard mapping, and environmental planning in mountainous regions. One of the DTA approaches proposed in this thesis aims to automatically recognize landslide crowns and features related to bank erosion of debris-flow channels starting from a high-resolution LiDAR DTM (Chapt. 1, Sect. *IV.DTA for feature recognition*). Different methods introduced by Tarolli and Dalla Fontana (2009), Pirotti and Tarolli (2010), and Lashermes et al. (2007), are tested compared to numerous statistical analysis of variability to define objective thresholds of landform curvature for feature extraction. An analysis on effects of the scale choice on curvature calculation is provided, suggesting guidelines and indentifying also limits and at the same times future challenges in automated methodologies for geomorphic feature extraction from high resolution topography.

b. Hydrological features: channel network

Drainage network delineation is one of the key steps when studying catchment hydrological responses to rainfall events (Tucker et al., 2001). Traditionally, extraction methodologies are based on the flow routing model, and various drainage algorithms offer possibilities of computing drainage networks all over the raster surface (O’Callaghan and Mark, 1984; Quinn et al., 1991; Tarboton, 1997; Orlandini et al., 2003). They generally follow the procedure of filling pits, computing flow direction, and computing the contributing area draining to each grid cell (Tarboton, 2003). The conversion from a drainage flow path to a meaningful network requires then the choice of a threshold to apply to label channels. However, these classical methodologies are not bias-free, and they present two main disadvantages*: i)* the flow direction approach is unable to operate effectively on flat areas (areas of equal elevation), where flow routing is unable to occur; and *ii)* the conversion from flow path to actual network requires the choice of a unique thresholds that is generally not able to fully characterize the network.

Considering i), a number of drainage enforcement algorithms have been developed to determine flow direction in flat areas of DTMs (Jenson and Domingue, 1988; Hutchinson, 1989; Tribe, 1992; Soille and Gratin, 1994; Saunders and Maidment, 1995; Garbrecht and Martz, 1997; Martz and Garbrecht, 1998; Mackay and Band, 1998; Turcotte et al., 2001; Soille et al., 2003). However, drainage enforcement is a computationally expensive operation that can cause the formation of artifacts such as double streams and meanders (Soille et al., 2003). Other authors worked on Triangulated Irregular Network (TIN), representing elevation dataset as an irregular mesh of triangular facets (Gandoy-Bernasconi et al., 1990; Jones et al., 1990; Nelson et al., 1994; Palacios-Velez et al., 1998; Tucker et al., 2001; Vivoni et al., 2005a,b) in order to better characterize surfaces, but the application of such models is computationally not feasible for large-scale analyses.

Considering ii), the traditional approach is to use a unique contributing area or slope-area threshold beyond which the hydrographical network is chosen (Mark, 1984; O`Callaghan and Mark, 1984; Marks et al., 1984; Jenson and Domingue, 1988; Fairfield and Leymarie, 1991; Freeman, 1991; Wichel et al., 1992; Costa-Cabral and Burges, 1994; Soille and Gratin, 1994; Tarboton, 1997; Soille et al., 2003; Colombo et al., 2007). This approach implies that the drained area is the most important factor to explain hydrographic networks distribution. The assumption is that the morphology of the thalweg, creating breaks of slope, concentrates both surface water and exfiltrations of sub-waterflows (Pilesjo, 1992). Physical location of channel heads, however, is not related just to topographic slope, but in some cases depends also on several factors as geomorphic processes involved, soil properties, climatic environment, land use, etc. (Montgomery and Dietrich, 1988; Prosser 1996; Wemple et al., 1996; Beven and Kirby, 1979; McGlynn and McDonnel, 2003). In these contexts, the identification of drainage network according to the area or slope-area thresholds does not necessarily correspond to the actual channel head location (Orlandini et al., 2011), because the use of a unique value is not enough to characterize all channels (Passalacqua et al., 2010b). Alternatively, some authors proposed morphological reasoning to establish this threshold (Rodriguez-Iturbe and Rinaldo, 1997; Heine et al., 2004).

Different works in literature (Passalacqua et al., 2010b; Orlandini et al., 2011) proved that classical methodologies are not suitable for some study areas. Orlandini et al. (2011) provided a comprehensive work where classical methods are evaluated by using accurate field observations of channel heads (Pirotti and Tarolli, 2010), gridded elevation data obtained from LiDAR surveys, and state-of-the-art methods for the delineation of drainage basins and surface flow paths (Orlandini et al., 2003; Orlandini and Moretti, 2009a, 2009b). Their work highlights how classic approaches show variable reliability and sensitivity over different drainage basins and grid cell sizes, with a general tendency to overestimate the network, and they do not provide reliable predictions of channel heads across drainage basins having different morphology and channel initiation depending on different processes. A clear comparison of classical channel network extraction and flow routing methodologies has been deeply and successfully addressed also by Passalacqua et al. (2010b). These authors state that “The large variability shown by channel initiation contributing areas […] presents a formidable challenge for any standard channel network extraction algorithm”, and they showed how the classical methodologies tend to predict channels that are actually not present in the field. The conclusion is in all cases, that classical approaches are unable to predict accurately channel heads in areas where the channel initiation depends on different processes.

As a consequence of the mentioned observations, several studies emerged, pointing out that a robust delineation of stream networks cannot always be achieved by the popular steepest descent algorithm, and in some case studies, it should be based on direct detection of morphology in the DTM (e.g. Molloy and Stepinski, 2007; Lashermes et al., 2007; Tarolli and Dalla Fontana, 2009; Thommeret et al., 2010, Pirotti and Tarolli, 2010; Passalacqua et al. 2010a,b; Sofia et al. 2011). These studies underlined how specific geometric properties of surfaces calculated directly from DTMs can effectively avoid the thresholding issue of classical methods on channel network extraction. The core idea of these approaches is to label convergent cells and connect them on a second step using classical flow routing procedures or cost functions based upon them. A large number of indexes directly derived from LiDAR DTMs exists to describe correctly the geometric properties of surfaces, and they are able to identify terrain convergences (Gallant and Wilson, 2000). Some of them have already been used for network extraction (Tarboton and Ames, 2001; Molloy and Stepinski, 2007; Lashermes et al., 2007; Tarolli and Dalla Fontana, 2009; Thommeret et al. 2010; Pirotti and Tarolli, 2010; Passalacqua et al., 2010a, 2010b; Sofia et al. 2011).

Tarboton and Ames (2001) suggested the use of a proxy of curvature stemming from the Peuker and Douglas (1975) algorithm to account for spatially variable drainage density. Upwards curved grid cells have been used by other authors to derive channel networks from digital elevation data (Band, 1986; Gallant and Wilson, 2000). Tarboton (2003) proposed a procedure in order to provide a weight matrix to apply on drainage area computation. He suggested the use of a statistical threshold based on the constant drop property of channel networks (Broscoe, 1959) in order to choose the most suitable weighted support area threshold to map channels. However, some authors argued that this thresholding procedure is not applicable when the network topology needs to be related to morphology (Thommeret et al., 2010).

Wavelet analysis to locally filter LiDAR elevation data and to detect threshold of topographic curvature and slope-direction change has been used by Lashermes et al. (2007) to define valleys and portions of probable channelized areas within the valley. Curvature maps derived from LiDAR DTMs have been used by Tarolli and Dalla Fontana (2009) and Pirotti and Tarolli (2010) to assess the capability of high resolution topography for the recognition of convergent hollow morphology of channel heads and for channel network extraction respectively. Thommeret et al. (2010) used a data-driven and data-derived threshold based on DTM noise to extract badlands network, identifying convergent areas from a combination of terrain morphology indices and a single flow drainage algorithm. Passalacqua et al. (2010a, 2010b) applied nonlinear diffusion filtering combined with a geomorphically-informed geodesic cost function to identify automatically channel initiation points and extract channel paths from LiDAR data.

The referenced studies dealt with a prior assessment of the input data (Thommeret et al. 2010), calibration of the kernel size by interactively testing its effectiveness related to the investigated features (Pirotti and Tarolli, 2010), fixed arbitrarily chosen scales to evaluate topographic parameters (Tarboton and Ames, 2001; Molloy and Stepinski, 2007; Tarolli and Dalla Fontana, 2009; Passalacqua et al. 2010a,b). Some open questions still remain, as in how to identify thresholds that are not data-driven and how to objectively select scale without calibrating it on results and without considering a previous analysis of the data and of the study area.

For the present work, to extract channel network, a methodology relatively independent of the input dataset or from the size of the analyzed features is proposed (Chapt. 2, Sect. *IV.DTA for feature recognition*). The approach is based on normalized topographic attributes, such as openness (Yokoyama et al., 2002; Prima et al., 2006) and minimum curvature (Evans, 1979) as a weight for the upslope area. The identification of the optimum scale to use to evaluate topographic parameters is based upon distribution analysis, and statistical thresholds provide the key for the choice of the parameters controlling the extracted network.

2.2 Features in engineered landscapes

Engineered landscapes cover as great an extent of Earth's land surface as do many other globally important ecosystems (Achard et al., 2002; Ellis, 2004; Foley et al., 2003). In such environments, direct anthropic alteration of processes is significant, and it is aimed toward servicing the needs of human populations (Ellis et al. 2006). In Northern Italy, and in particular in agrarian landscapes within floodplain, massive investments in land reclamation have always played an important role in the past for flood protection. In these contexts, human alteration is reflected by artificial (human-made or extensively modified) earth-surface features ('Anthropogenic features', NRCS,2005), such as banks, levees and drainage networks, that constantly increase and change, in response to the rapid land use changes and the growth of human populations. For these areas, various existing and emerging applications require up-to-date, accurate and sufficiently attributed digital data about these anthropogenic features, but such information is usually lacking (Kothe and Bock, 2009), especially when dealing with large-scale applications. These areas are complicated due to the mix of man-made features and natural features, and additional spatial indicators have to be extracted based on structural analysis in order to understand and identify spatial patterns or the spatial organization of features, especially for man-made feature. Additional attributes are generally derived by geomorphological mapping, field-based technique (Passmore and Macklin, 2001; Schrott et al., 2002) or provided by cartography, but these sources might present some issues as well. Ground-based geomorphological mapping, for example, is generally only performed on small areas (Burel and Baudry 2005), or with large investments in terrain surveys (Lagacherie et al. 2004), with clear constraints for generalization, and thus restricting its use as a tool for larger scale investigations. The official cartography (i.e. Regional Technical Map – RTM- at 1: 5000 scale) is generally considered as a large-scale source of data, but the provided information refers to the time the map is produced, and this presents a big limitation when maps are not updated frequently. In Italy, the updating of the RTM is supposed to be done approximately every 10–15 years, but no specific regulation exists: each regional government makes its own rules and specifications. It is therefore, clear that users, when working with the RTM, must cope with the oldness of the derived information, that cannot account for all the frequent changes the anthropogenic environment is subjected to. At the same time, map updating requires new information about topography, that are traditionally derived by aerial surveys, and subsequent user interpretation, a process that is not bias free.

More recently, National or Local Mapping Agencies, especially in Europe, are moving towards the generation of digital topographic information that conforms to reality and are highly reliable and up to date (Baltsavias et al. 2004). In combination with widely automated methods of data processing and image analysis, remote sensing can provide multiple options to support decision makers with accurate and up-to-date geoinformation in such environmental context. Available space-borne systems provide data sets with low spatial resolution (in the range of > 500m) and a broad swath (spatial coverage of one image). Thus, sensors like DMSP-OLS (night-time lights), MODIS or NOAA enable mapping on continental or national basis. On medium spatial resolution (>5m) sensors like Landsat, SPOT, IRS or RapidEye featuring a field of view of 60-185 km enable to separate urbanized from non-urbanized areas on a regional scale.

Highest geometric resolution (<5m) is provided by sensors like Ikonos or Quickbird, allowing the classification of the small-scale individual objects. The restriction here is that the swath of around 15 km often does not cover the full extent of the study areas. Also, radar sensors such as TerraSAR-X or CosmoSkyMed are operating from space. These active systems are weather-independent (all-time) systems, while the optical systems are restricted to cloud free skies. With spatial resolutions up to 1 meter these data sets are capable of detecting the small-scale structures, with swaths from 10 to 100 km. In addition, interferometric SAR has been applied widely to derive digital elevation models (DEMs). In particular, the Shuttle Radar Topography Mission (SRTM) of the year 2000 supports analyses with area-wide DEMs with a spatial resolution of up to 30m.

Next to satellite based sensors, airborne remote sensing provides complementary data sets especially suitable for small scale features: aerial imagery provides spatial resolutions up to few centimeters and laser scanning as well as stereo cameras enable producing digital elevation models on geometric resolutions of 1 meter or even higher, for example. However, advantages of using LiDAR for terrain analyses in engineered landscapes include the following: LiDAR allows rapid generation of large-scale DTMs (digital terrain models); LiDAR is daylight independent, is relatively weather independent, and is extremely precise. In addition, because LiDAR operates at much shorter wavelengths, it has higher accuracy and resolution than microwave radar.

LiDAR DTMs covering large areas are readily available for public authorities, and there is a greater and more widespread interest in the application of such information by agencies responsible for land management for the development of automated methods aimed at solving geomorphological and hydrological problems. Automatic feature recognition based upon DTMs can offer for large-scale applications a quick and accurate method that can help in improving topographic databases, and that can overcome some of the problems associated with traditional, field-based, geomorphological mapping such as restrictions on access, and constraints of time or cost. For mountainous environments, numerous recent studies demonstrated the reliability of LiDAR data for the automatic characterization of features (Tarolli and Dalla Fontana, 2009; Passalacqua et al., 2010; Pirotti e Tarolli, 2010; Tarolli et al. 2010, Sofia et al., 2011). In engineered landscape within floodplain, high-resolution digital terrain models have instead mainly been used for hydrological modeling purposes (e.g. Cobby et al., 2001; French 2003; Dal Cin et al., 2005), while some other studies focused on morphological aspects (e.g. Lohani and Mason, 2001; Challis, 2006; Challis et al., 2006; Nelson et al., 2006). Anthropogenic feature extraction from DTM in engineered landscape within floodplains is a relatively new field of application. In this thesis, digital terrain analysis for feature recognition in floodplain it is tested for two main types of features, drainage network and levees (Chapt. 3 and 4, Sect. *IV.DTA for feature recognition*). This choice is done considering that in floodplains, these two elements offer two of the main tools for flood protection, and they can be managed easily to control runoff; therefore, their identification and characterization can be a useful tool for hazard mapping and environmental planning.

a. Anthropogenic features: levees and scarps

This work considers on a first DTA the example of levees and scarps as typical anthropogenic features, since they are the most wide-spread man-made terrain features in engineered landscapes within floodplains. These particular features are strictly connected with hydrological analysis, considering that are originally created to manage and control runoff and consequently, the hydrologic behavior of these areas. In the mentioned context, for a long time, the only data sources, used for anthropogenic feature extraction, were aerial and satellite imagery, while when dealing with LiDAR topography, the identification of anthropogenic features is usually done directly on the filtered point cloud of LiDAR data, after filtering vegetation and any other non-ground elements. However, differently from buildings, anthropogenic features as levees and scarps are implicitly embedded in DTMs, even if they actually do not belong to what is usually defined as the bare ground surface (Krüger and Meinel, 2008; Kothe and Bock, 2009). They result in hybrid objects, which are man-made on one hand, but on the other hand, they are considered as belonging to the earth surface (Krüger and Meinel, 2008). A technique of extracting banks information from LiDAR DTMs has been investigated by Krüger and Meinel (2008). In their work, the authors proposed method to label pixels as banks when their height exceeds an operative threshold defined according to flood alert levels considering dikes height. Kothe and Bock (2009) analyzed an approach to post-processing DTMs in order to detect man-made features and reconstruct the natural surface. These authors applied a filter based on a resampling module to generalize grid data and to produce a smoothed DTM: the difference between the original DTM and the smoothed ones contained nearly all man-made features. In their work, additional skeletonization and manual adjustment of extraction were needed. More recently, when dealing with feature extraction in natural contexts, morphological indicators (as in landform curvature) have been proven to be feasible for applications. Questions as in what is the optimum scale to apply to evaluate parameters have been raised (Pirotti e Tarolli, 2010; Tarolli et al. 2010, Sofia et al., 2011) and statistical operators have been proven to offer reliable and objective threshold for geomorphic feature identification in such environments (Lashermes et al. 2007; Tarolli and Dalla Fontana, 2009; Passalacqua et al., 2010a,b; Pirotti e Tarolli, 2010; Tarolli et al. 2010, Sofia et al., 2011). The question is still open as in if these morphological indicators and objective thresholds can be feasible also in anthropogenic landscapes, where features assume different characteristics and other artificial disturbances are present.

In this work, three different topographic parameters are tested to verify their suitability for feature extraction in engineered landscapes (Chapt. 3, Sect. *IV.DTA for feature recognition*). Both the parameter introduced by Tarolli et al. (2010), and an approach similar to the one proposed by Krüger and Meinel (2008), Kothe and Bock (2009), Carturan et al. (2009), Humme et al. (2006) Hiller and Smith (2008), Doneus and Briese (2006) are tested. A new parameter based on a measure of randomness of surfaces is also proposed. All these parameters are evaluated according to different approaches, and they are computed for different scales. A statistical analysis of the produced datasets is applied, then, to identify outliers to define objective thresholds for feature extraction. The same statistical approach is used on the extraction to discard false positive and produce a map of the potential features.

a. Anthropogenic features: drainage network

Drainage networks in agrarian landscape within floodplains constitute man-made surface's discontinuities, and they are expected to affect hydrological response during flood events. Drainage networks, in fact, influence groundwater hydrology (Dages et al., 2009), but also overland flow paths (Duke et al., 2006; Gascuel-Odoux et al., 2011; Lavasseur et al. 2011). Considering agricultural ditch drainage networks, four effects are commonly accounted for*: i)* the interception of overland flow on hillslopes; *ii)* the drainage of groundwater by lowering the water table*; iii)* the infiltration from the ditch towards the groundwater, and *iv)* the conveyance of water towards downstream areas (Carluer and Marsily, 2004; Dunn and Mackay, 1996; Lavasseur et al. 2011). Clearly, these networks influence the water transfer (Moussa et al., 2002), and they play a key role in the control of floods generation (Gallart et al., 1994; Voltz et al., 1998; Marofi, 1999; Moussa et al., 2002).

In Northern Italy, and in particular in alluvial plains, massive investments in land reclamation have always played an important role for flood protection. The extensive drainage network designed for reclamation purposes was able, in the past, to control groundwater level, especially when dealing with long-term heavy rainfall, which are the most critical in these areas. During the last years, changes in agricultural techniques, and the simultaneous increase of urbanization and industrialization increased the extent of impervious areas and reduced the extent of agrarian drainage networks. As a consequence, an overall decrease in volumes of small reservoirs is generally registered, and some studies highlighted the consequent effect on flood risks (Brath et al. 2003), pointing out the impacts of urbanization and changing agricultural practices in flood flows. These land-use changes, on the one hand, greatly increased the capital that the reclamation must defend and, on the other hand, they greatly decreased the time of concentration of meteorological waters (i.e. the time it takes rainfall waters in a certain point to reach the drains). The old drainage network designed on the needs of agricultural lands, results often insufficient. As a consequence, many inundations have occurred causing great financial damages. An example is the major flood that affected the eastern part of North of Italy during November 2010 (Marra et al., 2011), and that underlined how the agrarian landscape and the urbanization are connected one to the other, and their deep connection represents a critical issue in flood risk management.

In Northern Italy, the agrarian drainage network consists generally of open main, sub-main, and lateral ditches, located both on the field boundaries but also within the plots. Some areas lay below the mean sea level, and consequently, the water fluxes on the network are either mechanically or alternately mechanically controlled by pumping stations. The whole network is subdivided into different drainage districts, each managed and monitored by a Land Reclamation Consortium (LRC). Each LRC has the responsibility to control, maintain and modernize the drainage network, and to guarantee the hydraulic safety of the territory from flooding. This proper programming of measures, especially for complex drainage systems, relies on a correct network characterization, starting from large-scale and up-to-date information about network positioning and geometry. Furthermore, drainage/reclamation service criteria determine the requirements for hydraulic infrastructure in the form of drainage density and storage capacity. Storage capacity within the network, in particular, plays an important role in the design of drainage channels and pumping stations, considering that a larger storage or retention capacity within the network system lowers the requirement for pumping capacity to achieve the same service objective (Malano and Hofwegen, 1999). Network storage capacity assessment, furthermore, is a crucial tool for flood management: low values of channel storage capacity can underline deficit in the network, and they can outline areas whose hydrological behavior is potentially critical during floods.

For the characterization of the network over large areas, problem arises in Italy for two main reasons: *i)* there are no technical manuals with precise indications, valid for the Country, regarding the suitable size and density of the in-field channel network, that remains a farmer choice; and *ii)* as in other European countries, each farm unit is very often not continuous: as a result of land inheritance and political action, properties are generally characterized by a high degree of fragmentation, and each farmer's land is divided into a collection of scattered plots. As a consequence, when scaling up from an agricultural plot scale to the LRC scale, the structure of drainage networks appears to be highly variable in space and hard to characterize.

For the localization of the network, Regional Technical Maps are the source of information, with the limits already expressed. When dealing with the geometric characterization of the network, channel geometries are generally homogeneous over each property, and they are related to the trenchers used to build the channel, but no constraints exist that require all the farmers to apply some specific machines. Consequently, channel geometries vary over the different plots, and no information at all about channel widths or cross sections are available, unless they are derived with large investments in field surveys (Lagacherie et al. 2004), with clear constraints for generalization. As a consequence, drainage length, drainage density and storage capacity within the network are generally hard to define, and tools for an accurate large-scale and up-to-date detection of the agrarian network, and for an efficient characterization of its characteristics are deeply needed.

With LiDAR surveys, high resolution data are available concerning the ground elevation, and considering the artificial network dimensions, i.e. width or height, this kind of data can be a good candidate for agrarian landscapes' linear elements mapping (Bailly et al., 2008). A first method to delineate artificial network reaches in agrarian landscape directly from the LiDAR point cloud has been assessed by Bailly et al. (2008). However, these authors underlined how their approach had two requirements: *i)* ditches are exclusively located at field boundaries, and *ii)* a geographical database of plot boundaries must be available. If both conditions are satisfied, ditch detection is defined for some pre-located sites, and for those specific locations, it is possible to estimate the ditches elevation from the scatter of LiDAR last pulse points. The two underlined constraints make the method not feasible for large-scale applications in the Italian context, where a dense in-field network exists, the official cartography cannot be considered as a valid and up-to-date network database to identify specific sites, and field surveys for large areas are cost-prohibitive and time-consuming.

How to objectively and automatically detect and characterize the channel network in a floodplain context where the network is highly variable and only few information are available, is still an open question. In other environmental contexts, automatic channel network detections benefit from the topographic information given by high resolution (3m and better) LiDAR Digital Terrain Models (DTMs) (Tarolli and Dalla Fontana, 2009; Passalacqua et al., 2010; Pirotti and Tarolli, 2010; Sofia et al., 2011). In a floodplain context, problems for network extractions arise because the accuracy with which a DTM is able to detect and correctly represent the hydrological asset of a catchment is determined by the strength of the landscape gradient (i.e. flatness and/or slope changes). Low-relief areas, such as great alluvial plains, are therefore, more challenging even when high-resolution DTMs are available. For cultivated landscapes, drainage algorithms used on DTMs are unable to represent anthropogenically modified overland flow paths (Duke et al., 2006 and Garcia and Camarasa, 1999). The detection of the network in these contexts benefits from morphological approaches, whereas channelized elements are defined from local morphologies, and hydrological connectivity is not accounted for.

In this work, a DTA methodology based on high resolution DTMs is assessed (Chapt. 4, Sect. *IV.DTA for feature recognition*), to *i)* detect the drainage networks (ditches and channels) in agrarian/floodplain context, and *ii)* to calculate some of the network summary statistics (i.e. network length, width, drainage density and storage capacity per unit of interest). The procedure starts from a grid DTM readily available for public authorities in Italy. The DTM (1 m resolution) derives from a LiDAR survey planned to have highly affordable costs: the survey can be easily repeated during time, providing up-to-date large scale topographic information. The procedure is applied in two typical alluvial-plain areas in the North East of Italy, and results are tested comparing automatically derived network information with field surveyed ones.

II. STUDY SITES

In this thesis, investigations using various techniques have been carried out towards a more detailed understanding of relationships and interactions between morphometry and processes at various scales and in different environments. Four main study areas have been considered, two representatives of mountainous context, and two representatives of engineered landscapes typical of floodplains.

1. Mountainous environment

1.1 Cordon basin

The Cordon basin is located in the Dolomites, a mountain region in the Eastern Italian Alps (Fig. 2, Fig. 3). The area is characterized by a large variety of geomorphological processes and related landforms (e.g. landslides, surface erosion, steep fluvial incisions of bedrock rivers, colluvial and alluvial channels).

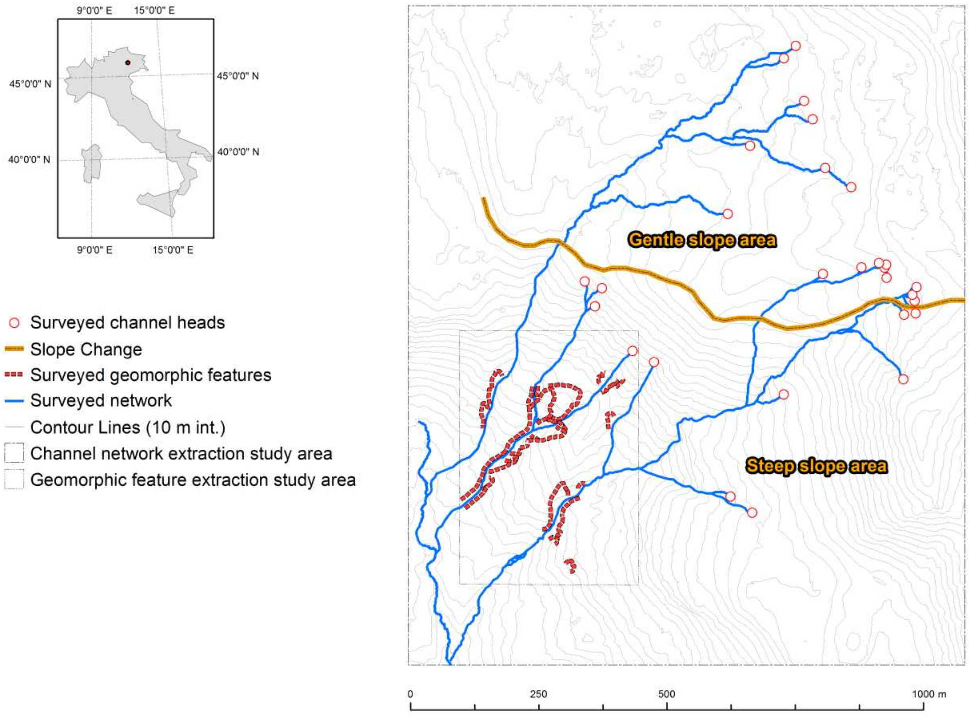

Fig. 2 Cordon basin: study areas and investigated features

The elevation ranges from 1969 to 2205 m above sea level (a.s.l.) with an average of 2064 m a.s.l.. The slope angle is 27.4° in average, and 69.6° at maximum. The area has a typical Alpine climate with a mean annual rainfall of about 1100 mm. Precipitation occurs mainly as snowfall from November to April. Runoff is dominated by snowmelt in May and June, and summer and early autumn floods represent an important contribution to the flow regime. During summer, storm events and long dry spells are common. During these events, several shallow landslides are triggered on steep screeds at the base of cliffs (Tarolli et al. 2008). Soil thickness varies between 0.2 and 0.5 m on topographic spurs up to depths of 1.5 m on topographic hollows. The vegetation covers the 96.1% of the area and consists in high-altitude grassland (89.7% of the area), and sporadic tall forest (6.4%). The remaining 3.9% of the area is un-vegetated talus deposits.

The Cordon morphology is extremely complex, both due to the presence of slope failures and erosional processes and, on the northern part of the site, due to the presence of erratic boulders, rocky outcrops, vertical cliffs and hummocky morphology (Fig. 3). Moreover the area is characterized by rapid slope changes, and these morphological complexities offer major issues for feature extractions.

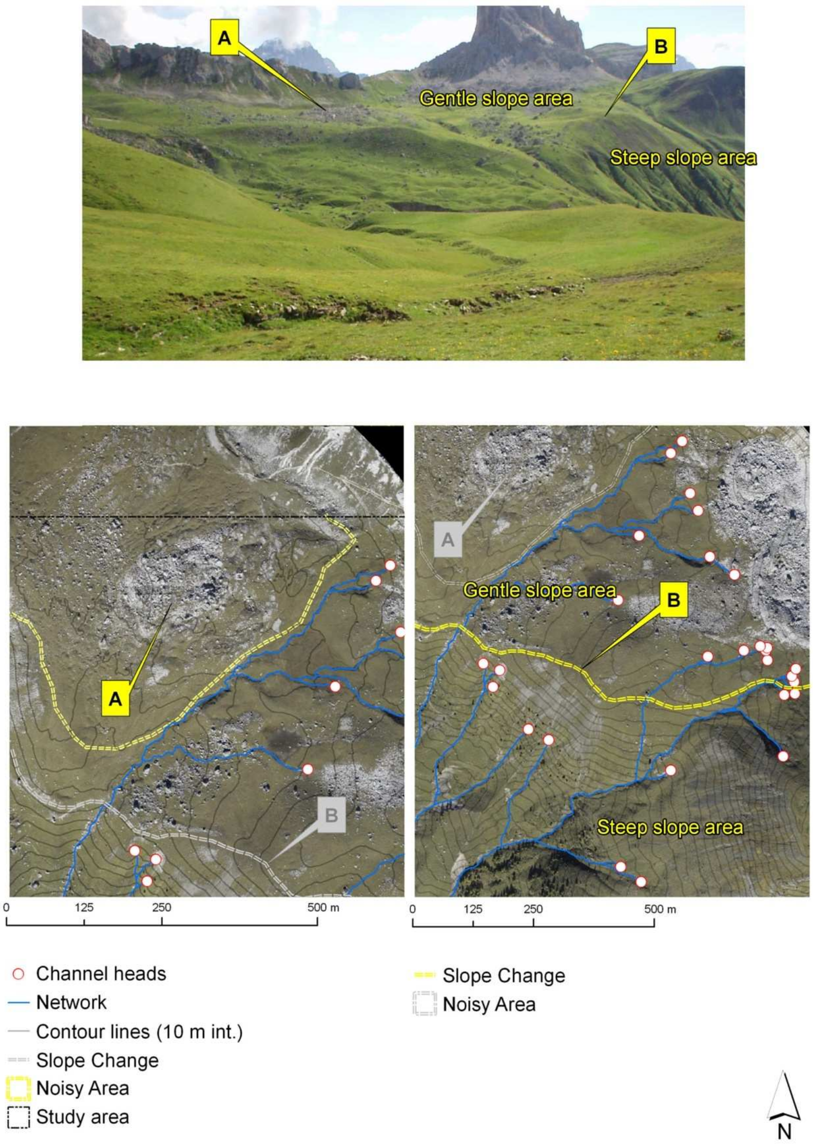

Fig. 3 Morphological settings of the upper part of the Cordon basin. The high degree of complexity (A) and the rapid slope change (B) define two of the main issues related to channel network extraction on this area according to topographic parameters and classic thresholding procedure respectively. (Sofia et al. 2011)

Available data of this area consist of several field surveys conducted during the past few years, including LiDAR survey (data acquired during snow-free conditions in October 2006), and DGPS (Differential Global Positioning System) ground observations carried out in the period 1995-2001 (Dalla Fontana and Marchi 2003) and during summer 2008-2009 (Pirotti and Tarolli 2010).

Two main features have been considered in this study area: shallow landslides and erosional features (Fig. 2 and Fig. 4) and channel network (Fig. 2).

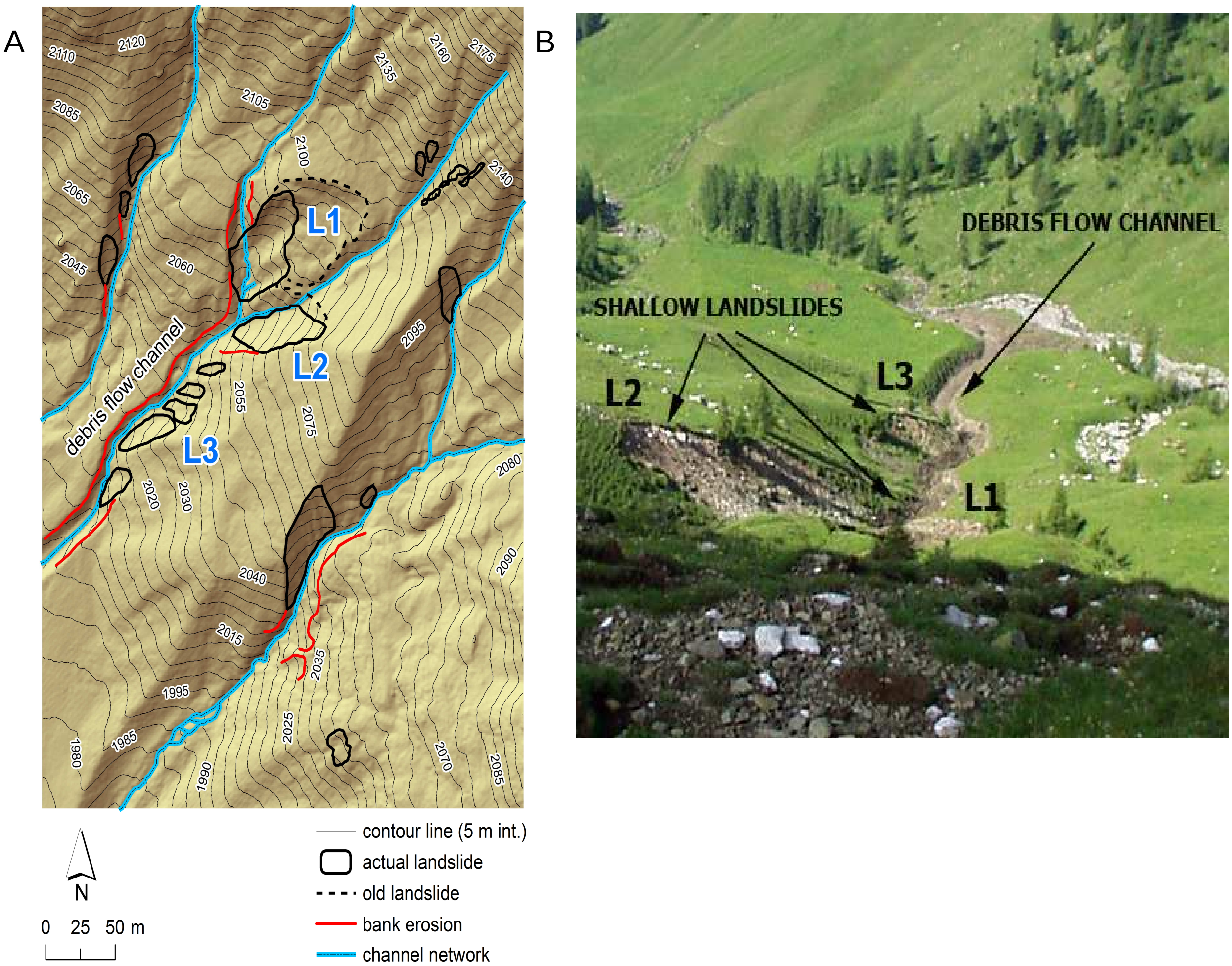

Fig. 4 Geomorphic feature details: (a) old landslides scars and bank erosion features and debris flow channel for the 2001 mud flow (b) (Tarolli et al. 2010)

Analysis of shallow landslides indicates that small, shallow debris flow scars heal rapidly, and they are difficult to detect after as few as 3-4 years. About 68% of the surveyed landslides were triggered by a very intense and short-duration storm on September 14th, 1994 (Lenzi 2001; Lenzi et al. 2004). The storm, with a duration of 6 hr, caused the largest flood recorded in 20 years of observation on the Rio Cordon basin. Due to the short duration of the storm, few slope instabilities were observed on entirely soil-covered slopes, while several landslides were triggered on slopes just below rocky outcrops (Tarolli et al. 2008). An important new sediment source was formed on May 11th, 2001, during an intense snowmelt event after a very snowy winter (Lenzi et al. 2003; Lenzi et al. 2004). Soil saturation mobilized a shallow landslide covering an area of 1905 m^2 that turned into a mud flow moving along a small tributary. A 4176 m^3 debris fan was formed at the confluence with the Rio Cordon, providing to the main channel fine sediments to be transported downstream (Lenzi et al. 2003). This new landslide area (Fig. 4A,B) triggered during 2001 is considered in this work, and it is located in a neighboring area of the Rio Col Duro basin where steep slopes, a narrow valley, and ancient landslide deposits are present as well. Along the small tributary affected by the mud flow of 2001, several shallow landslides were mapped (L3 in Fig. 4A,B). As a consequence, the whole tributary is considered to be a likely unstable region since different slope failures were checked in the field during the last survey of early June 2010. During the same field campaign, also other slope instabilities were found in proximity of the other two main landslide areas and channels.

The hydrographic network for the study area can be classified into three distinct types (Montgomery and Buffington, 1997) according to sediment supply, transport capacity and interaction with hillslope processes: alluvial channels that spatially organize sediment into distinct morphologies, colluvial channels comprise the transport-limited end member morphology where hillslope processes dominate. The final channel morphology is a bedrock channel where the transport capacity dominates the channel, leaving little to no deposition of sediment. To provide detailed information about the network, the area was systematically walked along all channels and surface flow paths up to the drainage basin divide (Passalacqua et al., 2010b). Twenty eight channel heads (Fig. 2) were mapped on the field with an accuracy of few centimeters. Channel heads were defined as points at which non-confined divergent flows on the hillslope converge to a drainage line with well-defined banks and flow paths, that is the upstream limit of concentrated flow (Dietrich and Dunne, 1993). For the Cordon area, contributing areas at channel head locations range between approximately 110 m^2 to 13000 m^2. Considering this high variability, area and slope-area threshold procedures using a unique value have been proven to be not reliable for channel network extraction if compared with the real channel network (Passalacqua et al., 2010b; Orlandini et al. 2011).

1.2 Miozza basin

The Miozza basin, located in Carnia (a seismically active area), an alpine region of north-eastern Italy, has been used most of all as a test site for the network extraction procedure. The test area (Fig. 5), in particular, refers to a sub-basin within the catchment. The area covers 4.4 km^2 and its elevation ranges from 834 to 2075 m a.s.l. with an average value of 1530 m a.s.l. The area is a typical alpine debris-flow dominated catchment (Tarolli and Tarboton, 2006).

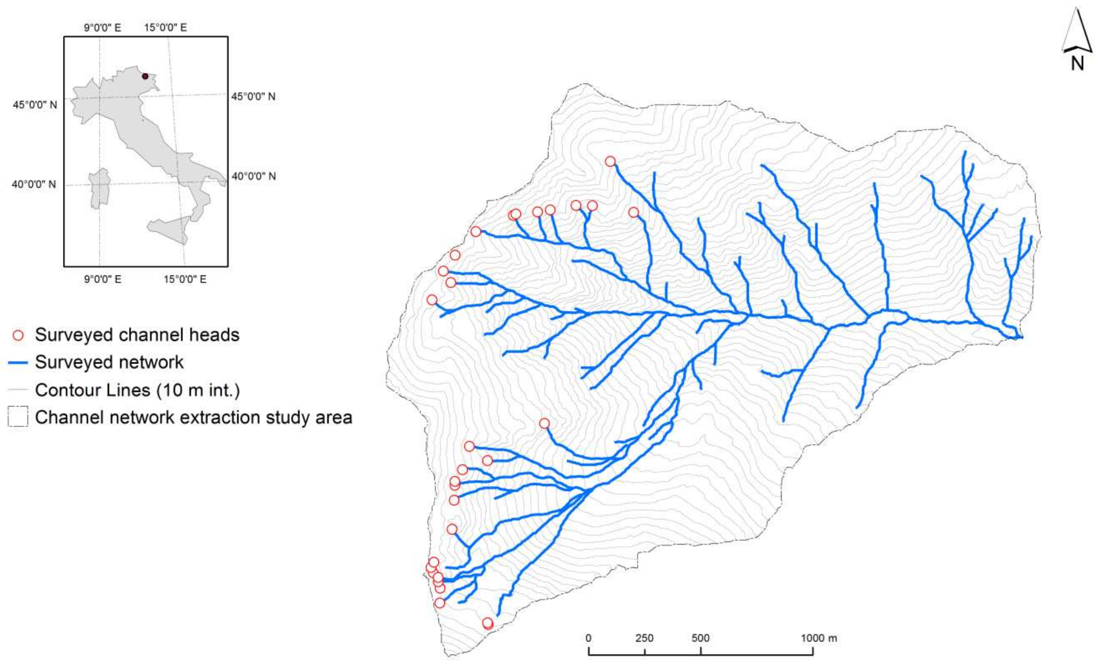

Fig. 5 Miozza basin: study area and investigated features.

Geomorphological settings of the basin are typical of north-eastern alpine region: deep valleys with high value of slope and significant erosion areas. Vegetation covers 90% of the area and consists of forest stands (40%), shrubs (20%) and mountain grassland (30%); the remaining 10% of the area is unvegetated landslide deposits. The Miozza basin is characterized by numerous landslide scars (Tarolli and Tarboton, 2006) object of several modelling applications (Tarolli and Tarboton, 2006; Tarolli and Dalla Fontana, 2008) and surveys (for example with Terrestrial Laser Scanner –TLS-). The average slope of the landslide scars area is 39°. Most of these areas, in particular, the largest single landslide area, are located at the head of the basin and occur in complexes that result from the aggregation of many shallow landslides. The occurrence of landslides in complexes is not the result of a specific event, but a combined effect of different events, including extreme short rainfalls, low intensity long duration rainfalls, snow melt, and also tectonic activity.

The area is quite wild, and the only significant human activity is related to occasional forest practices. The site is very representative of lithological and physiographical conditions frequently observed in Carnia areas, and detailed topographic information from various sources are available: data consist of field surveys conducted during the past few years (Tarolli and Tarboton, 2006), including LiDAR survey (data acquired during snow-free conditions in 2003) and a DGPS field campaign conducted during 2006-2007 (Tarolli and Dalla Fontana, 2009).

2. Engineered landscapes

For the present work, two main study sites have been selected as representative of engineered landscapes, and in particular of floodplains of the North East of Italy. The first site is a small area covering about 80 ha (Fig. 6), while the second area is a wider site, covering about 3000 ha (Fig. 8). Within study area b, a smaller site has been chosen to test the effectiveness of different topographic attributes in detecting anthropogenic features.

2.1 Site A

Site A (Fig. 6) is a 82 ha site located in the Friuli Venezia Giulia region (North East of Italy), in the municipality of Sacile (PN). This site has been chosen to apply Digital Terrain Analysis for network detection and characterization. The area contains a complex and dense artificial drainage network approximately 20 km long. The network (Fig. 6) consists of open main, sub-main, and lateral ditches, located on the field boundaries but also within the plots. The positioning of the ditches is regular, and it closely depends both on field subdivisions and agricultural practices. A detailed topographic survey was done, in order to provide a broad database of typical cross sections, retrieving 170 measures of channel geometries (Fig. 7). The survey was planned to obtain cross-section measurement for any relevant change on the sections for every significant network length (>30m).

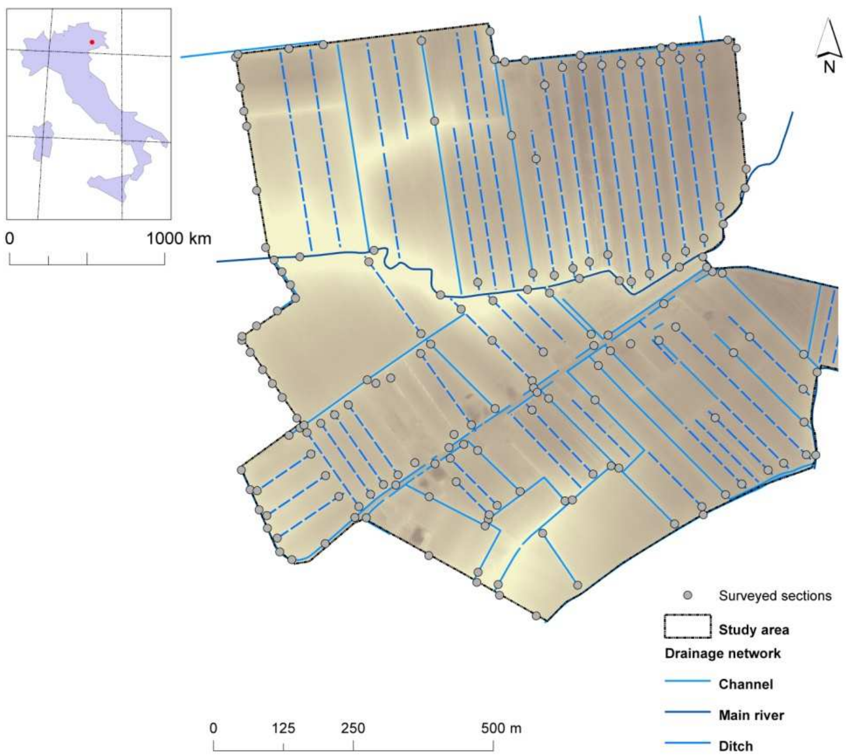

Fig. 6 Drainage network and field surveyed cross-sections retrieved for site A.

A database of network widths (W_{obs}), mean depths and cross-sectional areas (A_{obs}) has been created. Ditches and channels dimensions are characterized by widths ranging from 0.90 to 6.10 m (average of 1.2 m for ditches and 2.4 m for channels) and cross-sectional areas between 0.07 and 5.40 m^2 (average of 0.5 m^2 for ditches and 0.8 m^2 for channels). Being the drainage network artificial, its shape and characteristics are generally regular and homogeneous within the plots, and a strong relationship between the two parameters is registered (Fig. 7).

Considering that the network is artificial and generally built using trenchers with specific digging widths and depths, it is possible to relate some specific cross-sectional area to network widths, the assigned values in this case are 0.4 m^2 cross-sectional areas for widths lower than 2 m, 0.7 m^2 for widths up to 3 m and 1.5 m^2 for sections larger than 3 m. This characterization is area specific: it is an averaged characterization of cross-sections for widths ranges, and it may vary in different areas according to the digging techniques adopted to create the ditches.

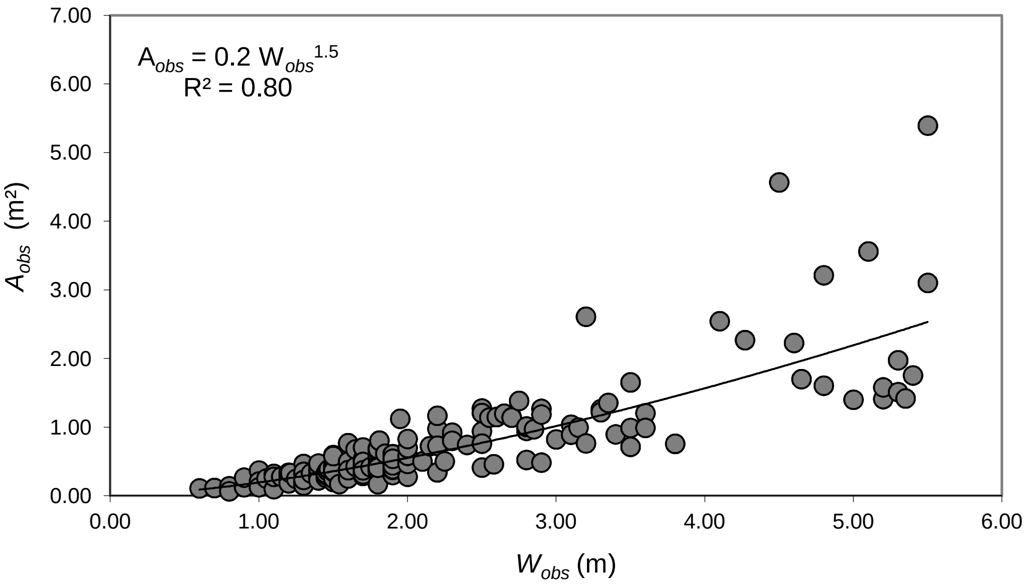

Fig. 7 Study site A: surveyed cross-sectional areas (A_{obs}) and bankfull widths (W_{obs}) and relationship between the values

2.2 Site B

Site B (Fig. 8a,b) covers the tract of the lower Veneto plain (North-Eastern Italy) stretching between Livenza and Tagliamento Rivers. The whole surface (about 3000 ha) is regulated by Hydro-geological Structure Plan (*PAI*) and it belongs to the Lemene River Basin Authority whose borders outline the area eastern boundaries. The west boundaries are underlined instead by the Livenza river embankments. On this area, two features are considered: levees and scarps, and drainage network.

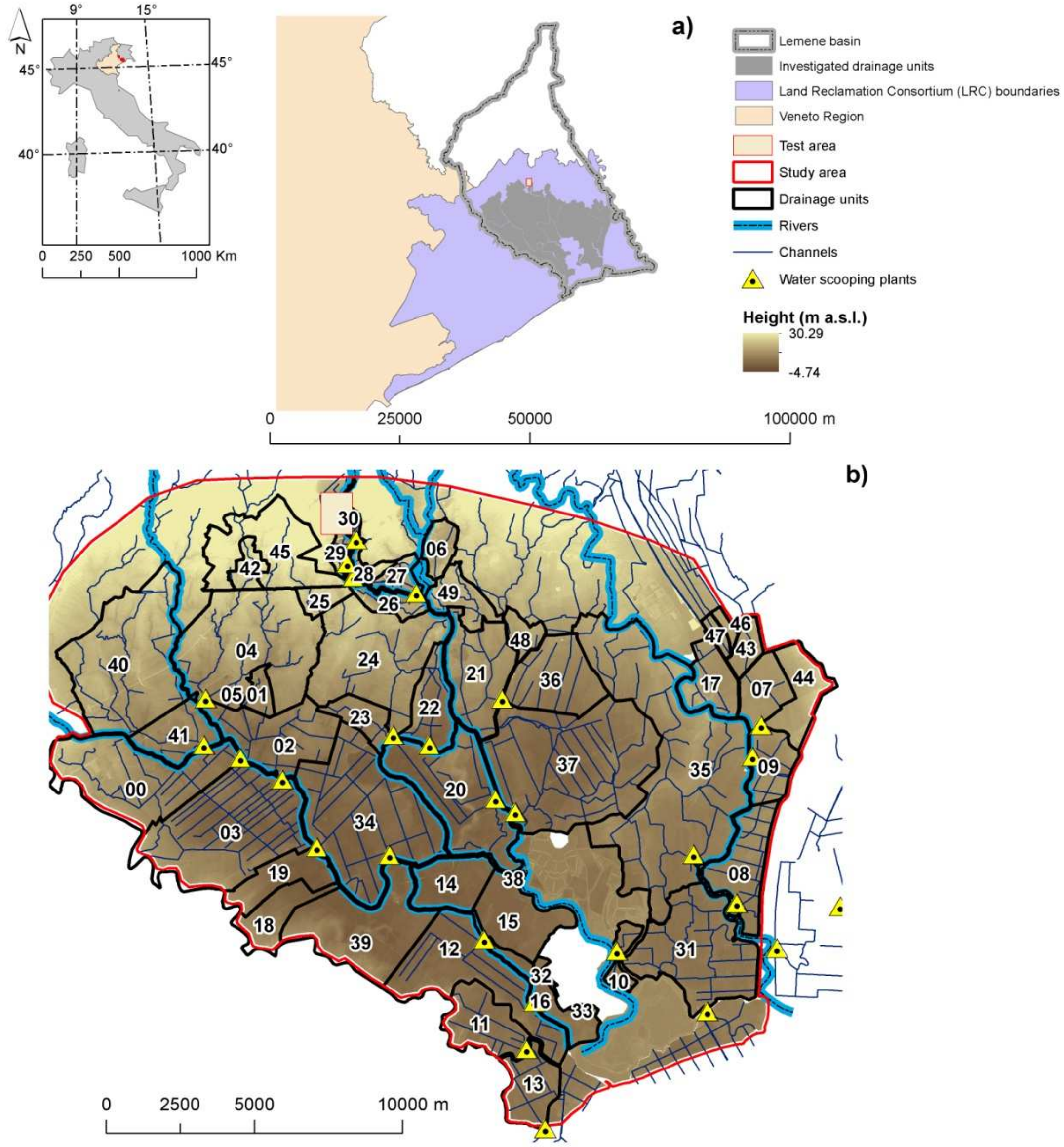

Fig. 8 Study site B. The considered drainage units are shown and labeled from 1 to 49, and the smaller site used for testing the different topographic parameters is showed.

The site is crossed from north to south by several natural and artificial water collectors (Fig. 8). These watercourses originate from the northern part of the area, in Friuli-Venezia Giulia, by waters emerging along the line of groundwater springs; they then flow through Veneto receiving the superficial outflows. In the southern part, the average ground elevation is at the sea level and declines to even 2 – 3 meters below it in the southernmost areas, close to the coast. For this reason, these watercourses in their final stretch become collectors of artificial outflows, which originate from water scooping plants. Almost 60% of the area is artificially drained: at the present time, about 30 water scooping plants are working, with a total circulation of about 200 m^3/s.

The drainage network spans for about 900 km, 30 % of which offers just drainage functions. The remaining 70% is characterized by both irrigational and drainage functionality making use of draining ditches either for irrigation or for drainage. This network is mainly composed by channels and ditches, as typical for agricultural landscapes (Fig. 8 and 9a). Ditches are generally small (<1 m), and they store excess water for drainage or irrigation purposes; channels are wider, and are characterized by permanent and constant discharge. According to the official cartography (RTMs), channels are defined as main channels when their width is greater than 2 m, while they are labeled as minor network when the width is smaller than 2 m. The whole area includes different drainage units, based mainly on a network of open channels and ditches, which guarantees the drainage of meteoric water, and on a complex embankments system, which prevents the whole area from being flooded. For this study, for network characterization, 50 drainage units have been considered (Fig. 8). Each drainage unit completely relies on artificial drainage by water scooping plants.

Within site B, a small test site (Fig. 9) has been selected to test the effectiveness of different topographic parameters for feature extraction.

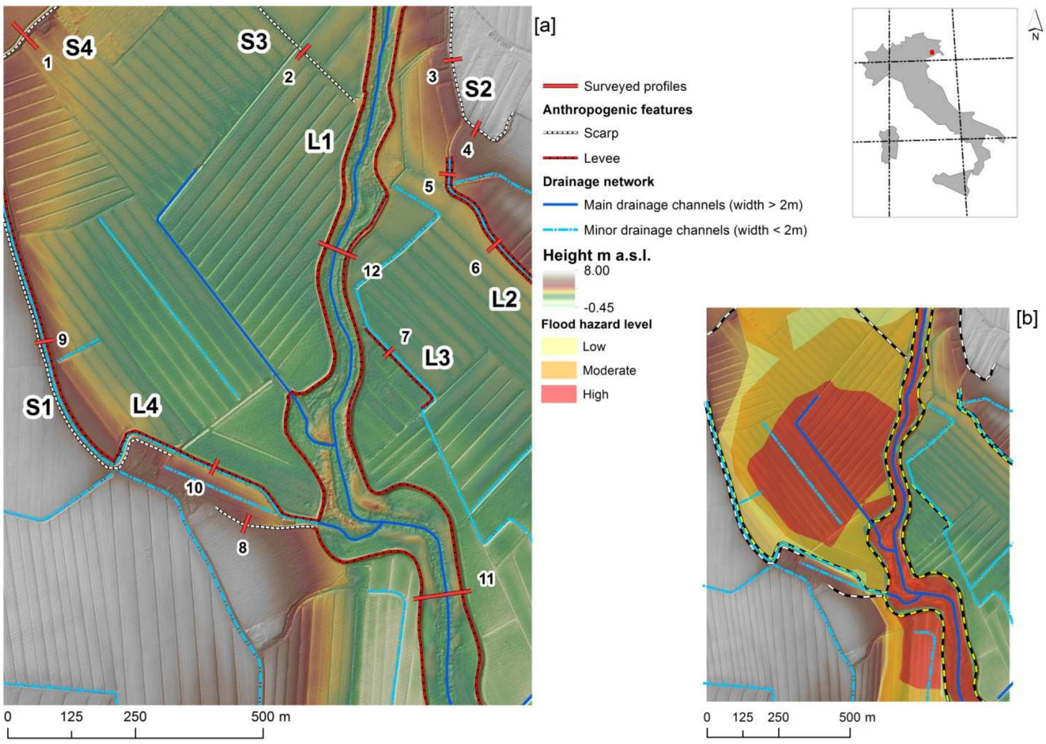

Fig. 9 Location of the test area for anthropogenic feature extraction, its main characteristic (a) and flood level hazards (b). Anthropogenic features (levees and scarps) as derived from official cartography are shown. Location that have been surveyed on the field to verify cartography, - labelled from 1 to 12- are identified.

Due to the dense network and the morphological context, the area is characterized by high levels of flood hazard (Fig. 9b), and banks, levees, and scarps offer the major flood protection, especially considering that the average ground elevation is at the sea level or lower.

For testing purposes, two different type of anthropogenic features have been analyzed (Fig. 9a): levees (L1, L2, L3, L4) and scarps (S1, S2, S3). Levees are built along both banks of the main channel (L1), or on one or both banks of some minor channels (L2, L3, L4) for flood protection purposes. They are usually characterized by width ranging from 10 to 30 m, trapezoidal cross-section, and heights that range between 1 and 3 m (Fig. 10), and they are generally passable. Scarps are instead abrupt differences in ground level, due to artificial causes (i.e. roads escarpments, or escarpments along channels that are too small to be considered as levees). S1 and S2 (in Fig. 9) are on the right side of some minor channels, while S3 and S4 are due to the construction of two small roads that run on a level higher than the surrounding plain. All the artificial features have been checked on the field, and 12 sections (1-12 in Fig. 9a and Fig 10) have been mapped on the input LiDAR DTM (1 m resolution) (Fig. 10), to gain insights about the shapes and measures of the features as they are represented on the digital terrain model, and to provide a database of position measurements to use as reference dataset.

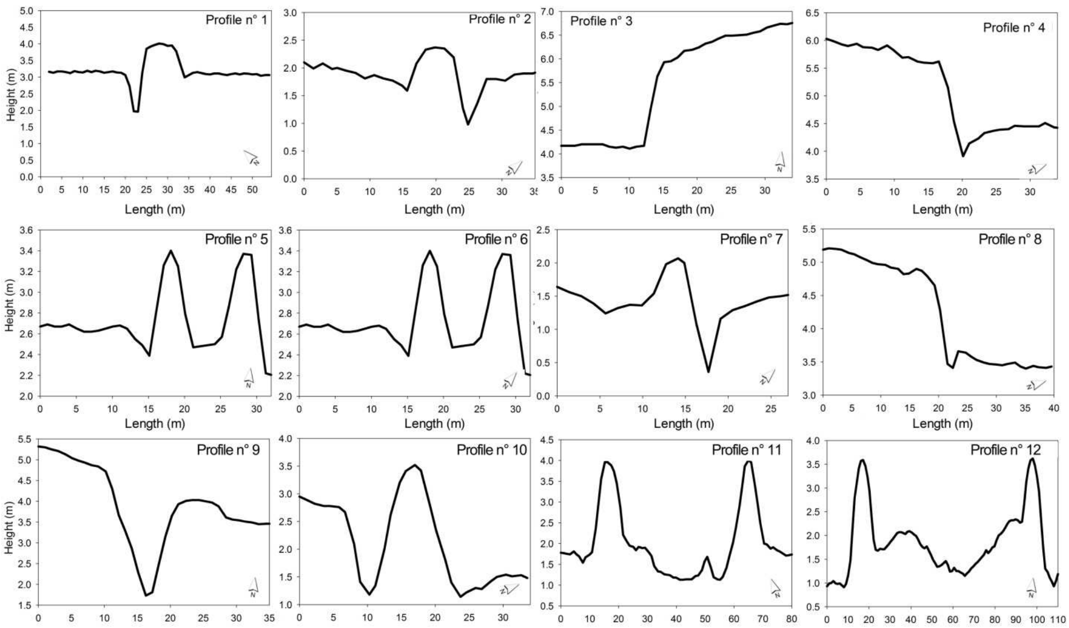

Fig. 10 Representation of anthropogenic features geometry according to the Digital Terrain Model.

III. MATERIALS AND METHODS

This chapter reviews and discusses the research that provides materials and methods for this study. It is not meant to be a deep and complete review of the literature about Digital Terrain Analysis, but more an indication of the theoretical basis of, and problems associated with its application for characterizing surfaces, landforms and hydrogeomorphic features using high resolution LiDAR- Digital Terrain Models.

With the term of Digital Terrain Analysis (Evans, 1980), literature usually identify the processes of geomorphological analysis, landform parameterization and land surface analysis (Shary et al. 2002). Wilson and Gallant (2000) give a comprehensive review of Digital Terrain Analysis, providing a deep overview of applications to geomorphology, hydrology, soil and vegetation mapping, offering a '*state of the art'* reference for this context. The increasing interested in DTA has been driven in the last decade by the growing availability of high-resolution models, such as the one derived from LiDAR. In this chapter, a brief review of this technology is provided. A more detailed approach is dedicated to Digital Terrain Models, their characteristics, and the main conceptual problems related to their use in the field of landform characterization for feature extractions. Using LiDAR data for DTM generation is becoming a standard practice in spatial related contexts, but their use for automated or semi-automated methods to detect landform and landform features is still a matter of research (Lashermes et al. 2007, Passalacqua et al. 2010a,b,; Tarolli et al. 2010, Sofia et al. 2011). A review of the main concepts related to surface representation is provided, offering the general background and framework for the terrain parameters considered in this thesis and applied for the research. The statistical approach that offer the basis of the objectivity of all proposed methodologies is also described.

1. Airborne LiDAR technology

Airborne Light Detection and Ranging (LiDAR) – also referred to as Airborne Laser Scanning (ALS), provides nowadays a valid tool for high-density and high-accuracy three-dimensional terrain point data acquisition. Two of the most appealing features in the LiDAR output are the direct availability of three dimensional coordinates of points in object space (Habib et al., 2005), and the capability to obtain ground information over areas with vegetation cover (Vosselman and Maas, 2010). LiDAR data have become a major source of digital terrain information (Raber et al., 2007) and they have been used in a wide of areas, such as building extraction and 3D urban modeling, hydrological modeling, glacier monitoring, landform or soil classification, river bank or coastal management, and forest management. However, terrain modeling has been the primary focus of most LiDAR surveys (Hodgson et al., 2005). As of today, the use of LiDAR for terrain data collection and Digital Elevation Models (DEMs) generation is the most effective way for digital surface mapping (Forlani and Nardinocchi, 2007), and it is becoming a standard practice in the spatial science community (Hodgson and Bresnahan, 2004).

An airborne LiDAR system is typically composed of three main components (Fig. 11): a laser scanner unit, a Global Positioning System (GPS) receiver, and an Inertial Measurement Unit (IMU) (Habib et al., 2005; Hollaus et al., 2005; Reutebuch et al., 2005; Webster and Dias, 2006; Pfeifer and Briese, 2007).

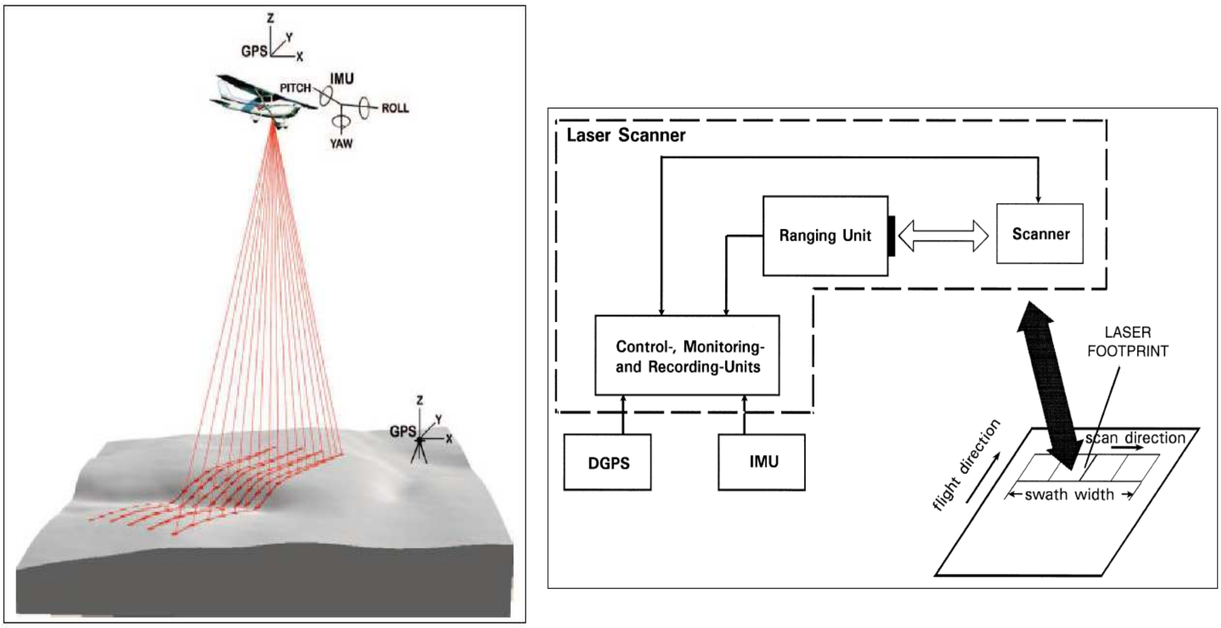

Fig. 11 LiDAR schematic, showing scanning laser unit and scan patterns on the ground (red), and aircraft positioning and altitude measurement systems (Carrier-phase DGPS for aircraft position and an inertial measurement unit -IMU- for recording pitch, yaw, and roll of the aircraft) (Reutebuch et al., 2005; Wehr and Lohr, 1999).

The laser scanner unit consists of a pulse generator of laser with a wavelength in the range of 0.8 μm to 1.6 μm (typically, with 1.064 μm or 1.500 μm) and a receiver to get the signal of scattered and reflected pulses from targets (Wehr and Lohr, 1999; Mukai et al., 2006; Pfeifer and Briese, 2007). The laser pulses are typically 4 to 15 ns in duration and have a peak energy of several millijoules (Wehr and Lohr, 1999; Acharya et al., 2004; Lemmens, 2007). Laser pulses are emitted to the Earth surface at a rate of up to 250 kHz (Lemmens, 2007).

The basic principles of the technology, relies on pulses of light toward a target: each emitted signal is backscattered and reflected by the objects, and the measurement mechanism is able to provide some of the properties (e.g. traveling time, signal intensity) of the reflected pulse (Wehr and Lohr, 1999). The distance (*range*) between the LiDAR sensor and the object can then be calculated by multiplying the speed of light by the traveling time of the light to be transmitted from and return to the sensor (Watkins, 2005; Weitkamp, 2005). With recently developed LiDAR sensors, range precision can reach 2-3 cm (Lemmens, 2007). Range measurements do define the target position through lasers, adopt two major principles: pulsed modulation and sinusoidal Continuous Wave (CW) modulations (Fig. 12).

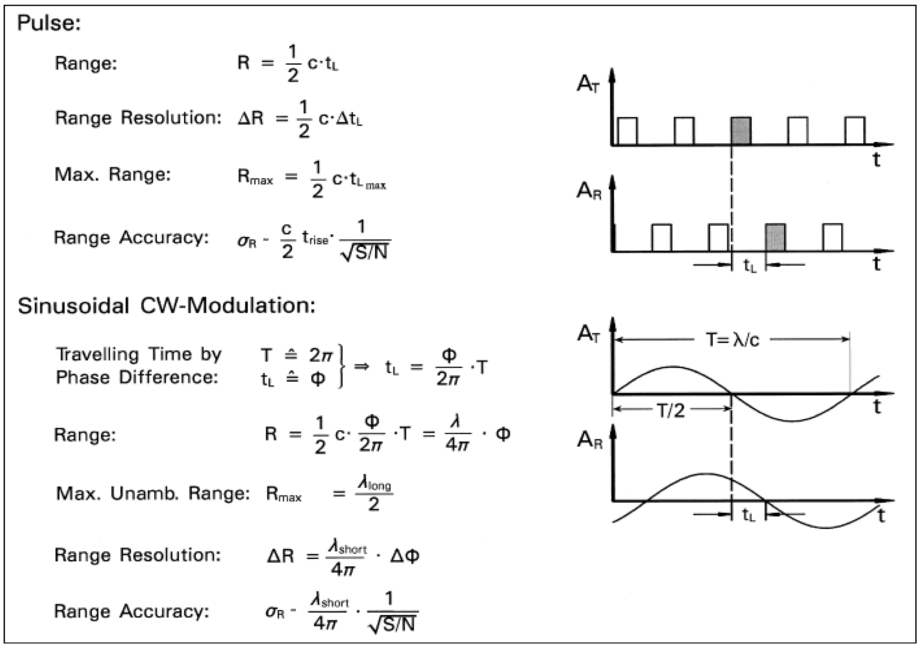

Fig. 12 Measuring principle of pulse and CW-lasers. On the right, the first and the third figures show the transmitted signal, the second and the fourth figures the received one. A_T and A_R are the amplitudes of the transmitted and received signal, respectively (Wehr and Lohr, 1999).

The GPS receiver is used to record the aircraft trajectory and position in absolute coordinates, while the IMU unit measures the altitude of the aircraft (roll, pitch, and yaw or heading) (Webster and Dias, 2006). By synchronizing the information derived by the scanner, the IMU and the GPS it is possible to determine the target location with high accuracy in three dimensional spaces (Liu, X. et al., 2007). The accuracy of LiDAR points is related to the accuracy of GPS and IMU. Airborne GPS is able to yield results in 5 cm horizontally and 10 cm vertically, while IMU can generate attitude with accuracy within a couple of centimeters (Liu, 2008). LiDAR data can get an overall accuracy of 15 cm root mean square error (RMSE) in vertical and 20 cm RMSE in horizontal (BC-CARMS, 2006).

One of the main advantages of the airborne LiDAR systems, is their capability of detecting multiple return signals for a single transmitted pulse (Wehr and Lohr, 1999; Charaniya et al., 2004; Reutebuch et al., 2005). Most LiDAR systems typically record first and last returns, but some are able to record up to six returns for a single pulse (Wagner et al., 2004; Lim et al., 2003). Recording multiple returns is quite useful for the topographic mapping in forested area or for the description of forest stand and structure (Sheng et al., 2003), and it is of great advantage, especially in mountainous environment.

In addition to the three dimensional coordinates, most LiDAR systems also have the capability of capturing the intensity of the backscattered laser pulse, which is referred to as the LiDAR intensity value for the particular return (Jelalian, 1992; Barbarella et al., 2004; Coren et al., 2005). This intensity data can assists surface classification, and therefore, is of potential to improve the generation of DEMs (Höfle and Pfeifer, 2007).

One important developments of airborne LiDAR systems include the integration of a high-resolution digital camera or video camera with a LiDAR system (Ackermann, 1999; Ahlberg et al., 2004). For each collected digital image, the position and orientation of the camera can be obtained by using the GPS and IMU data. Exterior orientation parameters for each frame of imagery are directly provided by these position and orientation data. Therefore, no stereo overlapping images and/or ground control points are needed. Orthorectification can be completely automatic by using the digital images and a LiDAR-derived DEM (Ahlberg et al., 2004).

LiDAR data sets contain a very large record of points, concerning both bare ground surfaces, and every feature on the surface. Such data are filtered and thinned using specific algorithms, providing a dataset for ground elevation and a dataset for feature information. From such information set, the construction of DEMs, such as Digital Terrain Models (DTMs) and Digital Surface Models (DSMs) can be computed. These high-quality models can have accuracies less than ± 25 cm depending on land cover, slope, flight parameters and environmental conditions (Hollaus et al., 2005).

2. Digital Terrain Models

The availability of data derived by laser scanning enabled rapid, accurate, and effective acquisition of geographic information (Ackermann 1999, Kraus and Pfeifer 2001, Briese 2004, Slatton et al. 2007, Tarolli et al. 2009). There has been a significant increase in the use of LiDAR data for Digital Elevation Models (DEM) generation over the last decade, as more reliable and accurate LiDAR systems are developed (Sithole and Vosselman, 2003). Lohr (1998) and Kraus and Pfeifer (1998) are pioneers who demonstrated the suitability of using airborne LiDAR for the generation of DEMs. Since then, DEMs generation from LiDAR data under various conditions has been documented by many authors (Lloyd and Atkinson, 2002; Wack and Wimmer, 2002; Lee, 2004; Gonçalves-Seco et al., 2006; Lloyd and Atkinson, 2006; Kobler et al., 2007).

Different digital elevation models have been developed to represent the terrain surface: the most common one are the regular grid (usually square grid), the triangular irregular network (TIN), and the contour line model (Ramirez, 2006). The form of dem used for this entire thesis is that of the regular grid Digital Terrain Model (DTM).

A DTM can be understood as a digital representation of a portion of the bare ground earth's surface, represented as 'fields': each grid cell with x and y coordinate has a constant elevation (z) value for the whole cell (Ramirez, 2006). In this sense, a DTM is a '2.5D' representation of terrain surface (Weibel and Heller, 1991) through a matrix of values. The georeferentiation of elements that comprise the surface is defined by the ordering of elevation values within the matrix, whose structure implicitly record topological relations between data points (El-Sheimy et al., 2005). The widespread use of such grid models for morphological quantification is mainly due to the fact that the matrix form is the simplest and the most efficient approach in terms of storage and manipulation, since this data structure is similar to the array storage structure in computer (El-Sheimy et al., 2005; Ramirez, 2006; Ziadat, 2007). This matrix form is the key element that allows the use of such models also in a non-GIS environment, as further explained in appendix A.

There are a number of conceptual problems that must be addressed when considering DTMs as models of terrain form. In this chapter, some main issues are addressed, and they follow two of the main general tasks related to digital terrain modeling for landform characterization: (1) DTM generation, analysis and interpretation: what is the morphological quality of the produced DTM? (2) DTM application: how do we apply a discrete surface (DTM) to represent continuous variables (slope, aspect, curvature…)?

2.1 DTM Generation, analysis and interpretation: quality of the DTM

It is well known that LiDAR DTMs, being an accurate representation of ground surface, allow automated direct extraction of hydrological features (Martz and Garbrecht, 1999), thus bringing advantages in terms of processing efficiency, cost effectiveness, and accuracy assessment, compared with traditional methods based. However, the quality of spatial analysis strictly depends on DTM quality, procedure relevance, and on the way they interact (Burrough and McDonnell, 1998). Researchers have found that DTM quality and resolution affect the accuracy of any extracted hydrological features (Kenward et al., 2000). Quality assessment of data is a critical parameter for DTM production and use: semantically reliable and high-quality data models should be always defined. Generic quality of a DTM can consist of many factors, as for example in the accuracy of the DTM in respect to the input points (interior quality), or its accuracy related to external control data (exterior quality) (Briese 2010). The common techniques for quality assessment are based on the statistical comparison of small reference areas of higher quality, or the use of higher resolution measurements of the terrain surface (i.e. Zandbergen, 2008 and Davis et al., 2001) with the created DTM in order to find outliers. However, one should consider that there is an inherent variability of landscapes across a very wide range of scales (McClean and Evans, 2000), therefore measurements of elevation at a finer spatial resolution may be measurements of a slightly different surface (Wise 2011). Another approach used in literature to assess DTM quality is the use of synthetic surfaces in which the true values of elevation and surface derivatives are known everywhere (Jones, 1998; Zhou and Liu, 2002; Zhou and Liu, 2004). One of the main weaknesses of this approach is that synthetic surfaces, even when complex polynomial or trigonometric surfaces (i.e. Jones, 1998), tend to be smoother than natural terrain, and they might lack of information in places where interpolation problems actually arise (Wise, 2000).

A number of studies have empirically assed the accuracy of DTMs under various conditions. Later works have examined errors in LiDAR derived DEMs as influenced by land cover and slope (Hodgson et al. 2003). Cowen et al. (2000) tested for a relationship between canopy closure and accuracy of the produced maps. In a more recent work, Hodgson and Bresnahan (2004) presented an error budget model for a LiDAR derived DTM surface, accounting for the contributing error from the LiDAR system, elevation errors induced from horizontal displacement, errors induced by interpolation techniques and errors in the survey used as reference to calculate the observed RMSE.

It is generally understood that there are a variety of factors influencing the accuracy of LiDAR derived DTMs. A general summary of the sources of these errors can be found in Maune (2001) and in Table 1.

Table 1: Concepts related to LiDAR surface accuracy variations (Hodgson et al. 2004)

Sensor	*Aircraft*	*Navigation*	*LiDAR point processing*	*Geography*
Pulse Length	Altitude	GPS	Return identification	Seasonality
Pulse Rat	Forward speed	INS	Automated labeling algorithm	Land cover
Wavelength			Human classification	Slope
Divergence			Interpolation algorithm	
Scan Angle				

In general, errors in a DTM appear as a consequence of constructing a model from a discrete distribution of points sampled on the terrain (Meneses et al. 2005). This approach is liable to introduce errors because of its discontinuous representation of the terrain surface. More specifically, the features which have an impact on DTMs accuracy are the point density and terrain slope (Karel and Kraus, 2006), the ratio of point resolution to grid resolution and the distance between each point and its nearest neighbor (Briese, 2010). There are approaches to DTM creation that try to solve the problem of assigning the appropriate sampling density to each type of surface, as a function of the accuracy required (Li 1991), but the relation between point density and model quality has not been appropriately parameterized. Usually, a higher level of accuracy might be achieved by increasing the point density, but in terrain with rough topography, this is not always feasible (Meneses et al. 2005). There are even anomalous situations where increasing the point density might increase the errors in the DTM as well (Makarovic 1973, 1977, 1980, 1984). The variety of available interpolation methods has led to questions about which is most appropriate in different contexts and has stimulated several comparative studies of relative accuracy (Zimmerman et al., 1999). To evaluate the performance of some commonly-used interpolation methods, a variety of empirical works have been conducted to assess the effects of different methods of interpolation on DTM accuracy (Zimmerman et al., 1999; Ali, 2004; Blaschke et al., 2004; Mardikis et al., 2005; Chaplot et al., 2006; Lloyd and Atkinson, 2006). There seems to be no single interpolation method that is the most accurate for the interpolation of terrain data (Fisher and Tate, 2006): no interpolation method is universal for all kinds of data sources, terrain patterns, or purposes. Many DTM creation methods produce distinctive artifacts that have a strong spatial signature (Berry et al., 2000, Brown and Bara, 1994, Guth, 1999,Wise, 2000 and Wood and Fisher, 1993). For example, linear interpolation of contour lines can create ramps (Hutchinson, 1988), spline interpolation can create deep pits (Wood, 1996), and inverse distance weighting interpolation can create terraces (Burrough and McDonnell, 1998).

Another point to consider is that, even by choosing the most appropriate interpolation method, the fidelity with which the DTM represents the true surface will depend on both surface roughness, and DTM resolution. There is therefore, an implicit scale of analysis implied by the grid cell resolution: the bigger the grid size, the more general the approximation of the terrain surface representation (Ramirez, 2006). LiDAR data have high density, and can overcome this kind of limitation of grid DTM, allowing the creation of models with sub-meter grids. However, selection of a suitable resolution for a DTM is also highly dependent on different applications. High resolution DTMs may significantly improve the predictive ability of terrain attributes (Lassueur et al., 2006), and the choice of input DTM data resolution depends on the output of interest (Chaubey et al., 2005). The general idea is to select a resolution that produces best predictive properties without giving computational constraints, and many researchers have investigated the effects of different resolutions on the accuracy of specific application models (Hengl, 2006, Garbrecht and Martz, 1993; Ackerman, 1993; Hodgson, 1995, Tarolli and Dalla Fontana, 2009). Other relevant researches can be seen in (Garbrech and Martz, 1994; Zhang and Montgomery, 1994; Florinsky and Kuryakova, 2000; Kienzle, 2004). In general, one must note that the grid DTM is commonly over-sampled in low relief areas and under-sampled in high relief areas (Hengl et al., 2003). Furthermore, the size of regular grids can not be adapted to the complexity of the relief. Feature specific points such as peaks and pits may be missed (El-Sheimy et al., 2005), and linear features such as breaklines are not well represented. One way to increase the details of the terrain representation is to increase the sample point density and decrease the grid size. Considering LiDAR data, anyway, the point density, even if high, is not regular, and changes in point density might results in errors and artifacts on the produced map that do not actually represent the ground surface (see i.e. Fig. 51, p. 116). LiDAR data, furthermore, need to be filtered before deriving the DTM, and filtering procedures is another fundamental issue that has been discussed in some recent researches (Jones et al., 2007; James et al. 2007; Cavalli et al., 2008a). The automatic filtering procedures of LiDAR raw data, may decrease the quality of DTM, mainly for the decreasing of bare ground points density, and it might result in systematic error on the filtered data. This fact has a strong influence on the representativeness of the derived DTM for morphological characterization of surfaces.

Small errors in elevation can produce large errors in derived values, especially second-order derivatives such as curvature (Florinsky, 2002; Wise, 1998). In Florinsky (2005) a thorough analysis is reported on artificial linear elements of topographic variables, where such linear elements can be a reflection of geological structures, but can also be a result of quality degradation due to the geometry of the DTM grid, errors in the DTM compilation, errors in the DTM interpolation, aliasing errors, imperfection of algorithms for DTM derivation, and anisotropy of operators. Kraus and Pfeifer (2001) have investigated on the geo-morphological quality of LiDAR-derived DTMs, mentioning the importance of the identification of breaklines and pits; the former to improve the quality of the DTM, the latter to improve applicability of hydrological models by elimination of the pits. Other related works on the theoretical bases of DTM modeling and quality assessment have been done by Li (1993) and McCullagh (1988). Haneberg (2006), Holmes et al. (2000), and Fisher (1998) showed that the effects of elevation errors on slope angles and other derivative values calculated from conventional 10 m and 30 m DEMs can impart significant uncertainty into slope angle calculations and values dependent upon them. McKean and Roering (2003), Hodgson and Bresnahan (2004), and Adams and Chandler (2002) have evaluated LiDAR elevation errors using root-mean-square (RMS) statistics. Haneberg (2008) evaluated instead the geostatistical variability of high resolution LiDAR DTM elevation errors and their effects on slope instability calculation. In Wise (2011) the general characteristics of DTM errors are issued and the capability of RMSE of elevation in characterizing these errors is addressed.

Other than the horizontal or vertical accuracy, therefore, a geo-morphological quality of the DTM should also be accounted, whereas a high geo-morphological quality DTM must include the absence of elements which limit successive interpretation. DTMs are normally only provided with a single RMS error, this is not adequate to determine the error associated with the derived topographic parameters, because this indicator shows only moderate correlation with the geo-morphological quality of the DTMs. In Fig. 13 for example, a visual assessment of four different 1 m LiDAR DTM underlines how the standard measure of error (RMSE ~ 0.3 m for all areas), shows only moderate correlation with the quality of the DTMs. All three datasets are characterized by errors, i.e. artificial lineaments and fault textures (b and c) and erroneous heights (pits) (a) (Fig. 13).

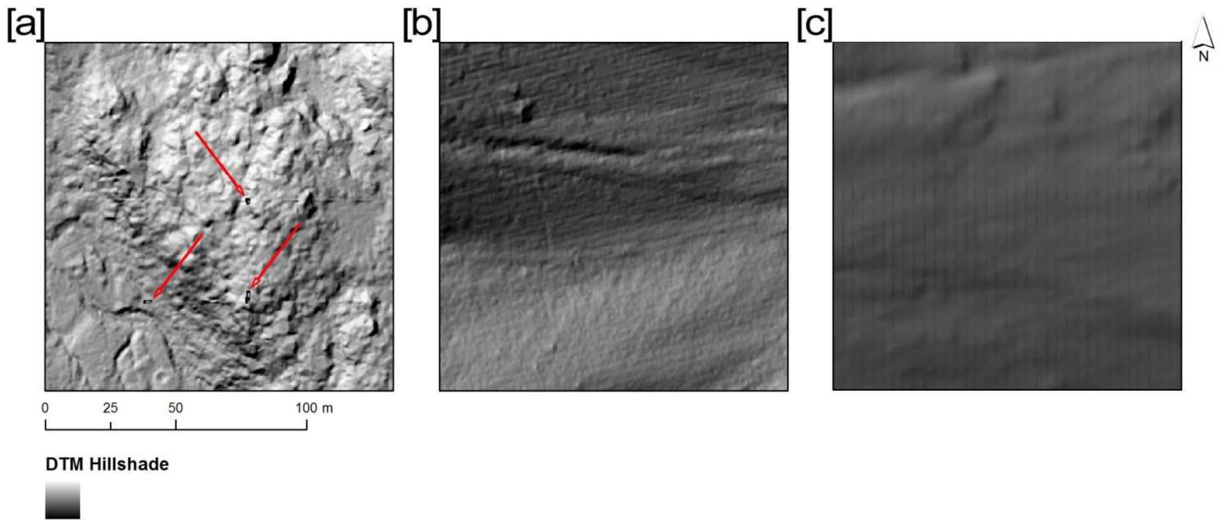

Fig. 13 Examples of errors on DTMs: (a) points with wrong elevation value and pits (red arrows), (b) fault texture oriented approximately east-west) (c) fault texture oriented north-south)(Sofia et al. under review)

DTMs provide the basic information required to characterize the topographic attributes of terrain. Projects which use LiDAR have a DTM as either main product or intermediate product, and often such projects are over very large areas, and they are based on a large number of tiled DTMs. Many algorithms have been developed to evaluate topographic attributes but less work has gone into determining the effects of DTMs uncertainty in these parameters, or the affect of this uncertainty in the scale choice. Assess the geo-morphological quality of DTMs is therefore fundamental, especially when dealing with their morphological applications for understanding earth and surfaces processes. Such analysis is provided in this thesis in Chapt. 4.3, Sect. *III.Materials and methods.*

2.2 Modeling continuous surfaces attributes through DTMs

Characterizing the shape of the terrain surface is important to environmental applications (Burrough and McDonnell, 1998). In the context of analyzing and understand earth surface processes, surface characterization moved towards a more practical approach, implying measurements and quantification of each surface forms, through geomorphometry (Wood, 1996). Various authors have presented a large number of geomorphometric measures, many of which are closely related and overlapping in terms of the surface form attributes they describe. For example, Nogami (1995) describes 37 such measures. Evans (1972, 1979, 1980) presents a synthesized and standardized set of measures, which provide a comprehensive description of surface form, while minimizing redundancy. Evans (1972, 1979, 1980) considers five terrain parameters that may be defined for any two dimensional continuous surface. These correspond to groups of 0, 1st and 2nd order differentials, where the 1st and 2nd order functions have components in the *xy* and orthogonal planes. In theory, these first and second order derivatives exist and can be calculated mathematically because terrain is a continuous surface. However, the raster grid format of a DTM, despite being a model of continuous surface, is a set of discrete elevation measurements (Wood, 1996). Therefore, the first and second order derivatives must be approximated by computing a local continuous surface patch for each cell. There are a variety of methods for making this approximation, which have been described and compared (Burrough and McDonnell, 1998; Evans, 1972; Florinsky, 1998; Hodgson, 1995; Jones, 1998; Skidmore, 1989). Figure 14 shows (in profile) different examples of ways in which adjacent grid values can be used to imply a continuous surface.

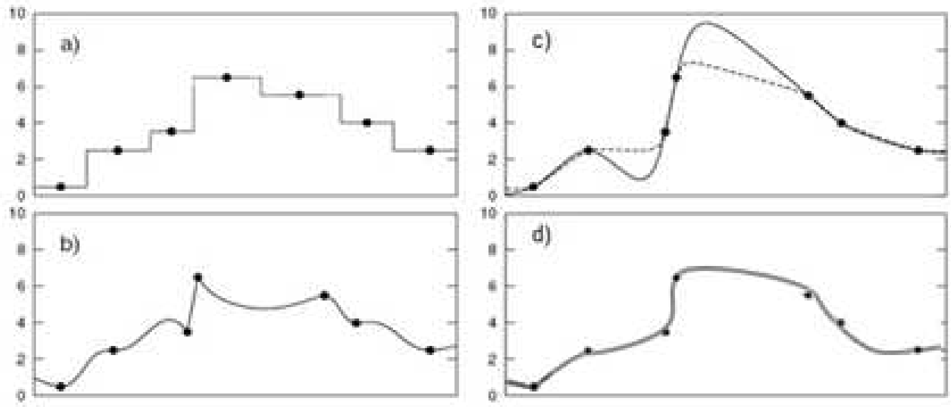

Fig. 14 Comparison of different interpolation to transform discrete DTM cell values into continuous surface models. (a) Proximal interpolation; (b) inverse distance squared; (c) spline interpolation; (d) quadratic interpolation (modified from Grayson and Bloschl, 2001)

The process of interpolating parts of surfaces from point values in a DTM is fundamental. In this work, the approximation considered for the application are mainly two: the proximal interpolation (Fig. 14a), and a quadratic interpolation (Fig. 14d) (e.g. Evans, 1979, 1980; Wood, 1996).

Proximal interpolation (Fig. 14a) is the native format of a grid DTM and it is used most commonly in raster visualization, where each grid location is the centre of an homogeneous rectangular grid cell (hence the ‘2.5 dimension’ of the DTM). It is also frequently used in many forms of DTM processing (e.g. viewshed analysis, Fisher, 1993). This kind of representation, even if continuous, it is also abrupt, meaning that processing requiring higher order continuity (such as slope derivation) cannot be applied directly. However, proximal interpolation can be the base to evaluate parameters as openness (Yokoyama et al. 2002, see Chapt. 3.1.d, Sect. *III.Materials and methods*), elevation residuals (see Chapt. 3.1.c, Sect. *III.Materials and methods*), and Entropy (see Chapt. 3.1.e, Sect. *III.Materials and methods*).

To measure terrain properties, such as slope or terrain curvature, the DTM interpolation needs to be more sophisticated. Figure 14c shows an example of fitting a spline function through adjacent cells in order to preserve second order continuity. Such a procedure has been used by Mitasova and Hofierka (1993) for various spatial and temporal analyses of DTMs.

The approximation considered in this work for curvature and slope evaluation, is the quadratic approximation (Fig. 14d) (e.g. Evans, 1979, 1980; Wood, 1996), based on the use of a bi-variate quadratic function. This function has been already applied in literature for many DTM analyses (e.g. Evans, 1979, 1980; Wood, 1996; Pirotti and Tarolli, 2010; Tarolli et al. 2010, Sofia et al. 2011), and it has the advantage that second order properties (curvature) can be identified directly (Wood, 1996). It is the highest order complete polynomial that can be estimated for a grid cell and its 8 connected neighbors. Other surfaces approximations are available, and have been referenced in numerous works (Evans, 1972; Horn, 1981; Zevenbergen and Thorne, 1987; Mitasova and Hofierka, 1993; Shary et al., 2002). However, empirical evidences (e.g. Skidmore, 1989) suggest that the bi-variate quadratic function represent a better form of continuous function for measuring slope magnitude and direction.

The continuous quadratic function can be represented as the sum of six terms based on a local coordinate system (*x,y,z*) centered on the DTM grid cell whose properties are to be measured (Eq. 1).

$$z = ax^2 + by^2 + cxy + dx + ey + f \qquad 1$$

The coefficients *a-f* in Eq. (1) can be solved within a moving window using simple combinations of neighboring cells: the standard method to solve them involves calculating the parameters for a central cell, related to its eight neighbors in a moving 3x3 cell window (Evans ,1980) (Fig. 15).

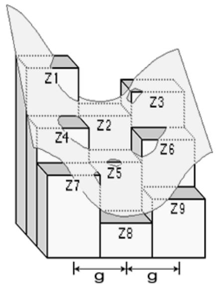

$Z = ax^2 + by^2 + cxy + dx + ey + f$

$a = (z_1 + z_3 + z_4 + z_6 + z_7 + z_9)/6g^2 - (z_2 + z_5 + z_8)/3g^2$
$b = (z_1 + z_2 + z_3 + z_7 + z_8 + z_9)/6g^2 - (z_4 + z_5 + z_6)/3g^2$
$c = (z_3 + z_7 - z_1 - z_9)/4g^2$
$d = (z_3 + z_6 + z_9 - z_1 - z_4 - z_7)/6g$
$e = (z_1 + z_2 + z_3 - z_7 - z_8 - z_9)/6g$
$f = (2(z_2 + z_4 + z_6 + z_8) - (z_1 + z_3 + z_7 + z_9) + 5z_5)/9$

Fig. 15 Solution of the bi-quadratic function according to a 3x3 neighborhood (modified from Evans, 1979)

More complete and complex analysis can be carried out considering a wider range of kernels, and this allows the classification of surfaces and their segmentation into specific units. Wood (1996) shows how the coefficients can be found for any sized window using matrix algebra. The larger the window size used for the computation, the smoother is the derived surface (Fig. 16).

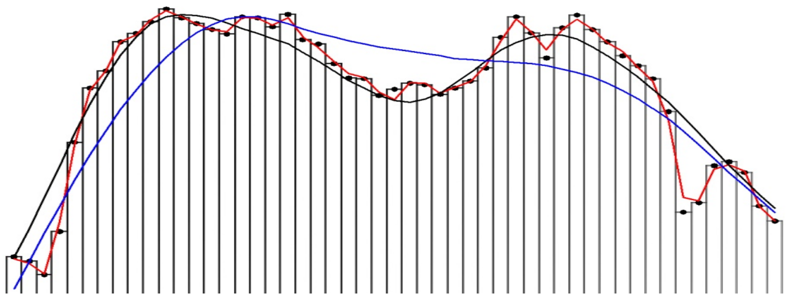

Fig. 16 Comparison of a profile of a squared grid DTM and the derived continuous bi-quadratic surfaces for different windows size: 3x3 (red), 15x15 (black), 33x33(blue). The reference grid DTM is showed, as well as the value for the centre of each pixel on the grid (black dots).

The advantage of a moving window approach is that it preserves some of the spatial variability inherent in the original dataset, providing at the same time a smoothing filter to the input data. Smoothing filters help to improve the classification of grid cells within the context of the landform features of interest, and filtering improves the extraction of hydrological features by reducing extraneous local detail (Pirotti and Tarolli 2010; Tarolli et al. 2010, Sofia et al. 2011). The core idea of the method is that the smoothing action of the filter provides a useful function in bringing out the longer-range signal (usually connected to meaningful processes signature among surfaces) and masking much of the local shorter-range noise connected to the presence of imbalanced or erroneous terrain elevation.

The choice of the window size range refers to two main issues: a computational constrain that sets the minimum size to apply, and operational choices supported by previous works (Pirotti and Tarolli 2010; Tarolli et al. 2010, Sofia et al. 2011). The window size needs to be large enough for a reasonable number of data to be processed, and the computational constraint for its minimum width relies on the fact that sampling windows are centered on the cell of interest, thus they consider (2*m*+1)x(2*m*+1) cells where *m* is an integer. The minimum width for a squared window is therefore, 3x3 cells. To choose the maximum window width, one can make considerations on literature review according to which over-sized windows have the tendency to incorporating irrelevant elevation data, smoothing surfaces, while undersized windows are less robust to noise (Pirotti and Tarolli 2010; Tarolli et al. 2010, Sofia et al. 2011). For a fuller discussion about the size constraint of moving windows, see Chapt. 3.1, Sect. *IV.DTA for feature recognition*.

In the following paragraphs, the main assumptions of the generalization procedures are explained. For a fuller description, see Evans, 1979 and Wood, 1996.

To solve the general case, the unknown coefficients in Eq. 1 are expressed as a set of six simultaneous equations, or *normal equations.* The normal equations can be simplified due to the regular nature of the DTM sampling (as Evans, 1979, Fig. 15).

The basic assumption of the polynomial interpolation is to create a surface that has a constraint through the central cell of the local DTM window. The regression surface becomes an *exact interpolator* (at the centre of the function) to use the nomenclature of Lam (1983). This can be achieved by creating a local origin through the central cell in both *X-Y* and *Z* directions. Thus all elevations in the local window are expressed as relative vertical changes from the central value. If all observed values z_i are taken from a local window with dimensions *n* by *n*, where *n* is an odd number, a local coordinate system can be defined with the origin at the central cell as a function of the grid spacing *g* (Fig. 17).

(- n·g , - n·g)	…	…	…	(- n·g , 0)	…	…	…	(-n·g , n·g)
…	(- (n-1)·g , - (n-1)·g)		…	(-(n-1)·g , 0)	…	…	(-(n-1)·g , (n-1)·g)	…
…	…	…	…	…	…	…	…	…
…	…		(-g,-g)	(-g, 0)	(-g, g)	…	…	…
(0, - n·g)	(0 , - (n-1)·g)	…	(0,-g)	**(0, 0)**	(0, g)	…	(0 , (n-1)·g)	(0, n·g)
…	…	…	(g,-g)	(g, 0)	(g, g)	…	…	…
…	…	…	…	…	…	…	…	…
…	((n-1)·g ,- (n-1)·g)		…	((n-1)·g , 0)	…	…	((n-1)·g , (n-1)·g)	…
(n·g , -n·g)	…	…	…	(n·g , 0)	…	…	…	(n·g , n·g)

Fig. 17 Local coordinate system defined with the origin at the central cell (0,0) for a window with dimensions n *by* n*, on a grid with pixel size* g

Once this coordinate system has been adopted, all coefficients of the equations can be found by solving a standard matrix equation (2)

$$G^T G \iota = G^T z \qquad 2$$

where z is the elevation matrix within the moving neighborhood, ι is the coefficient matrix according to (3), *G* for a *n x n* neighborhood is given by (4), and G^T is the transpose of the matrix *G,* where each *(i,j)* element of G^T is the *(j,i)* element of *G*.

For any application case, ι is given by

$$\iota = \begin{pmatrix} a \\ b \\ c \\ d \\ e \\ f \end{pmatrix} \qquad 3$$

and *G* for a *nxn* neighborhood is given by

$$G = \begin{pmatrix} x_1^2 & y_1^2 & x_1 y_1 & x_1 & y_1 & 1 \\ x_2^2 & y_2^2 & x_2 y_2 & x_2 & y_2 & 1 \\ x_3^2 & y_3^2 & x_3 y_3 & x_3 & y_3 & 1 \\ x_4^2 & y_4^2 & x_4 y_4 & x_4 & y_4 & 1 \\ x_5^2 & y_5^2 & x_5 y_5 & x_5 & y_5 & 1 \\ & \cdots\cdots\cdots & & & & \\ & & & & & \\ x_{n-1}^2 & y_{n-1}^2 & x_{n-1} y_{n-1} & x_{n-1} & y_{n-1} & 1 \\ x_n^2 & y_n^2 & x_n y_n & x_n & y_n & 1 \end{pmatrix} \qquad 4$$

where *x* and *y* are the coordinate of each pixel as a function of the grid size *g* (according to Fig. 17).

From Eq. (2), ι can be found as

$$\iota = \left(G^T G\right)^{-1} \cdot G^T z \qquad 5$$

For example, for a 3x3 neighborhood having the origin at the central pixel, for a *DTM* with pixel size *g*, the coordinates of each cell become:

(-*g*,-*g*)	(-*g*, 0)	(-*g*, *g*)
(0,-*g*)	**(0, 0)**	(0, *g*)
(*g*,-*g*)	(*g*, 0)	(*g*, *g*)

Thus G can be identified as

$$G_{3x3} = \begin{pmatrix} g^2 & g^2 & -g^2 & -g & g & 1 \\ 0 & g^2 & 0 & 0 & g & 1 \\ g^2 & g^2 & g^2 & g & g & 1 \\ g^2 & 0 & 0 & -g & 0 & 1 \\ 0 & 0 & 0 & 0 & 0 & 1 \\ g^2 & 0 & 0 & g & 0 & 1 \\ g^2 & g^2 & g^2 & -g & -g & 1 \\ 0 & g^2 & 0 & 0 & -g & 1 \\ g^2 & g^2 & g^2 & g & -g & 1 \end{pmatrix} \qquad 6$$

and $\left(G^T G\right)^{-1} \cdot G^T$ is found to be

$$\left(G^T G\right)^{-1} \cdot G^T = \begin{pmatrix} \frac{1}{6g^2} & -\frac{1}{3g^2} & \frac{1}{6g^2} & \frac{1}{6g^2} & -\frac{1}{3g^2} & \frac{1}{6g^2} & \frac{1}{6g^2} & -\frac{1}{3g^2} & \frac{1}{6g^2} \\ \frac{1}{6g^2} & \frac{1}{6g^2} & \frac{1}{6g^2} & -\frac{1}{3g^2} & -\frac{1}{3g^2} & -\frac{1}{3g^2} & \frac{1}{6g^2} & \frac{1}{6g^2} & \frac{1}{6g^2} \\ -\frac{1}{4g^2} & 0 & \frac{1}{4g^2} & 0 & 0 & 0 & \frac{1}{4g^2} & 0 & -\frac{1}{4g^2} \\ -\frac{1}{6g} & 0 & \frac{1}{6g} & -\frac{1}{6g} & 0 & \frac{1}{6g} & -\frac{1}{6g} & 0 & \frac{1}{6g} \\ \frac{1}{6g} & \frac{1}{6g} & \frac{1}{6g} & 0 & 0 & 0 & -\frac{1}{6g} & -\frac{1}{6g} & -\frac{1}{6g} \\ -\frac{1}{9} & \frac{2}{9} & \frac{1}{9} & \frac{2}{9} & \frac{5}{9} & \frac{2}{9} & -\frac{1}{9} & \frac{2}{9} & -\frac{1}{9} \end{pmatrix} \qquad 7$$

The advantage of this approach is that, by considering a local coordinate system centered at the central pixel of the moving window, Eq. (7) is only evaluated once, and it depends only on the size of the moving window and the resolution of the DTM (*g*). At any switch of the moving window, what changes is the height values stored in *z,* and ι is evaluated from Eq. 5. Properties of a continuous surface that could not be estimated from the discrete DTM values directly, can now be derived analytically from the continuous function. Such measures describe the properties of the surface at a point at the centre of the quadratic function. Given that this point is usually the centre of the grid cell to be assigned the property, the measurements are often regarded as characteristic of the cell they are associated with. The coefficients *a-f* (Eq. 1 and 3) depends on the local morphology captured within the moving windows used to compute the surface, and they are not a function of the window size, if by a function it means that there is a direct relationship between the window size measure and their values. The surface approximated according to the different moving windows is at any time a slightly different surface, accounting for the elevation values captured within the moving window, and the parameters vary consequently.

3. Hydrogeomorphological characterization of surfaces

High resolution terrain representation can be used at different levels, moving from a more qualitative approach to a quantitative one. A first and purely qualitative approach can be considered as a virtual tour of the landscape: the DTMs can be combined, for example, with high resolution orthophoto and can be used to produce a representation of the local terrain condition (Fig. 18). Numerous GIS software allow advanced visualization, analysis, and 3d surface generation starting from high resolution topography. Large sets of high resolution data can be seen in three dimensions from multiple viewpoints, creating a realistic perspective image that drapes raster and vector data over a surface. This first approach allows to create a realistic simulation of a project, environment, or critical situation to help the users on planning and preparing for and proactively mitigate potential issues.

Fig. 18 3d representation: ortophoto combined with a 1m LiDAR DTM.

The advantages of high resolution topography become more evident when DTMs are approached in a quantitative way, considering their capability to quantify and portray ground-surface form over large areas (Maune, 2001). Geomorphometry (or simply morphometry), terrain analysis, and quantitative geomorphology continue to grow through myriad applications to hydrology, natural hazards mapping, tectonics, sea-floor and planetary exploration, and other fields. Morphometric procedures are implemented routinely by commercial geographic information systems (GIS) as well as specialized software. Figure 19 shows two LiDAR DTMs (1 m vs 10 m) for a mountainous area and for a floodplain context. It is clear that elements on the surface are plainly visible and correctly mapped through the 1 m resolution topography.

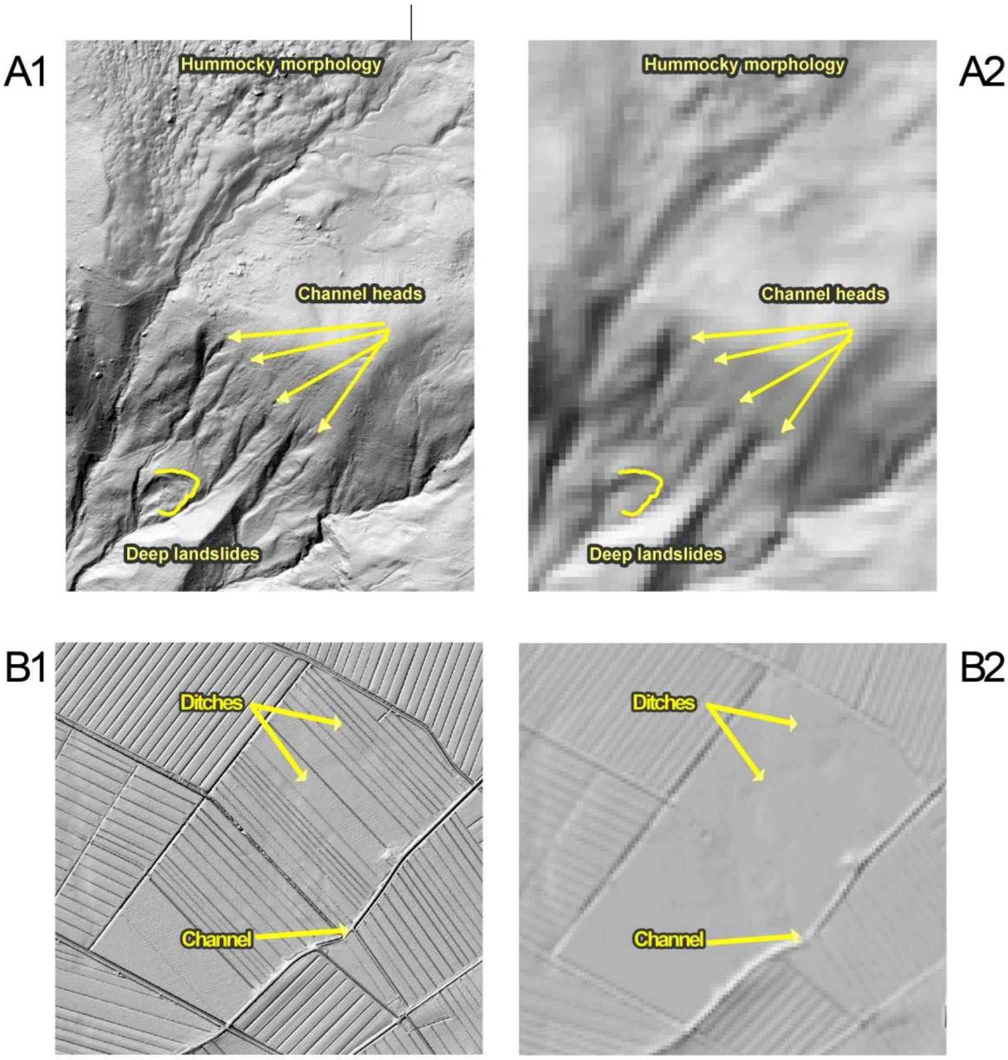

Fig. 19 Differences between a high-resolution DTM (A1, B1 1m) and a lower resolution one (A2 B2, 10m) for alpine environment (A) and for engineered landscapes (B).

Morphometric analysis of surfaces has been widely applied in order to relate morphology to hydrological processes at a wide range of scales. Various approaches have been used and applied to describe landform surfaces quantitatively. For the research problems investigated in this study, some morphometric concepts have been chosen to describe landforms at different spatial scales. The main tool for morphometric analysis is the approach to topographic attributes, spatial variables that are used to describe and represent the shape and pattern of the landscape surface. Speight (1974) described over 20 attributes that can be used to depict landforms. Moore et al., (1991, 1993) also described terrain attributes and divided them into categories: primary and secondary or compound attributes (Tab. 2). Primary attributes are directly calculated from elevation data and include variables such as elevation, slope, aspect, curvature etc. Secondary or compound attributes involve combinations of the primary attributes and are indices that describe or characterize the spatial variability of specific processes occurring on the landscape such as upslope area accumulation. The mathematical representation of most attributes and the methods for calculating them can be found in Moore (1991, 1993) and Gallant and Wilson (2000).

Table 2: Geomorphometric parameters and objects on different scales (Moore et al., 1991)

Primary morphometric parameters	Simple primary morphometric parameters	Slope Angle β Vertical Curvature ω_v Horizontal Curvature ω_h
	complex primary morphometric parameters	Flowlength l Flowaccumulation a Slope of downslope flowpath
	compound primary morphometric parameters	$ln(a/tan\beta)$ $ln(tan\beta/l)$ $a \cdot tan\beta \cdot \omega_h$
Morphometric objects	linear objects	flowpaths thalweg networks slopes
	areal objects	form elements catchments landform units
representative morphometric parameters	dimension parameters	object length or width, object area circularity elontation ratio
	relief parameters	statistic measures of primary parameters slope of 63ong est flowpath hypsometric integral portion of high curvature average height index of relief thickness (average height/area)

Recently, when dealing with feature extraction, morphological indicators (as in landform curvature) have been proven to be reliable for feasible applications (Lashermes et al. 2007; Tarolli and Dalla Fontana, 2009; Passalacqua et al., 2010a,b; Pirotti e Tarolli, 2010; Tarolli et al. 2010, Sofia et al., 2011). Questions as in what is the optimum scale to apply to evaluate parameters have been raised (Pirotti e Tarolli, 2010; Tarolli et al. 2010, Sofia et al., 2011), and the question is still open as in if these morphological indicators and objective thresholds can be feasible also in anthropogenic landscapes, where features assume different characteristics and other artificial disturbances are present.

In this chapter, the classification of terrain parameters primarily reflects the purposes of the analysis. Hence, two main group will be addressed: a) morphometric, and b) hydrological parameters.

3.1 Morphometric terrain parameters

The morphometric terrain parameters in this work are directly derived from a digital terrain model using local filter operations, where the term 'local' identify the analysis within neighboring pixels (moving windows environment) (see Chapt. 2.2, Sect. *III.Materials and methods*). For a fuller overview on morphometric parameters, the most recent study is given by Shary et al. (2002).

a. Slope

Several comparative studies of methods for the calculation of slope have been reported for terrestrial DTMs (e.g., Florinsky 1998; Jones 1998; Kienzle 2004; Warren et al. 2004), each of which reports a value in the direction of the steepest slope within the analysis window.

Suppose a surface can be expressed by a parametric function, $z=f_{(x,y)}$, (i.e. Eq. 1, p.56) then slope can be identified as

$$slope=\sqrt{\left(\frac{\partial z}{\partial x}\right)^2+\left(\frac{\partial z}{\partial y}\right)^2} \qquad 8$$

This formula is not based on a rise-over-run calculation over a fixed interval, but rather assumes that a plane surface can be placed at any point on the surface z(x,y) in such a way that it only just touches the surface: it is a tangential plane and relies on the notion of infinitesimally small distances. It is closely related to the formula for Euclidean distance, and simply shows how much of the surface *z=f(x,y)* rises with a small fixed increment in x and y. However, surfaces within GIS are rarely if ever represented by analytic functions: they are typically modeled as grids, with a finite resolution. Hence slope calculations will use approximations to the formula above depending on the surface model used, which is itself an approximate representation of the true surface.

The most general assumption, requires the computation of slope by solving the general surface equation within a 3x3 neighborhood. However, Evans' (1980) methods, reviewed by Wood (1996), allows to calculate slope (or other terrain parameter) considering an analysis window moved across the raster DTM surface such that each pixel in turn becomes the central pixel on which calculations are based (for a fuller discussion, see Chapt. 2.2, Sect. *III.Materials and methods*). The resulting calculations are still reported at the original pixel size; it is merely the window size or ground area considered in the analysis which varies. This generalization allows the parameter to be analyzed at a range of scales (different values of $k_{size} \geq 3$, Fig. 20) but also serves the function of overcoming short-wavelength noise in the data. In this case, the user will have to decide the trade-off between the analysis scale and the sensitivity of their investigations to noise/artifacts.

Slope is evaluated from Eq. 1 (p.56) and according to Eq. 8, starting from the computation of partial derivatives as

$$\frac{\partial z}{\partial x} = 2ax + cy + d \qquad 9$$

$$\frac{\partial z}{\partial y} = 2by + cx + e \qquad 10$$

By adopting a local coordinate system with the origin at the central point of the analysis window (x, y = 0), the slope at the centre of the (moving) analysis window is:

$$s = \arctan(\sqrt{d^2 + e^2} \qquad 11$$

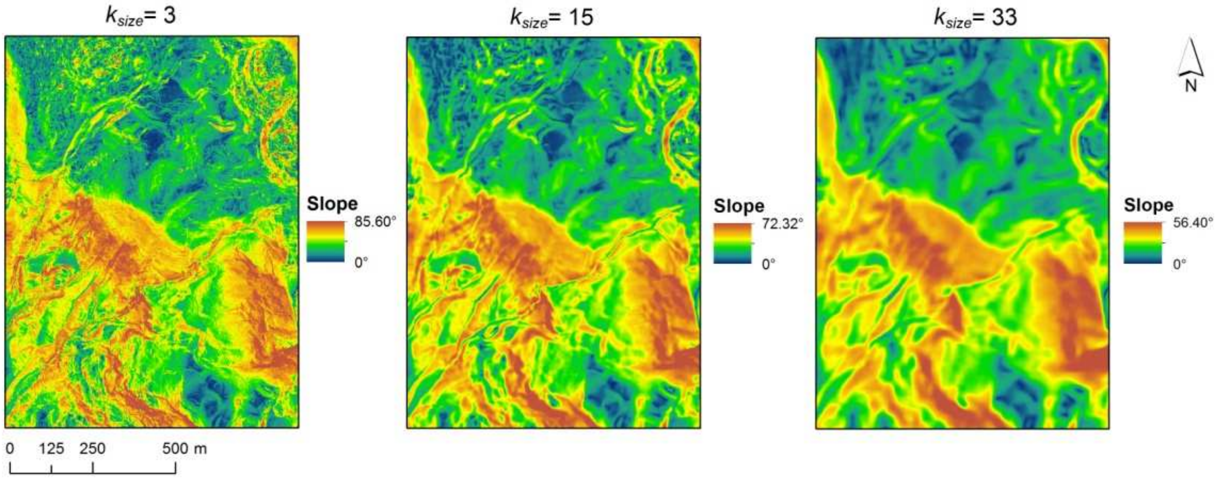

Fig. 20 Slope maps for different moving window sizes (k_{size}).

b. *Curvature*

Curvature is a second spatial derivative of the terrain elevations. It is one of the basic terrain parameters described by Evans (1979), and it is commonly used in terrestrial terrain analysis, being related to terrain concavity and convexity. Curvature can be defined also mathematically defined as the inverse of the radius of a circle that is best fitted to the surface at a given point.

Suppose a surface can be expressed by a parametric function, *z=f(x,y)*, (i.e. Eq. 1, p.56)) then curvature can be identified as

$$curvature = \frac{\frac{\partial^2 z}{\partial z^2}}{\left(1 + \left(\frac{\partial y}{\partial x}\right)^2\right)^{\frac{3}{2}}} \qquad 12$$

According to this formulation, the larger the curvature, the rougher the surface.

In general, the most appropriate curvature form depends on the nature of the surface patch being modeled: computational and interpretive simplicity may dictate a single measure for an entire DTM. The most effective way to introduce simple curvatures, is to consider some chosen directions (Shary et al. 2002). For any smooth surface, there are four such directions (Fig. 21).

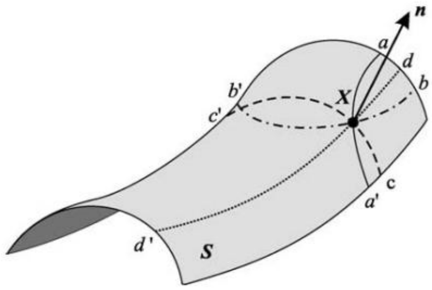

Fig. 21 The four directions naturally marked on a surface S. n *– the normal vector to* S *at point* X*;* aa′ *– the gradient line,* bb′ *– the contour line,* dd′*,* cc′ *– the main normal sections. (Olaya, 2009).*

Two of them (*aa'* and *bb'*) can be physically distinguished by the gravitational field of the earth, while the other two are marked by the surface itself: *cc'* by the maximal value of the curvature and *dd'* by the minimal value of it (Olaya, 2009).

The two most frequently calculated curvatures can be defined as (Gallant and Wilson 2000*) i)* Profile curvature (that of normal section aa'), and *ii)* Plan curvature (that of the normal section bb').

Profile curvature is the curvature of the surface in the steepest down-slope direction. It describes the rate of change of slope along a profile in the surface and may be useful to highlight convex and concave slopes across the DTM. Plan curvature is the curvature of a contour drawn through the central pixel. It describes the rate of change of aspect in a plan across the surface and may be useful to define ridges, valleys and slopes along the side of these features.

Shary et al. (2002) grouped surface curvatures into two main types and twelve minor ones. Only describing the geometrical structure of the surface, the curvatures of the first main type are independent of reference coordinates. In contrast, the ones of the second main type have to do with the direction of the coordinate system (Tab. 3).

Table 3: The information of terrain curvatures (modified from Youfu et al. 2008)

Curvature types	*Curvature names*	*Descriptive Geographical Themes*
First type independent from the reference coordinates	Mean Curvature	"Equilibrium" land form state
	Unsphericity Curvature	Extent to which land form differs from a sphere
	Maximum Curvature	Geometrical C-ridges
	Minimum Curvature	Geometrical C-valleys
	Total Gaussian Curvature	Does not change during surface bending
Second type dependent from the reference coordinates	Difference Curvature	Compares the 1st and 2nd mechanism
	Profile Curvature	2nd accumulation mechanism
	Contour Curvature	movement modes of terrestrial materials
	Profile Curvature Excess	splits flow-line twisting onto two components
	Horizontal Curvature Excess	splits flow-line twisting onto two components
	Total ring Curvature	Flow-line twisting
	Total accumulation Curvature	Relative accumulation and deflection zones
	Tangential Curvature	1st accumulation mechanism
	Longitudinal Curvature	Recognition and extraction of terrain features

Profile and plan curvature involves the calculation of the slope vector, therefore they remain undefined for quadratic patches with zero gradient (ie. the planar components d and e are both zero). In such cases, alternative measures independent of slope and based solely on surface geometry need to be substituted. Evans (1979) suggests two measures of minimum (concavity) and maximum curvature (convexity):

$$Curvature_{\max} = -a - b + \sqrt{(a-b)^2 + c^2} \quad 13$$

$$Curvature_{\min} = -a - b - \sqrt{(a-b)^2 + c^2} \quad 14$$

where *a-c* are the coefficient of the quadratic surface equation (Eq. 1, p.56)) derived according to the procedure already expressed in Chap. 2.2, Sect. *III.Materials and methods*.

Calculation of the first and second derivatives using a local window is scale dependent. The derived parameters are only relevant to the resolution of the DTM, and the neighboring cells used for calculation. Wood (1996) proposed a multiple-scale parameterization by generalizing the calculation for different window sizes. The Eq. (13) and (14) become then:

$$C_{\max} = k_{size} \cdot g \cdot Curvature_{\max} \quad 15$$

$$C_{\min} = k_{size} \cdot g \cdot Curvature_{\min} \quad 16$$

where g is the grid resolution of the DTM, k_{size} is the size of the moving window and $Curvature_{max}$ and $Curvature_{min}$ derive from Eq. 13 and 14 respectively.

The Eq. (15) and (16) have been used as a useful method for multi-scale terrain analysis (Wilson et al. 2007), and for morphometric feature parameterization (Eshani and Quiel 2008). A mean curvature (C_{mean}) derived from these two formulae has been used by Pirotti and Tarolli (2010) for channel network extraction. Cavalli and Marchi (2008) applied the same generalization procedure to plan curvature formulation, for the characterization of surface morphology. In the study cases presented in this work, crowns and features related to bank erosion correspond to convex slope breaks forming ridges within the likely unstable area, while channel network corresponds obviously to convex areas. Since ridges are related to surface convexity, for this work C_{max} (Eq. 15, Fig. 22b) is the optimal parameter applied for geomorphic feature recognition, while C_{min} (Eq. 16, Fig. 22a) is considered for channel network characterization. Minimum curvature, furthermore, has been considered in this work to account for DTM quality because it is more sensible to concavities/convexities when dealing with morphological feature extraction (Sofia et al. 2011), and a recent work by Wise (2011) underlined how errors induced by interpolation were similar for different interpolation techniques, showing larger values along narrow crest lines, and at the convex change of slope at the tops of ridges or in hillslope hollows, but also occurs along the valley sides and in the valley bottoms.

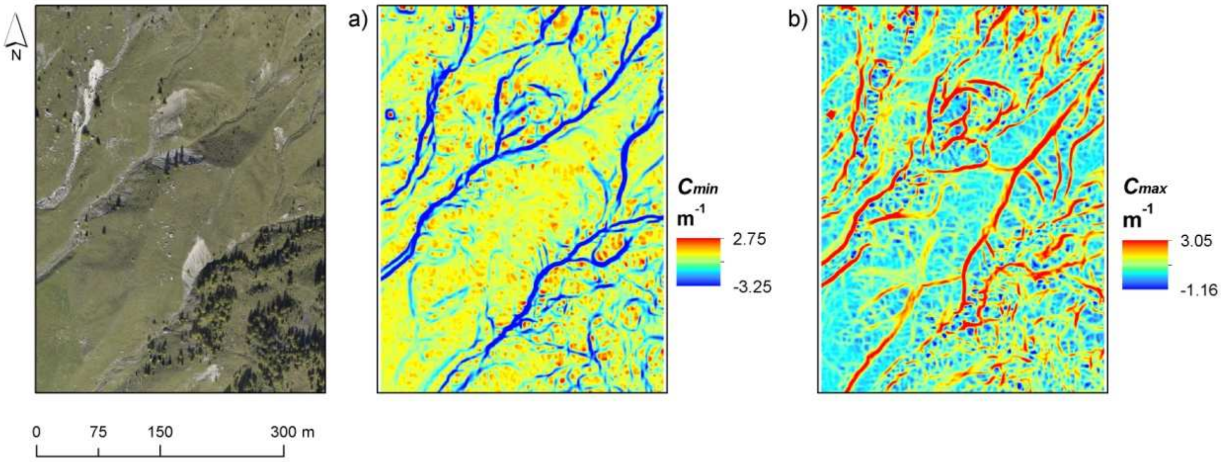

Fig. 22 Example of minimum (a) and maximum (b) curvature, and overview of the actual landscape on the area

c. Elevation residuals

In the context of feature extraction, sometimes features are controlled by local variations in topography (i.e. the change in elevation from one cell to the next). In some instances, it can be useful to consider the nature of each elevation point with reference to a wider context, as in the case of identifying ridges and valleys or elements that have a lower/higher values respect their surroundings. This kind of analysis ignores hydrological connectivity of the surface topography, considering instead the relationship of a point to the surrounding landscapes (Wilson and Gallant, 2000).

The basic element to consider as a reference against which to compare the elevation at the central point of the window is usually the mean elevation $\bar{z}$:

$$\bar{z}_w = \frac{1}{n_w}\sum_{i \in w} z_i \qquad (17)$$

where n_w is the number of pixel within the considered neighborhood and z_i is the elevation at each pixel.

The difference between the elevation at the centre of the window and the mean elevation is a measure of the relative topographic position of the central point, and its range depends on the range in elevation within the size of the window.

This terrain attribute can be useful in connection with processes/elements that are sensitive to local difference from regional elevations, as in application of DTMs for landform characterization (Carturan *et al.* 2009) or feature extraction (Humme *et al.,* 2006; Hiller and Smith, 2008; Doneus and Briese, 2006; Kothe and Bock, 2009; Cazorzi et al. *in press*).

The core idea shared by these works is to apply a low-pass filter to the DTM, providing a smoothed elevation model (Eq. 17) representing an approximation of the large-scale landscape forms. The

difference between this smoothed map and the original DTM is an approximation of the local relief, where only small-scale topographic features are preserved, in spite of large-scale landscape forms. In a similar fashion, two models can be derived, one represents a relative elevation map that can be termed Relative Elevation Attribute (REA, Carturan *et al.* 2009) (Eq 18, Fig. 23a), the other represents a map of Residual Topography (Cavalli et al. 2008) (Eq. 19, Fig. 23b).
These maps are evaluated as

$$REA_w = \bar{z}_w - z_{DTMw} \qquad 18$$

$$RT_w = z_{DTMw} - \bar{z}_w \qquad 19$$

where z_{DTMw} is the elevation at the central pixel within the considered neighborhood (w) and $\bar{z}_w$ is the average elevation of cells within the same neighborhood according to Eq. 17 (Carturan *et al.* 2009, Humme *et al.,* 2006; Hiller and Smith, 2008; Doneus and Briese, 2006, Cavalli et al. 2008).

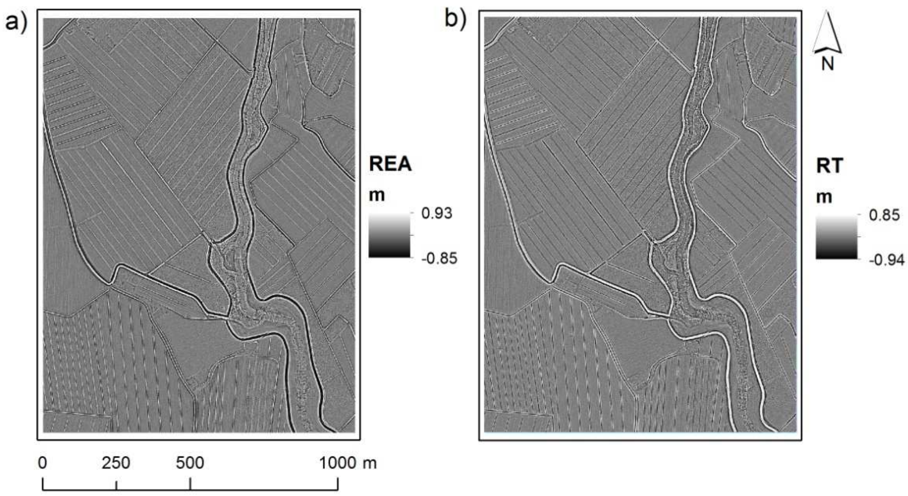

Fig. 23 Evaluation of REA (a) and Residual Topography (b) for a floodplain area.

The two formulation results in two maps that underline different features: the Relative Elevation Attribute is intended to represent concavities with higher values (i.e. Fig. 23a), while Residual Topography underlines convexities at the expense of concave-overall features (Fig. 23b).

d. Openness

Continuous topography is difficult to express, and many parameters have been proposed to quantify attributes of terrain that existing measures cannot describe. A new approach recently developed to describe topography, as distinguished from discrete landforms, is the DTM-based surface 'openness' of Yokohama et al. (2002), that expresses dominance (exposure) versus enclosure of a location on an irregular surface. Positive openness (Fig. 24b) is used to identify local convexities and it is equal to the mean zenith angle of all determined horizons; Yokohama et al. (2002) suggest also the negative openness, which is based on nadir angles, to identify local concavities (Fig. 24a).

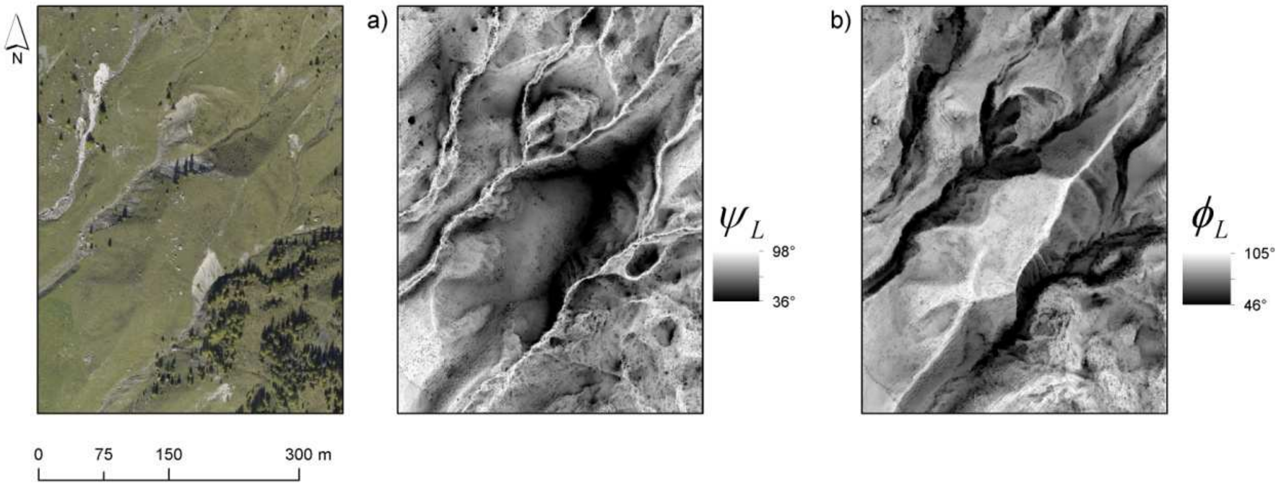

Fig. 24 Example of negative (a) and positive (b) openness.

Openness always assumes a positive sign, and its values range from 0 to 180°. The parameter is designated '*positive*' and '*negative*' in the same sense as has been used to express terrain-slope curvature (Pike, 1988).

Topographic openness is calculated as the average of either zenith (ϕ) or nadir (ψ) angles along eight azimuths *D* (0, 45, 90, 135, 180, 225, 270 and 315) within a radial distance *L* (Fig. 25, Yokoyama et al., 2002). To perform terrain analyses maintaining homogeneity with curvature, openness can be evaluated considering an *n* x *n* moving window (Wood, 2009). Instead of a radial distance, pixels are processed if they belong to the considered neighborhood as a function of the window size (k_{size}).

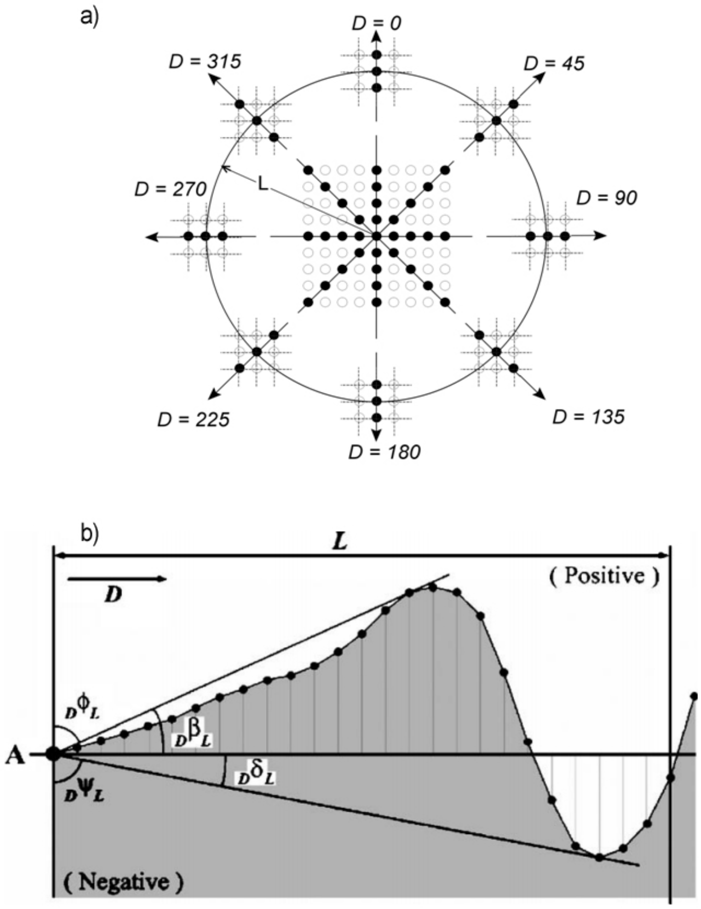

Fig. 25 a) Azimuths D (0, 45, 90, 135, 180, 225, 270 and 315) within a radial distance L*; b) Openness for a location A, according to azimuth and nadir, considering a defined* D*. (modified from Yokoyama et al., 2002).*

Positive openness ϕ_L is convex-upward and refers to the calculation with zenith angles; negative openness ψ_L is concave-upward and refers to evaluation with nadir angles (Yokoyama et al., 2002). Along the Azimuth *D,* the zenith angle $_D\phi_L$ at a grid location is

$$_D\phi_L = 90 - {}_D\beta_L \tag{20}$$

The nadir angle $_D\psi_L$ is

$$_D\psi_L = 90 - {}_D\delta_L \tag{21}$$

The procedure, therefore, starts from the computation of the elevation angles ($_D\beta_L$ and $_D\delta_L$) between the central point of the window and the element within the neighborhood for which the line of sight is unobstructed, along the straight line profiles in the eight azimuthal directions D (Fig. 25). For a computational approach, openness is essentially the solid angle subtended by the visible sky at each point. The Yokoyama et al. (2002) article does not mention this explicitly, but the procedure it describes can be interpreted as a discrete approximation to this angle, that needs to be computed for each location, as described in Fig. 26.

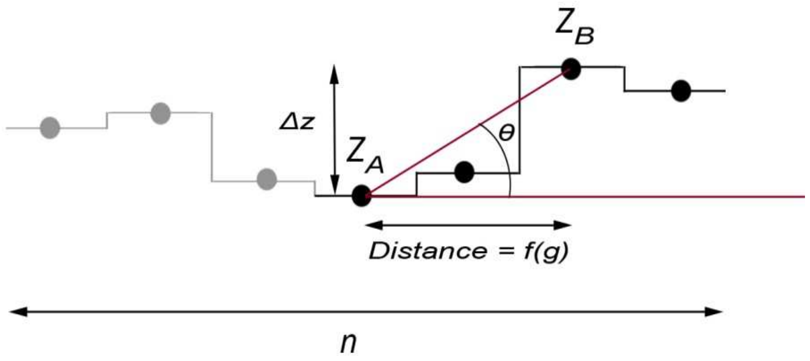

Fig. 26 Example of evaluation of elevation angle ϑ within a moving window of n *cells. Z_A is the elevation measured at the central cell, while Z_B is the elevation of the cells for which the line of sight is unobstructed. The distance between the two points is a function of the DTM grid size* (g)*.*

The elevation angle at each location is calculated in an identical manner to the calculation of profiles gradients (Eq. 22).

$$\theta = \tan^{-1}\left(\frac{\Delta Z}{\text{distance}}\right) \quad (22)$$

Where *distance* is the distance between points along the azimuthal direction according to Fig. 27 and ΔZ is the difference in elevations between the central cell and the considered ones.

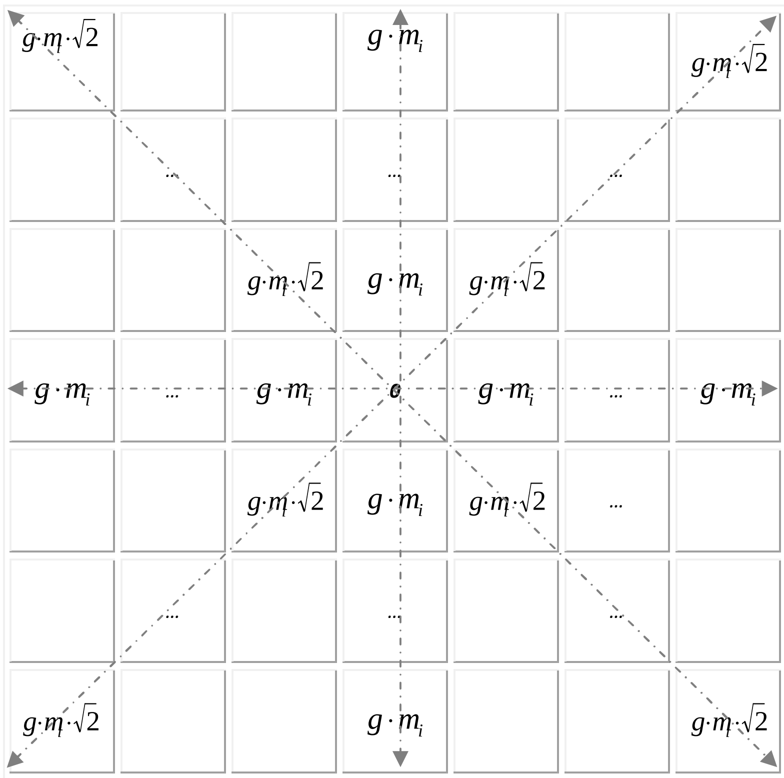

Fig. 27 Example of distances to be computed within a moving window of n x n *for elevation angle computation.* g *is the DTM resolution and* m_i *is an integer number that goes from 1 (the eight nearest neighbor) to* (n/2)+1 *(the boundary cells).*

This angle is referenced to the level of the origin point, and as a consequence it is positive when the profile is higher than the origin point, and negative if the origin is lower than the profile point. Once the elevation angles are identified, zenith and nadir are computed for each location within the moving window according to (20) and (21). The values to be considered to evaluate openness, are the maximum ${}_D\psi_L$ or ${}_D\phi_L$ value along the considered azimuth for positive and negative openness respectively.

Positive openness ϕ_L of a location on the surface is then derived as

$$\phi_L = ({}_0\phi_L + {}_{45}\phi_L + \dots {}_{315}\phi_L)/8 \qquad 23$$

and negative openness ψ_L is

$$\psi_L = ({}_0\psi_L + {}_{45}\psi_L + \dots {}_{315}\psi_L)/8 \qquad 24$$

Maps of negative openness emphasize drainage (higher values) at the expense of convex-overall features (Fig. 24a), while maps of positive openness emphasize ridges (higher values) (Fig. 24b) (Yokoyama et al., 2002).

Openness has been used for surface characterization and visual assessment of landform (Prima et al. 2002, Cavalli et al. 2011), because it offers a clear vision of the landscape without the constraints of the more classical hillshade. Hillshaded images are sometimes used to guide surveys, but comparing multiple images requires the user knowledge (Fig. 28) and might be time consuming, because the user needs to produce multiple outputs by illuminating a surface from multiple directions, to enhance visualization of the relief morphology.

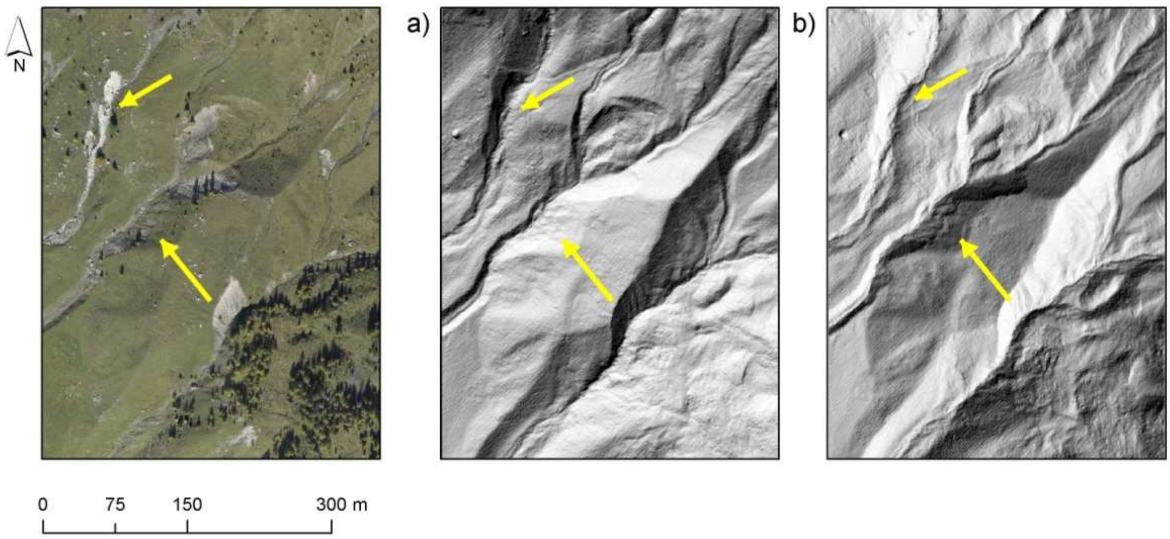

Fig. 28 Angle dependence of analytical hill-shading: 315° azimuth illumination (a), and 135° azimuth (b). Note the missing features (landslides) that are not visible using some particular azimuths.

In the published article, Yokoyama et al. (1999) focused on the interpretation of openness to identify the basic relief features, and did not elaborate the physical background and the optimal visualization parameters. Other works dealing with this parameter for landform characterization (Yokoyama 2002, Prima et al. 2006) used scale of analysis operationally derived, without testing the effect of openness scale on the parameter evaluation according to feature extraction. In this thesis, a scale approach has been considered elaborating the effect of the dimension of the considered neighborhood on the effectiveness of the parameter for feature extractions (Sofia et al. 2011).

Yokoyama et al. (2002), described openness as a method that is based on estimating the mean horizon elevation angle (in eight directions) within a defined neighborhood. The parameter, differently from curvature, bases its computation on the native format of a grid DTM (cfr *proximal interpolation*, Chapt. 2.2, Sect. *III.Materials and methods*), where each grid location is the centre of an homogeneous rectangular grid cell: it is actually a proxy for a diffuse relief illumination, and it is not a mathematical derivative of the surface. Some authors (Sofia et al. 2011) underlined how its computational basis, not depending on differential approaches, might define a more robustness of the parameter to DTMs errors. As already described in Chapt. 2.1, Sect. *III.Materials and methods*, depending on the spatial variation of the accuracy and density of the data, and on the suitability of the interpolation method for a certain relief, in fact, DTM quality might vary locally and regionally (Karel et al. 2006).

e. Entropy

A further topographic parameter that can quantify attributes of terrain, offering a measure of the elevation organization and its degree of randomness, is the entropy. The concept of entropy has its roots in the second law of thermodynamics, being a measure of the degree of organization in a system (Resnikoff, 1989). Calculating entropy provides an analytical treatment of information by measuring the degree of organization within a system, which can be also interpreted as a measure of the quantity of information incorporated in it. Shannon and Weaver (1949) introduced the concept of Entropy as a measure of randomness for digital signal processing. From a geographical point of view, entropy can be seen as a measure of how many categories are present in the parameter map at a given sampling interval. As Vieux (1993) and Mendicino (1996) reported, in the field of topographic surfaces described by a DTM, entropy can become a measure of spatial variability, since the total amount of disorder in elevation data distribution, is interpretable, indirectly, as the DTM information content. For a complete and deep review of entropy in hydrology and connected fields, see Singh (2011). Entropy has been used in this thesis for feature extraction, in particular as a filter to discard noises (Sofia et al. 2011) and as a topographic parameter to identify anthropogenic features.

Entropy is evaluated as

$$Entropy = -\sum_{i=1}^{N_{bins}} p_i \cdot \log p_i \qquad 25$$

where p_i is the proportion of pixels within the considered neighborhood that are assigned to each class *i* according to (26)

$$p_i = \frac{N_i}{N_{bins}} \qquad 26$$

where N_i is the number of pixel within the considered class *i* and N_{bins} is the number of considered bins.

For class and bins evaluation, in this work two approaches have been used. On the channel network extraction procedure, the approach was to considered entropy of flow movements (Fig. 29b), therefore each class is representative of a particular direction. In another instance to extract anthropogenic features, Entropy is considered directly for the DTM elevation values (Fig. 29d). Entropy is low when the heights within a local window have similar values (smooth surface) and high when they vary significantly.

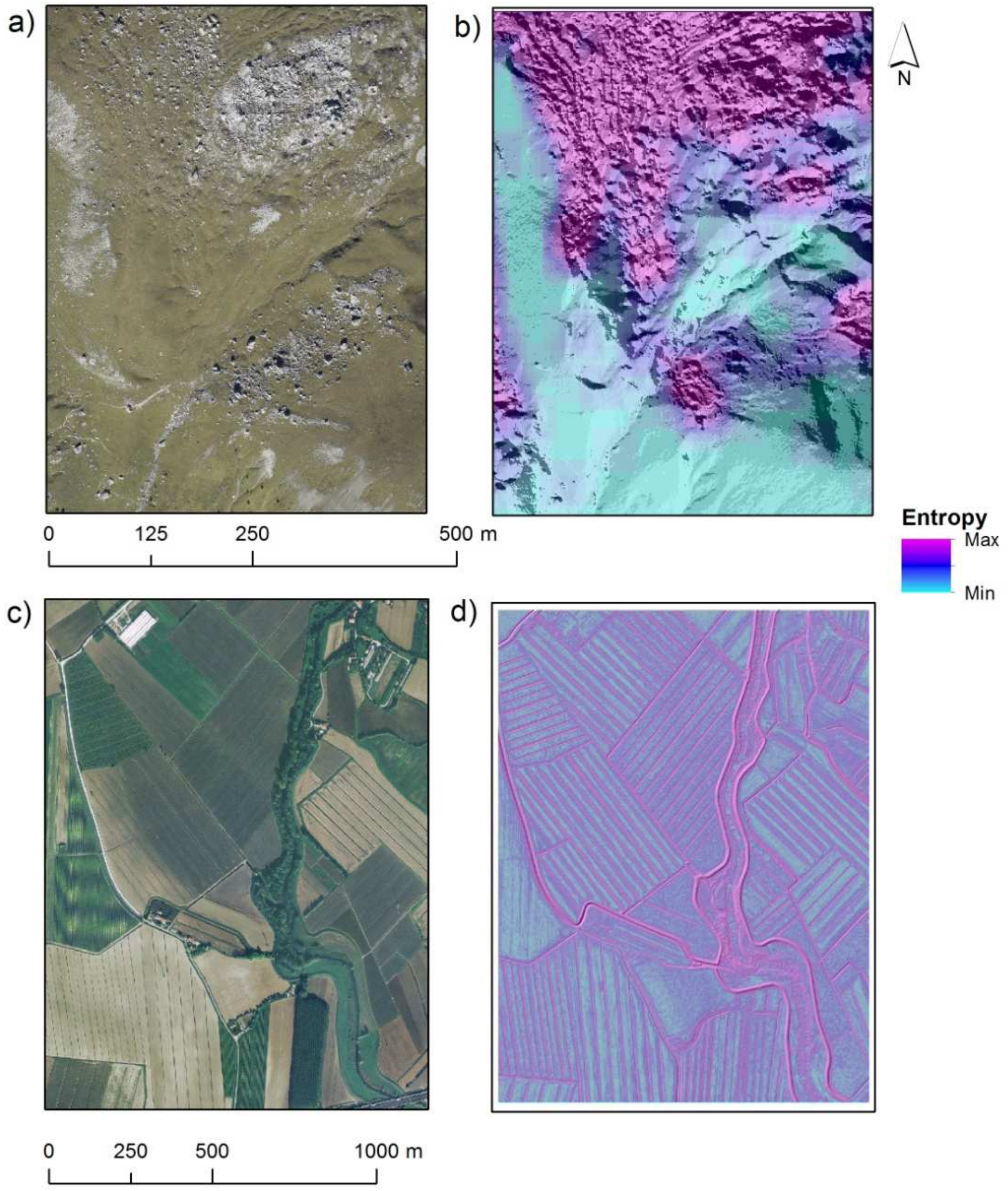

Fig. 29 Two approaches to evaluate entropy for a mountainous context (a,b) and floodplain (c,d). Map b represent Entropy of flow movements on surfaces, whereas higher entropy values correspond to irregular morphologies. Map d represents entropy of elevations, whereas higher entropy values are related to the presence of human disturbances (river levees or surface roughness due to farming activities).

3.2 Hydrological terrain parameters

One of the major tasks in digital terrain analysis is the computation of hydrological parameters used to model the hydrological behavior of a watershed. A number of important parameters have been proposed, and they are commonly derived from a more fundamental element: the flow model. A detailed discussion about hydrological terrain parameters can be found in Wilson and Gallant, 2000. In this section, only a brief commentary about the flow model is discussed.

Calculation of upslope area depends on the way the accumulated area of upstream cells is routed to downstream cells. The two main approaches to evaluate flows over a surface are the *Single-Flow direction (SFD)* where the total amount of flow is received by a single neighboring cell that has the maximum downhill slope to the current cell, and the *multiple-flow direction (MFD)*, where the flow from the current cell is distributed to all lower neighboring cells, according to some specific criteria as slope and flow width (Quinn et al. 1991).

The distribution of area to each downslope cell is generally based on slope according to the term

$$Flow_i = \tan \beta_i^{\,h} / \sum \tan \beta_i^{\,h} \qquad 27$$

where tanβ is the local slope measured at that location and *h* is a parameter that controls the flow distributions and its ranges is given by $0 \le h \le \infty$ (Holmgren, 1994b).

This formulation can be seen as a generalization of the flow direction approaches, where the parameter *h* determines the transition from single directional flow ($h = \infty$) to multidirectional flow ($h = 1$). For *h*>1 steeper slopes receive a higher proportion of the accumulated area (i.e. Tarboton 1997), while for *h* values smaller than one are more evenly distributed among the down slope directions. A high exponent (*h*) means that more accumulated area will be distributed in the steepest direction, i.e. more similar to single directional flow. The lower the exponent the more equally the flow will be distributed among the downslope cells (for a more detailed description see Holmgren, 1994b, or Quinn et al., 1995).

Several studies have shown differences connected to the choice of single- and multiple-flow direction algorithms on predicting channel networks (McMaster, 2002; Endreny and Wood, 2003), on the location of ephemeral gullies (Desmet and Govers, 1996), on modeled erosion and sedimentation rates (Schoorl et al., 2000), spatial patterns of saturated areas (Guntner et al., 2004), and on the statistical distributions of terrain attributes (Quinn et al., 1991; Wolock and McCabe, 1995; Desmet and Govers, 1996; Tarboton, 1997). Locations of ephemeral gullies and channel networks are better identified by algorithms with limited flow divergence, but upslope area computed through multiple flow algorithms could make it possible the identification of the most depressed parts of the channels, likely to be active also under conditions of low or moderate flow and it allows the recognition of minor channel features which are involved in flow processes during floods. Multiple direction algorithms tend to produce a more realistic looking spatial patterns than the single flow ones by avoiding concentration to distinct lines (Seibert and McGlynn, 2007). The negative outcome of this, however, is that multiple flow algorithms tend to produce a dispersive flow pattern, since the area from one cell is routed to all downslope cells and thus is dispersed to a large degree even for convergent hillslopes. Flow randomization and concentration can be implemented (Schwanghart and Kuhnn, 2010) providing correction to this unrealistic behavior, and other algorithms based on triangular facets have been developed to overcome these weaknesses (Tarboton, 1997; Seibert and McGlynn, 2007).

In the context of this work, the choice of the algorithm to apply to correctly evaluate flow directions is based on literature review. This work is carried out considering high resolution topography, and literature underlined that multiple-flow algorithms should be preferred for applications of upslope contributing area derived from higher-resolution DTMs (Erskine et al., 2006). Furthermore, previous studies demonstrated that computing total contributing area properly when dealing with divergent topography, involves suitable algorithms for handling multiple-flow directions (Tucker et al. 2001) as the one proposed e.g. by Quinn et al., 1991; Costa Cabral and Burges, 1994; Tarboton, 1997. In general, it has been underlined that multiple-flow algorithms are more robust than single-flow (Seibert and McGlynn, 2007): using single-flow, a tiny elevation difference between two of the neighboring cells can have a large effect as one of the cells receives all the area. With multiple-flow, these differences have a less influential effect because both cells receive about the same portion of the accumulated area.

Considering these observations, in this work the attention has been focused on the multiple-flow algorithms (Quinn et al., 1991; Costa Cabral and Burges, 1994; Tarboton, 1997). Algorithms such as digital elevation model networks (DEMON) (Costa-Cabral and Burges, 1994), anyway, have not been applied because, even if they might have theoretical advantages, they are too complex and case specific to be implemented for most applications (Tarboton, 1997).

The evaluations of flow paths for this thesis have been carried out using as a basis the Quinn et al. (1991) multiple-flow algorithm (Eq. 23 with $h = 1$), according to two main considerations: a) previous studies (Endreny and Wood, 2001) demonstrated that, compared to other flow algorithms, MDF (Quinn et al., 1991) was the least sensitive to terrain uncertainties, thus it can provide a more robust estimation; b) the main disadvantage of Quinn's MDF (large degree of dispersion even for a convergent hillslope), can be supplied by incorporating a weight depending on local topographic conditions. Point b) can be found in Kim and Lee (2004), where the authors compared different flow direction methods according to their ability to predict the observed stream network, and found that a modification of the multidirectional flow accumulation algorithm suggested by Quinn et al. (1991) was needed to solve the problem of flow dispersion overestimation in near-stream cells.

For the present work, the Quinn' (1991) flow accumulation algorithm has been modified using a weight factor *W* dependent on local morphology:

$$A_w = f(W, r) \qquad 28$$

where A_w is the weighted upslope contribution area for a given pixel and *r* is the pixel location on the DTM. The main difference from a conventional MDF flow accumulation is to provide a map of *W*, directly related to geomorphologic form, where surface concavities and convexities are detected. Similar modification procedures can be found in Tarboton (2003) and Liu J. et al. (2007), for different upslope area computational approaches.

The weighted upslope area is an implicit description of how much water can be accumulated according to the degree of convergence of the surface. Given a defined upslope value, the weighted amount depends on upslope contributing area and local convergence of morphology, represented by the weight matrix *W* (Eq. 28, Fig 56D p.124, and 57D p.125). This weight depends on local convexities and is derived by their quantification through openness and curvature (see Chapt. 2, Sect. *IV.DTA for feature recognition*). If a pixel relies on a convergent morphology, the value of the upslope area will be increased proportionally to its degree of convergence, while if it lies on divergent morphology, its value will be diminished.

4. Statistical Background

In this section, some elementary statistical concepts that provide the necessary foundations for more specialized statistical data analysis (Chapt. 4.2 and 4.3) are explained. The selected topics illustrate the basic assumptions of most statistical methods applied on the present thesis. Further information on each of those concepts can be found in Kachigan (1986), and Runyon and Haber (1976); for a more advanced discussion of elementary theory and assumptions of statistics, see the classic books by Hays (1988), and Kendall and Stuart (1979).

Variables differ in how well they can be measured, i.e., in how much measurable information their measurement scale can provide. There is obviously some measurement error involved in every measurement, which determines the amount of information that we can obtain. Another factor that determines the amount of information that can be provided by a variable is its type of measurement scale. Referring to the application of digital terrain analysis in this work, two are the mail goals searched by applying a statistical approach: *i)* measure the relation between each topographic attribute and its location, and quantify the significance of this relation in terms of scales; and *ii)* Once the appropriate scale is defined, the goal is to extract the feature of interest in an automatic or semiautomatic way.

Specifically, the relationship between topographic attributes and features depends mostly on the scale of analysis and on the morphology of the area. In very large samples, even very small relations between variables might be significant, whereas in very small samples large relations cannot be considered reliable (significant). Thus, in order to determine the level of statistical significance, a function is needed, that represents the relationship between “magnitude" and "significance" of relations between the value of the observed topographic attribute and the hydrogeomorphic processes involved in it, depending on the scale. The probability distribution function is an important characteristic which gives significant space domain information regarding the signal, and distributive analysis can be considered for these applications.

Distributive analysis typically consists in estimating summary measures capturing aspects of the distribution of every sample points beyond central tendency (i.e. Fig. 30). Simple descriptive statistics can provide some information, and they are related to the distribution moments: the first moment refers to the mean, the second to the variance (the positive square root of which is the standard deviation, σ), the third and fourth moments refers respectively to *skewness* and *kurtosis*.

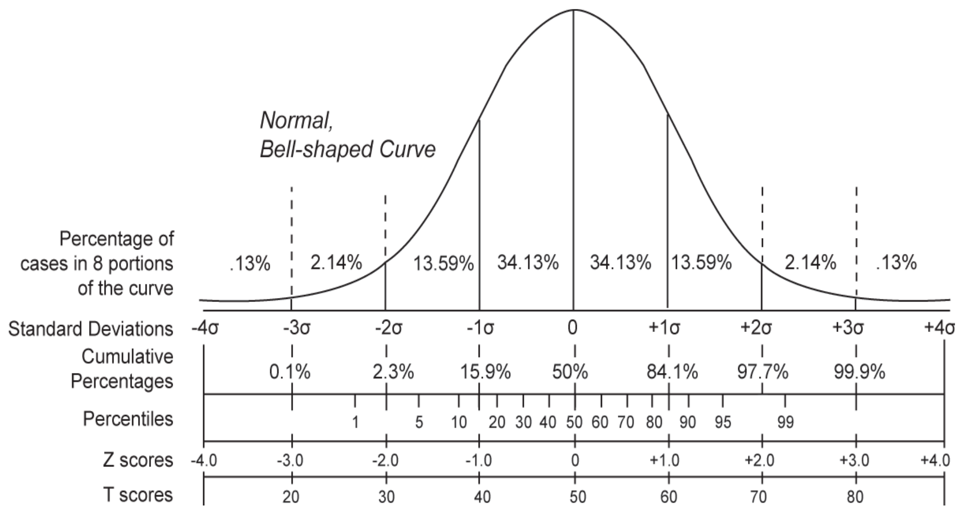

Fig. 30 Chart comparing the various dispersion measures in a normal distribution. Includes: Standard deviations, cumulative percentages, percentile equivalents, Z-scores and T-scores. Inspired by Ward et al. (1999).

4.1 Basic statistics

a. Standard Deviation

Standard deviation is a widely used measurement of variability or diversity used in statistics and probability theory. It shows how much variation or 'dispersion' there is from the 'average' (mean, or expected/budgeted value). A low standard deviation indicates that the data points tend to be very close to the mean, whereas high standard deviation indicates that the data are spread out over a large range of values. Technically, the standard deviation of a statistical population, data set, or probability distribution is the square root of its variance. Three standard deviations account for 99.7% of the sample population being studied, assuming the distribution is normal (bell-shaped). In addition to expressing the variability of a population, standard deviation is commonly used to measure confidence in statistical conclusions. The reported margin of error is typically about twice the standard deviation–the radius of a 95% confidence interval. In science, researchers commonly report the standard deviation of experimental data, and only effects that fall far outside the range of standard deviation are considered statistically significant—normal random error or variation in the measurements is in this way distinguished from causal variation. A useful property of standard deviation is that, unlike variance, it is expressed in the same units as the data.

Standard deviation is usually defined as

$$\sigma = \sqrt{E(t-\mu)^2} \qquad (29)$$

where E() represents the expected value of the quantity, and µ is the mean of the sample.

Tarolli and Dalla Fontana (2009) and Pirotti and Tarolli (2010) used threshold ranges identified as m-times the standard deviation σ of curvature as an objective method for hollow morphology recognition, and channel network extraction from high resolution topography. In Tarolli et al. (2010), the standard deviation has been tested also for convexity detection, and in Cazorzi et al (*in press*) it has been used to define a threshold to identify channel network in agrarian landscapes. Always for channel network recognition, Thommeret et al. (2010) used thresholds range identified by the standard deviation of DTM altimetrical errors spatial distributions.

b. Interquantile Range

The Interquartile Range (IQR) is a measure of statistical dispersion, being equal to the difference between the third and first quartiles.

$$\mathrm{IQR} = Q_3 - Q_1 \qquad (30)$$

where Q_3 and Q_1 are third and first quartiles.

The IQR is essentially the range of the middle half (50%) of the data, and because of this, is less affected by outliers or extreme values.

c. Boxplot

Different authors (Lashermes et al. 2007, Tarolli and Dalla Fontana, 2009, Passalacqua et al. 2010a,b, Tarolli et al. 2010, Pirotti and Tarolli, 2010, Sofia et al. 2011) underlined how statistical operators can describe natural process signatures on surfaces. However, when moving from a natural context to a more engineered one, a statistical approach can be used also to describe anthropogenic features. The basic idea is that man-made elements normally show a much sharper shape than natural terrain features. Furthermore, they mark local maxima of the elevation, and their heights represent outliers in the elevation matrix. Consequently, they represent outliers also within the derived geomorphometric parameters.

One of the most frequently used graphical techniques to analyze a univariate data set and to identify outliers is the boxplot, proposed by Tukey (1977). If $X_n=\{x_1,x_2,\ldots,x_n\}$ is a univariate data set, the boxplot is constructed by identifying the sample median (Q_2) and the sample first and third quartile (Q_1 and Q_3). The length of this box equals the interquartile range (*IQR*, Eq. 30) which is a robust measure of the scale.

An interval (*fence*) is then defined, by considering a lower bound (Fnc_{low}, Eq. 31) and an upper bound (Fnc_{up}, Eq. 32).

$$Fnc_{low} = Q_1 - 1.5 \cdot IQR \qquad 31$$

$$Fnc_{up} = Q_3 + 1.5 \cdot IQR \qquad 32$$

According to Tukey (1977), points outside the fence can be classified as potential outliers.

d. Mean Absolute Deviation

The Mean Absolute Deviation (or "MAD") of a data set is the average of the absolute deviations from the mean, and it is a summary statistic of statistical dispersion of variability. It is a more robust estimator of scale than the sample variance or standard deviation since it is more resilient to outliers in a data set. In the standard deviation, the distances from the mean are squared, so on average, large deviations are weighted more heavily, and thus outliers can heavily influence it. In the MAD, the magnitude of the distances of a small number of outliers is irrelevant.

The formula is expressed as follow

$$\mathrm{MAD} = \frac{1}{n}\sum_{i=1}^{n}\left|t_i - \mu\right| \qquad 33$$

where where μ is the mean of the sample.

e. Quantile-Quantile Plot

The quantile-quantile plot (Q-Q plot) is a probability plot consisting in a variable plotted against quantiles of a specific theoretical distribution representing the relative likelihood for this random variable to occur at a given point in the observation space. The deviation from a straight line indicates a deviation of the variable from a standard (normal) distribution. In the work of Lashermes et al. (2007) and Passalacqua et al. (2010a,b) Q-Q plots of landform curvature were used to objectively define curvature thresholds for channel network extraction. They suggested that the deviation from the normal distribution records an approximate break in which higher curvature values delineate well organized valley axes and lower (but still positive) values record the disordered occurrence of localized convergent topography.

f. Skewness

In probability theory and statistics, skewness is a measure of the asymmetry of the probability distribution of a real-valued random variable. The skewness can assume positive or negative values. Qualitatively, a negative skew indicates that the tail on the left side of the probability density function is longer than the right side and the bulk of the values (including the median) lie to the right of the mean. A positive skew indicates that the tail on the right side is longer than the left side and the bulk of the values lie to the left of the mean. A zero value indicates that the values are relatively evenly distributed on both sides of the mean, typically but not necessarily implying a symmetric distribution.

Skewness can be defined as:

$$Sk = \frac{E(t-\mu)^3}{\sigma^3} \qquad 34$$

where μ is the mean of the sample, σ its the standard deviation, and E() represents the expected value.

Skewness empirical computation for a topographic parameter dataset refers to

$$Sk_0 = \frac{\frac{1}{n}\sum_{i=1}^{n}\left(TA_i - \overline{TA}\right)^3}{\left(\sqrt{\frac{1}{n}\sum_{i=1}^{n}\left(TA_i - \overline{TA}\right)^2}\right)^3} \qquad 35$$

Where *n* is the sample size (in this case, the number of pixels of the input grid), TA_i is the value of the topographic parameter at each cell $_i$, and $\overline{TA}$ is the mean value of the parameter for the considered map.

d. Z-Score

Z-score is a statistical measure that quantifies the distance (measured in standard deviations) a data point is from the mean of a data set.

The standard score (z-score) is a dimensionless quantity and for the i_{th} observation of a random variable *x* at a point *i* is given by:

$$zscore_i = \frac{t_i - \mu}{\sigma} \qquad 36$$

where μ and σ are respectively the mean and the standard deviation of the distribution.

Values that are larger than the mean have positive z-scores and values that are smaller than the mean have negative z-scores. If a value equals the mean, then that location has a z-score of 0. The mathematics of the z score transformation are such that if every value in a distribution is converted to its z score, the transformed scores will necessarily have a mean of zero and a standard deviation of one. Z scores are sometimes called "standard scores". The z score transformation is especially useful when seeking to compare the relative standings of items from distributions with different means and/or different standard deviations. Z scores are especially informative when the distribution to which they refer is normal. In every normal distribution, the distance between the mean and a given Z score cuts off a fixed proportion of the total area under the curve.

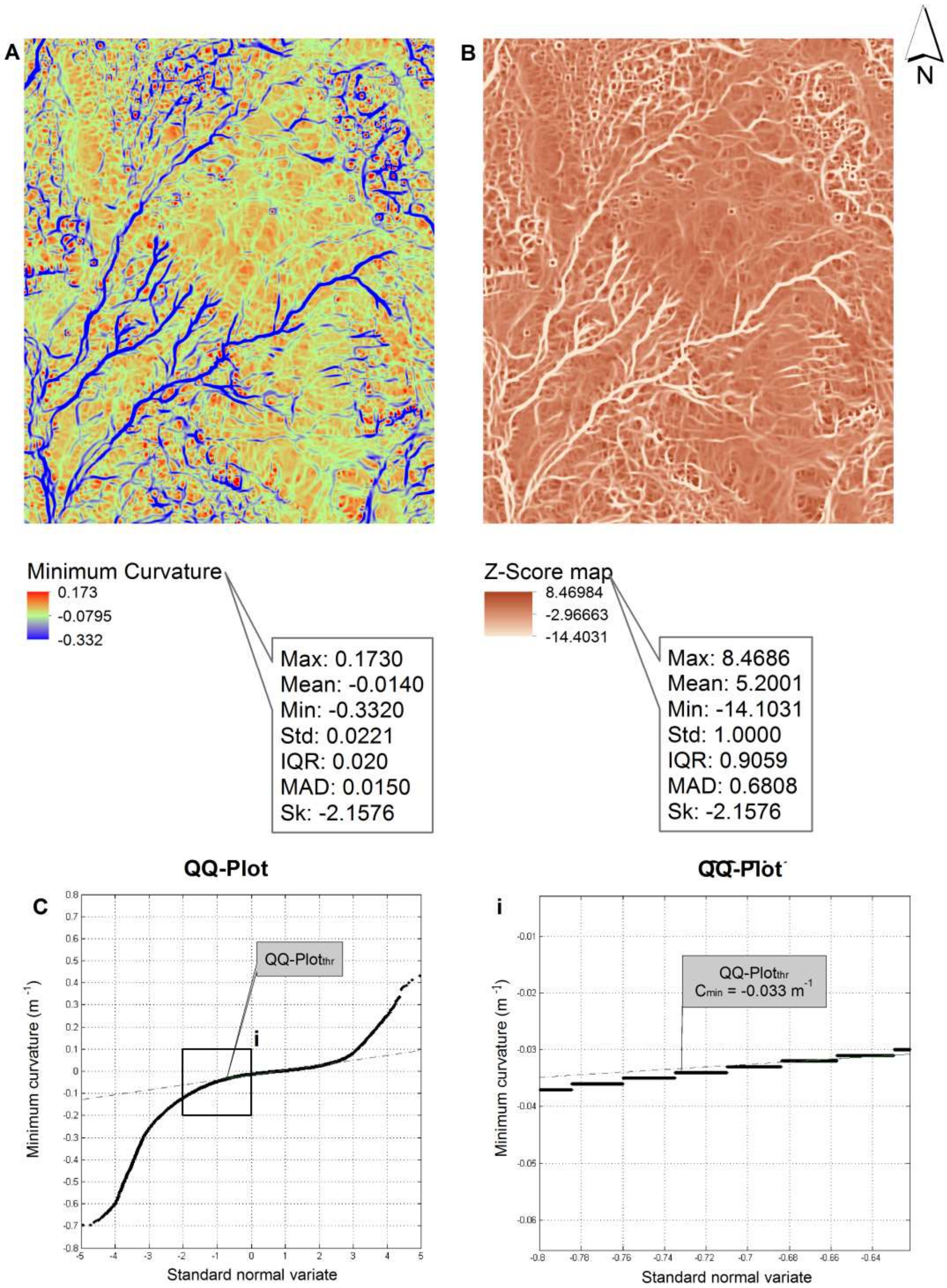

Fig. 31 Example of a topographic attribute map (minimum curvature, A), its Z-Score normalization (B), the basic statistics for both maps, and the evaluation of minimum curvature QQplot (C)

4.2 Statistics, scales of analysis, and feature recognition

As already said, an important aspect of the description of a variable is the shape of its distribution, which tells the frequency of values from different ranges of the variable. Considering a normally distributed sample, the 99.7% of the sample lies between negative three times and positive three times the standard deviations. Similar percentages can be found by considering the other measures of variability. When dealing with topographic attributes and landform, one must consider that only values of the elevation of a smoothed terrain tend to have a symmetric distribution in a well selected window with slow-changing terrain (Bartels et al., 2005). In the presence of noises, terrain roughness or particular morphologies, imbalanced terrain elevation affects the histogram distribution (Yuan et al., 2008): hydrogeomorphic features appear with lower frequencies, and they enhance the tails of the topographic parameter distribution, increasing or decreasing its skewness. This allows to consider that different processes leave their signature on the statistical properties of landform geometry, and by quantifying and labeling these signatures in detail, we can have an inference tool, to define the optimum scale of analysis, to identify a threshold to label where a process starts.

In the context of feature recognition, the key is to consideranalysis of dispersion focusing on the tail of the distribution which is more influenced by the presence of features, according to the topographic parameter in analysis. This means that if the topographic parameter is meant to describe in detail surface convexities, assigning to ridges higher values in the positive domain, the side to be analyzed is the positive side (Fig 32). On the opposite, if the topographic parameter is meant to underline surface concavities, labeling them with higher values in the negative domain, the side of the distribution to be considered is the negative side (Fig 32). In the tail of interest, then, the dispersion of the topographic attribute values can be a measure of the presence/absence of features.

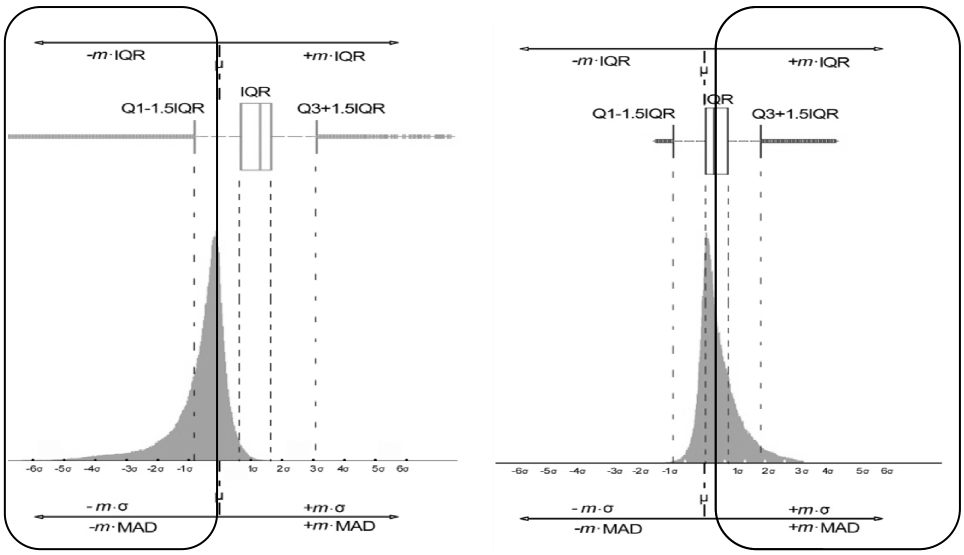

Fig. 32 Area of interest considering the main measures of dispersion (MAD, IQR, standard deviation and boxplots) for feature extraction from minimum curvature (left) and maximum curvature (right) for channel network and geomorphic features respectively.

Same consideration can be done for the QQ-Plot as a measure of disruption from normality: if the topographic parameter is meant to enhance concavities on the positive side, the area to be considered for channel extraction has to be the right tail of the distribution (Fig 30).

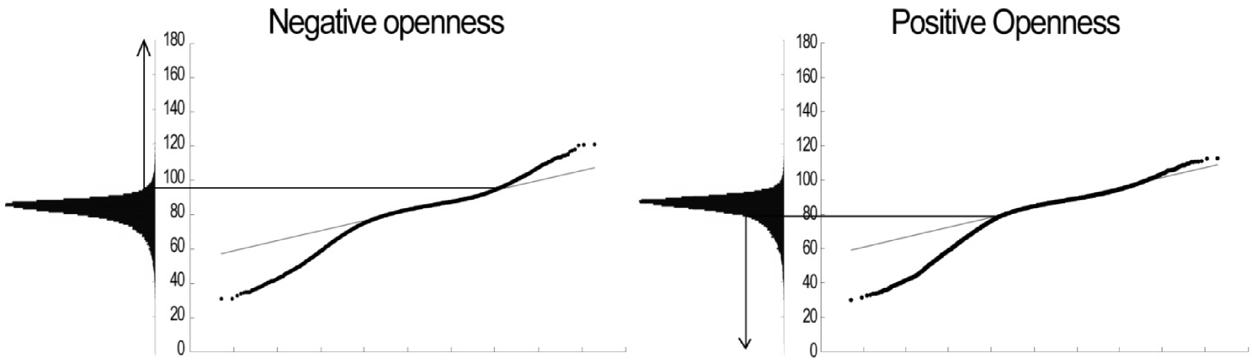

Fig. 33 Area of interest considering the qqplot as a measure of dispersion for feature extraction from negative (left) and positive openness (right) for channelized features. The same considerations are valid when considering maximum curvature for geomorphic feature extraction (where the approach is the same of the one proposed on the left), and minimum curvature for hydrologic feature extraction (where the approach is the same of the one proposed on the right).

Feature thresholding at this point can be based on standard deviation, interquartile range and median absolute deviation. Graphical operators can also be used: Q-Q plots can underline thresholds where the distribution is not linear and where deviation from a straight line can indicate a deviation of the pdf from Gaussian, underlying different morphological structures (Lashermes et al. 2007, Passalacqua et al. 2010, 2010b, Tarolli et al. 2010, Sofia et al. 2011).

With quadratic approximation (Chapt. 2.2, Sect. *III.Materials and methods*), it is possible to calculate the topographic variables at different scales using a range of window sizes. The minimum possible scale is dictated by the resolution of the DTM grid and the computational constraint, while the maximum possible scale is limited by the extent of the DTM itself. Clearly, not all these scales will produce meaningful results because of limitations of the elevation data, as well as limitations of the analysis method: *i)* very small windows are most influenced by errors in the DTM elevations, especially if the error has very low spatial autocorrelation (Fisher 1998,Heuvelink 1998a, Liu and Jezek 1999), and by local morphologies not necessarily connected to features (Pirotti and Tarolli, 2010, Tarolli et al. 2010, Sofia et al. 2011); and *ii)* as the evaluation window gets larger, it is less likely that the quadratic equation will be a good descriptor of the topographic surface in the neighbourhood of the evaluation point, because the approximation will be rougher.

In the works available in literature, where curvature was evaluated for different scales, the optimum one was either identified a posteriori, or selected arbitrarily a priori. The first approach is a time-consuming approach, considering that the optimum scale is defined through a comparison of all extractions for all possible kernel sizes with the reference features (Pirotti and Tarolli, 2010; Tarolli et al. 2010). In the second case cases, the scale of analysis is simply an operational choice [i. e. Lashermes et al. (2007) and Passalacqua et al. (2010a,b)]. In general, it has been argued that the scale of analysis should be about the twice of three times the size of the analyzed features (Pirotti and Tarolli 2010, Tarolli et al. 2010), but when there is no information available about, and in the absence of scale optimization techniques, how to select objectively a scale of analysis is an open question.

Giving that the presence of hydrogeomorphic features enhances the tail of the distribution of the topographic parameters, the shape of the distribution at different scales can be a diagnostic tool to identify the optimum scale of analysis (Sofia et al. 2011). Considering the observations done about feature identifications, where features are identified by lower frequencies of values in one specific tail of a distribution, Sofia et al. (2011) underlined how the optimum scale size is the one that results in the highest values of skewness. It is practically the scale that most enhances the tails of the distribution that represent the considered feature.

This scale can be mathematically identified by having a function defining a continuous relationship between skewness of the distribution, and the windows size used to evaluate the topographic parameter:

$$skew_{k_{size}} = t_1 k_{size}{}^{n} + t_2 k_{size}{}^{n-1} + ... + t_n k_{size} + t_{n+1} \quad (37)$$

Where k_{size} is the size of the moving window adopted for the evaluation, and t are the polinomial coefficients.

By representing this function, and identifying its 'extreme value' or 'inflection points'(Fig. 34), it is possible to define the optimum scale of analysis (Sofia et al. 2011).

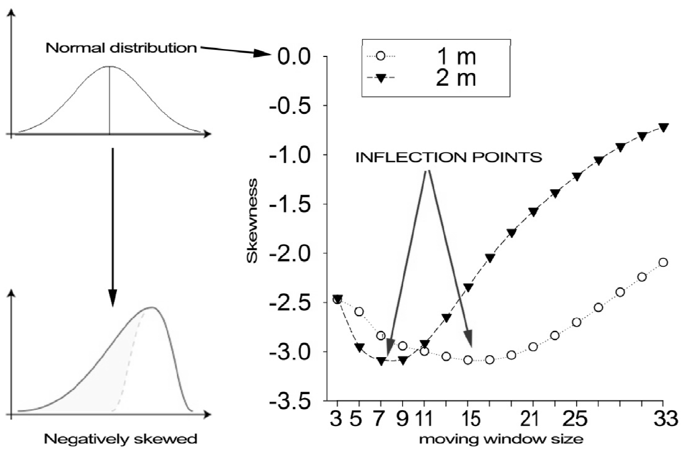

Fig. 34 Example of the polynomial identifying skewness of Minimum Curvature as function of the moving windows size for two DTMs (1m and 2m) of the same area. Inflection points are identified between 7 and 9 cells (~15m) on the 2m DTM and around 15 cells (~15m) on 1m DTM.

The stationary points are by definition those points where the derivative of the function itself is equal to zero, thus they can be automatically identified through a mathematic approach. In figure 34, an example is shown for minimum curvature evaluated starting from two different DTM resolution, 1m and 2m, for the same area. It is clear that for both resolutions, the increasing of the window size determines an increasing of the skewness in the negative domain until a maximum value is reached. After that point, the increasing of the window size determines a decreasing of the skewness and a progressive normalization of the distribution shape (skewness moves towards 0). The stationary points of both curves identify automatically an optimum kernel width of about 15 m (7 cells on the 2m grid, and 15 cells on the 1m grid). By digitally measuring on the map the channelized element of the area, their average width results to be about 15 m (Fig. 35a).

The curvature map derived with the defined window, is able to identify correctly these elements (Fig. 35b), and by considering curvature values lower than 2 times the standard deviation of the map, these features can be extracted with a high level of effectiveness.

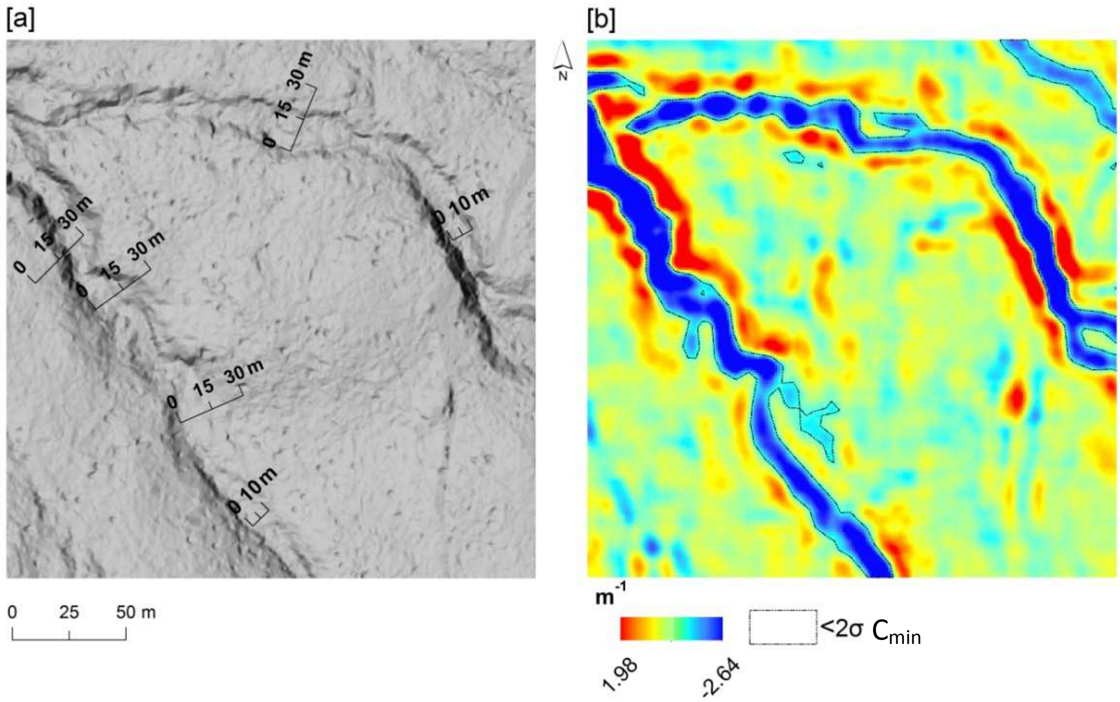

Fig. 35 Example of channelized element (a) as depicted on the DTM, and curvature derived for the same area (b) using an automatically defined 15 m kernel. Channels are correctly labeled by considering curvature values lower than 2 times the standard deviation of the map.

4.3 Statistics and scales of analysis: effects of DTM errors

The identification of optimal scale expressed in the previous chapter, consider that the shape of a topographic parameter distribution is influenced only by morphology. However, it is well known that also imbalanced or erroneous terrain heights affect the elevation histogram distribution, increasing or decreasing its skewness (Yuan et al., 2008), and topographic derivatives strictly depend on elevation distribution. The presence of errors in the DTM, therefore, might also be reflected in the relationship skewness/window size (Eq. 37, p.89). In the following section, the effect of errors on the skewness-window size relationship is assessed. The method can be summarized by the following steps: (1) dataset preparation; (2) processing curvature for different moving windows; (3) evaluating skewness of curvature for each map; (4) comparing the relationship between skewness values and moving windows over the different maps to identify different behavioral patterns, connected to the presence or absence of errors.

a. Error simulation: Monte Carlo approach

The Monte Carlo simulation is the approach commonly applied to assess DTM uncertainty. This can be attributed to its relative simplicity in concept, advances in computing power that have facilitated the computational demands of this brute force approach, and the “simplifying approximations” required of analytical methods in the face of complexity (Heuvelink and Burrough, 2007). The Monte Carlo method has been cited as the best method for determining the influence of error on DTM derivatives (Veregin, 1997). It is also advantageous because it is not affected by the complexity or non-linearity of the model (Burrough, 2002), and is thus generally applicable. Monte Carlo simulation is a technique for producing estimates of ‘true’ outcomes of stochastic processes by simply running many iterations of the model process and comparing its outcomes. The main disadvantage is the numerical load as the process is repeated for typically 50–2000 simulation runs (Heuvelink 1998), but the method remains widely recommended. The basis for using the Monte Carlo method in error propagation analysis is that the original data is perturbed repeatedly by the realization of the modeled error, and the analyses are performed on the perturbed data set (Heuvelink and Burrough, 2007; Openshaw et al. 1991). Using the results from all the iterations, it is possible to calculate a mean value that corresponds to the actual outcome of the algorithm under analysis. In this study case, this mean value is considered to be the ‘true’ value that the algorithm would produce in the presence of a specific error. The outline for the Monte Carlo process used here is shown in Fig. 36.

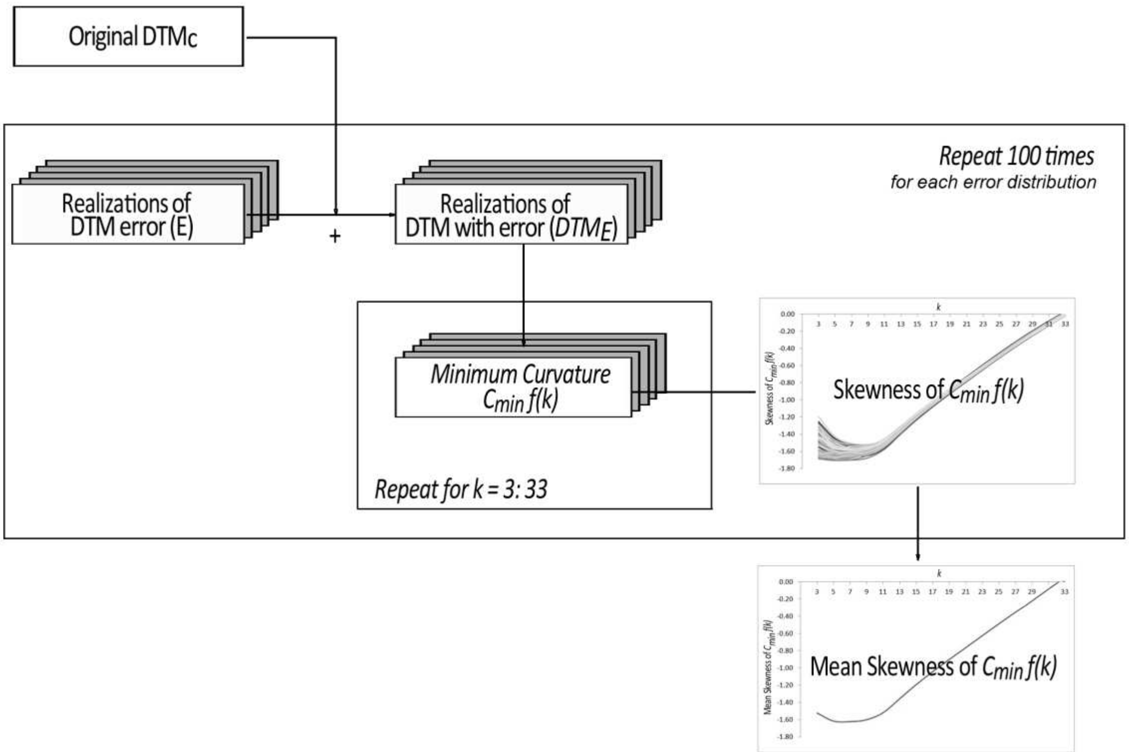

Fig. 36 Outline of the considered Monte Carlo process. Input clean DTM (DTM_c), multiple realizations of errors (E), multiple realizations of DTMs with errors (DTM_E), computation of minimum curvature for different moving windows and evaluation of skewness of curvature for each specific moving window. Using the results from all the iterations, it is possible to calculate a mean value of skewness for each moving window, considered to be the 'true' value that the algorithm would produce in the presence of a specific error.(Sofia et al. under review)

The main assumption of Monte Carlo simulations procedure is that errors exist and their nature and extent is unknown, but they can be modeled through a simplified approach considering random fields. Without having detailed information, the error simulation process starts from the generation of disturbance term consisting of random fields that have the same dimensions as the original DTM. These random maps (*E*, Eq. 38,39) can be repeatedly added to the true value of the DTM (*DTM_c*, Eq. 38), creating different realizations of the DTM (*DTM_E*, Eq. 38).

$$DTM_E = DTM_c + E \qquad (38)$$

Where

$$E = \lfloor t_{i,j} \rfloor_{m \cdot m} \qquad (39)$$

Differences in the Monte-Carlo approach rely on the definition of the error grids *E*, and in particular, on the shapes of error distributions, and the spatial correlations of errors. Theoretically speaking, the accuracy of the Monte-Carlo method is proportional to the square root of the numbers of runs (Temme et al. 2008). Heuvelink (1998) defines that as a general rule, 100 simulations can be considered as being large enough, and everything below 20 as insufficient. For the present work, 100 DTM realization for each error type have been created.

A potential problem with the Monte Carlo error simulation as it has been described, is that it does not preserve the spatial structure of the landscape elevation. Some authors approached error propagation by describing the spatial structure of the original DTM with geostatistical tools, and attempted to preserve it by preserving the variogram. However, other authors underlined how the variogram estimated from a DTM does not necessarily reflect that of the landscape, and preserving it in each realization would be an arbitrary choice (Raaflaub and Collins, 2006). As an operative choice, in this work the variogram characterization is not implemented.

To test the effects of errors on skewness of curvature at multiple scales, curvature evaluation is applied considering the same kernel size range of Tarolli et al. 2010 and Sofia et al. 2011, and three different DTMs resolutions have been considered (0.5, 1 and 2 m).

b. Considered DTMs

The test is carried out on seven different LiDAR DTMs (Fig. 37). The seven datasets belong to two selected areas in the Veneto Region in the northern part of Italy (Fig. 37), within the context of Alpine environment and morphology. The height (m a.s.l.) of the areas ranges between 1410 m a.s.l. and 1930 m a.s.l. (average of 1780 m a.s.l.) for the study site A, and between 1870 m a.s.l. and 2600 m a.s.l. (average 2220 m a.s.l.) for the study site B. The sites present different morphologies, and they were therefore considered ideal for this type of study.

The LiDAR data were acquired by an ALTM 3100 OPTECH, flying at an average altitude of 1000m above ground level under snow free conditions. The flying speed was 80 knots, the scan angle 20° and the pulse rate 71 kHz. During the LiDAR survey, high-resolution (0.15 m) digital aerial photos were also collected (camera Rollei H20). The spatial sampling density of the LiDAR-derived topographic datasets is high, with an average density of 7 point/m^2. Point cloud data were filtered to classify terrain and off-terrain points using the Terrascan™ software classification routines and algorithms. The vertical accuracy of the final datasets, evaluated by a direct comparison between LiDAR and ground DGPS elevation points, was estimated to be about 0.3 m (RMSE) for all the areas, an acceptable value for LiDAR analyses in the field of geomorphology (Mckean and Roering, 2004; Frankel and Dolan, 2007; Tarolli et al. 2009).

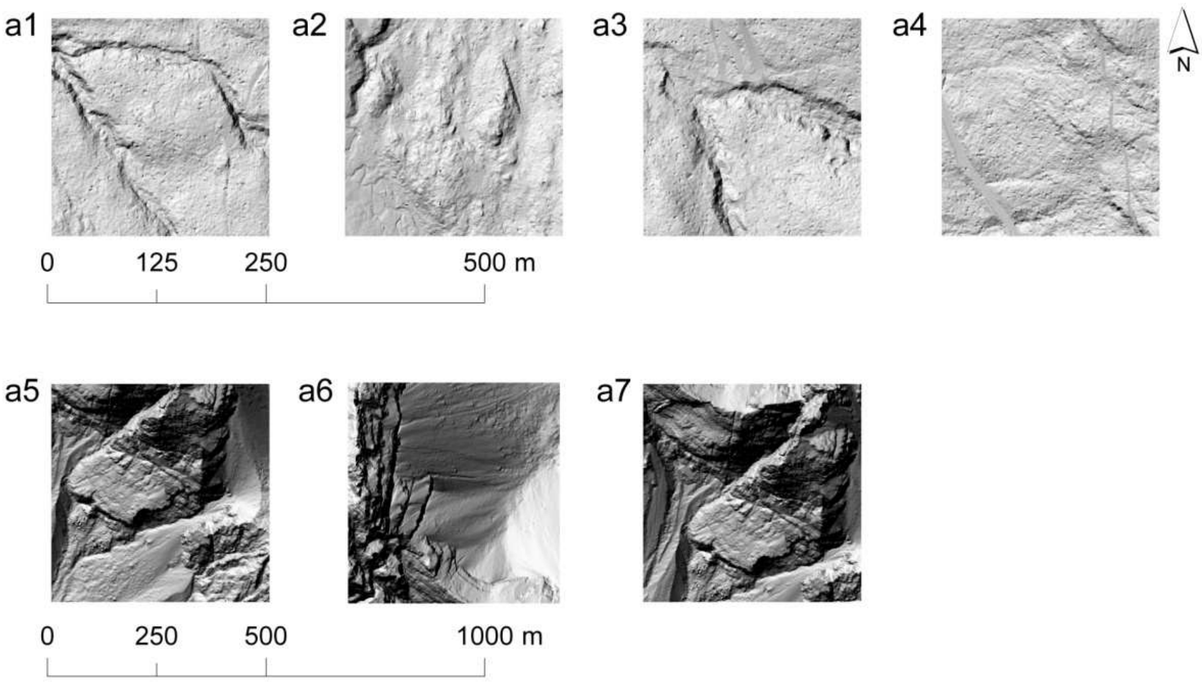

Fig. 37 Overview of the seven DTMs (a1-a7) considered for the analysis

c. Datasets preparation

For each test area, DTMs were obtained by rasterization - at the three different resolutions - of the triangulated surface created from the ground points. This procedure was adopted because it is a common processing workflow for extracting DTMs from LiDAR point clouds: to achieve a uniformly spaced DTM, data-producers typically start with mass points, produce a TIN, and then interpolate the TIN triangles to obtain elevations at the DTM's precalculated x/y coordinates (Maune, 2001).
The choice of three different resolution was done according to literature, considering that the grid cell size of a DTM significantly affects derived terrain attributes (Kienzle, 2004), and higher resolution might contribute more to the propagation of errors to DTM derived topographic parameters. The considered dataset shows different morphologies and different characteristics: a1, a3 and a4 are representative of high quality DTMs. They represent areas characterized by different morphological structures (Fig. 37): a1 and a3 have channelized elements, whereas a4 has no channels but it presents some roughness due to vegetation point filtering. Considering a2, a5, a6 and a7, a first analysis underlined how the standard measure of error (RMSE ~ 0.3 m for all areas), shows only moderate correlation with a visual assessment of the quality of the DTMs. All four datasets are characterized by errors, such as artificial lineaments and fault textures (a5 a6 a7) and erroneous heights and local outliers (pits) (a2) (see Fig. 13, p.54 for an example of each error types).
Both errors are visible on the hillshade representation, but the lower quality of the datasets and the different nature of the errors is not quantified by the RMSE. To be able to identify artificial

lineaments and fault textures through visual assessment, however, a user needs to produce multiple hillshade outputs by illuminating the surface from multiple directions. One of the possible outcomes is that light direction might not be correct to highlight the lineaments, and these errors might remain unknown. While local outliers are often randomly distributed over a study area, fault texture/striping artifacts are systematic (‘spatially structured errors of a systematic nature’, Albani and Klinkenberg, 2003), and they have a strong anisotropy in the autocorrelation of the error (Albani and Klinkenberg, 2003). Striping artifacts, in particular, have been described in Albani and Klinkenberg, 2003; Brunson and Olsen, 1978; Hassan, 1988; Klinkenberg and Goodchild, 1992; Brown and Bara, 1994; Garbrecht and Starks, 1995; Oimoen, 2000; Arrel et al. 2008.

The seven DTMs have been grouped into a training dataset (a1, a3 and a4) and a test dataset comprising maps with errors (a2 a5 a6 a7). The core idea was to provide a set of data representative of high-quality DTMs ($a1_c$, $a3_c$ and $a4_c$) and, on a second step, to simulate the presence of errors on the same dataset. The effects of errors are then learned from the training data and compared to the test dataset.

The error generation is carried out in three steps: at first, the error distribution is modeled, then the random fields are generated with no spatial correlation, and finally, spatial correlation is added (Fig. 38).

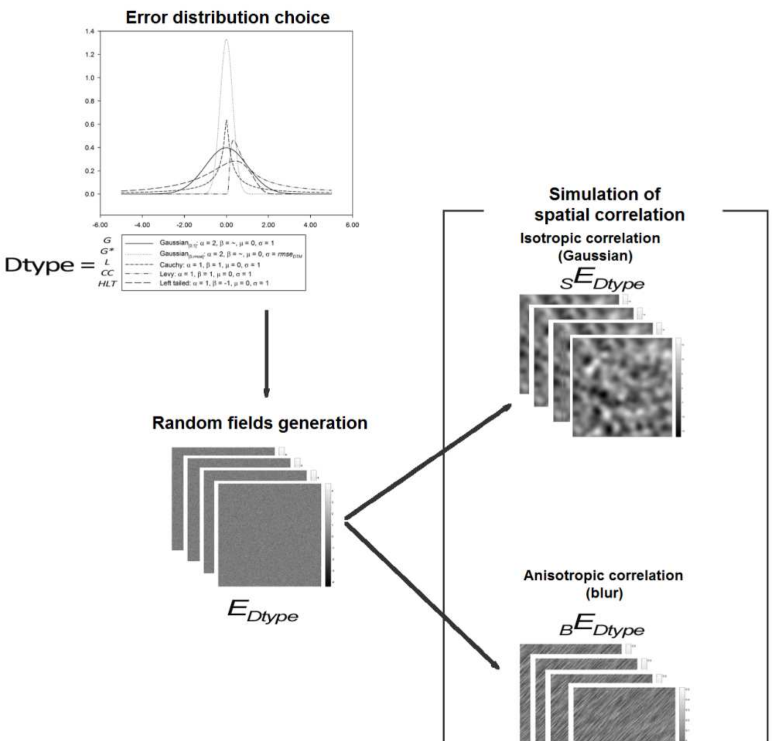

Fig. 38 Proposed approach to model errors. Modeling the different error distribution shapes through alpha-stable variables according to the different parameters (μ σ α β); creation of random fields and simulation of error spatial correlations. (Sofia et al. under review)

1) Modeling error distribution

Without knowing the detailed shape of the error distribution, there is a clear danger of over- or underestimating the actual error (Oksanen and Sarjakoski, 2006). The most common assumptions consider Gaussian or Normal distribution of random errors, with a specific mean and standard deviation. Hunter and Goodchild (1995) considered normal random errors with mean 0 and standard deviation 1. Other authors (Van Niel, et al. 2004; Wechsler, 2000; Wechsler and Kroll, 2006) applied this basic model considering normal values from distributions with mean 0 and standard deviation equal to the DTM RMSE. This technique is useful, as it doesn't require the comparison of DTM data with higher accuracy data; however, the limitations of a global accuracy measure have been presented (e.g. Wise, 2011). The Gaussian model makes only the most general assumptions about the processes by which the error has accumulated (Hunter and Goodchild, 1995) and it is not accurate to simulate impulsive, heavy-tailed noise (Nolan, 2006). Recently, literature review underlined how errors on DTMs have strongly non-Gaussian distributions with long tails (Kyriakidis, et al.1999; Lopez, 2000; Bonin and Rousseaux, 2005). Similar error distributions, with long and thick tails in the histogram, have also been found in other DTM accuracy studies (Fisher, 1998), which confirm that the phenomenon is general (Oksanen and Sarjakoski, 2006).

After this literature review, the generation of errors in this works starts from the creation of the random noise field (*E*, eq. 35, 35) with values derived from an Alpha-stable random distribution. This choice has been done considering that i) In cases of impulsive heavily tailed noise, modeling it through stable models offers a robust approach (Nolan, 2006); ii) the Gaussian distribution, as well as other well known distributions (i.e. Cauchy and Levy), are special cases of stable distributions, and they can be easily modeled through Alpha-stable random formulation, by adjusting some specific parameters.

The Alpha-stable distributions have been evaluated according to the Chambers-Mallows-Stuck (1976) formulation. Many other approaches have been proposed in the literature, to evaluate alpha-stable variables (i.e. Bergström, 1952; LePage et al. 1981; Borak et al. 2004). However, Chambers' method is regarded as the fastest and the most accurate one (Weron, 1996). For a fuller and complete bibliography on stable distributions, with references and applications examples in numerous fields, refer to Nolan (2006). For a detailed discussion on the Chambers-Mallows-Stuck method for simulating skewed stable random variables, see Weron (1996).

Any stable distribution requires four parameters to be described: a characteristic exponent α (0-2), a skewness parameter β (-1- 1), a scale parameter σ and a location parameter μ. For $\alpha = 2$ the distribution reduces to a Gaussian distribution with variance σ^2 and mean μ; the skewness parameter β has no effect (Nolan, 2006). For $\alpha = 1$ and $\beta = 0$ the distribution reduces to a Cauchy distribution with variance σ^2 and mean μ (Nolan, 2006). For α = 0.5 and β = 1 the distribution reduces to a Lévy distribution with variance σ^2, mean μ, and a positive skewness β (Nolan, 2006). By setting α = 1, it is possible to simulate tails longer than a normal distribution, and by choosing a negative value of β it is possible to simulate left heavily tailed distributions.

By opportunely setting the characteristic parameters (Tab. 4), it is possible to simulate different types of errors distribution shapes. For the present work, for all alpha-stable distributions, the considered scale and location parameters are σ *=1 and* μ *= 0* respectively, basic parameters of a standard normal distribution, considering that a recent literature underlined how errors in DTMs are characterized by a strong clustering of values around the mean of zero (Wise, 2011). The first considered error is set to have a Gaussian distribution with mean 0 and σ *=1* (E_G). A second error type is simulated to have the same distribution with equal mean, and standard deviation equal to the RMSE of the DTMs (E_{G^*}). This particular σ has been set only for the Gaussian distribution and not for the other as an operational choice, considering that a) setting the RMSE as a parameter, would require the DTM quality to be evaluated first, with the limit that comes from the DTM error determination, and b) the RMSE of elevation might not be good predictors of RMSE in curvature (Wise, 2011). Cauchy and Levy distributions have been considered as well [E_L and E_{CC}]. A particular error distribution (E_{HLT}) has been considering, by setting the characteristic exponent α = 1, to simulate tails longer than a normal distribution, and the skewness parameter β = -1. These parameter values were operationally decided: the result of such approximation is a random heavily left tailed distribution whose parameters have no mean of any morphological interpretation other than simulate a skewed distributed noise in order to create pits in the map (such as the ones detected in the test site a2).

To simulate all these errors, each $t_{i,j}$ (Eq. 39) within E, is simply represented by a value from one of the Alpha-stable random variables (Fig. 38). The considered input DTMs with errors have been labeled with a subscript according to table 4 (i.e. a DTM with an uncorrelated error with a levy distribution, will be labeled as DTM_L; a DTM with an uncorrelated error with a heavily left tailed distribution, will be labeled as $DTM_{HLT.}$)

2) *Modeling error spatial correlation*

The above described approach assumes that DTM error is uncorrelated from one elevation to the next. However, error models without spatial autocorrelation are known as the 'worst-case scenario' (Fisher, 1998; Hunter and Goodchild, 1995). Some authors argued that positive spatial autocorrelation in the DTM error yields smaller variance in the analysis results, but the nature of autocorrelation is difficult to assess due to the complexity associated with DTM errors and potential anisotropic nature of error (Wechsler, 2000).

To investigate the effects of error spatial correlation in this study, two cases are accounted for: an isotropic spatial correlation and an anisotropic spatial correlation. This choice was done in order to consider a standard case of correlation (isotropic), and in addition, to simulate the effects of fault textures and striping artifacts, that have by nature a strong anisotropy in the autocorrelation of the error.

The isotropic correlation in this work is obtained by applying to the original error matrices a spatial moving averages approach according to Oksanen and Sarjakoski (2005). Other approaches are available in literature to produce autocorrelation. However, techniques such as pixel swapping (i.e. Fisher, 1998; Lee et al. 1992; Veregin, 1997) are too slow to be implemented in a Monte Carlo approach (Oksanen and Sarjakoski, 2005), and the use of spatial correlation indexes might give a limited perspective to spatial autocorrelation of the data organized in regular matrices (Oksanen and Sarjakoski, 2005).

The spatial moving averages approach, is based on a filter applied to the input random field to increase its spatial autocorrelation, while generally keeping the shape of the original distribution. Other works in literature underlined how these filters range from 3x3 low pass filters to those that account for the distance of spatial dependence as computed on the input DTM (Lee et al. 1992; Wechsler, 2000). Considering that there is no practical information about the error correlation range in the considered DTMs, its value has been operatively set to be a random number equal to or lower than the one applied by Oksanen and Sarjakoski (2005), therefore it varies with the stated constraint at each error realization. The Oksanen and Sarjakoski (2005) approach was originally defined for errors with a Gaussian distribution, while in this study case, the filter is applied to all the noise matrices (*E)* with different errors distribution. Consequently, the preservation of the error distribution shapes has been verified through several numerical tests. A mathematical proof of the shape invariance of the filter was not achieved nor looked for, but the preservation of the error distribution shape has been checked: distributions are not preserved exactly, but their main characteristics (shape, standard deviation, mean, skewness) are maintained.

The considered error matrices with isotropic autocorrelation, are labeled as $_{S}E$ and followed by the subscript representative of the error distribution (Tab. 4).

The anisotropic spatial correlation is obtained by using an approach derived from image analysis. Through the use of motion blur, a static spatial correlation in the direction of motion can be obtained.

Assuming a user might not know the texture orientation, the input *E* is modified, and a motion blur is applied, in order to provide fault noises oriented with random directions, and at the same time maintaining the error distribution (Fig. 38).

The ‘blurred’ noise matrix can be approximately described by this equation

$$_{B}E = E \cdot h(\Phi) \qquad 40$$

where $_{B}E$ is the distorted noise with anisotropic spatial correlation, that simulates the striping artifacts, E derives from one of the Alpha-stable random variables (Tab. 4), and $h(\varphi)$ is the distortion operator, also called the point-spread function (*PSF*). The *PSF* describes the degree to which $p_{i,j}$ is blurred, in terms of the angle of the blur φ in degrees, set to be a random value between 0° and 360°. The distortion operator, when convolved with the input noise matrix E, creates the distortion.

Again, the Monte Carlo error propagation to spatially correlated errors is the same, the only difference is that the error grids are spatially correlated (adding either isotropic or anisotropic correlation) before being added to the original DTM.

Table 4: distributions parameters and derived error matrices

Distributions parameters					Spatial correlation		
Shape	α	β	σ	μ	None	Isotropic	Anisotropic
Gaussian	2	-	1	0	E_G	$_{S}E_G$	$_{B}E_G$
Gaussian	2	-	DTM_{rmse}	0	E_{G*}	$_{S}E_{G*}$	$_{B}E_{G*}$
Levy	0.5	1	1	0	E_L	$_{S}E_L$	$_{B}E_L$
Cauchy	1	0	1	0	E_{CC}	$_{S}E_{CC}$	$_{B}E_{CC}$
Heavily left tailed	1	-1	1	0	E_{HLT}	$_{S}E_{HLT}$	$_{B}E_{HLT}$

d. Error effects analysis

Using the results from all the realizations of each error type, it is possible to calculate a mean value of skewness for each specific moving window, and this can be considered to correspond to the ‘true’ value that the algorithm would produce in the presence of that specific error. The behavior of skewness is expressed as a function of the window size ($Skew_k$, Eq. 37 p.89). Figure 39 shows the $Skew_k$ functions obtained from the clean high quality datasets ($a1_C$, $a3_C$, $a4_C$) and from the lower quality dataset (a2*, a5*, a6*, a7*). Figures 40-44 show the $Skew_k$ results for $a1_E$, $a3_E$, $a4_E$ with each of the simulated error type (E).

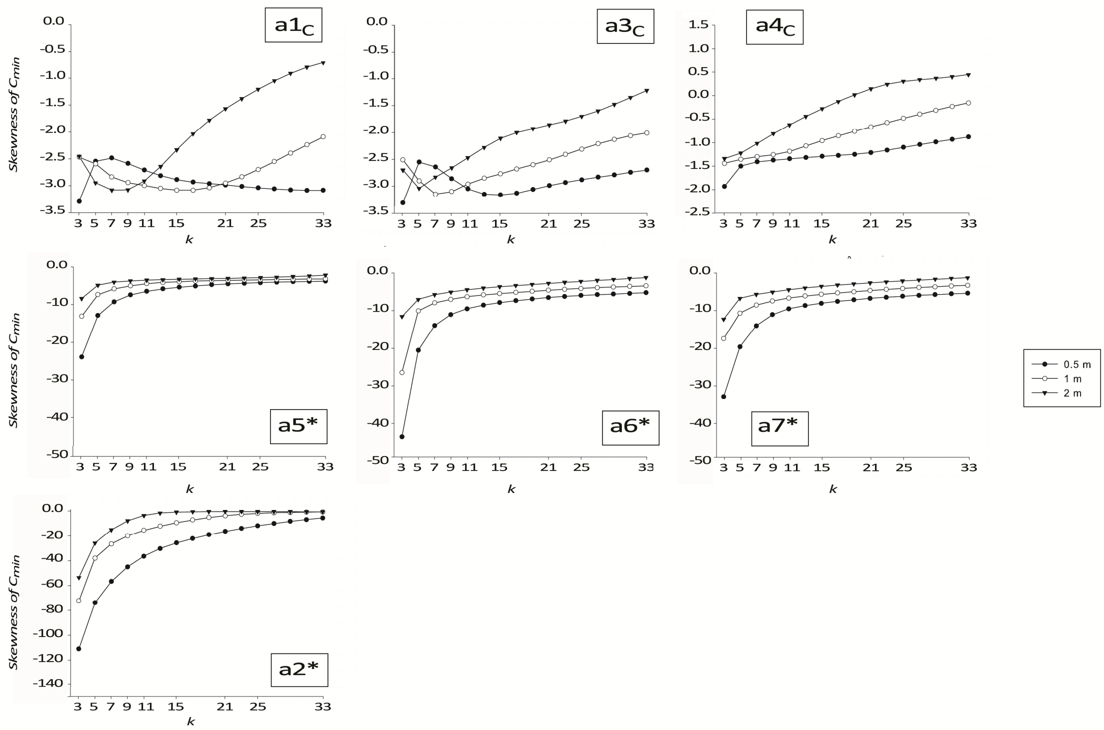

Fig. 39 Values of Skewness for each minimum curvature (C_{min}) map evaluated for different windows size (k) and for the different grid resolutions (0.5, 1, 2 m) for the clean test dataset (DTM_c) and the training dataset (DTM) with errors (Sofia et al. under review).*

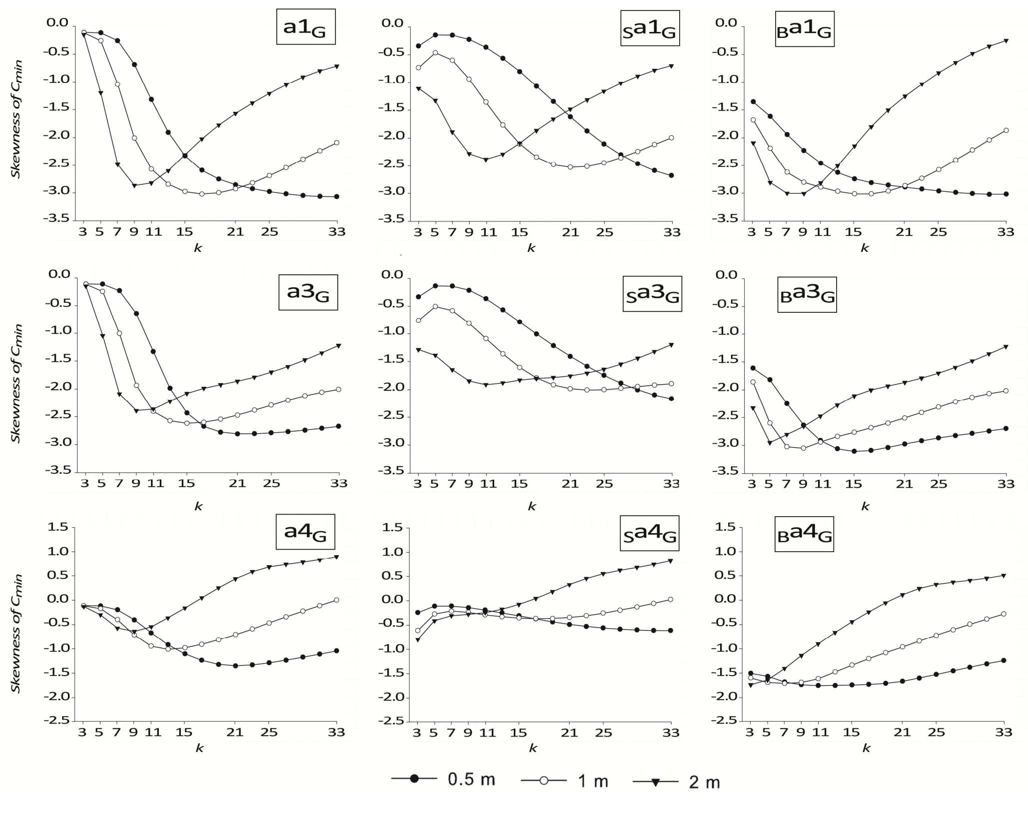

Fig. 40 Values of Skewness for minimum curvature (C_{min}) evaluated at different windows size (k) and for the different grid resolutions (0.5, 1, 2 m) considering DTMs with Gaussian error (μ =0 and σ =1), without spatial correlation (DTM_G), with isotropic correlation ($_SDTM_G$), and with anisotropic correlation ($_BDTM_G$). (Sofia et al. under review).

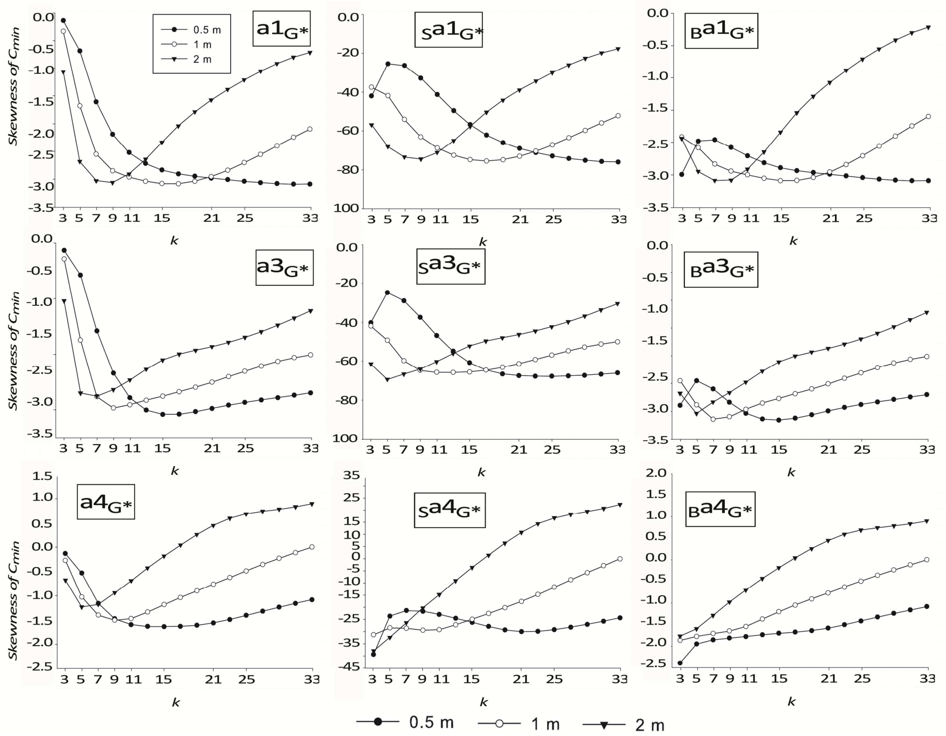

Fig. 41 Values of Skewness for minimum curvature (C_{min}) evaluated at different windows size (k) and for the different grid resolutions (0.5, 1, 2 m) considering DTMs with Gaussian error (μ =0 and σ = DTM_{RMSE}), without spatial correlation (DTM_{G*}), with isotropic correlation ($_{S}DTM_{G*}$), and with anisotropic correlation ($_{B}DTM_{G*}$).(Sofia et al. under review).

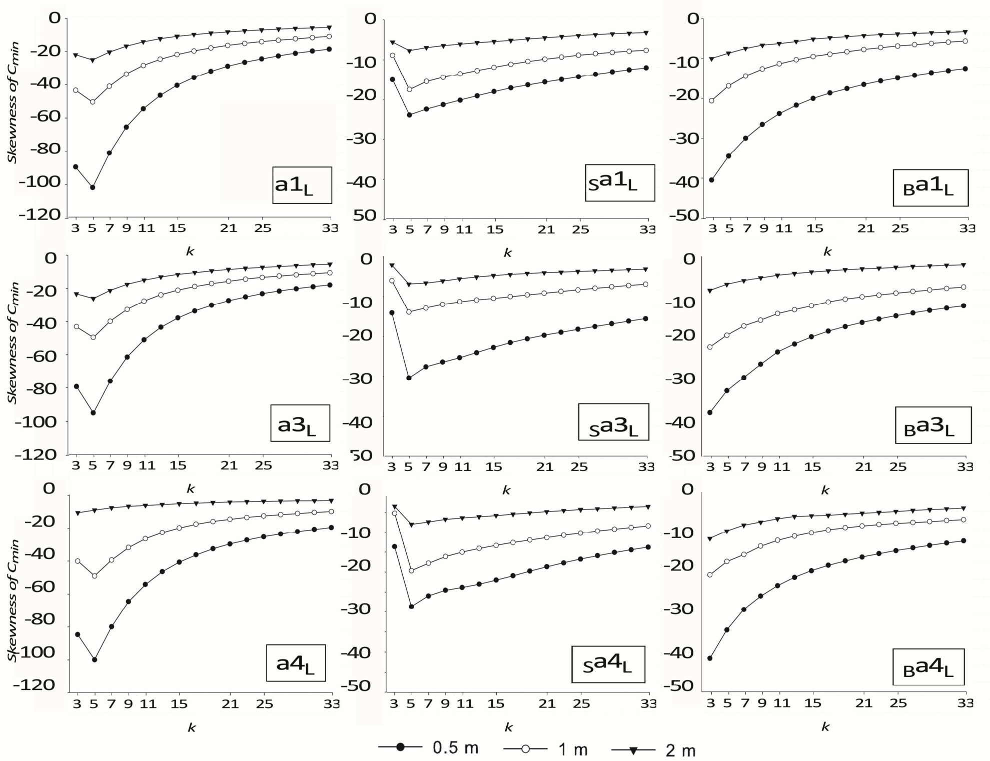

Fig. 42 Values of Skewness for minimum curvature (C_{min}) evaluated at different windows size (k) and for the different grid resolutions (0.5, 1, 2 m) considering DTMs with Levy errors, without spatial correlation (DTM_{L}), with isotropic correlation ($_{S}DTM_{L}$), and with anisotropic correlation ($_{B}DTML_{L}$). (Sofia et al. under review).

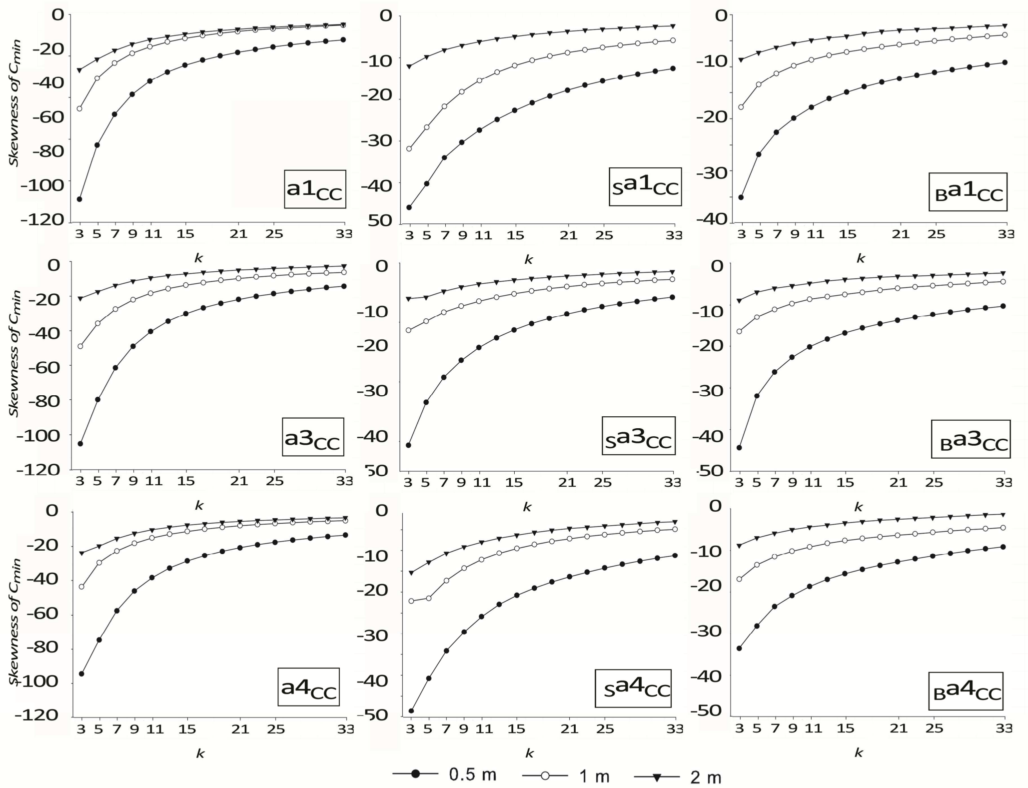

Fig. 43 Values of Skewness for minimum curvature (C_{min}) evaluated at different windows size (k) and for the different grid resolutions (0.5, 1, 2 m) considering DTMs with Cauchy errors, without spatial correlation (DTM_{CC}), with isotropic correlation ($_SDTM_{CC}$), and with anisotropic correlation ($_BDTM_{CC}$). (Sofia et al. under review).

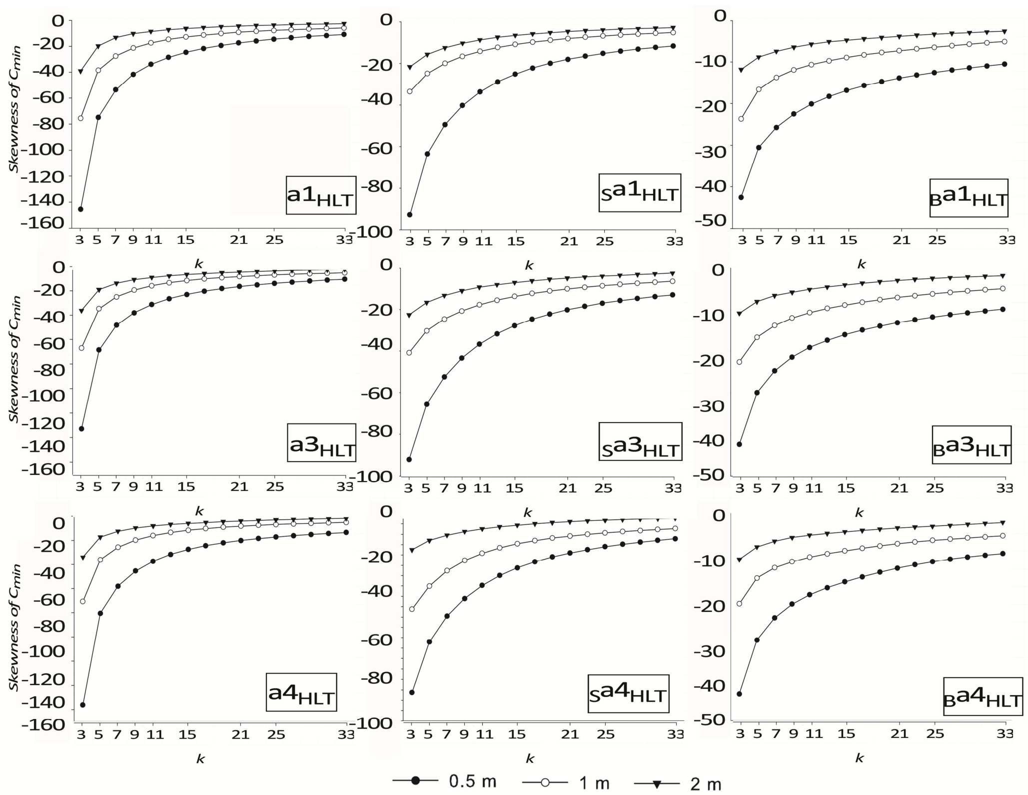

Fig. 44 Values of Skewness for minimum curvature (C_{min}) evaluated at different windows size (k) and for the different grid resolutions (0.5, 1, 2 m) considering DTMs with heavily-left tail errors, without spatial correlation (DTM_{HLT}), with isotropic correlation ($_SDTM_{HLT}$), and with anisotropic correlation ($_BDTML_{HLT}$). (Sofia et al. under review).

This section is divided in two parts. In the first part, the presence of errors is simulated on the high quality dataset, and compared to a test dataset with lower geomorphological quality, in order to provide realistic noise patterns.
On the second part, effects of all error types on curvature distribution are assessed.

1) *Actual errors effect VS simulated errors effects*

Two error types are accounted for: artificial lineaments and fault textures (a5,a6,a7), hereby labeled as *type(t)* errors, and erroneous heights and local outliers (a2), hereby named *type(o)* errors.
Considering that no information exists about the distributions that characterize the two errors, they have been simulated by considering different error distribution shapes, and by modeling in a different way the error spatial correlation. The aim of this part is, therefore, to a) identify the most suitable error distribution for *type(o)* and *type(t)* errors; and b) to test what spatial correlation better accounts for them.
If we are able to simulate correctly the error distribution and its spatial correlation, the $Skew_n$ behavior will be constant in all the datasets, independently from the DTM resolution and from the morphology of the area, and it will be similar to the reference behavior as registered in the lower quality dataset. The similarity between curves is evaluated considering as index the Modified Hausdorff Distance (MHD) (Dubuisson and Jain, 1994). Such distance measure is based on the Hausdorff distance between two point sets: the smaller the distance, the more similar the curves. In this instance, MHD values have been normalized so that their range goes from 0 (complete similarity between curves) to 1 (complete dissimilarity between curves). In table 5, mean MHD values between $Skew_k$ with each of the different error types, and the reference behavior are reported.

Table 5: average Modified Hausdorff Distance between each simulated error type and reference type(o) and type(t) errors.

	0.5 m			1 m			2 m		
	E_G	$_sE_G$	$_BE_G$	E_G	$_sE_G$	$_BE_G$	E_G	$_sE_G$	$_BE_G$
Type(o)	0.64	0.53	0.50	0.62	0.52	0.46	0.59	0.49	0.41
Type(t)	0.61	0.49	0.49	0.59	0.48	0.43	0.51	0.42	0.34
	E_{G*}	$_sE_{G*}$	$_BE_{G*}$	E_{G*}	$_sE_{G*}$	$_BE_{G*}$	E_{G*}	$_sE_{G*}$	$_BE_{G*}$
Type(o)	0.60	0.49	0.41	0.57	0.51	0.40	0.50	0.43	0.37
Type(t)	0.59	0.46	0.39	0.54	0.47	0.37	0.43	0.36	0.31
	E_{CC}	$_sE_{CC}$	$_BE_{cc}$	E_{CC}	$_sE_{CC}$	$_BE_{cc}$	E_{CC}	$_sE_{CC}$	$_BE_{cc}$
Type(o)	0.07	0.12	0.10	0.08	0.14	0.12	0.11	0.16	0.15
Type(t)	0.07	0.12	0.10	0.07	0.12	0.10	0.06	0.10	0.08
	E_L	$_sE_L$	$_BE_L$	E_L	$_sE_L$	$_BE_L$	E_L	$_sE_L$	$_BE_L$
Type(o)	0.15	0.26	0.20	0.17	0.28	0.23	0.19	0.31	0.24
Type(t)	0.15	0.28	0.19	0.14	0.28	0.20	0.13	0.26	0.16
	E_{HLT}	$_sE_{HLT}$	$_BE_{HLT}$	E_{HLT}	$_sE_{HLT}$	$_BE_{HLT}$	E_{HLT}	$_sE_{HLT}$	$_BE_{HLT}$
Type(o)	0.05	0.07	0.07	0.03	0.09	0.10	0.04	0.11	0.12
Type(t)	0.07	0.07	0.04	0.07	0.07	0.06	0.06	0.06	0.05

It appears that both error types (*type(o)* and *type(t)*) are better represented by distributions with longer tails (i.e. Cauchy, Levy and Heavily Left Tailed). Gaussian distributions, correlated or uncorrelated, are not able to represent the actual effect of *type(o)* nor *type(t)* errors, while by considering distributions as the Cauchy or the Levy one, $Skew_k$ is more resembling. However, errors with Levy's distributions and no spatial correlation or random isotropic correlation, seem to determine a ‘check-mark’ shape for $Skew_k$ that is never registered in the low quality available datasets.

When considering *type(t)* errors, distributions with longer tails better account for the effect of this type of error on curvature skewness. Between them, the Levy distribution produces the less realistic noise pattern (average MHD= 0.20 for the 0.5 m datasets), while the Cauchy and the Heavily Left Tailed distribution seem to better resemble the reference $Skew_k$ pattern (average MHD=0.10 and 0.06 respectively for the 0.5 m datasets). The most suitable error distribution appears to be the Heavily Left Tailed (average MHD= 0.06), however, only a slight difference is visually assessable between the $Skew_k$ functions produced by the datasets with these errors.

The more realistic pattern is produced by errors having a Heavily Left Tailed distribution and no spatial correlation, for *type(o)* errors, or anisotropic spatial correlation (blurred) for the *type(t)* errors. Considering this type of error distribution and the specified correlation, both $Skew_k$ shape and skewness ranges are consistent with the ones registered in the low-quality datasets (a2, a5, a6, a7). One must note that the direction of blur, for the *type(t)* errors, has no influence at all. By simulating randomly all the maps, the average simulated behavior of $Skew_k$ reflects the reference one.

2) *Effects of errors on Skew$_k$*

Considering a gaussian error with *μ = 0* and *σ = 1* (Fig. 40)*,* correlated or uncorrelated, skewness values range remains consistent with that of the original DTMs (Fig. 39): skewness has in all instances 0 as the nearest order of magnitude. However, differently from what expected, this particular error determines a normalization of curvature distributions for the smallest window size (*k*=3 cells). This normalization is more evident for non-correlated noise: while on the clean datasets, the smallest window size determined a highly skewed curvature, when adding a Gaussian noise with no spatial correlation, skewness of curvature is close to 0 in all instances and for all grid sizes. For all the datasets, it appears that the *Skew$_k$* function becomes independent from errors with this specific distribution when curvature is evaluated for windows greater than ~20 m. As expected, the errors have greater effects on the DTM 0.5 m. For this grid resolution, the shape of *Skew$_k$* appears hardly modified if compared to that the original dataset, and it assumes a peculiar shape that is constant independently from the morphology of the area.

When the Gaussian error is not correlated (DTM_G in Fig. 40), *Skew$_k$* for the 0.5 m datasets assumes a sigmoidal shape. If isotropic spatial correlation is added to the same error distribution ($_SDTM_G$ in Fig. 40), the *Skew$_k$* function for the 0.5 m datasets assumes a wave shape. The peculiar shapes are registered just for the defined errors, and appear not to be correlated with the morphology of the area, rather they appear to be peculiar of the Gaussian error with the defined parameters suggesting their suitability to label a lower geomorphological quality of the dataset and, in particular, to label the presence of a non-correlated Gaussian error with *μ = 0* and *σ = 1* (sigmoidal shape) or correlated Gaussian error with *μ = 0* and *σ = 1 (*wave shape*)*.

When anisotropic spatial correlation is added to the error matrix ($_BDTM_G$ in Fig. 40), effects of errors on *Skew$_k$* function are slightly visible only for the 0.5 m datasets. One must note that this error distribution is not able to account for actual systematic errors, even when the spatial correlation is simulated to be similar to the one typical of striping artifacts (DTM_B).

When considering an error with a Gaussian distribution with *μ = 0* and *σ = RMSE* (DTM_{G*} in Fig. 41)*,* *Skew$_k$* has a hyperbolic shape: starting from a normal shaped curve, skewness progressively increases in the negative domain. For this error distribution, if isotropic spatial correlation is added ($_SDTM_{G*}$ in Fig. 41) *,* the shape of *Skew$_k$* does not change, however skewness values increase of about one order of magnitude. Differently, from what expected, by adding a Gaussian noise with no correlation, the smaller window size used for curvature evaluation results in normal-shaped curvature distributions (*skewness* is close to 0). When considering the DTMs at 1 and 2 m, in all datasets the effect of errors on curvature maps disappears when the window size used for curvature calculation increases. This is consistent with the fact that too wide window sizes results in a smoothed morphology, that, on the one hand, is not able to correctly capture morphological features, and on the other hand, smoothes errors.

When the anisotropic correlation is applied *($_BDTM_{G*}$* in Fig. 41) to simulate *type(t)* errors (trying to obtaining striping artifacts as recorded on a5, a6, a7), it is clear, that even if we try to simulate the spatial structure of errors (stripes), Gaussian distributions of values with the considered shape parameters are not able to account for the effect of actual striping artifacts on curvature. Again, the higher error influence is registered for the 0.5 m datasets, while curvature evaluated from the 2 m datasets appears to be independent from errors. However, the $Skew_k$ function is slightly modified only for the 0.5 m datasets.

When considering an error with a Levy distribution *(DTM_L* in Fig. 42)*,* $Skew_k$ function is modified in all instances, independently from the DTM resolution. If the error has no spatial correlation *(DTM_L* in Fig. 42), $Skew_k$ function assumes a check-mark shape. If an isotropic spatial correlation is added ($_SDTM_L$ in Fig. 42), $Skew_k$ assumes a V shape, and skewness after reaching a minimum value for *k*=5, increases almost linearly. If anisotropic spatial correlation is considered ($_BDTM_L$ in Fig. 42), $Skew_k$ slightly resemble the pattern obtained from the test low quality dataset (a5* a6* a7* in Fig. 42), but for the 0.5 m resolutions, $Skew_k$ is almost linear.

Considering errors with a Cauchy distribution *(DTM_{CC}* in Fig. 43)*, a*nd errors with heavily left tailed distributions *(DTM_{HLT}* in Fig. 44)*,* their effects on $Skew_k$ are similar. However, the Cauchy distributed errors show some variability between the different datasets when isotropic spatial correlation is added *($_SDTM_{CC}$* in Fig. 43)*,* suggesting that in the presence of this type of errors, morphology of the area might still have some influence on curvature skewness.

This analysis underlines that in the presence of noise/errors, $Skew_k$ function does not depend on morphology, but it is strictly dependent on these errors. Some specific shapes of the $Skew_k$ function, furthermore, can identify the presence of specific error types: i.e. a checkmark shape is representative of errors with a Levy distributions and no spatial correlations, a sigmoidal shape of the function is a symptom of the presence of a non-correlated Gaussian error with $\mu = 0$ and $\sigma = 1$, or again, a wave shape can be an hint of the presence of isotropic correlated Gaussian error with $\mu = 0$ and $\sigma = 1$. When $Skew_k$ assumes an asymptotic shape, with value increasing from a highly negative value toward 0, the DTM might be characterized by the presence of striping artifact (if skewness higher values have at their maximum 1 as the closest order of magnitude), while for the same $Skew_k$ shape but with skewness values that have at their maximum 2 as the closest order of magnitude, pits and outliers might be present. Also, this analysis underlined the suitability of $Skew_k$ in identifying the optimum scale to analyze channelized features, when dealing with DTMs with high quality (Chapt. 4.2, *sect III.Materials and methods*).

IV. DTA FOR FEATURE RECOGNITION

1. Geomorphic features recognition

The study area considered for this first DTA application, is the Cordon basin (Chapt. *1.1,* Sect. *II.Study sites*), and the background framework for this application can be found in Chapt. *2.1,* Sect. *I.Introduction*. The addressed features are landslide crowns and bank erosion: this type of geomorphic features correspond to convex slope breaks forming ridges within the likely unstable area. Since ridges are related to surface convexity, for this DTA, maximum curvature (C_{max}, Eq. 15) has been considered as optimal for feature recognition.

This first DTA approach aims: 1) to test the effectiveness of different landform curvature maps with different smoothing factor for feature extraction; and 2) to test the effect of the choice of different statistical parameters as thresholds to label features. Considering 1) a progressively increasing moving window size has been considered for the calculation of curvature, in order to incorporate the majority of scale variations, and extractions are performed on all curvature maps and compared to the reference features. The considered kernels are 3x3, 5x5, 7x7, 9x9, 15x15, 21x21, 23x23, 25x25, 29x29, 31x31 and 33x33 cells, on a 0.5 m DTM resolution, and they are consistent with the kernel size range adopted in other works in literature (Pirotti and Tarolli, 2010). Considering 2), different statistical thresholds have been adopted and compared (Tab. 6): a) multiples of curvature standard deviation (as proposed by Tarolli and Dalla Fontana (2009) for channel head recognition, and channel network extraction), b) interquartile range, c) median absolute deviation (MAD), d) quantile-quantile plot (Q-Q plot) defining the threshold of curvature (as proposed by Lashermes et al. 2007). The reference statistical background of each parameter is described in Chapt. 4, Sect. *III.Materials and methods*.

Geomorphic features such as landslide crowns and features related to bank erosion correspond to convex slope breaks forming ridges within likely unstable area, and they are related to a lower frequency of values (for a fuller discussion, see the statistical background already defined in Chapt. 4.1 and 4.2 Sect. *III.Materials and methods*). Consequently, the basic idea of the method, according to the background theory expressed in Chapt. 4.2, is to identify potential features where:

$$C_{\max} > m \cdot \sigma_{C_{\max}} \qquad 41$$

$$C_{\max} > m \cdot \mathrm{IQR}_{C_{\max}} \qquad 42$$

$$C_{\max} > m \cdot \mathrm{MAD}_{C_{\max}} \qquad 43$$

$$C_{\max} > m \cdot \mathrm{QQ\,plot}_{\mathrm{thr}} \qquad 44$$

where *m* is a real number (Tarolli et al. 2010).

Each statistic is evaluated according to the procedures described in Chapt. 4.1.

The procedure to identify the QQ-Plot threshold is exemplified in Fig. 33, p. 88. The only difference, in this instance, is that the threshold is to be identified in the positive side of the tail.

Table 6: Descriptive statistics for C_{max} *maps according to window size (*k*, see Eq. 15 p.67) used for curvature evaluation (Tarolli et al. 2010)*

k	IQR_{Cmax}	MAD_{Cmax}	$QQ\text{-}Plot_{Cmax}$	σ_{Cmax}
3	0.72	0.47	0.81	0.63
5	0.60	0.39	0.62	0.53
7	0.55	0.38	0.62	0.52
9	0.55	0.38	0.61	0.53
15	0.62	0.43	0.66	0.59
21	0.70	0.48	0.74	0.64
23	0.73	0.49	0.76	0.65
25	0.75	0.50	0.78	0.67
27	0.77	0.52	0.81	0.68
29	0.79	0.52	0.83	0.69
31	0.81	0.53	0.85	0.70
33	0.83	0.54	0.86	0.70

1.1 Scale and threshold effects

To test the effect of windows size in curvature calculation, a visual comparison can provide some insightful information. In Fig. 45 maps of C_{max} obtained respectively with different kernels of 3x3 (a) 15x15 (b) and 33x33 (c) cells, and the potential features identified considering $\sigma_{C_{max}}$ as threshold (a-c_{EXT}) are showed. The smaller window (3x3, Fig. 45a) does not appear to be suitable for a good recognition of surface features. This, because only a limited area is investigated, and as a consequence, the map is highly noisy. The 3x3 kernel is the minimum kernel required for any topographic parameter, and before the generalization procedure proposed by Wood (1996), scale was never considered. This analysis, however, shows that by considering only the 8 nearest neighbors for each pixel, the parameter evaluation is negatively influenced by any surface changes caused by 1 meter scale features (rocks, boulders and non-significant morphology), and this results in a not suitable map to extract the features of interest (a_{EXT} in Fig. 45). Wider window sizes decrease noises, resulting in a better surface morphology recognition (Fig. 45 b, b_{EXT}). It can be easily noted how ridges (that correspond to positive $C_{max,}$ red color in the map) are highlighted in detail.

However, if on the one hand (until an optimum point) the increasing of the moving window corresponds to an improvement of the feature identification, when the considered neighborhood becomes too wide (i.e. 33x33 cells, Fig. 45c, c_{EXT}) curvature maps are too smooth to be suitable for a correct representation of morphology. For evaluation carried out using such window sizes, the investigated area is too large and morphological features sited in place far from erosion areas could be reached in the curvature analysis providing a misinterpretation of erosional features. Based on these visual considerations a better result is related to a not too small or too large kernel. These considerations are similar to those obtained in the work by Pirotti and Tarolli (2010), where the authors suggested that window size for curvature calculations has to be related to size of the features to be detected. In general, the best ratio between information and noise, and thus the best results for feature recognition, is found when the window size is about twice-three times the maximum size of the investigated features.

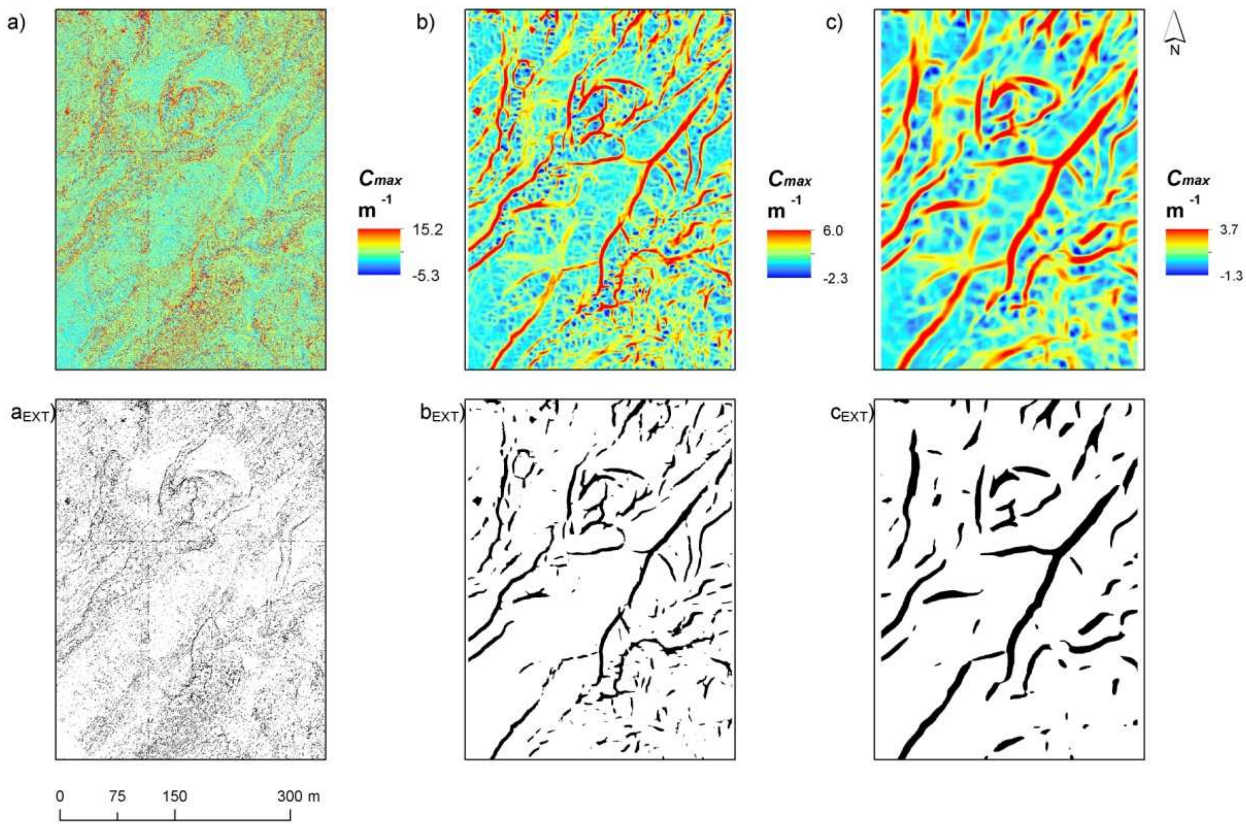

Fig. 45 Landform curvature maps obtained with moving window of a) 3x3, b) 15x15, c) 33x33, and derived extractions.

The other parameter that influences the quality of the feature extraction process is the choice of the threshold to label meaningful convexities. Fig. 46 shows features derived from a curvature map evaluated for k_{size}=15 cells and using 1, 2, 3 times the $QQplot_{thr}$ (a-c) and the *MAD* value (d-f) as thresholds.

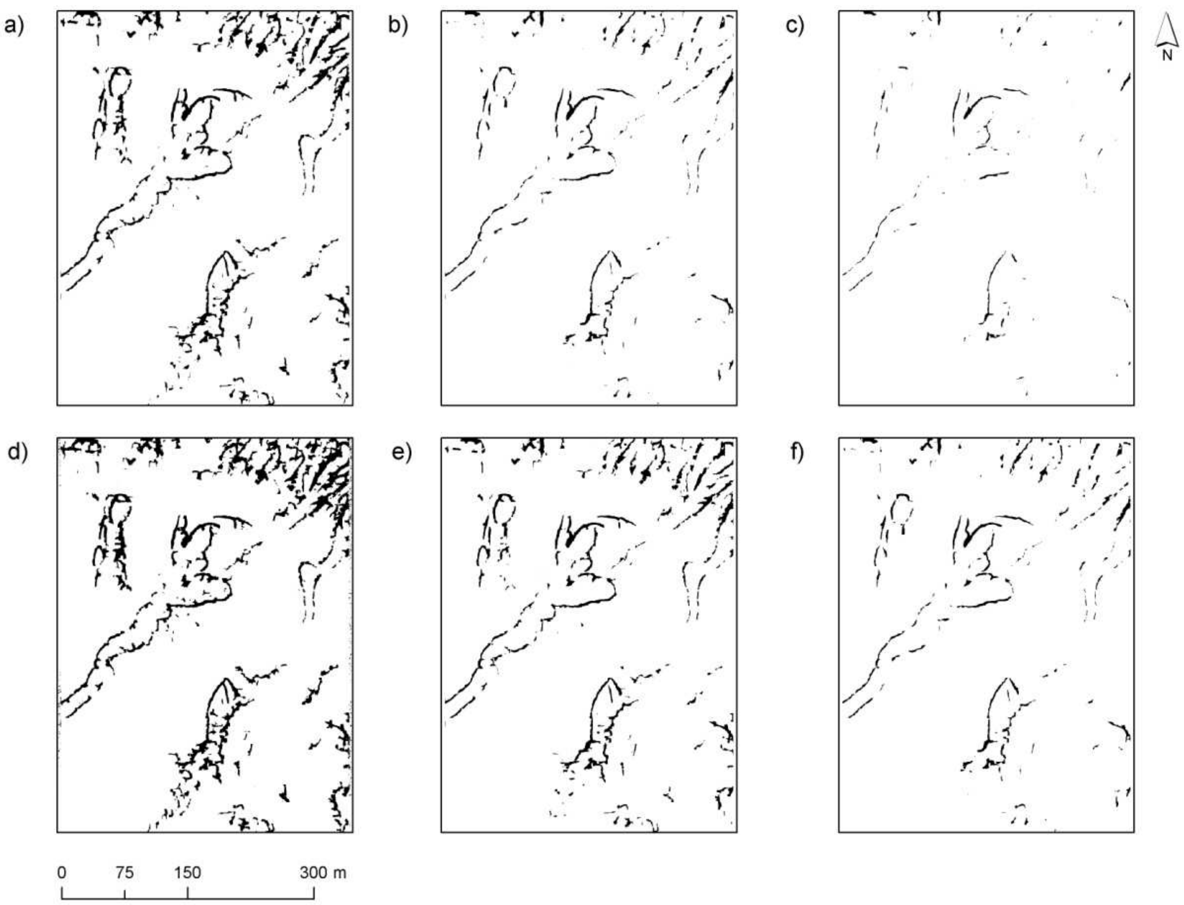

Fig. 46 Geomorphic features extracted using the threshold of 1, 2, 3 QQ-Plot$_{thr}$ (a-c) and 1,2,3 MAD *(d-f)*

The progressively increase of *m* value (Eq. 41-44) is related to a better ridges recognition, and a progressively decrease of noises on hillslopes. However larger values of *m* are at the same time related to a progressive loss of information of extracted features. This behaviour is constant for all the considered thresholds, however, different thresholds might lead to slightly different extraction quality, considering that the value of each statistic varies (i.e. Tab. 6).

However, elements identified from curvature only through the thresholding approach, are not necessarily related to ground failures and geomorphic features: local convexities might also be related to ridges or local changes in morphology (see i.e. Fig. 45). Considering the high morphological complexity of the study area (Fig. 3 p.37), and considering that the analysis is focused only on ground failures, an improvement of extraction can be obtained by filtering the results. The idea is to label as noise, and therefore, discard, elements that are extracted in areas having a slope lower than the internal frictional angle at which most of the instabilities in the area occur. Such slope threshold is area specific, and it can be identified through laboratory analyses: for the considered study areas, it corresponds to 35° (Borga et al. 2002; Tarolli et al. 2008). Potential geomorphic features are therefore, only extractions that belong to areas with slope greater than 35° (Fig. 47). Different methods are available in literature for slope calculation (i.e. Zevenbergern and thorn, 1978); in this instance, slope is computed through the same background theory and kernels used for curvature calculation (Evan's 1980) (See Chapt. 3.1.a, Sect. *III.Materials and methods*), in order to guarantee a consistency in the analysis. Figure 47 shows the improvement obtained on the extracted features by considering different slope maps, and using 35° as the slope threshold.

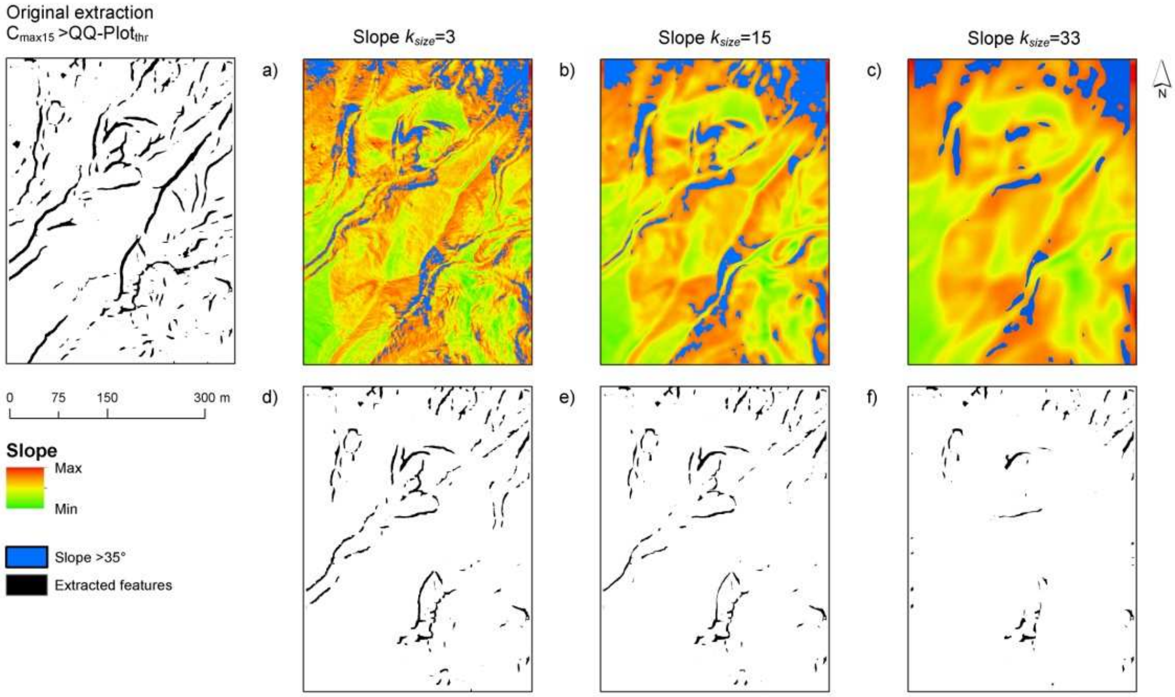

Fig. 47 Use of slope to improve the extraction derived from curvature evaluated for k_{size}*=15 using the threshold of QQ-Plot*$_{thr}$ *. Different slope maps (a-c), evaluated considering the different* k_{size}*, underline areas with slope greater than the internal frictional angle (35°) (in blue). Extraction improvement considering each mask are shown in d-f.*

1.2 Accuracy assessment

After the considerations done by visual assessment, the different statistical thresholds are compared to identify the optimal algorithm for feature extraction. Such kind of evaluation is not meant to evaluate the extraction and the matching results in an absolute way, rather, it is used to compare the results of different algorithms (Heipke et al., 1997). The final product to test is a raster map segmented into two classes: during the thresholding process, individual pixels on the maps are marked as 'object' pixels (feature) if their value satisfies the thresholding formulation and as 'non-object' pixel otherwise.

Two significant statistical error may occur during this classification process, type I Error and type II Error. The "null hypothesis" corresponds to a default situation (in this case, that an area is not related to an erosional feature), while the "alternative hypothesis" is that the area refers indeed to an erosion process. The goal is to determine if the null hypothesis has been correctly discarded in favor of the alternative by the extraction methodology. If methodology rejects the null hypothesis when it is indeed true (non-erosion areas labeled as erosional features) a type I Error (False Positive) is shown, if it accepts the null hypothesis when it is false (actual erosional element marked as non-erosional features), a type II Error (False Negative) is provided.

To assess how well results represent the ground truth, the landslide crown and the instability areas polylines digitized in the field by DGPS were converted to raster with a buffer of 2 m on each side for a total of 4 m width. The buffer size was chosen because it soundly envelopes the convex slope breaks among erosion location and allows the correction of issues like the likely shift (< 1 m) due to horizontal accuracy that could be present in the DTM respect to GPS ground survey. The resulting raster was used as reference and compared with each of the results derived from each of the twelve window sizes and multiples of the σ_{Cmax} , MAD_{Cmax}, IQR_{Cmax}, $QQ\text{-}Plot_{thr}$ as thresholds. The matching extracted areas are defined as true positive (TP) underlining the fact that the extraction method has correctly detected the features (null hypothesis has been correctly discarded), while the un-matching extracted areas are considered as false positive (FP) because the extracted features are not correct. The areas within the buffer that are not extracted by the methods are interpreted as false negative (FN).

A quality evaluation on performances aims to find the best cutoff value that gives the best result according to user's expectation and that reduces the two types of potential mistakes (FP and FN) in the semi-automatic process (Lee et al. 2003). According to Heipke et al. (1997) it is possible to measure the "goodness" of the final extraction results through an index (Eq. 45) that takes into account the percentage of the reference data, which is explained by the extracted areas as well as the percentage of correctly extracted features.

$$\mathrm{QUALITY} = \frac{\mathrm{TP}}{(\mathrm{TP}+\mathrm{FP}+\mathrm{FN})} \qquad 45$$

Quality therefore vary between 0 for extraction with no overlap between extracted and observed features and the optimum value of 1, for extraction where these coincide perfectly.

The evaluation of cutoff methodologies has been done considering quality results that have been compared according to the following factors:

i. kernel size used for slope evaluation (Fig. 48a)
ii. kernel size used for curvature evaluation (Fig. 48b)
iii. choice of m for thresholding (Fig. 48c)

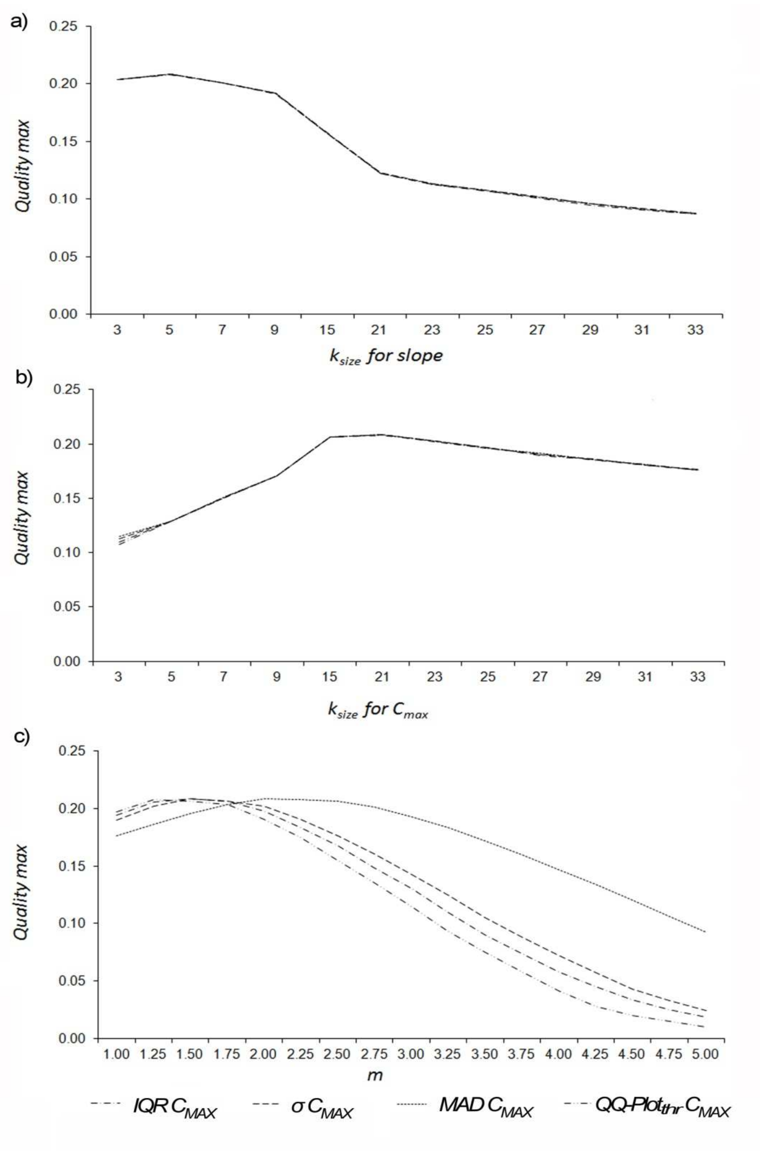

Fig. 48 Plots of maximum values of quality index according to (a) k_{size} *for slope (for all the considered curvature maps and* m *values), (b)* k_{size} *for curvature (for all the considered slope filtering and* m *values), (c) and m (for all the considered kernel sizes). (modified from Tarolli et al. 2010)*

According to the overall accuracy, all the methodologies show higher precision in classifying the features using maps filtered for slope evaluated for k_{size} of 5 (2.5 m); considering slopes derived from wider moving windows, the accuracy of pixel segmentation decreases (Fig 47e-f and 48a). Analyzing the choice of k_{size} for curvature (Fig. 48b), better performances are obtained when k_{size} reaches 10.5 m. This result underlines something that was already clear from a visual assessment of the different curvature maps: map suitability is optimal when curvature derives from window sizes that are nor too small nor too big (fig 48b).

Referring to the thresholding approach (Fig. 48c), the different statistics give almost the same optimal results when *m* ranges between 1.25 and 1.75 (Fig. 48c). The only registered differences appear for extraction based on *MAD* as thresholds, where highest quality is obtained for *m* ranging from 2 to 2.5 (fig 48c). This is consistent with the fact that the value *MAD* is for all maps, the lowest, if compared to the other statistics (see i.e. Tab. 6).

The best approach (*Quality* = 0.21) considering all the combinations of slope, curvature, and *m,* is to extract features using 1.5 IQR_{Cmax} on curvature evaluated for a k_{size} of 21, and to filter then in a second step considering slope evaluated for k_{size} equal to 5 (Fig. 49). Other algorithms provide similar results (Fig. 48c), since the thresholds values for feature extractions are similar (Tab. 6). The best results, anyway, always refers to curvature maps evaluated for k_{size} equal to 21 and filtered according to slope evaluated for k_{size} of 5.

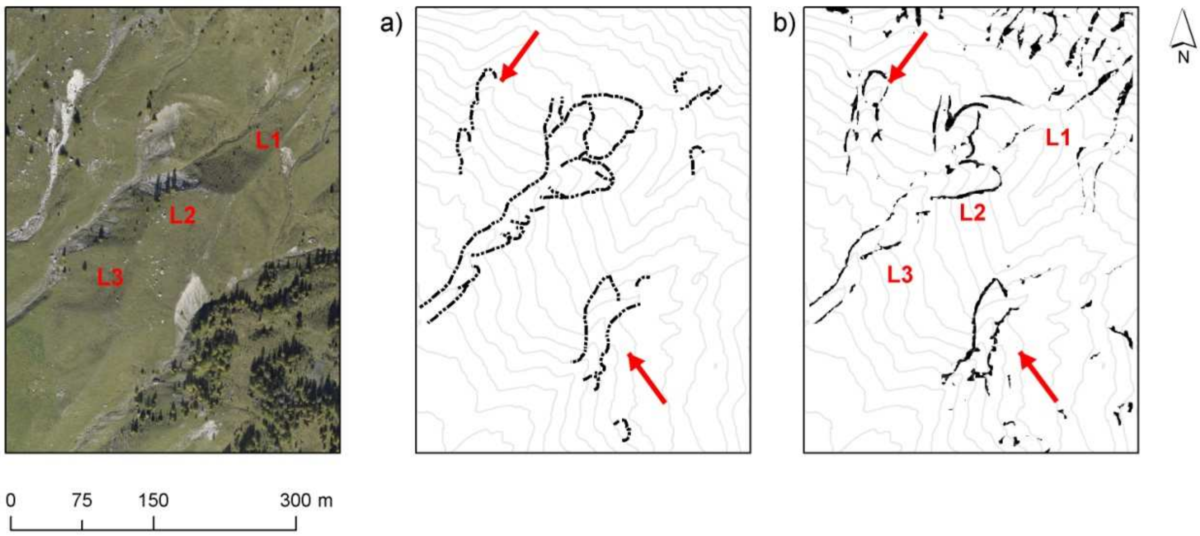

Fig. 49 The figure shows (a) the surveyed features for a comparison (red arrows are related to the extracted features representing the main slope instabilities investigated) and (b) the geomorphic features corresponding to the best extraction of all proposed methodologies (threshold value of 1.5 IQR of Cmax calculated with a 21x21cells moving window). (modified from Tarolli et al. 2010)

Looking at Fig. 49, one can note that the features (red arrows) related to shallow landslide crowns, and bank erosions are correctly labeled. However, at the top of the study area, where the morphology is complex, the methodology tends to recognize features where convex slope breaks are not related to instability. This explains the relatively low values of the quality index of 0.21.

These results show that a completely-automated feature recognition it is not fully reliable in areas with complex morphology. Nevertheless, this methodology should be considered as a first, and relatively fast approach to slope instabilities hazard mapping when using high resolution topography. According to Fig. 49b, even if a significant number of false positives is detected, it is easy to discriminate areas where the main instabilities are located, since these clearly show organized patterns of discontinuity, very similar to investigated features (Fig. 49b).

2. Channel network recognition

The procedure proposed in this chapter for feature extraction, even if focused on a different type of feature (channel network), is based on the same background considerations of the previous one, and it is carried out on the same study area, the Cordon Basin (hereby defined as '*study area'*). The background framework for this application can be found in Chapt. *2.1,* Sect. *I.Introduction*. The DTA is also tested in another site (Miozza basin, Chapt. *1.2,* Sect. *II.Study sites)*, hereby defined as '*test area'*). The two areas are different, both in morphological complexity and network characterization (Fig. 50). .

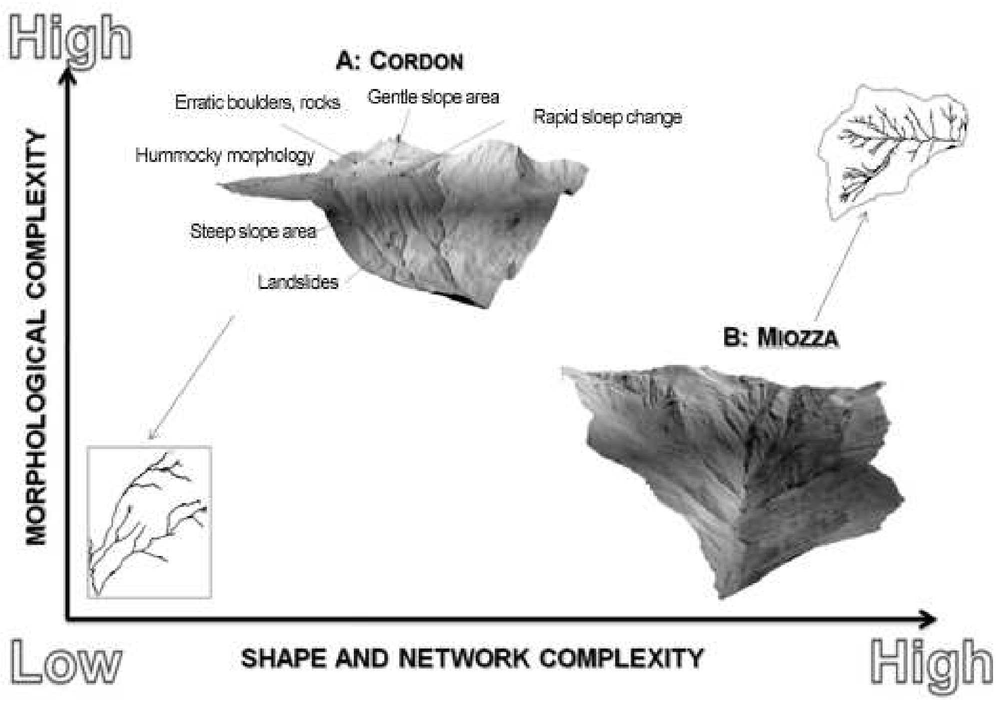

Fig. 50 Different complexity of the study sites.

The Cordon area is a squared area selected site, chosen without any reference to a defined watershed, with the only constraint to have a network and a pour point. The Miozza site, instead, is a full watershed, with a more complex network. The Cordon area, furthermore, is characterized by a highly complex morphology on the northern part (Fig. 3 p.37), while the Miozza morphology is more smooth and with fewer abrupt changes.

For the present DTA application, DTMs were derived with two different interpolation procedures: the natural neighbor interpolator (Sibson, 1981) for the Cordon study site, and an algorithm with a spline function in the ESRI TOPOGRID tool for the Miozza one (Tarolli and Tarboton, 2006; Tarolli and Dalla Fontana, 2009). Depending on the spatial variation of the accuracy and density of the data, and on the suitability of the interpolation method for a certain relief, DTM quality might vary locally and regionally (Karel et al. 2006), and for some parts of the Cordon study area, the presence of some small artifacts is registered on the DTM, probably due to changes of the bare ground point density (Fig. 51).

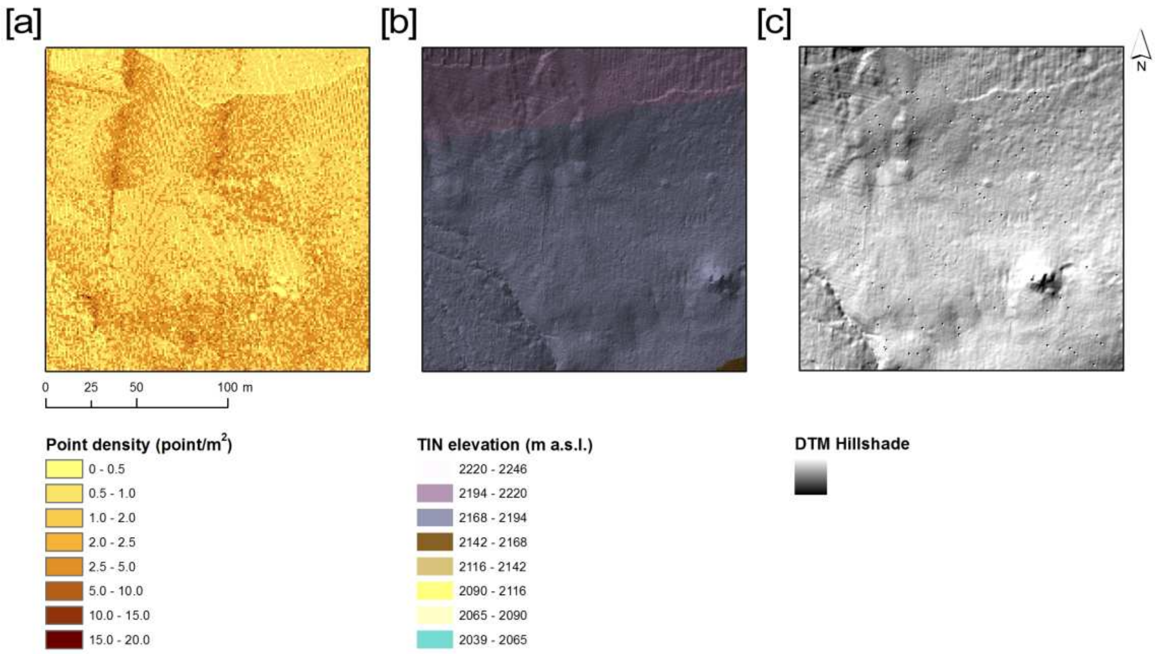

Fig. 51 Detail of (a) LiDAR point density, (b) generated TIN, and (c) DTM derived from triangulated points. Artifacts are visible both on TIN and DTM, where striping artifact oriented approximately north-south or east-west, corresponding to change in point density, are visible.

When dealing with surface derivatives, one of the limits of their use is that these artifacts constitute errors that, even when controlled and limited by appropriate methods, might amplify when differentiating (Burrough and McDonnell, 1998; Gallant and Wilson, 2000), and Chapt. 4.2, Sect. *III.Materials and methods*, provided a deep analysis about the matter.

Considering the different morphology of the areas and the issues related to DTM quality, in this application, there was the need to obtain a sound method to detect features, and to resolve some of the issues previously identified: 1) independency from errors, 2) choice of the optimum scale of analysis and 2) noise discarding in areas with complex morphology.

Figure 52 shows a flow chart of the complete DTA approach considered in this framework. The proposed approach is a three-step method based (a) on the normalization of topographic parameters (openness and minimum curvature, see Chapt. 3.1.b and 3.1.d, Sect. *III.Materials and methods*) to highlight local morphology, (b) a weighting of the upslope area according to such normalization to identify flow convergences (Chapt. 3.2, Sect. *III.Materials and methods*), and (c) the choice of a statistical parameter as an objective threshold for channel network detection. As a final step, according to the presence/absence of noises, an indication is provided on how to perform a filtering approach and then how to connect the network.

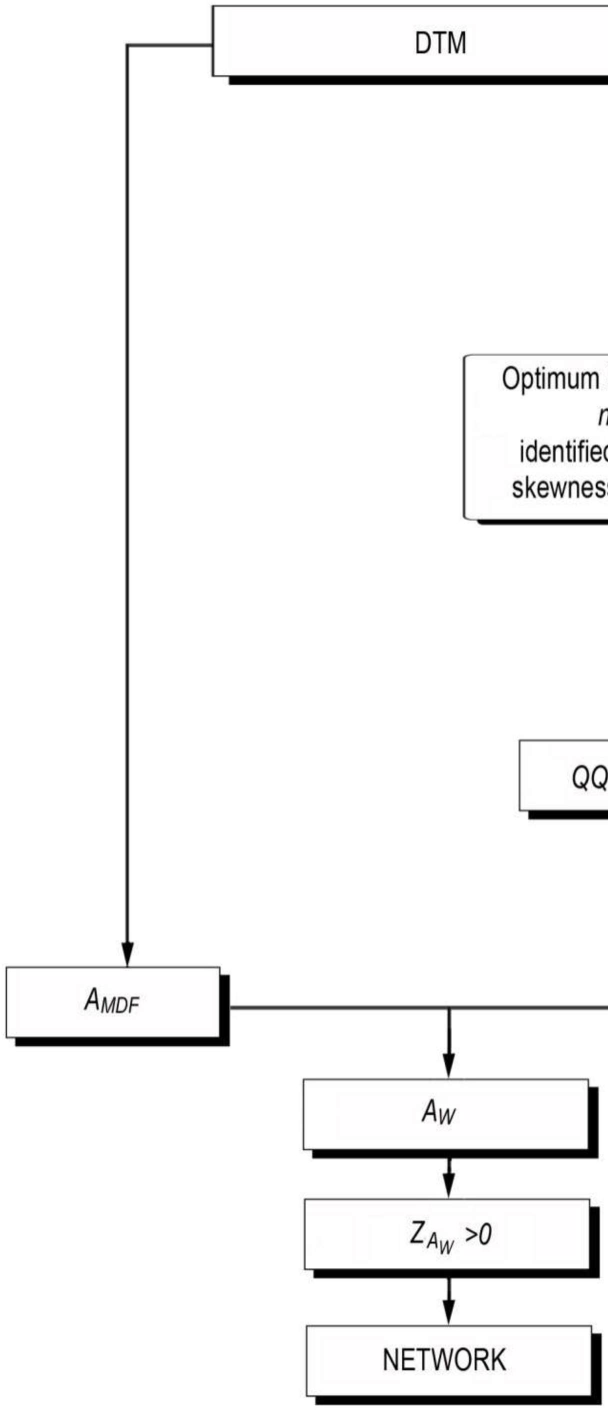

Fig. 52 Flow chart of the proposed methodology. Local morphology is enlightened through Topographic Attributes (Minimum Curvature Cmin, Positive Openness φL, Negative Openness ψL). The choice of the optimum kernel size (n) is done through the analysis of the relationship between skewness and kernel width. Topographic attributes computed considering the optimum kernel are analyzed through QQ-Plot to identify thresholds to normalize each map. Flow convergence is done through multiple flow upslope area (A_{MDF}) weighted according to a matrix depending on the normalized topographic attributes. Network is then identified as positive values of the weighted area standard score. (Sofia et al. 2011)*

The objective of this study is to delineate the network where surface allows flows to converge. This analysis is done through a direct detection of morphology from the digital terrain maps. On the idea of proposing an unsupervised extraction of network that did not require an assessment of the input data, no correction of DTMs artifacts has been done, but two indexes have been joined to enforce local concavity detection: a direct surface derivative (Minimum Curvature, Evans', 1979), and an image of shaded relief and slope angle (Openness, Yokoyama et al., 2002; Prima et al. 2006). The choice of curvature has been done considering that numerous works proved its effectiveness for feature extraction (e.g. Molloy and Stepinski, 2007; Lashermes et al., 2007; Tarolli and Dalla Fontana, 2009; Thommeret et al., 2010, Pirotti and Tarolli, 2010; Passalacqua et al. 2010a,b). The choice of openness is based on the fact that its measure of convergences relies on an averaging procedure: openness values are calculated as averaging angles along azimuths (Yokoyama et al., 2002; Prima et al., 2006). This averaging procedure is assumed to be less affected by artifacts in the input data due to interpolation techniques. As suggested by Yokoyama et al. (2002), values of both positive and negative openness have been compiled. All parameters are carried out through the classical moving window approach, providing maps of curvature and openness for window sizes from 3x3 up to 33x33 cells (Fig. 53).

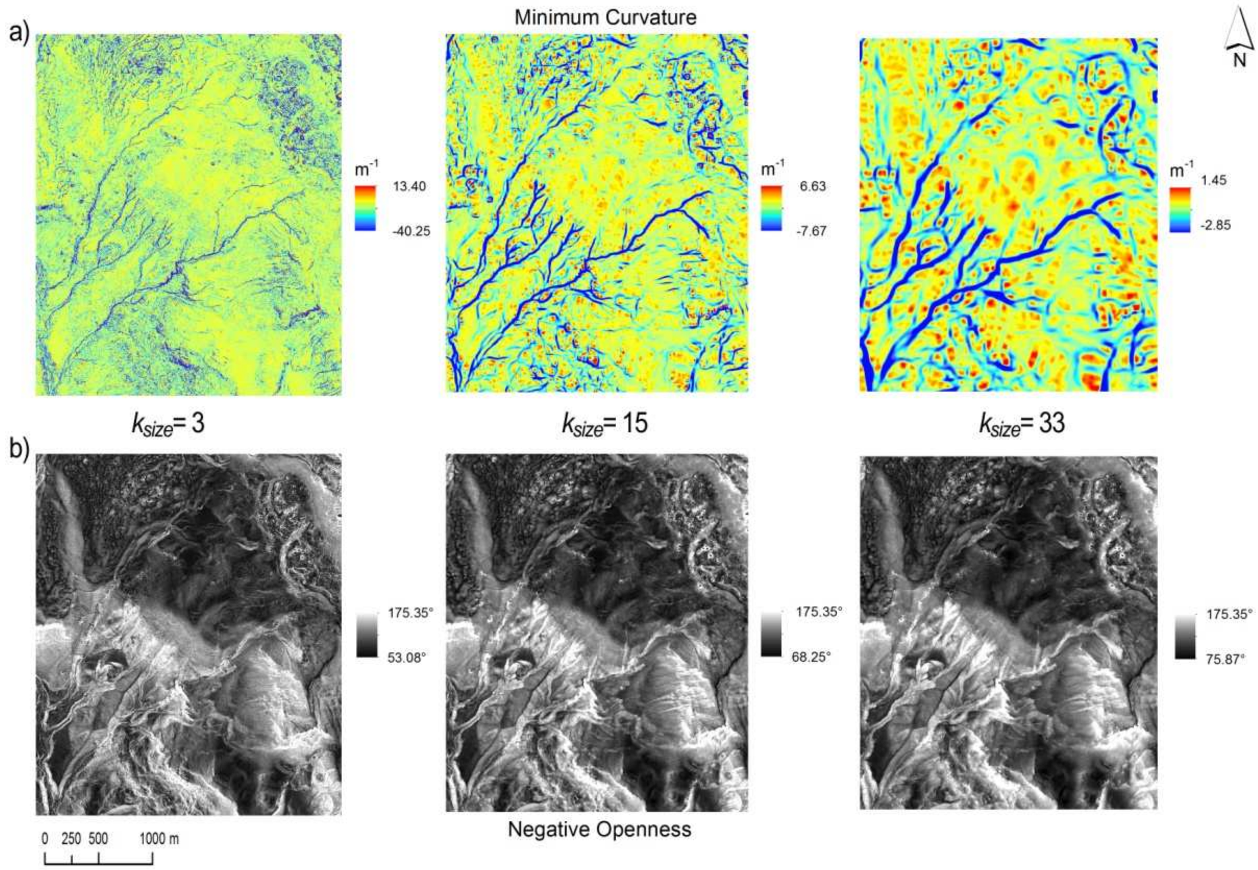

Fig. 53 Example of kernel size effect on minimum curvature (a) and negative openness (b) for the Cordon area according to an increasing window size (k_{size}) of 3, 15 and 33 cells. (modified from Sofia et al.2011)

2.1 Optimum scale selection

Considering the previous experience, in this approach the idea was to find a way to objectively select the scale of analysis. This is carried out through the procedure described in Chapt. 4.2, Sect. *III.Materials and methods*. Values of the height of a smoothed surface tend to have a symmetric distribution in a well selected window with slow-changing terrain (Bartels et al., 2005), but in a complex and hilly region, imbalanced terrain elevation affects the histogram distribution, increasing or decreasing its skewness (Yuan et al., 2008). Values of concavities connected to channels, furthermore, have low frequencies, and are usually located in the tails of the distribution. The shape of the distribution, therefore, is influenced both by the morphology but also by the kernel size used to evaluate the topographic parameters, since the aim of the kernel size approach is to provide a filter to mask noises and bring out the meaningful concavities related to channels. An analysis of how skewness varies at increasing windows size has been carried out (Fig. 54). Skewness has been computed for each topographic parameter according to Eq. (37)

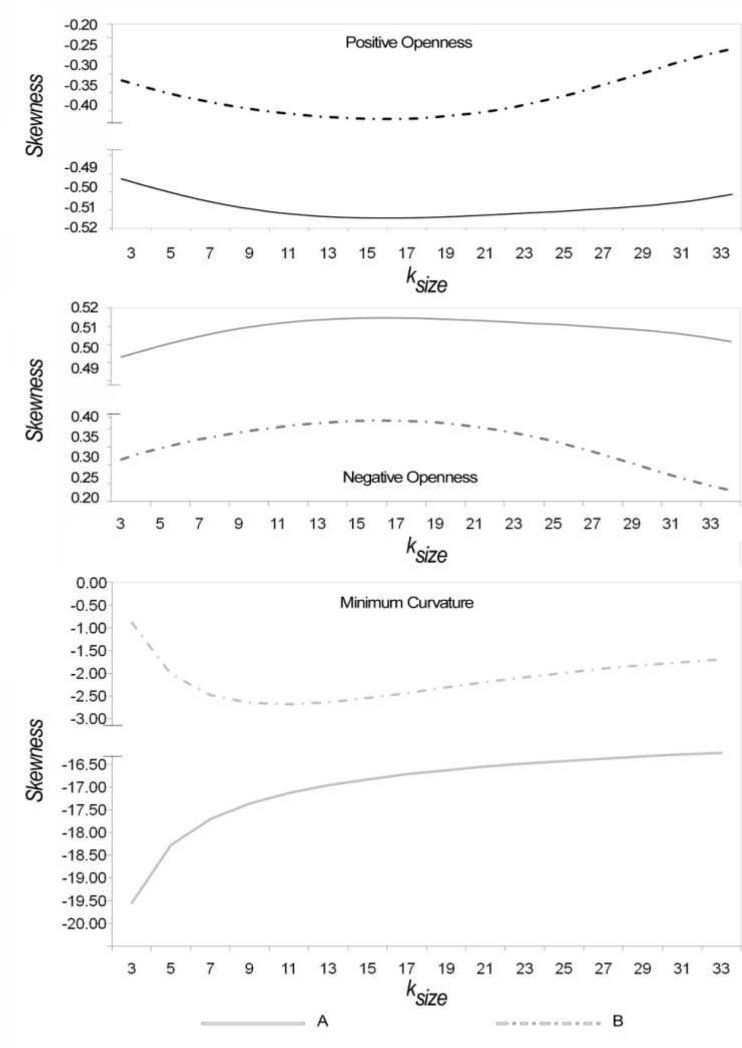

Fig. 54 Skewness for each parameters according to window size (k_{size}) for the Cordon study site (A) and the Miozza basin (B). (modified from Sofia et al.2011)

Considering minimum curvature on the Cordon area (Fig. 54) the increasing of widths of the moving window causes a progressive and slight decreasing of the skewness of the distributions. This is related to the presence of small artifacts in the original DTM that are magnified using a direct surface derivative (minimum curvature). The pattern identified by the $skew_k$ function is comparable both in shape and values with the pattern analyzed in Chapt. 4.3, Sect. *III.Materials and methods*, related to the presence of striping artifacts (i.e. a5, a6 and a7 in Fig. 39 p.100).

Analyzing positive and negative openness in both study cases, instead, and observing minimum curvature for the Miozza basin, it is clear that the increasing the window size causes a skewing of the distributions of these parameters up to a certain point: skewness values become higher in the negative or positive domain until a maximum value is reached. After that, the increasing of the window size is related to a decreasing of skewness: the distributions slightly and slowly move toward less skewed shapes (Fig. 54a and 54b). This behavior is related to the fact that up to a certain scale (the optimal one), the kernel size approach succeeds on enhancing channelized features in spite of noises, but when the kernel size becomes too wide, the resulting maps are too smooth, masking all noises but at the same time, losing important feature details (Pirotti and Tarolli, 2010; Tarolli et al., 2010), therefore, the distributions move toward less skewed shapes (skewness slightly decreases in the negative domain). Based on the theory expressed in Chapt. 4.2 Sect. *III.Materials and methods*, the optimum kernel width is the one identified at the first point where the change in the window size loses its meaningful effect: it refers to the minimum kernel size that determines a break in the feature enhancing and noises decreasing effects. To correctly represent the effect of kernel sizes on the skewness, for each of the datasets (minimum curvature, positive and negative openness), the polynomial defining skewness as a function of window widths in a least square sense ($Skew_{k,}$ Eq. 37 p.89) has been computed. The identification of stationary points is then mathematical and objective, and it is based on a differentiation approach: the stationary point is the point where the derivative of $Skew_k$ is equal to zero.

In this peculiar case, considering that, due to errors on the DTM, in the Cordon basin minimum curvature $Skew_k$ does not have a real inflection point, the approach of defining the polynomial and identifying its stationary point is defined as polynomial "fitting/enforcing". The polynomial orders (*n* in Eq. 37 p.89) is automatically and iteratively chosen in order to provide a curve having at least a derivative equal to zero at one point n included within the adopted kernel size range (3–33). It is a fitting procedure that is enforced, when it is necessary, to obtain a stationary point within the kernel size range. The polynomial "fitting/enforcing" is totally automatic and does not require the user to observe the data or to assess them: it is a recursive fitting/differentiating procedure automatically executed in a loop, that continues until the condition (stationary point is a real number within the window size range) is verified. The accomplishment of the condition forces an immediate exit of the loop code, providing the equation of the polynomial and the value of the optimum kernel size to apply. The polynomial "fitting/enforcing" approach has also a further meaning for future practical application of the method. The first aim is to avoid some evaluation of topographic parameters: it is necessary to compute fewer maps, considering fewer windows; the only constraint is to have the minimum (k_{size} = 3), some average sizes (k_{size} = 15; k_{size} = 17) and the maximum width (k_{size} = 33), to evaluate the $Skew_k$ behavior. The second aim refers to the objectivity of the method.

In this case, the "fitting/enforcing" approach allows to define the stationary point even for the Cordon case, by forcing the representative minimum curvature $Skew_k$ (Fig. 55).

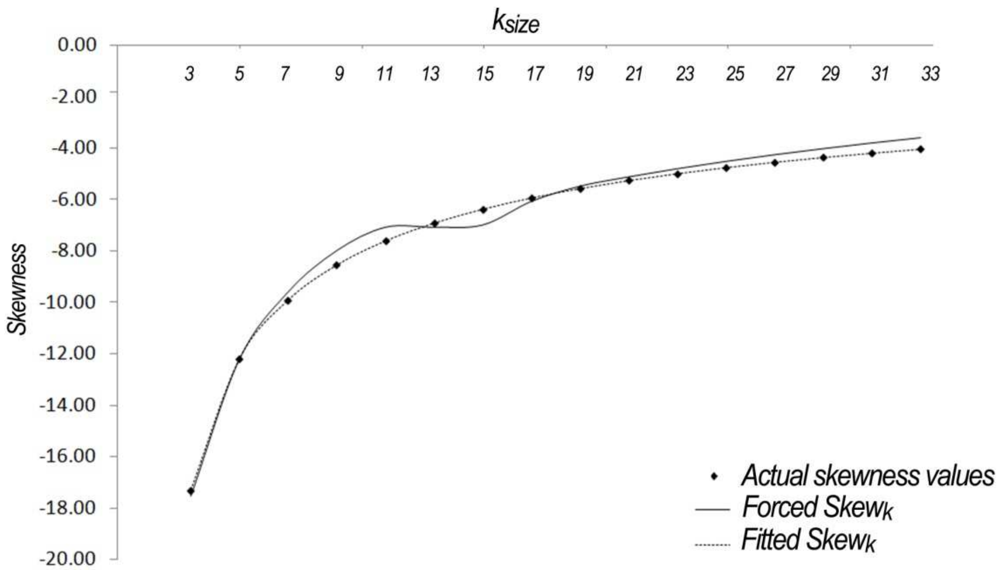

Fig. 55 Example of the result of the fitting/enforcing approach for the Minimum Curvature in the Cordon study area. The fitted $Skew_k$ represents the first attempt to define a relationship between the actual values of skewness and each moving window size, that has no stationary point. The forced $Skew_k$ obtained by the proposed procedure, defines a function with an actual inflection point, at about k_{size}=11.

Once each $Skew_k$ is defined, the identification of the stationary point is automatic. For minimum curvature, this value refers to k_{size} = 11.56 for the Cordon area (Fig. 55) and k_{size} = 10.54 for the Miozza one. On the Cordon area, considering positive and negative openness, skewness derivative vanishes at k_{size} = 15.54 for both cases. On the Miozza basin, positive and negative openness derivatives vanish for k_{size} = 15.16 for both cases.

For topographic parameters elaboration, the kernel size has to be an integer odd number. Therefore, stationary point values have been rounded to the closest odd integer. According to the proposed procedure, a kernel of k_{size} = 11 has been chosen for minimum curvature on both areas. To give homogeneity to the evaluation of the parameter among zenith and nadir angles, the mean value between the values of positive and negative openness' stationary points coordinates (15.54 and 15.16 for the Cordon and the Miozza site, respectively) have been rounded to k_{size} = 15. One should note that for both the study areas, according to this methodology, the same windows sizes have been chosen, without any subjective decision. These values are statistically derived, but they do not imply a similarity on the areas morphology. The optimum values (15 and 11 cells, corresponding to 15 and 11m) identified with the proposed procedure coincide with kernel widths that have been proven to be the best for feature extractions in the works by Pirotti and Tarolli (2010) and Tarolli et al. (2010), respectively.

2.2 Flow convergences recognition

Once the scale of analysis is automatically chosen, the approach proceeds with the recognition of flow convergences. This operation is based on a multiple flow direction algorithm (Quinn et al., 1991), slightly modified in order to incorporate local morphological conditions depending on local concavity (evaluated according to the two proposed indexes) (See Chapt. 3.2, Eq. 28, p.79). The weight matrix applied to the upslope area, derives from the combined use of openness and curvature. Obviously, the two parameters do not have comparable values (m^{-1} for curvature and degrees for openness), but the interest here is focused on their capability to highlight meaningful concavities. The idea is therefore, to normalize both maps, according to a threshold able to highlight these concavities.

For maps normalization, for each attribute map the QQ-Plot threshold is computed (same approach as described for maximum curvature and described in Fig. 33 p.88). The choice of the QQ-Plot in this instance, has been done considering that the same threshold has been proven to be highly effective for network extraction in other studies (Lashermes et al. 2007, Passalacqua et al. 2010a,b). Furthermore, while for curvature, the different statistics assume similar values (see i.e. Tab. 6 p. 108), when using openness, classical statistics as standard deviation assumes values that are too low to be considered as thresholds (σ for example, is in all cases lower than the minimum registered value), while the QQ-Plot assumes ranges comparable to the actual values registered in the map (Tab. 7).

Table 7: Comparison of descriptive statistics for openness maps for the Cordon area, according to window size (k_{size}*)*

	Negative openness (°)					Posotive openness (°)				
k_{size}	*Min*	*Max*	*Mean*	*σ*	*QQ-plot$_{thr}$*	*Min*	*Max*	*mean*	*σ*	*QQ-plot$_{thr}$*
3	34.37	140.62	87.43	9.85	95.42	33.30	136.21	88.68	9.41	96.42
5	34.07	128.85	85.02	8.97	90.15	33.30	124.03	86.28	8.60	91.23
7	33.40	123.54	83.76	8.57	88.70	32.82	119.62	85.03	8.30	89.89
9	32.54	121.67	82.95	8.37	87.79	32.21	117.80	84.24	8.22	89.13
11	31.98	121.67	82.36	8.26	87.15	31.90	116.31	83.68	8.25	88.61
13	31.31	121.61	81.89	8.19	86.68	30.81	115.05	83.25	8.35	88.27
15	30.86	121.01	81.51	8.16	86.31	29.98	113.07	82.89	8.47	88.00
17	30.40	120.81	81.18	8.14	86.00	29.73	110.80	82.59	8.61	87.80
19	30.01	120.81	80.89	8.13	85.73	28.32	109.79	82.33	8.75	87.65
21	29.76	120.81	80.63	8.12	85.49	27.52	108.75	82.10	8.87	87.53
23	29.59	120.14	80.40	8.11	85.27	27.45	107.84	81.89	8.98	87.41
25	29.37	119.58	80.20	8.09	85.08	27.45	107.28	81.70	9.07	87.28
27	29.25	118.70	80.01	8.08	84.92	27.45	106.49	81.53	9.15	87.19
29	29.15	117.82	79.83	8.07	84.74	27.38	105.07	81.37	9.22	87.11
31	29.01	117.19	79.67	8.05	84.60	27.06	103.94	81.22	9.27	87.04
33	28.85	116.26	79.52	8.04	84.44	26.79	103.38	81.09	9.32	86.96

For negative openness (ψ_L), the break is considered for the higher values (right tail of distribution), while for positive openness (ϕ_L), the break is considered for the lower values -left tail- (Eq. 46, 47). For C_{min}, we evaluate the break on the negative side that, following Evans' approach, corresponds to convergent topography (Evans, 1979; Wood, 1996).

Resuming these formulations, channels are identified where

$$\psi_L > \mathrm{QQplot_{thr}} \quad 46$$

$$\phi_L < \mathrm{QQ\ plot_{thr}} \quad 47$$

$$C_{\min} < \mathrm{QQ\,plot_{thr}} \quad 48$$

Maps normalization has been evaluated according to QQ-Plot$_{th}$ using the procedure

$$N_{TA} = f\left(\frac{1}{QQplot_{thr}}, TA_{(x,y)}\right) \quad 49$$

where N_{TA} stands for the normalized parameter (openness or curvature) considered for a given pixel, and $TA_{(x,y)}$ is the topographic attribute at the pixel of interest.

The obtained weight grid W (Eq. 28 p. 79, Eq. 50, Fig. 56D and 57D) refers to:

$$W = \frac{\left(N_{C_{\min}}\right)\cdot\left(N_{\psi_L}\right)}{\left(N_{\phi_L}\right)} \quad 50$$

where N stands for normalization procedure according to Eq. (49). To assign higher values to convergent topography, the positive openness normalized map appears as 1/ $N\phi_L$.

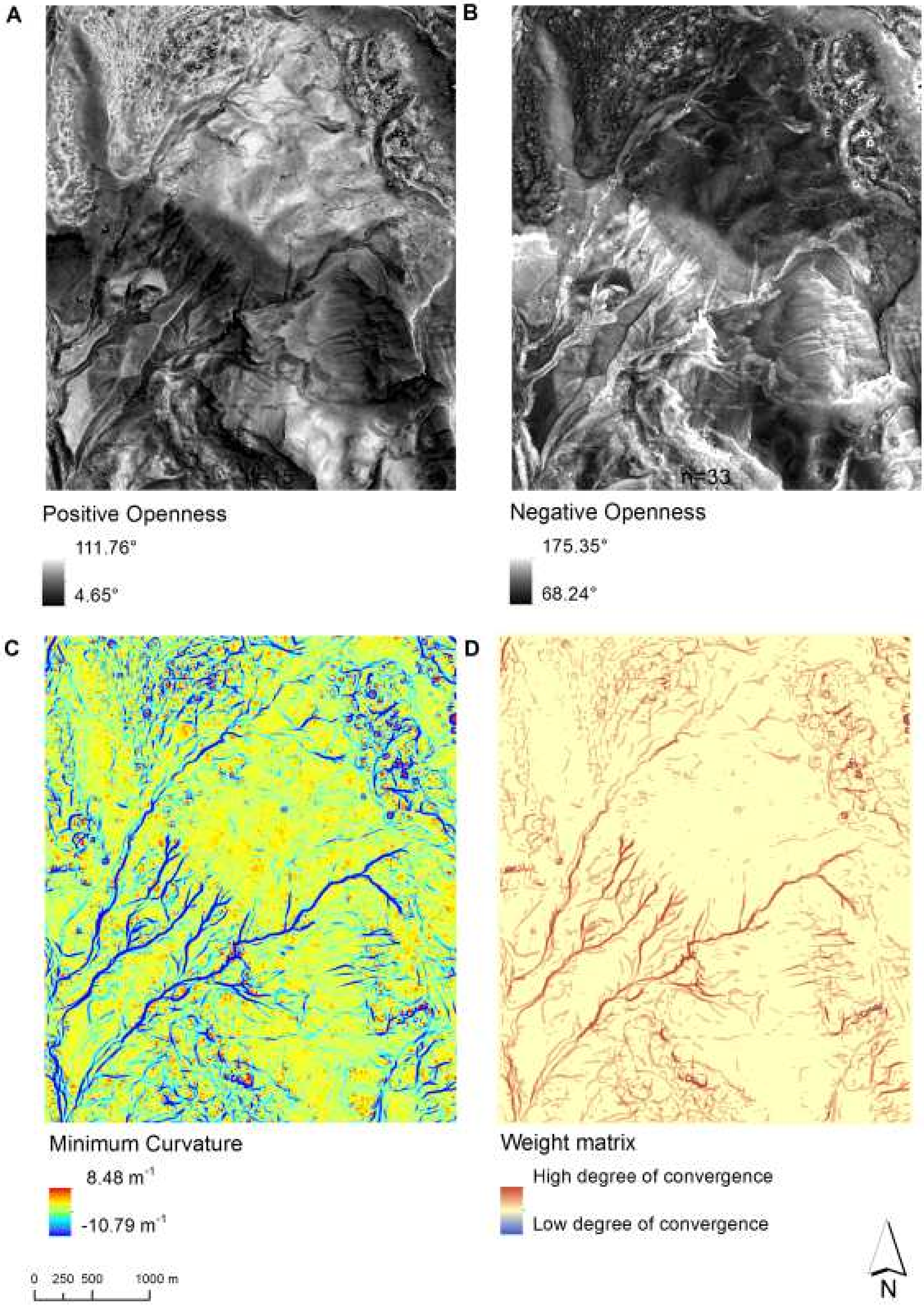

Fig. 56 ***C****ordon study area: positive (A) and negative (B) openness, minimum curvature (C) and weight matrix (D) derived through normalization and overlapping.*

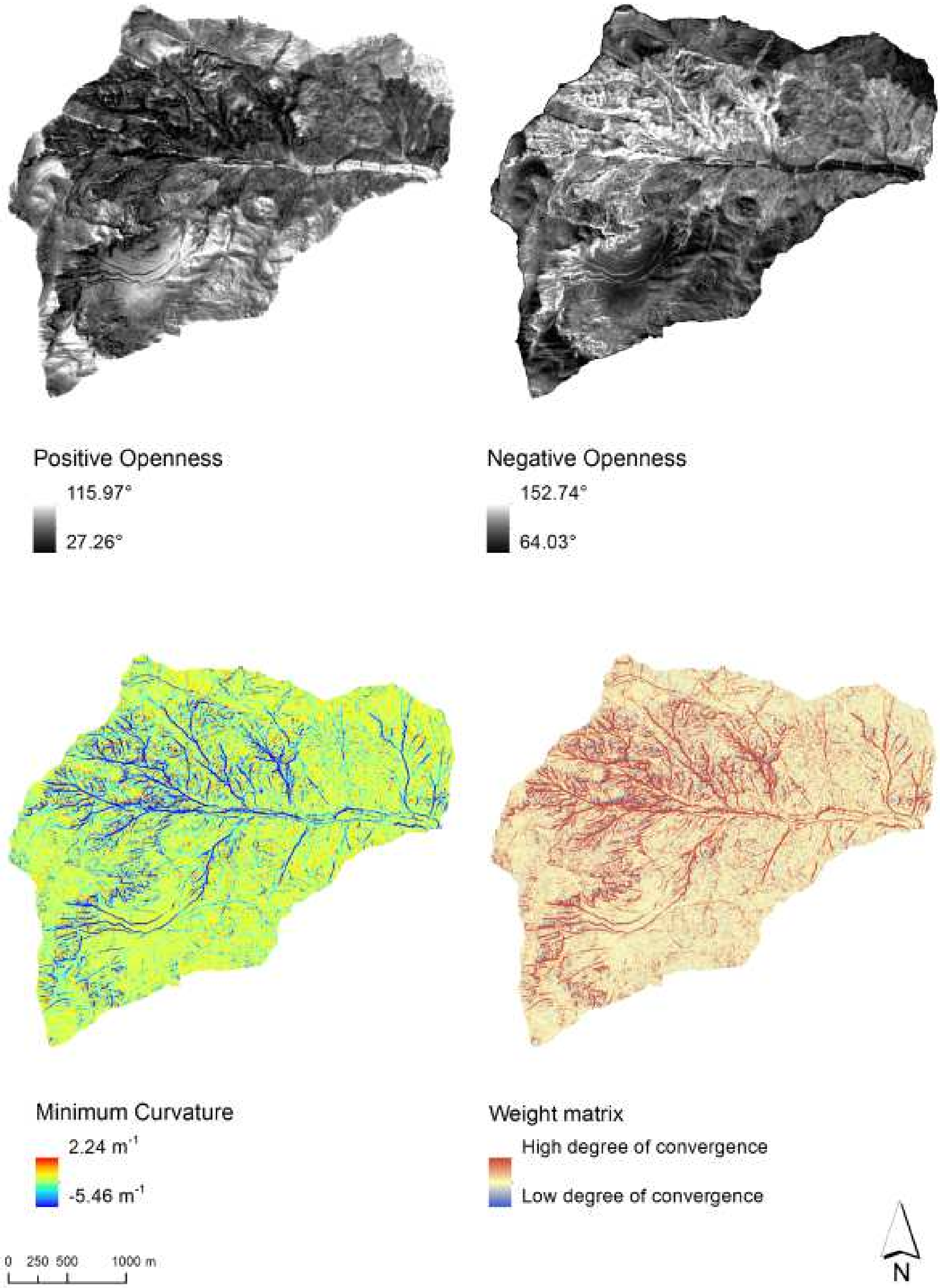

Fig. 57 Miozza basin: positive (A) and negative (B) openness, minimum curvature (C) and weight matrix (D) derived through normalization and overlapping.

2.3 Network detection

Field surveyed channel heads for the study area show that observed contributing areas vary significantly (Chapt. 1.1, Sect. *II.Study sites*) and this suggests that a constant value for network extraction might not be a good assumption (Passalacqua et al., 2010b). Average contributing area can be used, but the resulting drainage densities are too high (Passalacqua et al., 2010b). Accurate and objective location of channel network remains therefore, a challenge. For the present work, the idea is to identify these features using an objective threshold dependent on the weighted upslope area distribution. Considering that the datasets derived from different distributions, both weighted upslope maps have been normalized in order to allow comparison, according to a standard score approach (Eq. 36, p.85), indicating how many standard deviations each observation is above or below the mean. The network is then identified for $zscore_i$ greater than 0, a position in the exact middle of the distribution. After this thresholding, the obtained network is still fragmented: direct application of openness and curvature produce typically segmentation of the resulting raster, because of the numerous local convergences that exist in real surfaces due to inherent noise. To compute correct hydrological characterization of the network, its connectivity need to be accounted for. The use of the weighted upslope area allows a better connection of the network, but noises are still relevant (i.e. Fig. 59). For areas with a low degree of morphological complexity (Miozza), noises can be easily discarded on the produced map through simple filtering based on the majority of contiguous neighboring cells. When the procedure is applied to areas with complex morphology (Cordon, Fig. 3, p.37), noise detection becomes more challenging, as already underlined in the previous DTA approach.

It is generally difficult to obtain relevant indicators automatically without any interaction by the user. The approach proposed in this instance is not fully automatic, but it can be used to assist on the task of identifying the network and of discarding objectively meaningless extractions.

To discard false positives (noises), it is useful to analyze regions that show high fragmentation. For these areas, it is possible to evaluate disruption magnitude to mark a morphological disorder. The idea is that noises can be related to higher randomness of values of the original elevation data, while concavities related to channels refer to patterns with a better structure. A good representation of the elevation organization can be identified through the analysis of water movement for each cell. The basic assumption of the flow function is that if the value of a cell in the immediate eight-cell neighborhood is greater than the value of the processed cell, it will flow into the ita. This flow corresponds to the way water moves into locations at lower elevations or to the way contaminants migrate to areas with less concentration. To test whether a particular neighborhood cell will flow into the processing cell, the value of each neighborhood cell is subtracted from the processing cell. If a value is positive, the neighborhood cell does not flow into the processing cell; if it is negative, it does.

If no cells flow, the location will receive a value of zero. The representation of the combination of flow from multiple neighborhood cells is accomplished through a binary representation of the considered neighborhood. Each bit of the binary representation for the processing cell correlates to a neighborhood cell location—the neighbor to the immediate right is 1, the neighbor to the lower right is 2, and so forth—until the value of 128 (powers of two, since representation occurs in binary), the neighbor to the upper right, is reached (Fig.58).

A — *Binary values*

32	64	128
16		1
8	4	2

B — *Elevation (m)*

11	8	13
7	10	9
6	12	8

C — *Flow*

	164	

Fig. 58 Binary representation of a 3x3 neighborhood (A). The central pixel is the processed one for which flow accumulation is computed. In (B) an example of elevation for the neighborhood is given, and in C the computation of flow for the central pixel is shown: in this case, pixels that contribute to the flows (highlighted in this figure by light grey) are the one having higher elevation than the central one. The computed flow is given by the sum of their binary values, in this case 128+32+4 =164.

The above encoding assigns a unique number to each possible combination of upstream numbers. The total number of combinations of flow into a processing cell is 255, and flow values range from 0 to 255. A cell into which no adjacent neighbor flows assume value 0, while a cell into which all adjacent neighbors flow would receive a value of 128 + 64 + 32 + 16 + 8 + 4 + 2 + 1 = 255.

In order to test the degree of organization of this map, a statistical measure of randomness, Entropy (Chap 3.1.e) can be considered, measuring the distribution of flow direction within a considered neighborhood. For class definition (to use in Eq. 26, p.75), 256 classes have been identified, so that each bin corresponds to a possible flow value. To maintain homogeneity with the full procedure, cell neighborhood for entropy evaluation has been defined according to an average window size (k_{size} = 13) between the chosen ones for curvature and openness.

Minimum entropy occurs when the cell values are all located in the same class, while maximum entropy occurs when each cell value is located in a different class interval. The most homogeneous areas have therefore, a low spatial entropy; this is the case for channel patterns. The most irregular regions have a high entropy. This entropy map can be used as a guidance tool on areas where extraction produces not clear results. Extractions obtained in areas with values of entropy higher than the average should be discarded (Fig. 59).

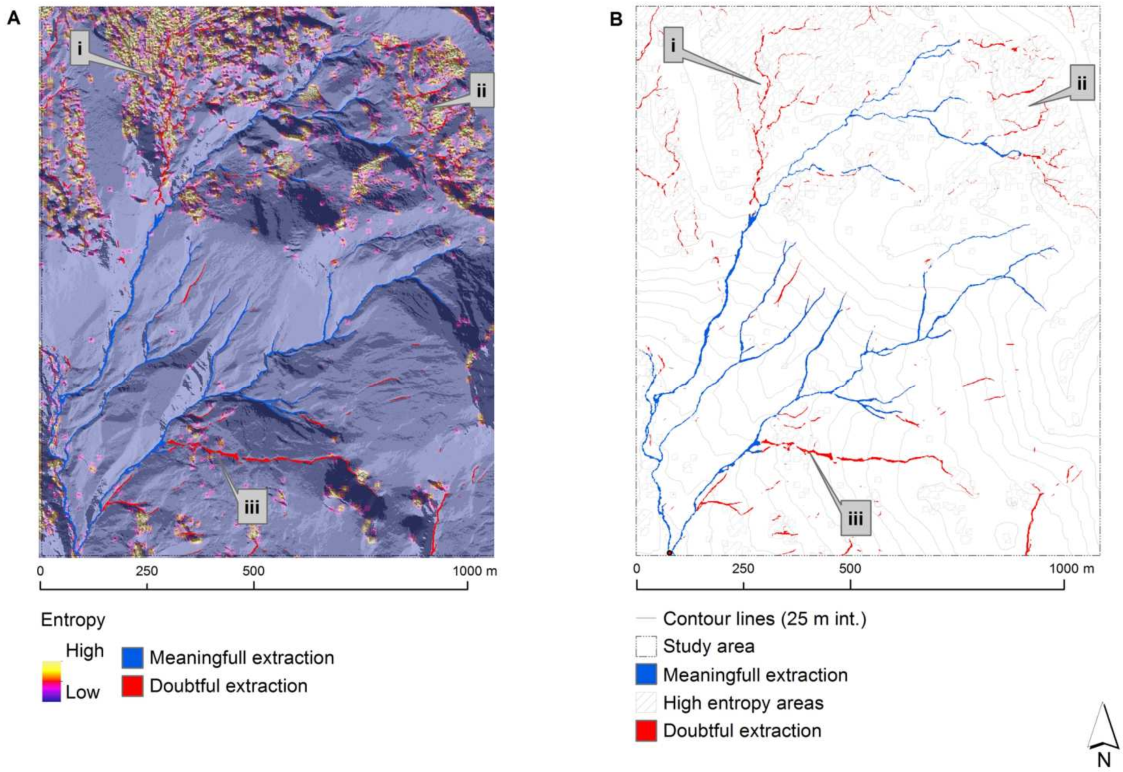

Fig. 59 Cordon study area: local entropy according to flow convergences (A) and identification of meaningful (blue) and doubtful (red) pixels (B) (Sofia et al. 2011)

Some noises can be withdrawn according to this analysis (El. i, ii in Fig. 59). Element iii in Fig. 56 refers to a channel referenced on maps but actually not active on the area. Therefore, consistently with other works (Passalacqua et al., 2010b), it has not been considered for quality evaluation.

2.4 Network connection

Once the two filtering approaches are applied (majority filter for the Miozza basin and entropy analysis for the Cordon area) the remaining network needs a connection procedure. Approaches to network connection have been successfully tested in the work of Passalacqua et al. (2010a,b) where channel networks were detected using non linear diffusion and geodesic path. Considering a pour point (maximum value of flow convergences), it is possible to identify the most suitable (shortest) flow path from each channel head to the pour point. This path is defined as the least accumulative cost distance to the pour point over a cost surface. A fuller discussion of accumulated cost surface methods, and representational accuracy can be found in Douglas (1994) and Eastman (1989).

The challenge is to choose among all the possible connecting paths for the missing features the one that minimizes the cost of traveling from the channel heads to the pour point. This cost is represented by the distance between each possible location and the extracted features. The computational approach is to define, for each pixel, this cost value *j* (Eq. 47 and 48).

The cumulative cost evaluation is then based on an eight-neighbour-cell algorithm. For any given movement to a cell *i* the cumulative cost ($J_{(i)}$) is calculated as the accumulated cost to reach cell *i* ($\sum_{m=1}^{i-1} j_m$) plus the average cost to move through two contiguous cells, multiplied by the cell size (*g*) (Eq. 50 and 51).

For vertical and horizontal generic movements, the cost evaluation refers to:

$$J_{(i)} = \frac{g}{2}\left[j_i + 2\sum_{m=1}^{i-1} j_m \right] \qquad 51$$

while for diagonal movements the cumulated cost is evaluated through

$$J_{(i)} = \sqrt{2}\,\frac{g}{2}\left[j_i + 2\sum_{m=1}^{i-1} j_m \right] \qquad 52$$

where *j* is the numerical value representing the cost for each cell (Corry and Lafortezza 2006).

The ‘shortest path evaluation’ is then carried out using the standard Dijkstra algorithm (Dijkstra 1959). Dijkstra’s algorithm implementations allow the finding of shortest path by systematically generating different path nodes and testing them against a destination node (*v*). For a given pair of vertices *s* and *v*, the algorithm finds the path from *s* to *v* with lowest cost (Lee and Stucky 1998). The algorithm works by keeping for each vertex *v* the cost *d*[*v*] such that some path from s to v has a total cost of *d*[*v*]. Initially, this value is 0 for the source vertex *s* (*d*[*s*]=0), and infinity for all other vertices. By proceeding in the computation, the tentative costs decrease until for each vertex v, *d*[*v*] represent the cost of a minimum-cost path from *s* to *v* (Tarjan 1983). The basic operation of Dijkstra's algorithm is vertices partitioning into three sets: unlabeled vertices (with infinite tentative of *d*[*v*] evaluation), labeled vertices (with finite tentative of cost evaluation whose minimum is yet unknown) and scanned vertices (with *d*[*s*] corresponding to minimum cost). Computation is applied and in each step sets are updated until all values *d*[*v*] represent the cost of the shortest path from *s* to *v* and all vertices are labeled. Main advantage of such kind of approach is that the computation can be terminated as soon as each *v* become definitely labelled and this can be usually translated to significant computational savings if the destination nodes are in relatively close proximity to the source node (Zhan and Noon 1998).

2.5 Accuracy assessment

The final product is a map representing the channel network (Fig. 60b and 61b).

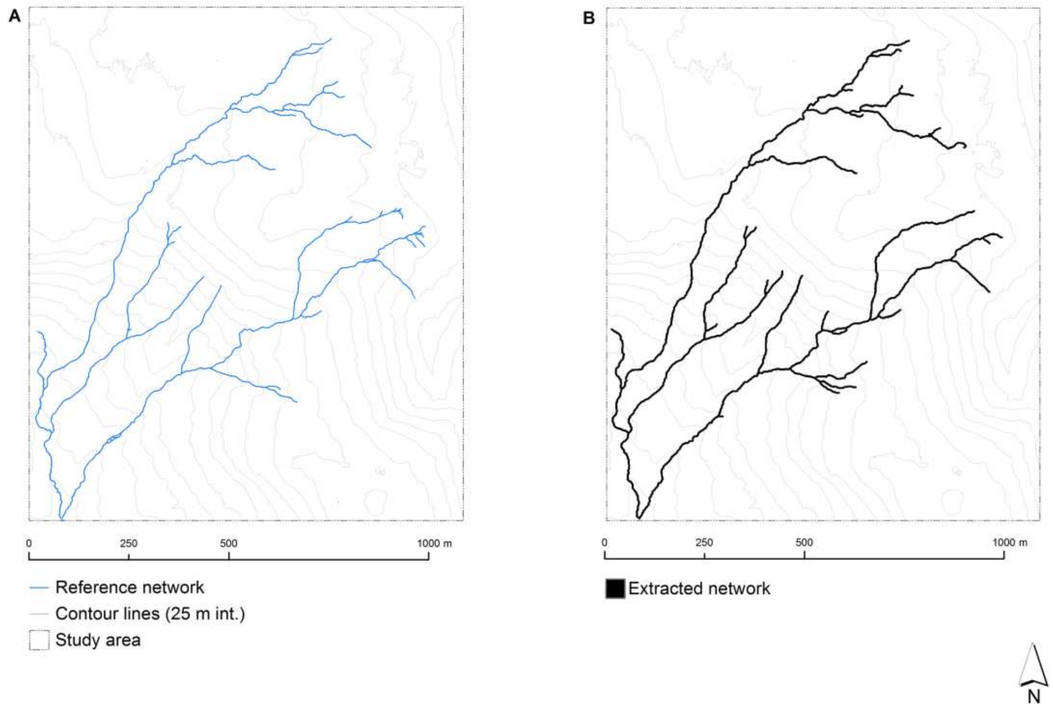

Fig. 60 Cordon study area: reference network (A) and network extracted through the proposed methodology (B). (Sofia et al. 2011)

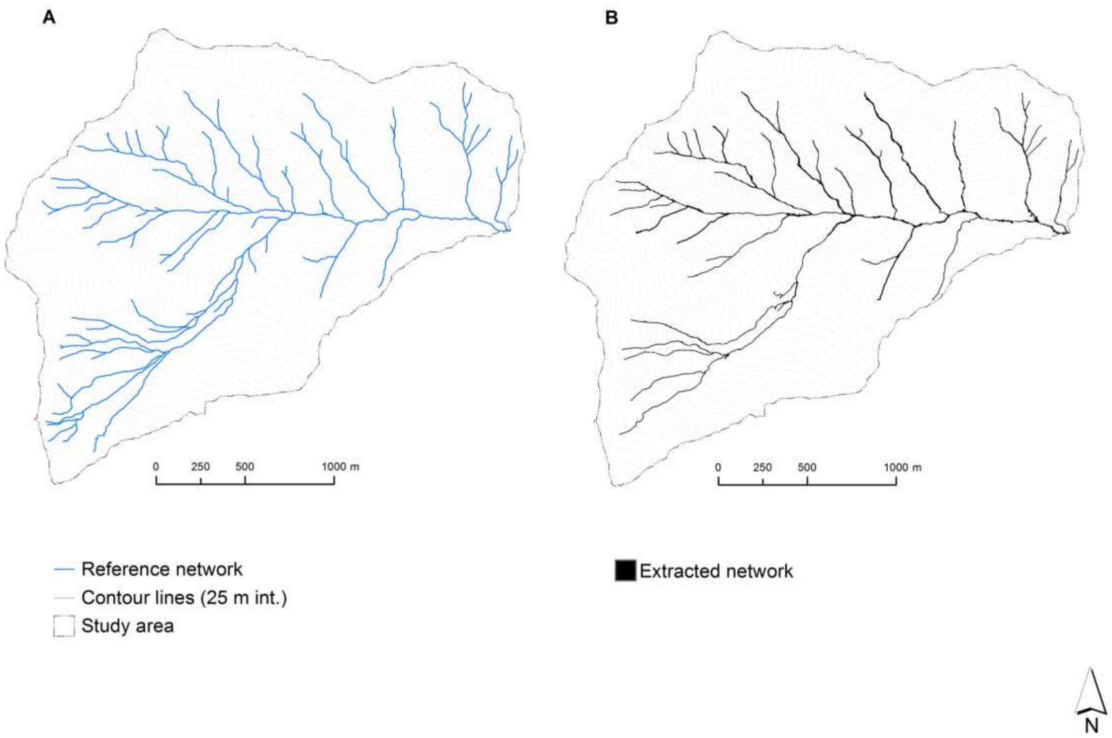

Fig. 61 Miozza basin: reference network (A) and network extracted through the proposed methodology (B) (Sofia et al. 2011)

For accuracy assessment, the extracted networks have been compared with a DGPS surveyed network (Tarolli and Dalla Fontana, 2009; Pirotti and Tarolli, 2010) (Fig. 60a and 61a). The overall quality has been evaluated considering Cohen's *k* index of agreement (Cohen, 1960).

The quality measure used for this accuracy assessment was defined as

$$k_{Cohen's} = \frac{P_a - P_e}{1 - P_e} \qquad 53$$

where P_a is the total agreement probability evaluated according to Eq. (54), and P_e is the agreement probability due to chance, according to the formulation in Eq. (55) (Cohen, 1960).

$$P_a = \sum_{i=1}^{l} P(x_{ii}) \qquad 54$$

$$P_e = \sum_{i=1}^{l} P(x_{.i})P(x_{i.}) \qquad 55$$

where *i* is the number of class values, $P(x_{.i})$, $P(x_{i.})$ are the columns and rows marginal probabilities, respectively and $P(x_{ii})$ are the agreeing extracted values.

Perfect agreement results in a Cohen's *k* value of 1.0, while a value of 0 indicates a level of agreement due to chance alone. A reference scale does not exist for Cohen's *k* for hydrological applications, but some reports about the application of this index in other fields exist. These studies suggested a scale for Cohen's *k* and its level of agreement between datasets: values of *k* lower than 0.20 indicate slight agreement, 0.20-0.40 represent a fair agreement, 0.40-0.60 moderate agreement, 0.60-0.80 substantial agreement, and 0.80-1.00 indicates almost perfect agreement (Landis and Koch, 1977).

To evaluate the index, buffer zones were generated around the extracted network as well as the reference one. The chosen buffer width was set to 5 m according to a previous work carried out on the Cordon area, where analysis of results had been performed using the same quality measure (Pirotti and Tarolli, 2010). To maintain homogeneity, the same buffer width has been considered for both the Cordon and the Miozza case study.

The extraction procedure generates a network characterized by a substantial agreement between extracted features and reference ones for both applications: Cohen's *k* are 0.78 and 0.63 for the Cordon area and the Miozza basin respectively.

A comparison between the proposed morphological approach, and a network derived through a constant contributing area threshold is presented in Fig. 62, for the Cordon study site. In the proposed example, the extraction based on contributing area uses as threshold the average value of the upslope area measured for each actual channel head. Clearly, the more classic area-threshold is not able to correctly represent the network, even if the threshold is computationally realistic. This is in line with other works in literature, that underlined how a unique value of contributing area is not able to fully characterize the network, and classic methodologies do not provide a reliable prediction of channel heads across drainage basins having different morphology and channel initiation depending on different processes (i.e. Passalacqua et al. 2010b, Orlandini 2011).

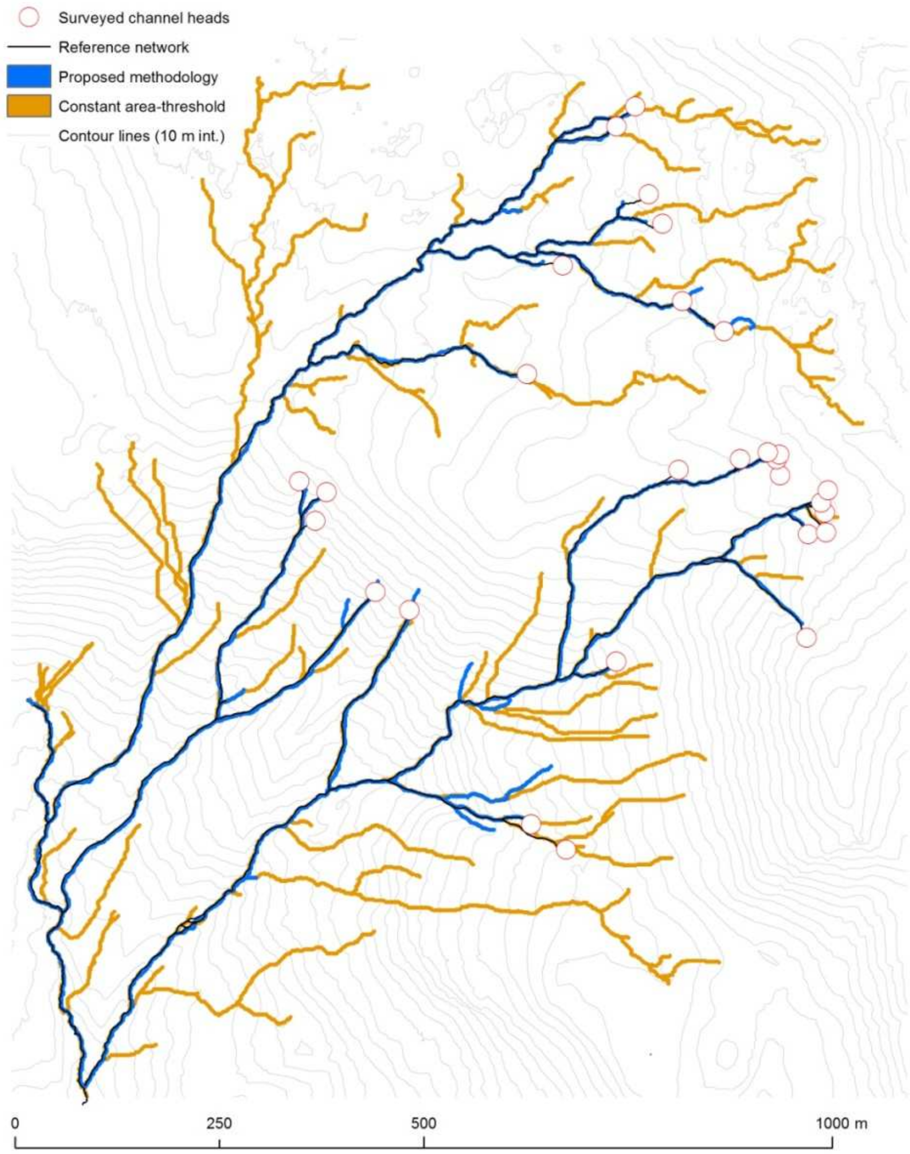

Fig. 62 Comparison with a constant threshold accumulation area extraction for the Cordon study site.

3. *Testing morphometric parameters for features recognition in engineered landscapes*

The DTA proposed in this section can be considered a comparative work, where different topographic parameters at various scales are compared to extrac features in engineered landscapes. In this context, and in particular in floodplains, the creation of the drainage network is strictly connected with the creation of a complex system of embankments, and the conformation of the plain usually brings to operative choices of building roads and structures on scarps. Topographic parameters can be a useful tool to identify these features. The background framework can be found in Chapt. 2.1.a, Sect. *I.Introduction*. The parameters here considered are maximum curvature (Eq. 15), Residual Topography (Eq. 19) and Entropy (eq. 25) (see Chapt. 3.1, Sect. *III.Materials and methods*, for a fuller description). For entropy evaluation, classes to be used in Eq. 26 are computed considering an interval of 0.01 times the DTM standard deviation, and they range from zero to 100 times the DTM standard deviation. This choice is in line with the choice of standard deviation for network extraction in other works in literature (Pirotti and Tarolli, 2010, Tarolli et al. 2010). The DTA starts from a DTM (1 m) available for public authorities in Italy. This DTM derives from a LiDAR survey planned to have highly affordable costs: the survey can be easily repeated during time, providing up-to-date large scale topographic information.

3.1 Testing different approaches to account for scale

Some practical considerations need to be done for the DTA approach expressed in this chapter. It has already been proven that geomorphometric parameters are strongly scale-dependent (Pirotti and Tarolli, 2010; Tarolli et al. 2010, Sofia et al. 2011), and the effects of scales have already been assessed in this thesis dealing with natural features in chapts. 1 and 2, Sect. *IV.DTA for feature recognition*. However, scale effects in different environments have not been tested, and scale accounting through a square moving window (see Chapt. 2.2, Sect. *III.Materials and methods,* and Chapt. 1 and 2 Sect. IV.DTA *for feature recognition*) in engineered landscapes might not be the best approach. Within the context of feature classification, in fact, appropriate scales for derivation of the local geometry have to be selected according to the semantic terrain model implied by the application (Schmidt et al., 2003), and the elevation characteristics captured by terrain are of course different, in mountainous environments and floodplains.

In the two DTA approaches reported in Chapt. 1 and 2 Sect. IV.DTA *for feature recognition*, as in other examples reported in literature (Wood, 1996; Pirotti and Tarolli, 2010; Tarolli et al. 2010; Sofia et al. 2011), filters are computed among a squared window with a local coordinate system (x, y, z) defined with the origin at the pixel of interest (central pixel, see Chapt. 2.2, Sect. *III.Materials and* *methods).* In some other applications, however, it is preferable to compute the moving filters in a non-rectangular window (Glasbey and Jones, 1997). In particular, for rotationally invariant (i.e. isotropic) filters, the window should be circular (Glasbey and Jones, 1997). For example, Davies (1984) showed the benefits of circular windows, and octagonal approximations, in the context of edge detection. This type of filter is at the base of REA (Eq. 14) evaluation, as it has been applied i.e. in Carturan et al. (2009).

Considering this literature review, and considering that the addressed features are different in shape and morphology from the features previously analyzed, for the present DTA example, three different shapes of moving window have been applied and tested: rectangular (Fig. 63a), circular (Fig. 63b) and annulus (63c) shaped kernels.

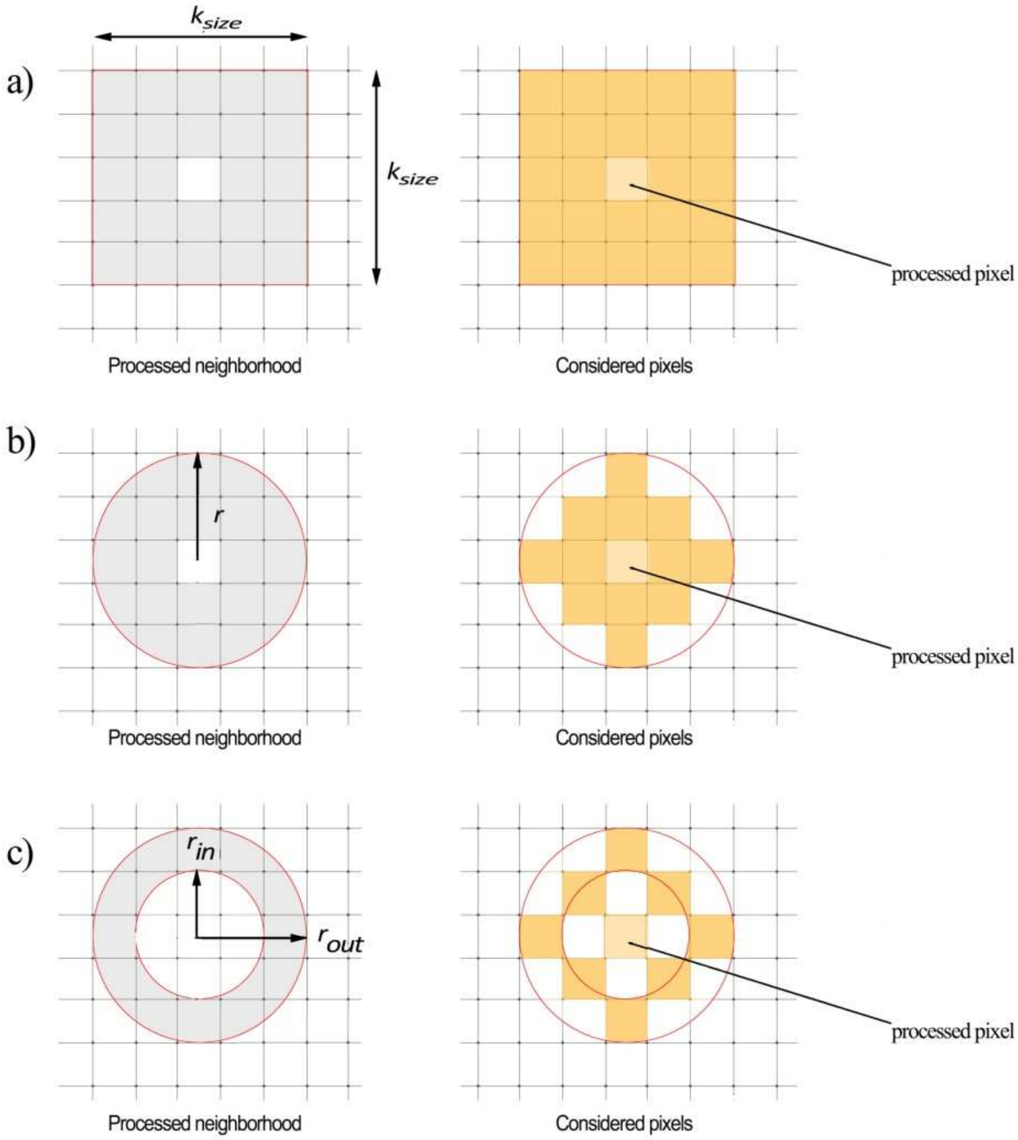

Fig. 63 Tested kernel shapes: rectangular (a), circular (b) and annulus (c).

By defines the shape of a neighborhood as a *rectangle* (Fig. 63a), the processed pixels defined by the kernel size correspond to the same cells in the output block. The kernel sizes need to be large enough for a reasonable number of data to be processed, and its minimum width relies on the fact that sampling windows are centered on the cell of interest. Size constraints refers to Eq. (56).

$$k_{size} \geq (2m + 1) \tag{56}$$

where k_{size} is the width of the kernel and *m* is a positive integer number greater than 0.

When defining the shape of the kernel as a *circle* (63b), the corresponding processed block on the output raster will be the minimum-bounding square who encompasses the circular neighborhood with the diameter *2r*. Any cell completely encompassed by the circle will be included in processing the neighborhood (Fig. 63b). For the circle shaped kernel, the diameter parameter is measured in cells and the computational constraints for the minimum size are two: a) in order to evaluate curvature, the minimum number of processed cells is six (considering that surface is approximated by a quadratic function with six coefficients (Eq. 1, p.56), and b) as for the rectangular kernel, the sampling windows are centered on the cell of interest. Size constraints for the circular kernel, therefore, refer to Eq. (57).

$$2r \geq \left(2\bar{m}+1\right) \tag{57}$$

where 2r is the chosen diameter and $\bar{m}$ is a positive integer number greater than 2.

By defining the shape of the kernel as an *annulus*, the considered neighborhood comprises a smaller circle within a larger circle (a donut shape, fig 63c). The corresponding processed block on the output raster will be the minimum-bounding square who encompasses the annular neighborhood. The required parameters are the inner ($2r_{in}$) and outer ($2r_{out}$) diameters: cells that fall outside the diameter of the inner circle, but inside the diameter of the outer circle will be included in processing the neighborhood. For the annulus shaped kernel, the main size constraint is that the inner diameter must be smaller than the outer one. Further constraints are express in Eq. (58) and (59).

$$2r_{out} \geq \left(2\bar{n}+1\right) \tag{58}$$

$$2r_{in} \geq (2m+1) \tag{59}$$

where $\bar{n}$ is a positive integer number greater than 3, while *m* is a positive integer number greater than 0.

The choice of using different shape of the kernel brings to some algorithm modification for the evaluation of Maximum curvature. It has already been underlined that to perform analysis at multiple scales, maximum curvature can be evaluated generalizing its computation according to a moving window approach (see Chapt. 2.2. and 3.1.b, Sect. III.Materials and methods). For this DTA analysis, the generalization of curvature is carried out according to Eq. 60

$$C_{\max} = q \cdot Curvature_{\max} \qquad (60)$$

where $Curvature_{max}$ derives from Eq. 13, and q is a generalization parameter connect to the size of the processed neighborhood and to the DTM grid size.

In this example of DTA, curvature generalization has been done considering q evaluated according to Eq. 61.

$$q = g \cdot \sqrt{n} \qquad (61)$$

where g is the grid size and n is the number of pixels in the processed neighborhood.

By applying this generalization, if the kernel shape is rectangular, the parameters equal the generalization proposed by Wood (1996), described in 3.1.b, Sect. *III.Materials and methods,* and applied in Chapt. 1 and 2 Sect. *IV.DTA for feature recognition.*

Considering that in this application features dimensions vary up to 50 m, the analysis has been carried out considering scales from 3 up to 55 m for the rectangular kernel, and from 5 up to 55 cells for the circular kernel and the annulus shaped one.

Table 8 shows for the squared kernel and the circular one, the kernel sizes (diameter or width), the value of the corresponding analyzed neighboring (in cells), and the correspondent q considered for curvature generalization (Eq. 60 and 61). For the annulus kernel, table 9a shows the inner and outer diameter sizes and the value of the corresponding analyzed neighboring (in cells), while table 9b shows for the same cases the corresponding q.

Table 8:Considered kernel shape (Rectangle or Circular) and sizes (k_{size}*) for the rectangular and (*$2r$*), extent of the analyzed neighboring (in cells) and the correspondent* q *considered for curvature generalization.*

	Rectangle		Circle	
k_{size} or $2r$	number of cells	q	number of cells	q
3	9	3	-	-
5	25	5	13	5
7	49	7	29	7
9	81	9	49	7
11	121	11	81	9
13	169	13	113	11
15	225	15	149	13
17	289	17	197	15
19	361	19	253	17
21	441	21	317	19
23	529	23	377	21
25	625	25	441	21
27	729	27	529	23
29	841	29	613	25
31	961	31	709	27
33	1089	33	797	29
35	1225	35	901	31
37	1369	37	1009	33
39	1521	39	1129	35
41	1681	41	1257	37
43	1849	43	1373	39
45	2025	45	1517	39
47	2209	47	1653	41
49	2401	49	1793	43
51	2601	51	1961	45
53	2809	53	2121	47
55	3025	55	2289	49

Table 9a: Annulus kernel: diameters sizes ($2r_{in}$ and $2r_{out}$) and extent of the analyzed neighboring (in cells)

$2r_{out}$ \ $2r_n$	3	5	7	9	11	13	15	17	19	21	23	25	27	29	31	33	35	37	39	41	43	45	47	49	51	53
3	-	-	-	-	-	-	-	-	-	-	-	-	-	-	-	-	-	-	-	-	-	-	-	-	-	-
5	8	-	-	-	-	-	-	-	-	-	-	-	-	-	-	-	-	-	-	-	-	-	-	-	-	-
7	24	16	-	-	-	-	-	-	-	-	-	-	-	-	-	-	-	-	-	-	-	-	-	-	-	-
9	44	36	20	-	-	-	-	-	-	-	-	-	-	-	-	-	-	-	-	-	-	-	-	-	-	-
11	76	68	52	32	-	-	-	-	-	-	-	-	-	-	-	-	-	-	-	-	-	-	-	-	-	-
13	108	100	84	64	32	-	-	-	-	-	-	-	-	-	-	-	-	-	-	-	-	-	-	-	-	-
15	144	136	120	100	68	36	-	-	-	-	-	-	-	-	-	-	-	-	-	-	-	-	-	-	-	-
17	192	184	168	148	116	84	48	-	-	-	-	-	-	-	-	-	-	-	-	-	-	-	-	-	-	-
19	248	240	224	204	172	140	104	56	-	-	-	-	-	-	-	-	-	-	-	-	-	-	-	-	-	-
21	312	304	288	268	236	204	168	120	64	-	-	-	-	-	-	-	-	-	-	-	-	-	-	-	-	-
23	372	364	348	328	296	264	228	180	124	60	-	-	-	-	-	-	-	-	-	-	-	-	-	-	-	-
25	436	428	412	392	360	328	292	244	188	124	64	-	-	-	-	-	-	-	-	-	-	-	-	-	-	-
27	524	516	500	480	448	416	380	332	276	212	152	88	-	-	-	-	-	-	-	-	-	-	-	-	-	-
29	608	600	584	564	532	500	464	416	360	296	236	172	84	-	-	-	-	-	-	-	-	-	-	-	-	-
31	704	696	680	660	628	596	560	512	456	392	332	268	180	96	-	-	-	-	-	-	-	-	-	-	-	-
33	792	784	768	748	716	684	648	600	544	480	420	356	268	184	88	-	-	-	-	-	-	-	-	-	-	-
35	896	888	872	852	820	788	752	704	648	584	524	460	372	288	192	104	-	-	-	-	-	-	-	-	-	-
37	1004	996	980	960	928	896	860	812	756	692	632	568	480	396	300	212	108	-	-	-	-	-	-	-	-	-
39	1124	1116	1100	1080	1048	1016	980	932	876	812	752	688	600	516	420	332	228	120	-	-	-	-	-	-	-	-
41	1252	1244	1228	1208	1176	1144	1108	1060	1004	940	880	816	728	644	548	460	356	248	128	-	-	-	-	-	-	-
43	1368	1360	1344	1324	1292	1260	1224	1176	1120	1056	996	932	844	760	664	576	472	364	244	116	-	-	-	-	-	-
45	1512	1504	1488	1468	1436	1404	1368	1320	1264	1200	1140	1076	988	904	808	720	616	508	388	260	144	-	-	-	-	-
47	1648	1640	1624	1604	1572	1540	1504	1456	1400	1336	1276	1212	1124	1040	944	856	752	644	524	396	280	136	-	-	-	-
49	1788	1780	1764	1744	1712	1680	1644	1596	1540	1476	1416	1352	1264	1180	1084	996	892	784	664	536	420	276	140	-	-	-
51	1956	1948	1932	1912	1880	1848	1812	1764	1708	1644	1584	1520	1432	1348	1252	1164	1060	952	832	704	588	444	308	168	-	-
53	2116	2108	2092	2072	2040	2008	1972	1924	1868	1804	1744	1680	1592	1508	1412	1324	1220	1112	992	864	748	604	468	328	160	-
55	2284	2276	2260	2240	2208	2176	2140	2092	2036	1972	1912	1848	1760	1676	1580	1492	1388	1280	1160	1032	916	772	636	496	328	168

Table 9b: Annulus kernel: diameters sizes ($2r_{in}$ and $2r_{out}$) and correspondent q considered for curvature generalization

	$2r_n$																									
$2r_{out}$	3	5	7	9	11	13	15	17	19	21	23	25	27	29	31	33	35	37	39	41	43	45	47	49	51	53
3	-	-	-	-	-	-	-	-	-	-	-	-	-	-	-	-	-	-	-	-	-	-	-	-	-	-
5	3	-	-	-	-	-	-	-	-	-	-	-	-	-	-	-	-	-	-	-	-	-	-	-	-	-
7	5	5	-	-	-	-	-	-	-	-	-	-	-	-	-	-	-	-	-	-	-	-	-	-	-	-
9	7	7	5	-	-	-	-	-	-	-	-	-	-	-	-	-	-	-	-	-	-	-	-	-	-	-
11	9	9	9	7	-	-	-	-	-	-	-	-	-	-	-	-	-	-	-	-	-	-	-	-	-	-
13	11	11	11	9	7	-	-	-	-	-	-	-	-	-	-	-	-	-	-	-	-	-	-	-	-	-
15	13	13	11	11	9	7	-	-	-	-	-	-	-	-	-	-	-	-	-	-	-	-	-	-	-	-
17	15	15	13	13	11	11	7	-	-	-	-	-	-	-	-	-	-	-	-	-	-	-	-	-	-	-
19	17	17	15	15	15	13	11	9	-	-	-	-	-	-	-	-	-	-	-	-	-	-	-	-	-	-
21	19	19	17	17	17	15	13	11	9	-	-	-	-	-	-	-	-	-	-	-	-	-	-	-	-	-
23	21	21	19	19	19	17	17	15	13	9	-	-	-	-	-	-	-	-	-	-	-	-	-	-	-	-
25	21	21	21	21	19	19	19	17	15	13	9	-	-	-	-	-	-	-	-	-	-	-	-	-	-	-
27	23	23	23	23	23	21	21	19	17	15	13	11	-	-	-	-	-	-	-	-	-	-	-	-	-	-
29	25	25	25	25	25	23	23	21	19	19	17	15	11	-	-	-	-	-	-	-	-	-	-	-	-	-
31	27	27	27	27	27	25	25	23	23	21	19	17	15	11	-	-	-	-	-	-	-	-	-	-	-	-
33	29	29	29	29	27	27	27	25	25	23	21	19	17	15	11	-	-	-	-	-	-	-	-	-	-	-
35	31	31	31	31	29	29	29	27	27	25	23	23	21	17	15	11	-	-	-	-	-	-	-	-	-	-
37	33	33	33	31	31	31	31	29	29	27	27	25	23	21	19	15	11	-	-	-	-	-	-	-	-	-
39	35	35	35	33	33	33	33	31	31	29	29	27	25	23	21	19	17	11	-	-	-	-	-	-	-	-
41	37	37	37	35	35	35	35	33	33	31	31	29	27	27	25	23	19	17	13	-	-	-	-	-	-	-
43	37	37	37	37	37	37	35	35	35	33	33	31	31	29	27	25	23	21	17	11	-	-	-	-	-	-
45	39	39	39	39	39	39	37	37	37	35	35	33	33	31	29	27	25	23	21	17	13	-	-	-	-	-
47	41	41	41	41	41	41	39	39	39	37	37	35	35	33	31	31	29	27	23	21	17	13	-	-	-	-
49	43	43	43	43	43	41	41	41	41	39	39	37	37	35	33	33	31	29	27	25	21	17	13	-	-	-
51	45	45	45	45	45	43	43	43	43	41	41	39	39	37	37	35	33	31	29	27	25	23	19	13	-	-
53	47	47	47	47	47	45	45	45	45	43	43	41	41	39	39	37	35	35	33	31	29	25	23	19	13	-
55	49	49	49	49	47	47	47	47	47	45	45	43	43	41	41	39	39	37	35	33	31	29	27	23	19	13

An example of the effect of kernel size and shape on Maximum Curvature is shown in Fig. 64.

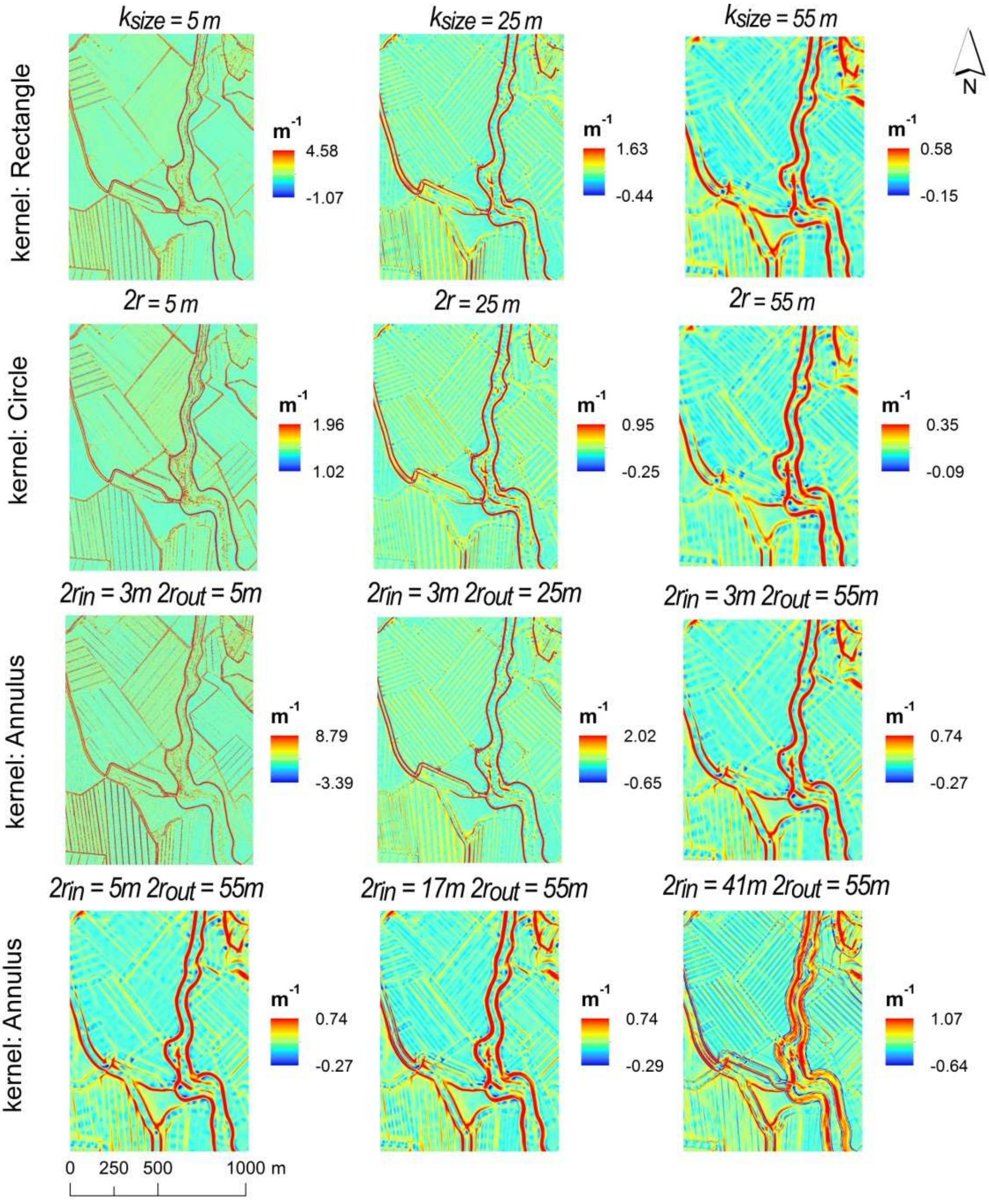

Fig. 64 Effect of kernel shape and size on Maximum Curvature

3.2 Feature recognition

Different authors (Lashermes et al. 2007, Tarolli and Dalla Fontana, 2009, Passalacqua et al. 2010a,b, Tarolli et al. 2010, Pirotti and Tarolli, 2010, Sofia et al. 2011) proved how statistical operators can describe natural process signatures on surfaces and the previous three DTA approaches, underlined the same aspects. The idea to test in the present work is that a statistical approach can be used also to describe anthropogenic features. In the context of floodplains and agrarian landscape, the basic idea is that embankments normally show a much sharper shape than natural terrain features. Furthermore, levee crests mark local maxima of the elevation, and their heights represent outliers in the elevation matrix. Consequently, they represent outliers also within the derived topographic parameters (Maximum Curvature, Residual Topography and Entropy). In this case, the outliers are identified according to the boxplot approach by Tukey (1977) (Chap 4.1.c Sect. *III.Materials and methods*), where points outside the fence can be classified as potential outliers. The idea is that features can be identified by geomorphic parameters values falling outside the upper bound (Eq. 62)

$$TA > Fnc_{up_{TA}} \tag{62}$$

Where *TA* is the considered topographic parameter (Maximum Curvature, Entropy, Residual Topography) and Fnc_{up} is the upper bound as defined in Eq. 32 p.83.

Figure 65 shows an example of Residual Topography map (a) evaluated for the rectangular kernel (k_{size}=21), the derived boxplot and the identified threshold, and the features derived after thresholding the map (b).

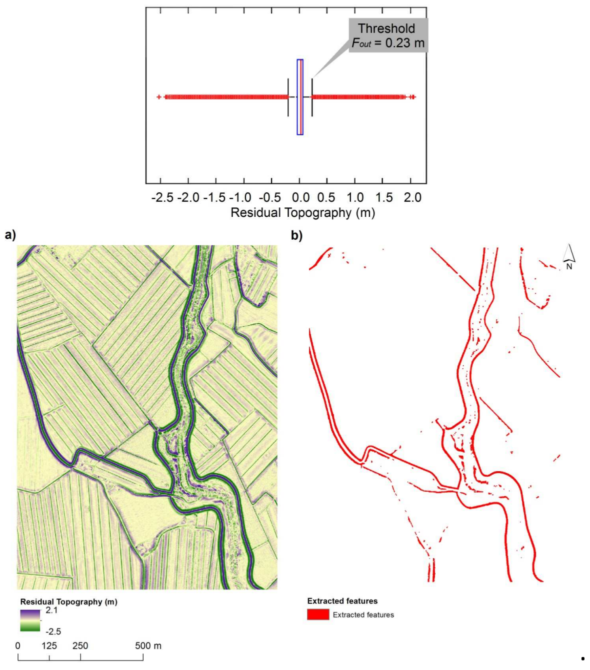

Fig. 65 Example of Residual Topography map (a) evaluated for the rectangular kernel (k_{size}=21), the derived boxplot and the identified threshold (Fnc_{out}=0.23 m), and the features derived after thresholding the map (b).

3.3 Extraction improvement

As in all the other DTA application, after the thresholding, the product is a binary map with pixel values 1 for potential features and 0 for landscape pixels. The binary map can be automatically clustered into fragments (potential features) having the same values (i.e. elements A and B in Fig. 66). These fragments might comprise extraneous details as well as the actual features, and this usually requires the user to select manually which elements are features and which ones are instead false positives. In this section, an automatic procedure is proposed, to improve further the quality of the extractions. The proposed idea is to discard automatically extractions according to their dimension, eliminating small details that can be considered as background noise. The basic assumption is that scarps and levees are elongated elements; therefore, the length of each fragment within the extraction can be a diagnostic tool: when the length of a fragment is an outlier respect the whole extraction, that is the element is '*too short*', that fragment can be eliminated. Outlier lengths are identified with the same technique described for the extraction procedures (Eq. 62), but considering, in this case, elements with lengths shorter than the lower fence (Eq. 31 p.83).

A simplified approach is proposed to evaluate fragment length, where the length of each fragment is defined to be the ratio between the area (number of pixels) of the potential feature and its width. The main advantage of this approach is that it does not require any skeletonization procedures to measure an actual length, avoiding common errors, such as loops or neckings, that are difficult to resolve through automatic procedures, and might require manual interpretation. A further advantage is given by the fact that in this way, also the extent of each fragment (areas and widths) are accounted when evaluating lengths: elements with more round shapes results in smaller lengths and are therefore discarded. In this evaluation the width of each element is computed considering an *inverse Euclidean distance transform* of the binary map. For each potential-feature pixel, the *inverse Euclidean distance transform* assigns a number that is the distance between the centre of that pixel and the nearest zero value pixel (landscape pixel). Higher distances are related to pixels that are on the centerline of the fragment (thus they potentially represent half of the actual width of the fragment in that location) (Fig. 66).

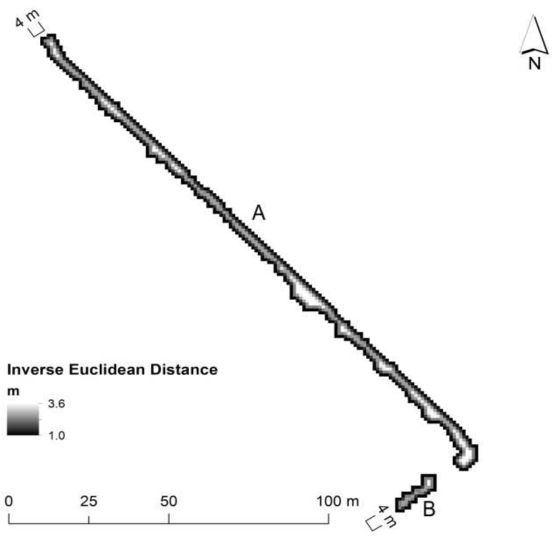

Fig. 66 Example of inverse Euclidean distance for two separate clusters of pixels. Higher values of distance are located on the clusters centerlines. In the considered example, the derived features width is 4.05 m for cluster A, and 4.01 m for cluster B.

To evaluate the overall fragment width, local maximum distance values are computed among a given neighborhood (8 nearest connected neighborhood), and the potential-feature width is assumed to be twice the average value of this local maxima. Lengths, as in the ratio between the area and the width of each fragment, are then automatically evaluated for all the potential features in the area, and their lower fence (Eq. 31 p. 83) is identified. Extractions to discard are at this point the ones having a length smaller than the lower fence. By eliminating from the input map the fragments identified through the proposed procedure, the extraction result more clean, and local extraneous details are automatically removed (Fig. 67).

Fig. 67 Extraction derived after thresholding procedure (a) and the improvement obtained after automatic filtering (b): local extraneous details are automatically removed.

3.4 Accuracy assessment

The evaluation of the proposed methods is made by comparison of the automatically extracted features with the field surveyed ones used as reference data, and is processed in two steps: (1) matching of the extraction with the references and (2) calculation of quality measures. For the matching process, a buffer is created around the reference features with variable widths, according to the average actual width of the anthropogenic feature as measured on the field. Extractions that agree with the surveyed features are labeled as *True Positive* (*TP*), missing extractions are labeled as *False Negative (FN)* and extractions that do not correspond to actual features are marked as *False Positive (FP)*, as already described in *Chapt. 1, Sect. IV.DTA for feature recognition.*

The evaluation of the different methodologies has been done considering at first an overall quality and how this quality is influenced by the following factors:

i. kernel size used for evaluation (ksize for rectangular kernel, 2r for circular kernel and $2r_{in}$ and $2r_{out}$ for annulus kernel)
ii. choice of topographic parameters.

On a second step, three different measures have been evaluated in order to underline better the differences between the approaches, and to underline how the filtering procedure improved the results.

The overall quality is evaluated considering Cohen's *k* index of agreement (Cohen, 1960), defined as already explained in Eq. 53-55. This overall quality measure, as used in Pirotti and Tarolli (2010) and Sofia et al. (2011), aims at assessing exhaustivity as well as geometrical accuracy of the results. In this study case it is also used to compare the results of the different geomorphic parameters and kernel approximations.

To provide a complete quality evaluation on performance, to better underline the differences between the approaches, and to underline how the filtering procedure improved the results, three further quality measure have been proposed (Eq. 63-65) and evaluated (before and after the filtering approach): Correctness, Completeness, and Branching (Heipke et al. 2007, Lee et al, 2003).

$$Correctnes\ s = \frac{TP}{TP + FP} \qquad 63$$

$$Completene\ ss = \frac{TP}{TP + FN} \qquad 64$$

$$Branching\ = \frac{FP}{TP} \qquad 65$$

Correctness is related to the probability of an extracted linear piece to be indeed a scarp or a levee; it is a measure of the accuracy of the correctly extracted features. *Completeness* instead expresses how much is missing of the features of interest. *Branching* offers a measure of the overestimation of the extractions. Values of *correctness* and *completeness* range between 0 and 1, where 1 represent a perfect extraction. *Branching* values instead range from 0 to + ∞, where 0 represent perfect extractions.

To quantify the improvement offered by the proposed filtering approach, quality measures (Cohen's *k*, Completeness, Correctness and Branching) have been evaluated before and after the filtering approach for all extractions, and their maximum values have been analyzed according to the kernel shape, without considering the kernel sizes (Tab. 10).

Table 10: Maximum values of quality indexes for all extractions before and after filtering.

		Cohen's *k*		Completeness		Correctness		Branching	
		Before	After	Before	After	Before	After	Before	After
Rectangular	*RT*	0.74	0.80	0.73	0.72	0.81	0.97	2.75	0.18
	Entropy	0.73	0.75	0.91	0.91	0.76	0.79	4.33	1.34
	C_{max}	0.68	0.75	0.78	0.78	0.65	0.97	2.67	1.26
Circular	*RT*	0.74	0.80	0.72	0.71	0.81	1.00	5.46	2.16
	Entropy	0.73	0.75	0.91	0.90	0.78	0.79	5.46	0.86
	C_{max}	0.66	0.75	0.90	0.90	0.55	0.79	1.94	1.22
Annulus	*RT*	0.75	0.80	0.73	0.72	0.82	0.99	2.07	0.28
	Entropy	0.73	0.75	0.91	0.90	0.80	0.80	39.63	15.86
	C_{max}	0.61	0.76	0.99	0.80	0.55	0.82	15.70	2.28

It is clear how the filtering approaches enable an increase of the overall quality of the extractions, for all parameters, with Cohen's *k* increasing of about 10% for C_{max} and *RT* for all applications. Maximum curvature is the parameter that more benefits from the filtering, with an increase of the maximum overall quality of about 10% for the rectangular kernel up to 15% for the annulus one (Cohen's *k* passes from 0.61 to 0.76).

The filtering approach guarantees an increase of the correctness of the extractions and contributes to a diminishing of the false positives (Branching diminishes for all instances). Extractions derived from residual topography, showed higher quality even before the filtering approach, but the application of the filter allows to obtain almost 100% of correctness (all extractions are indeed actual features). Entropy is the parameter that is less influenced by the filtering approach, and this suggests a higher suitability of the parameters if the users do not want to post-process results: overall quality and correctness of extractions carried out through entropy show values comparable with the ones obtained by residual topography, and entropy derived extractions show a higher completeness.

Cohen's *k* is evaluated for each final extraction, after the filtering procedure, are represented for all geomorphic parameters for the rectangular kernel in Fig. 68, for the circular kernel in Fig. 69 and for the annulus kernel in Fig. 70. All quality measures (Cohen's k, Completeness, correctness and branching) are also shown in Table 11 for the extractions considered as optimal according to Cohen's *k,* and they are expressed for the same extractions before and after the filtering. Best extractions according to Cohen's *k* are shown in figure 71.

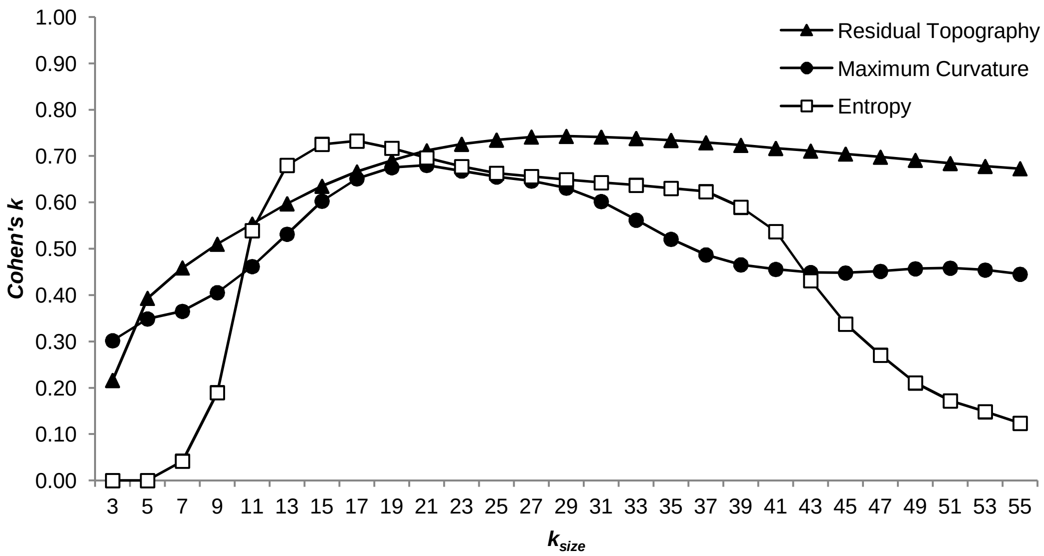

Fig. 68 Cohen's k values for all geomorphic parameters for the rectangular kernel

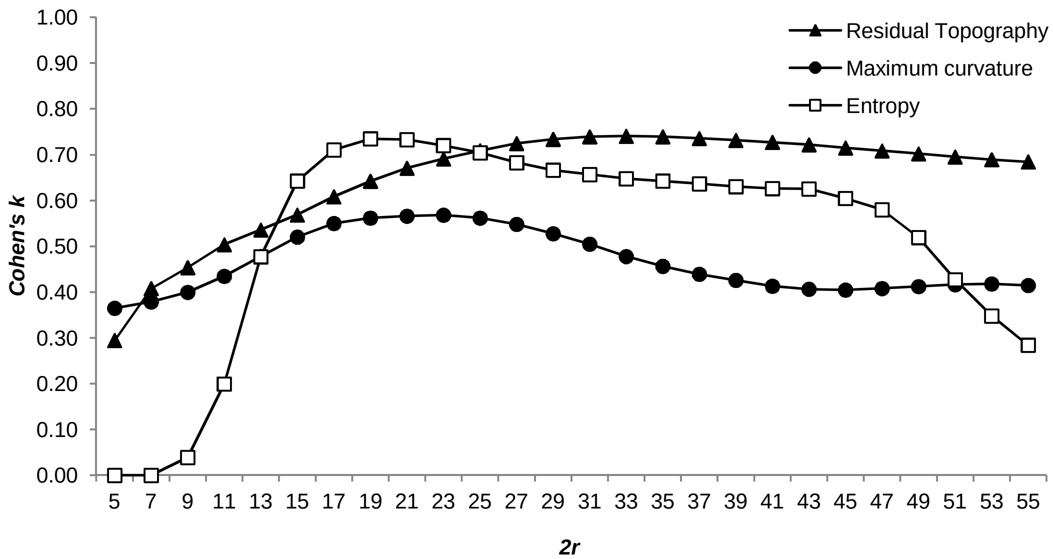

Fig. 69 Cohen's k values for all geomorphic parameters for the circular kernel

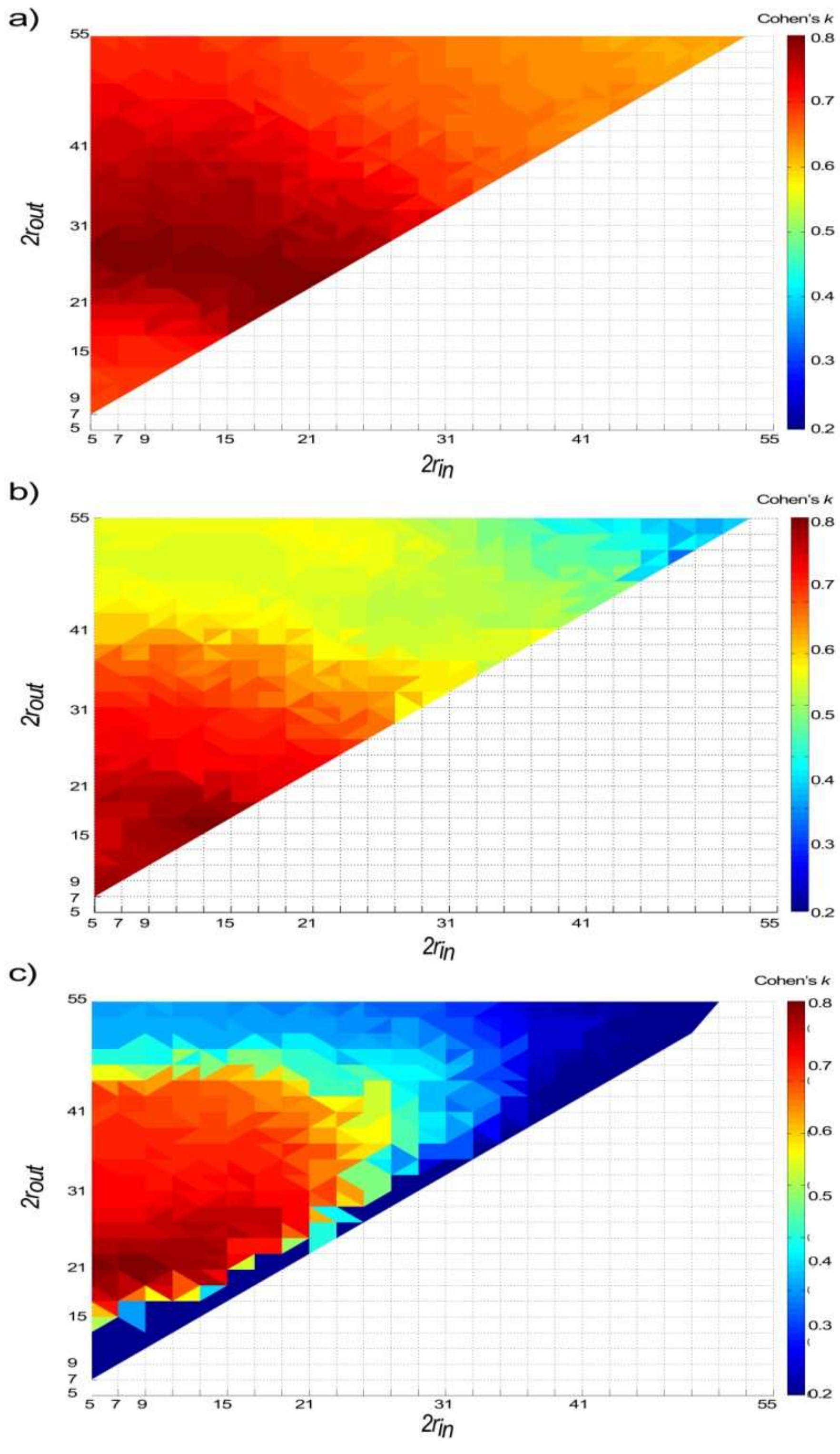

Fig. 70 Cohen's k values for all geomorphic parameters for the annulus kernel: Residual Topography (a), Maximum curvature (b) and Entropy (c).

Table 11: Quality indexes for the best extractions, before and after filtering.

		Cohen's *k*		Completenes		Correctness		Branching	
		Before	After	Before	After	Before	After	Before	After
	k_{size}								
RT	23	0.73	0.80	0.73	0.72	0.75	0.93	0.34	0.08
Entropy	17	0.73	0.75	0.82	0.80	0.69	0.73	0.45	0.36
C_{max}	17	0.65	0.75	0.78	0.78	0.59	0.75	0.71	0.34
	2r								
RT	29	0.73	0.80	0.72	0.71	0.77	0.92	0.30	0.09
Entropy	17	0.73	0.75	0.84	0.82	0.68	0.73	0.47	0.38
C_{max}	19	0.64	0.75	0.85	0.82	0.54	0.73	0.85	0.38
	$2r_{in}$; $2r_{out}$								
RT	13;15	0.75	0.80	0.73	0.72	0.78	0.93	0.27	0.07
Entropy	21;25	0.73	0.75	0.83	0.82	0.68	0.72	0.47	0.38
C_{max}	3;21	0.55	0.76	0.76	0.74	0.47	0.82	1.13	0.22

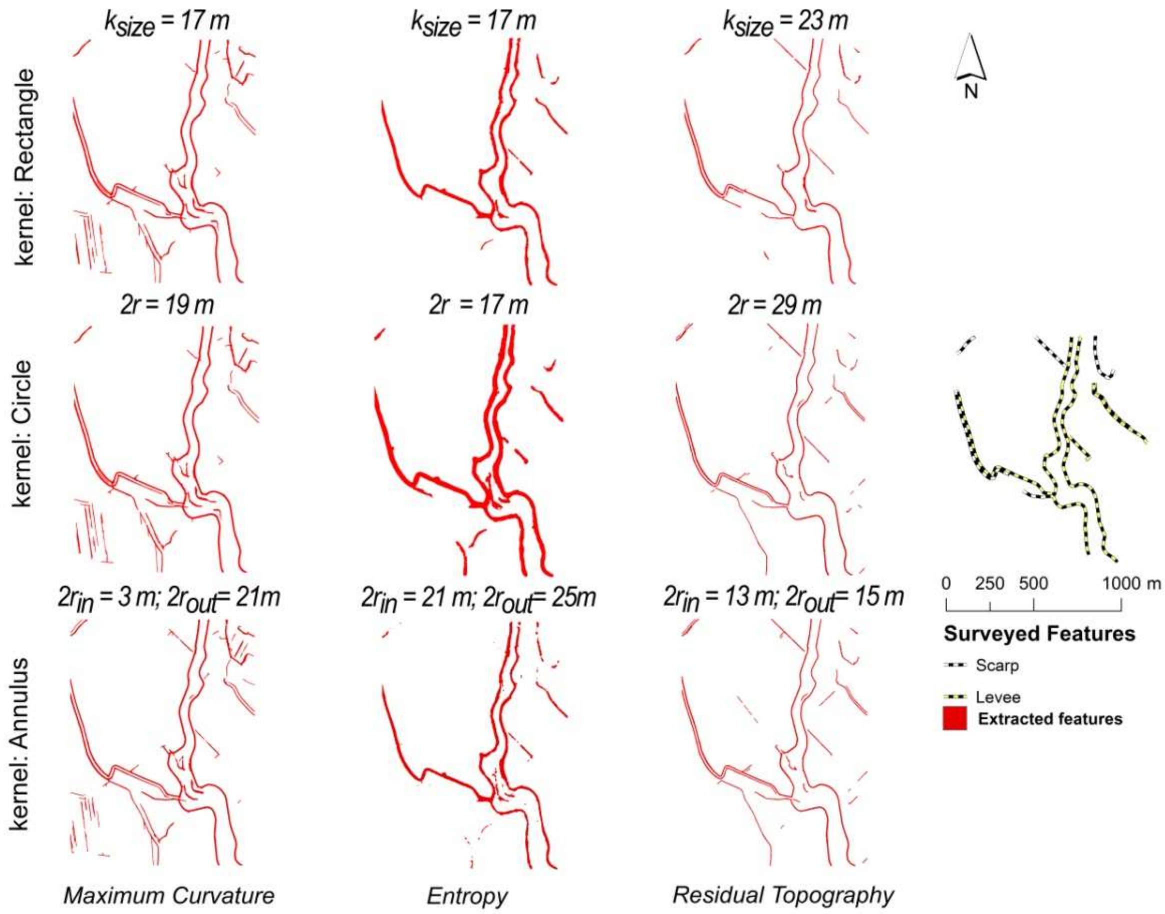

Fig. 71 Best extractions according to Cohen's k for each geomorphic parameter and kernel shape. Reference features are also shown.

The main element influencing the quality of the extractions, independently from the chosen topographic parameters, is the size of the neighborhood considered when evaluating the indexes. The increasing of the area of analysis (increasing k_{size} or $2r$), results in a progressive increasing of the quality of the extraction, until a maximum value is reached. Then, the increasing of the window size corresponds to a decreasing of the overall quality of the extraction (Fig. 68,69 and 70). When considering the annulus shaped kernel, the increasing of the inner diameter contributes as well to an increase of the overall quality until a maximum is reached. As suggested for other parameters in this work, if the area is too wide resulting maps are less noisy, but they lack of precision. At the same time, if investigated area is too small, quality is negatively influenced by noises that are extracted and wrongly labeled as features (Sofia et al. 2011, Pirotti and Tarolli, 2010; Tarolli et al. 2010). The overall quality of the extraction seems to be just slightly influenced by the shape of the adopted kernel: similar Cohen's *k* are obtained for the three geomorphic parameters by considering different shapes at different scales (Tab. 11). Overall quality slightly benefits of the annulus shaped kernel when considering maximum curvature. For the same topographic parameter, the annulus shaped kernel offers also a better correctness and reduces the number of false positives.

One must note, anyway, that the similarities between extractions carried out considering parameters evaluated for different kernel shapes are mostly determined by the post processing of the extractions (filtering). When reading the quality measures for the same maps, before the filtering (Tab. 11), clearly the shape of the kernel has more importance, accentuating or diminishing the number of false positives and thus decreasing or increasing the quality of the extraction (i.e. quality and correctness of Residual Topography were higher when considering the annulus shaped kernel instead of the rectangular or the circular ones). Analyzing in detail the best extractions, results underlined that Residual Topography, independently from the shape of the analyzed area, shows the higher correctness of extraction and the lower degree of overestimation (minimum branching). The use of the annulus shaped kernel, results in a slight diminishing of branching. A better completeness of extractions is guaranteed by the use of Maximum Curvature (especially when evaluated with the circular or the annulus shaped kernels) and Entropy (evaluated with the rectangular kernel), but this is also connected to a higher overestimation of extractions (higher branching). One must note (Fig. 71) that for Entropy, the overestimation is due to the fact that identified features are larger than the surveyed one, while for Maximum Curvature overestimation is actually due to the fact that wrong features are extracted. Among all parameters, Maximum Curvature is the most sensitive to change in surface concavities-convexities also related to tillage practice and convexing, and these false positives are not entirely discarded by the automatic post processing filtering.

By visually assessing the extractions, the best product is obtained by Residual Topography evaluated with a 23 m rectangular kernel: for this extraction, all features are correctly identified and the number of false positive is almost null.

4. *Drainage network detection in engineered landscapes*

The background framework for this DTA application can be found in Chapt. *2.1.b,* Sect. *I.Introduction,* while information about the considered study sites are provided in Chapt. 2, Sect. *II.Study sites*. The study areas will be hereby labeled as '*control area*' (site *A*, Chapt. 2.1, Sect. *II.Study sites*) and '*application area*' (site *B* in Chapt. 2.2, Sect. *II.Study sites*). This nomenclature has been chosen considering that for study site A, an accurate field survey was carried out, providing detailed information about the considered features. In this site, a comparison between actual measurement and derived measurement can be carried out, assessing the correctness of the procedure (hence the definition of 'control area'). Study site B instead, has been chosen to test if the proposed approach can be feasible for large scale applications. The procedure starts from a grid DTM readily available for public authorities in Italy, the same DTM considered in the previous application.

The proposed DTA aims to the detection of an artificial drainage network, and to its geometric characterization. In particular the aim is to assess over specific areas the network total length, drainage density, and storage capacity within the channels. The proposed procedure does not consider at this stage any hydrological characterization of the network: neither its connectivity nor the flow directions are accounted for.

The method can be conceptualized in two main steps: 1. From a high resolution DTM, the network is automatically detected, and, always in an automatic fashion, a width and a length index are computed. From these indexes, network length and network drainage density are computed directly. 2. In a second step, by associating some characteristic cross-section area to specific width ranges, it is possible to derive the network storage capacity. While the first step is completely automatic, the second step requires the user to identify roughly some width ranges and cross section shapes. Once these are defined, the network storage capacity is evaluated automatically.

The width and length indexes are evaluated directly from a raster map, without any skeletonization procedure. This because even if algorithms for such operations are available in many contemporary GIS, they usually produce highly irregular skeletons that are a poor representation of the channel itself, and they require additional filtering and connection. However, considering that the DTM has a constraint due to the grid size (1 m) that is constant all over the map, two assumptions need to be underlined: i) this constraint makes inapplicable the reading of cross section geometry directly on the DTM (Fig. 72), but it allows an approximation of the ditches widths, considering that their minimum width is about 1 m (equal to the DTM grid size); ii) an exact local characterization of the ditches is not expected, rather the aim is a characterization of the network for each considered drainage unit.

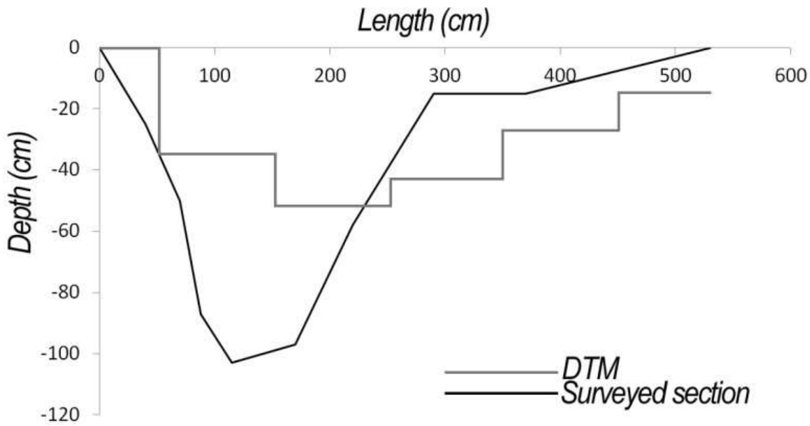

Fig. 72 Example of cross section geometry as depicted by the DTM (gray) compared to the surveyed ditch geometry (black).

4.1 Network detection

Drainage network such as ditches and channels in agrarian landscapes are usually represented by linear and regularly distributed features. Land reclamation ditches are commonly low ‘amplitude’ elements, considering amplitude as the difference in relief between low points on the ditch and height areas to either side, and they are topographically subtle in comparison with the underlying plain, especially for areas where the landscape gradient is relatively low. The proposed approach is based on consideration of having to extract local small-scale, low-relief features from the DTM and to eliminate as far as possible the large-scale landscape forms from the data. The considered parameter is the REA (Eq. 18 p.69). Such choice is done considering the previous DTA assessment (*Chapt. 3*, *Sect. IV.DTA for feature recognition*), when compared to other topographic parameters, the use of residual topography was assessed to be optimal for the floodplain context.

When working in engineered landscapes, some issues arise due to human disturbances. DTM based on laser scanning are highly accurate, buildings as well as vegetation are normally already filtered. However, laser-based DTMs also show all man-made modifications of the earth's surface such as large roads, stamps of urban areas, high banks etc. For extraction procedure based on relief control, prior to local relief evaluation, it is necessary to identify and roughly mask these manmade terrain features on the original DTM, at least where their density is high. This masking approach allows a better detection of the actual channels, decreasing considerably false detections, avoiding peak values on the relief index due to artificial elements.

Once the DTM has been roughly masked, Eq. 17 and 18 are applied, obtaining a map that carries only the signature of the main topographic features, detrending the landscape.

In figure 73 the input DTM for an area is shown (a). On the DTM some narrow linear element representing the drainage network are visible. In figure 73b the derived REA map is shown, highlighting the network features with higher values of the parameter.

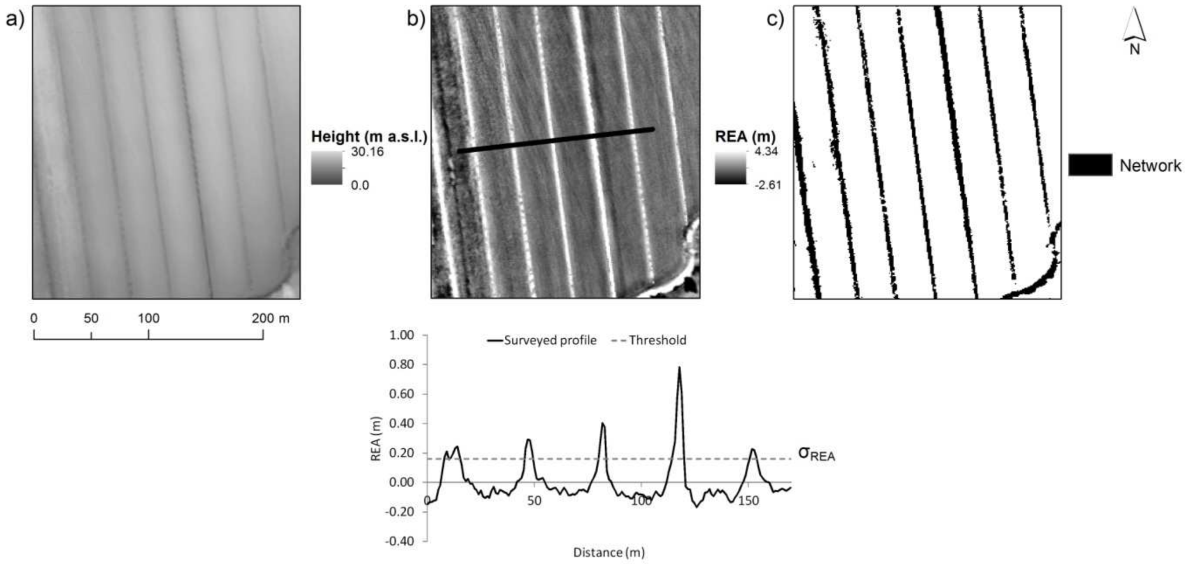

Fig. 73 Input DTM (a), derived REA map (b), and the threshold identified to detect the network. REA peak values corresponding to ditches for the sections surveyed in b are shown in the profile graph. The boolean map detecting the drainage network derived after thresholding is shown (c)

To detect the network it is necessary to label the REA peak values, and this is done through a thresholding approach. The theoretical basis of such approach are the same ones described in Chapt. 4.2, Sect. *III.Materials and methods*. In this instance, the chosen threshold is the standard deviation of REA (Fig. 73). The result (Fig. 73c) represents a boolean map with features taking only binary values, 1 or 0 for network pixels and landscape pixels respectively.

4.2 Network geometric characterization

Once the network is detected, the interest moves toward its geometrical characterization, that starts from the Boolean map (Fig. 73c). This map is composed by clusters of pixels (groups of connected cells having the same value). A single cluster does not necessarily imply the identification of a single network reach: each cluster might be a composed by multiple reaches with different geometries. Figure 74 shows an example of three different clusters: while cluster B corresponds to a single ditch with a specific and constant width, cluster A comprises two ditches with different widths.

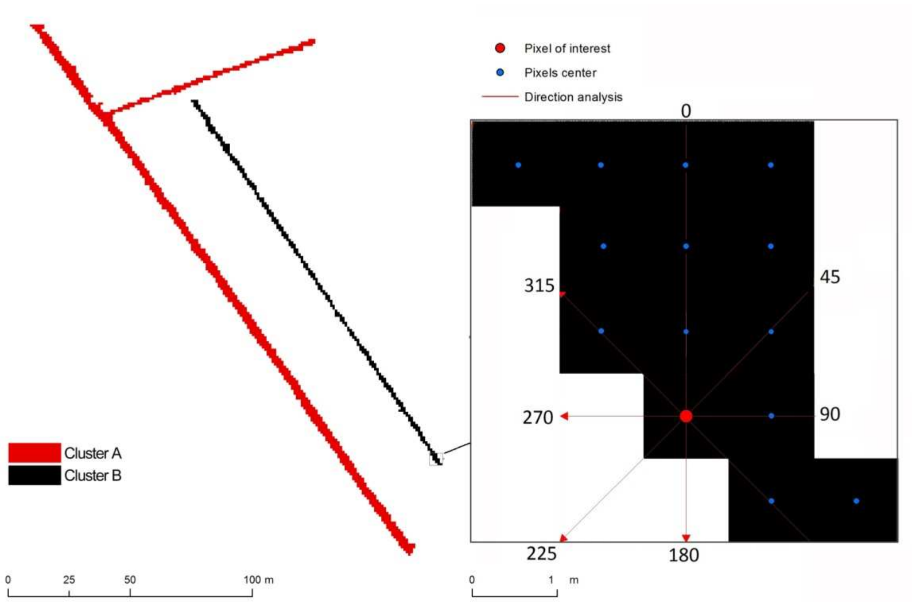

Fig. 74 Clusterization approach and cluster parameters evaluation. Cluster A is composed by reaches with different geometries, while cluster B is a single reach with constant width. On the overview, an example of the pixel width evaluation is proposed: the red arrows show, for the considered pixel (red dot), the four directions D (0-180, 45-225, 90-270, 135-315) used for width evaluation (modified from Cazorzi et al. In press). In this example, the derived pixel width for the pixel in analysis is 2.

Simple shape-related quantities, as area, width and length can be consistently calculated for each cluster. Knowing the DTM grid size, the surface for each cluster (s_c) simply refers to the sum of the areas of the pixel within the cluster.

In the previous DTA, cluster width was approximated by the use of the inverse distance transform. In this DTA, instead, the procedure is slightly different and the network width index is computed for each cluster according to the following steps.

For each pixel on the cluster, the connected neighboring cells along four directions *D* (0-180, 45-225, 90-270, 135-315) are counted (Fig. 74), and the width w_{px} associated to each pixel is computed as

$$w_{px} = \min({}_{0-180}count_{px}, {}_{45-225}count_{px}, {}_{90-270}count_{px}, {}_{135-315}count_{px}) \qquad 66$$

where ${}_{D}count_{px}$ is the number of pixels connected to the considered one (*px*) along the direction *D* (Cazorzi et al. *in press)*.

In the example provided in Fig. 74, for the pixel of interest the evaluated w_{px} is 2.

The width index W_{index} for each cluster is then represented by the average value of pixel widths

$$W_{index} = \frac{\sum_{px=1}^{n} w_{px}}{n} \qquad 67$$

where w_{px} derives from Eq. (66) and n is the number of pixel within the cluster (Cazorzi et al. *in press)*.

The length index L_{index} is analytically derived as the ratio between the cluster area and the cluster width index (W_{index}) *(*Cazorzi et al. *in press)*.

$$L_{index} = \frac{s_c}{W_{index}} \qquad 68$$

In Fig. 75, an example of the two indexes is provided.

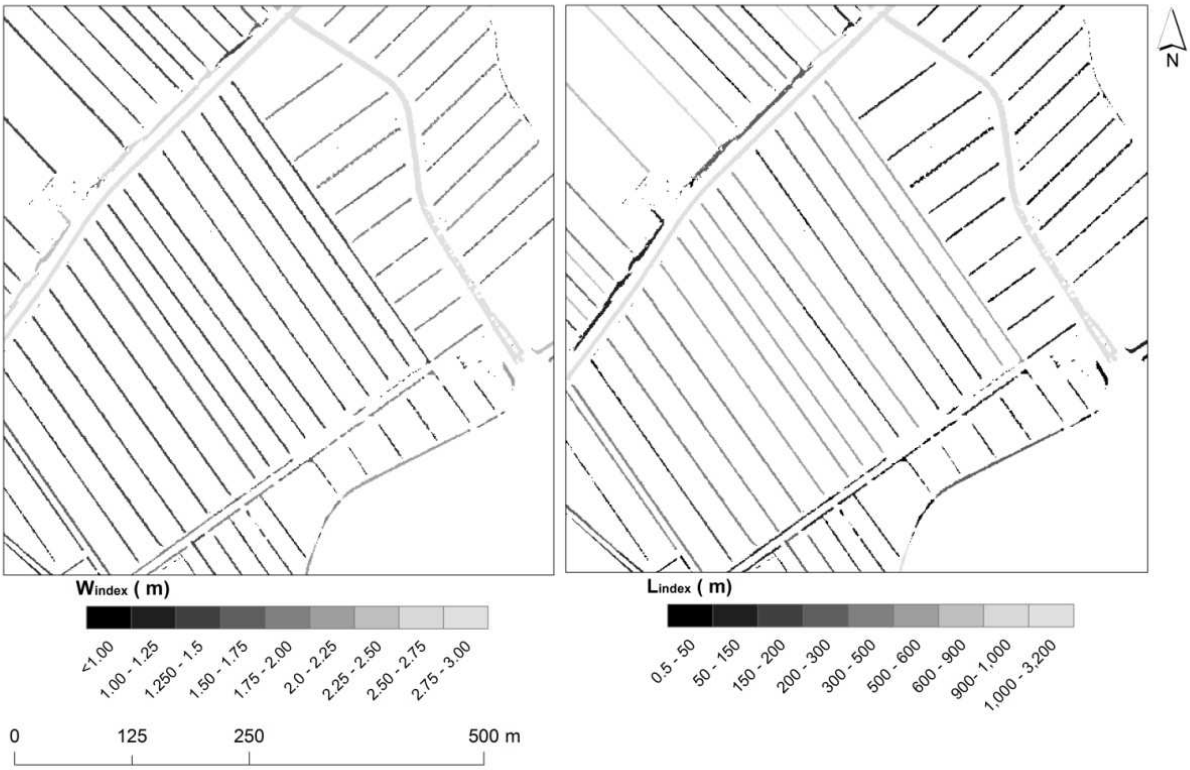

Fig. 75 Example of indexes derived for a drainage unit: width (W_{index}) and length (L_{index}) index for each clusters of pixels.

Knowing both indexes for each cluster, it is possible to evaluate the areal drainage length (DL_u) and drainage density (DD_u). Drainage Length is evaluated as the sum of Length indexes of the clusters belonging to the considered unit. Knowing the unit surface, drainage density (DD_u) is evaluated as the ratio between drainage length and the actual surface of the unit of interest *(*Cazorzi et al. *in press)*.

The definition of network storage capacity starts from the availability of some field measures: field surveying allows to define some representative cross-sectional areas for specific width ranges (see Chapt. 2.1, Sect. *II.Study sites*). This characterization is a user choice: it is an averaged characterization of cross-sections for widths ranges, and it may vary in different areas according to the digging techniques adopted to create the ditches.

This approach considers a simplified representations of ditches cross-sections such as nested trapezoids, single trapezoids, or rectangular cross-sections, as derived by field survey. An optimal stream channel description should include detailed measurements of how depth varies with increasing widths, but, due to the highly regular shape of agrarian drainage networks, this simplified estimation procedure is justified, and the averaging characterization accounts also for the differences in network geometry that might be present over different plots due to farmer choices. It should be pointed out, anyway, that a) this process results in an average characterization of the network per unit of interest; and b) the relationship between width ranges and cross-sectional areas as it is formulated, cannot be applied for watersheds with a more natural network, such as mountainous watersheds of similar drainage area that are not likely to have regular channel geometries.

Once the width index is automatically derived, it is possible to associate the user-defined cross-sectional areas (A_{index}) to the whole network, and the network storage capacity for drainage unit (SC_u) is defined as

$$SC_u = \frac{\sum_{j=1}^{n} \left(L_{index_j} \cdot A_{index} \right)}{S_u} \qquad 69$$

where L_{index} is the length index for each cluster (j), S_u is the surface of the considered drainage unit (Cazorzi et al. *in press)*, and A is the associated cross sectional areas such as

$$A_{index} = f\,(W_{index\ j}) \qquad 70$$

Where W_{index} derives from Eq. 67 (*Cazorzi et al.* in press).

4.3 Accuracy assessment

The accuracy of the methodology has been tested considering some comparisons based on the availability of actual network statistics. Whereas channel lengths and channel geometries (bankfull width, depth and cross-sectional areas) are available in detail for the control area, acquiring channel geometry measurements for the whole network of the application area (total length about 900 km) would have been time-consuming and cost-prohibitive due to the large extent of the site (3000 ha). Available reference network statistics listed by sources are express in table 12.

Table 12: Reference statistics availability.

Network reference statistics	Control Area (80 ha)	Application Area (3000 ha)
Network positioning	DGPS field survey	Manually Updated RTC
Drainage Length	Field survey	Manually Updated RTC
Channel Geometry	Field survey (170 control points)	Field survey (15 control point)
Storage Capacity	Field survey	None

Considering the problems of the Regional Technical Map, high-resolution digital aerial photos collected for the application area during the same flight that provided the LiDAR dataset have been used in a time-consuming approach to update manually the RTMs where needed, in order to provide a better information for quality assessment.

Assessment of drainage network positioning accuracy was performed by calculating distances between the location of channels of the available reference data, and the corresponding derived network. Median distance of reference points to extracted drainage network for the study site is registered to be about 1 m (consistent with the DTM grid size constraint). In some instances, the procedure detects localized pixels, that do not correspond to the actual network location, and that can be classified as either noises or localized macro-depression on the soil. When compared to the actual land use, the proposed procedure represents the network in its real conformation, while the original RTMs are not updated (Fig. 76).

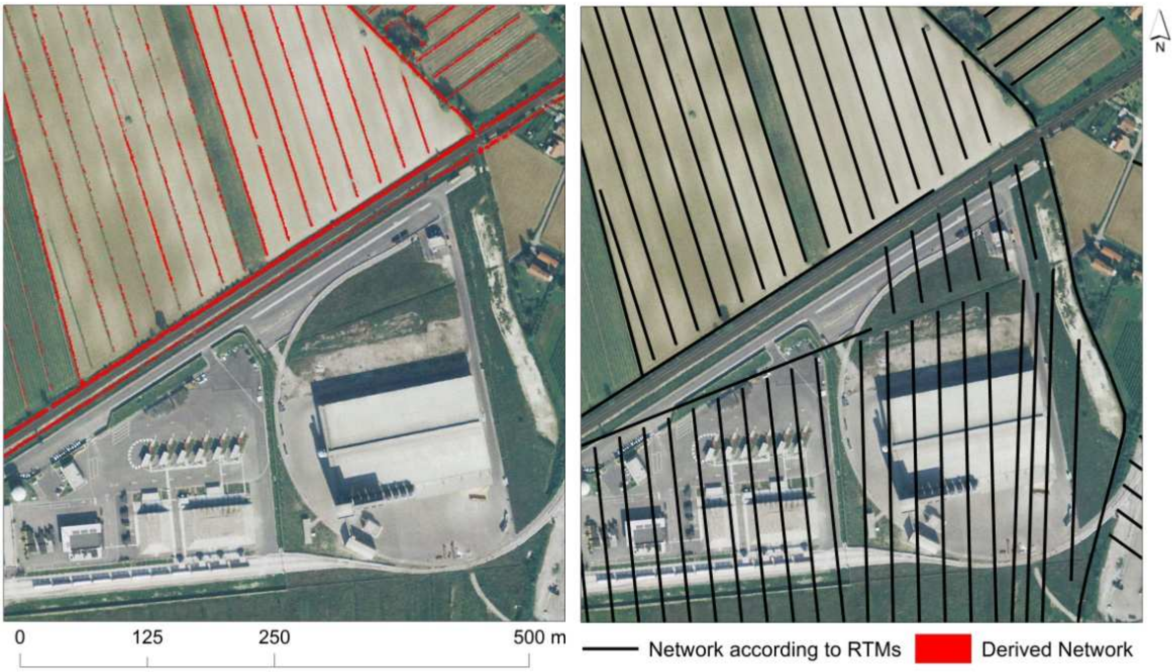

Fig. 76 Accuracy of evaluated network (red) and network as digitalized from official cartography (Regional Technical Map –RTMs-) (black) before updating. The underlying ortophoto shows how official cartography needs some update and adjustment.

A first quality assessment has been done considering the width index (W_{index}) and the actual width derived from field survey (W_{obs}). One must note that, by definition, the proposed indexes are a unique averaged value for each cluster of pixels, and each cluster does not necessarily represent an individual reach, but it might be composed by multiple network reaches with different cross-section geometries (see i.e. Fig. 74). To test the effectiveness of the procedure, some specific locations have been considered, where the considered cluster was actually a single reach of the network with a constant surveyed width (Fig. 77a). For the same clusters, the length index (L_{index}) has been compared to the field surveyed length (L_{obs}) (Fig. 77b).

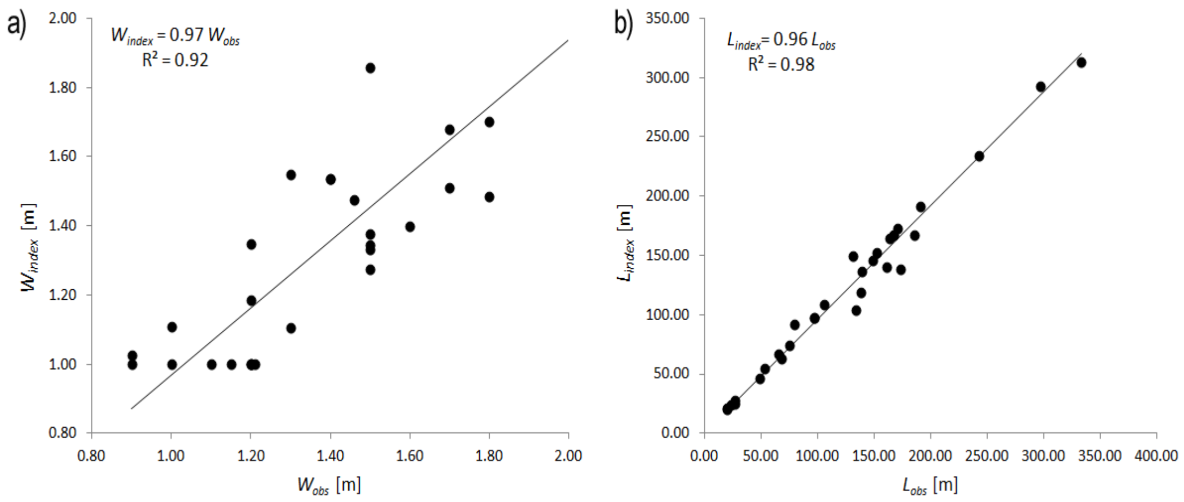

Fig. 77 Comparison between a) width (W_{index}) and b) length (L_{index}) indexes and the correspondent surveyed measures (W_{obs} and L_{obs}). (Cazorzi et al. In press)

The result shows that when the considered cluster is representative of a reach, the width index is generally also a correct local estimation, with a measured RMSE of about 0.2 m. The same consideration can be done about the length index: in this case, the RMSE is estimated to be about 2 m.

Using a transitive relationship, if the field measured cross-sectional areas (A_{obs}) are strictly correlated to the field measured widths (W_{obs}), and the field measured width (W_{obs}) is in turn related to the width index (W_{index}) (Fig. 7 p.42), then cross-sectional areas can be also related to width index. By associating some characteristic cross-section area to specific width ranges, it is possible to automatically derive the network storage capacity.

When the storage capacity is compared to the field surveyed one in the control area, a good concordance among measures is registered: the field surveyed storage capacity for the area is about 156.14 m^3/ha and the one estimated by the procedure is 154.11 m^3/ha. The procedure slightly underestimates the surveyed storage capacity (SC_u= 0.98 SC_{obs}), and this is consistent with the approximation in the width and length indexes (W_{index}= 0.98 W_{obs} and L_{index}= 0.96 L_{obs}). For the application area, storage capacity ranges between 50 m^3/ha to about 300 m^3/ha: low values of channel storage capacity can underline deficit in the network, and they can outline areas whose hydrological behavior is potentially critical during floods.

The regression technique was chosen to investigate the relationship between evaluated network statistics (Drainage length, drainage density and storage capacity) versus control values considering at the same time values derived from the field survey for the control area with the values derived from the updated Regional Technical Map for the application area. The underlying assumption is that a similarity exists between the two sites. The main idea is to integrate the RTC-derived information with the field surveyed one, even if derived on a different site. The quality evaluation of the methodology can be then estimated more accurately by using the existing field surveyed values as an auxiliary base.

Evaluated drainage lengths (*DL_u*) have been tested against drainage length derived from field survey (in the control area) and updated from cartography (application area) highlighting how a strong linear relationship (R^2= 0.97) exists between the evaluated characteristic and the measured one in all cases (Fig. 78). The evaluated RMSE for the network length is estimated to be around 1.5 m and it is consistent with the values registered for the cluster length index.

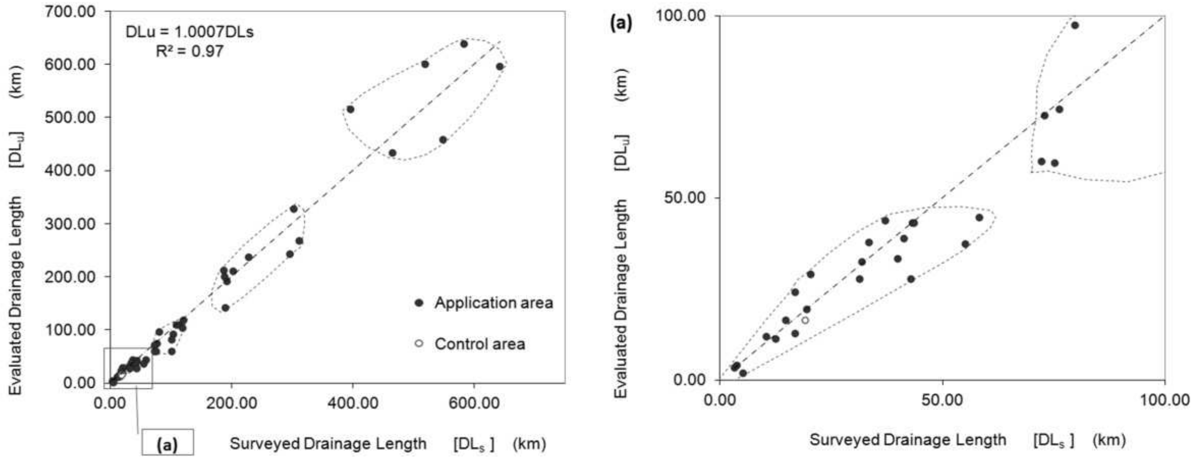

Fig. 78 Drainage length derived by the proposed procedure (DL_u) and field surveyed Drainage Length (DL_{obs}) for the control area and for each one of the drainage units of the application area (Cazorzi et al. in press)

The values of evaluated drainage length and field derived one for the control area, behave in a similar way when considering length ranges between 0 and 60 km (Fig. 78a). For the control area, the evaluated Drainage Length is about 17 km, while the surveyed one is 19.50 km. In this case, the procedure slightly underestimates the measures.

When evaluating drainage density (Fig. 79), correlation between the measured values and the evaluated ones is less strong, but still valuable (R^2= 0.67). Testing R^2 with two-tailed Student's t-tests for statistical significance and α = 0.05, anyway, shows that this value represents a significant linear relationship between the two variables for the considered datasets.

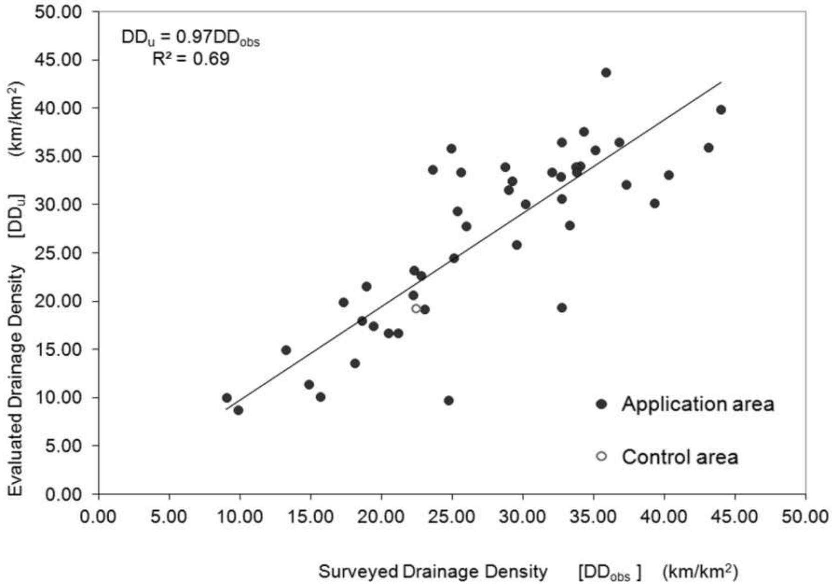

Fig. 79 Drainage density derived by the proposed procedure (DD_u) and field surveyed Drainage density (DD_{obs}) for the control area and for each one of the drainage units of the application area. (Cazorzi et al. in press)

As mentioned before, due to the large extent of the application area, it was not possible to have detailed information about storage capacity within the network, but for this study case, regression techniques, anyway, indicated that the evaluated storage capacity is strongly related (R^2 = 0.83) to drainage density (Fig. 80), that has been proven to be related to the correspondent control values (Fig. 79).

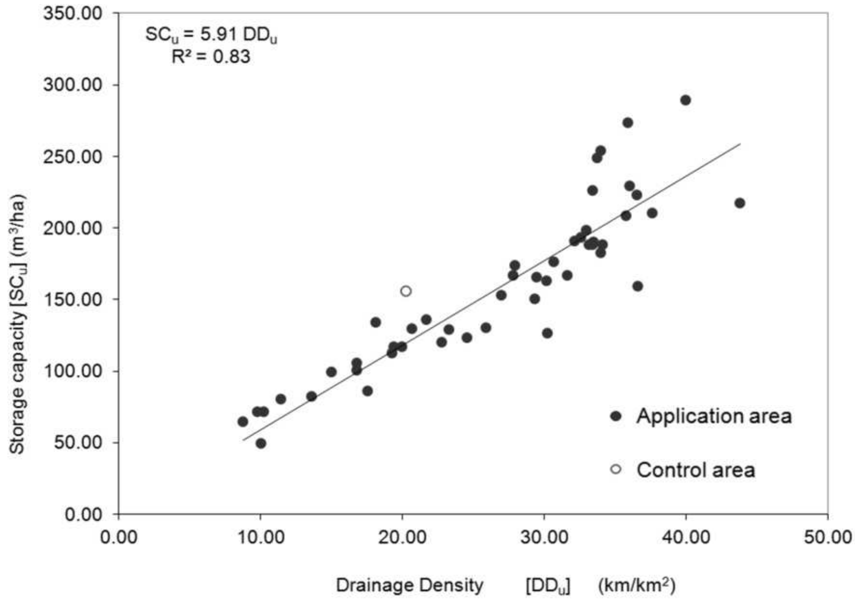

Fig. 80 Relationship between the Storage Capacity (SC_u) derived by the proposed procedure and the evaluated Drainage Density (DD_u) for the control area and for each one of the drainage units of the application area Cazorzi et al. in press)

The strength of correlation between REA derived values and the surveyed ones, in the majority of the instances, suggests a high reliability of the method. Some small inconsistencies between values exist, due to the DTM grid cell constraint that determines a slight underestimation of the derived parameters.

However, the method allows the definition of indexes generally available only through time-consuming and cost-prohibitive field surveys, such as information about storage capacity within the channels and drainage density (Fig. 81). This assessment is a crucial tool for flood management: low values of channel storage capacity can underline deficit in the network, and they can outline areas whose hydrological behavior is potentially critical during floods.

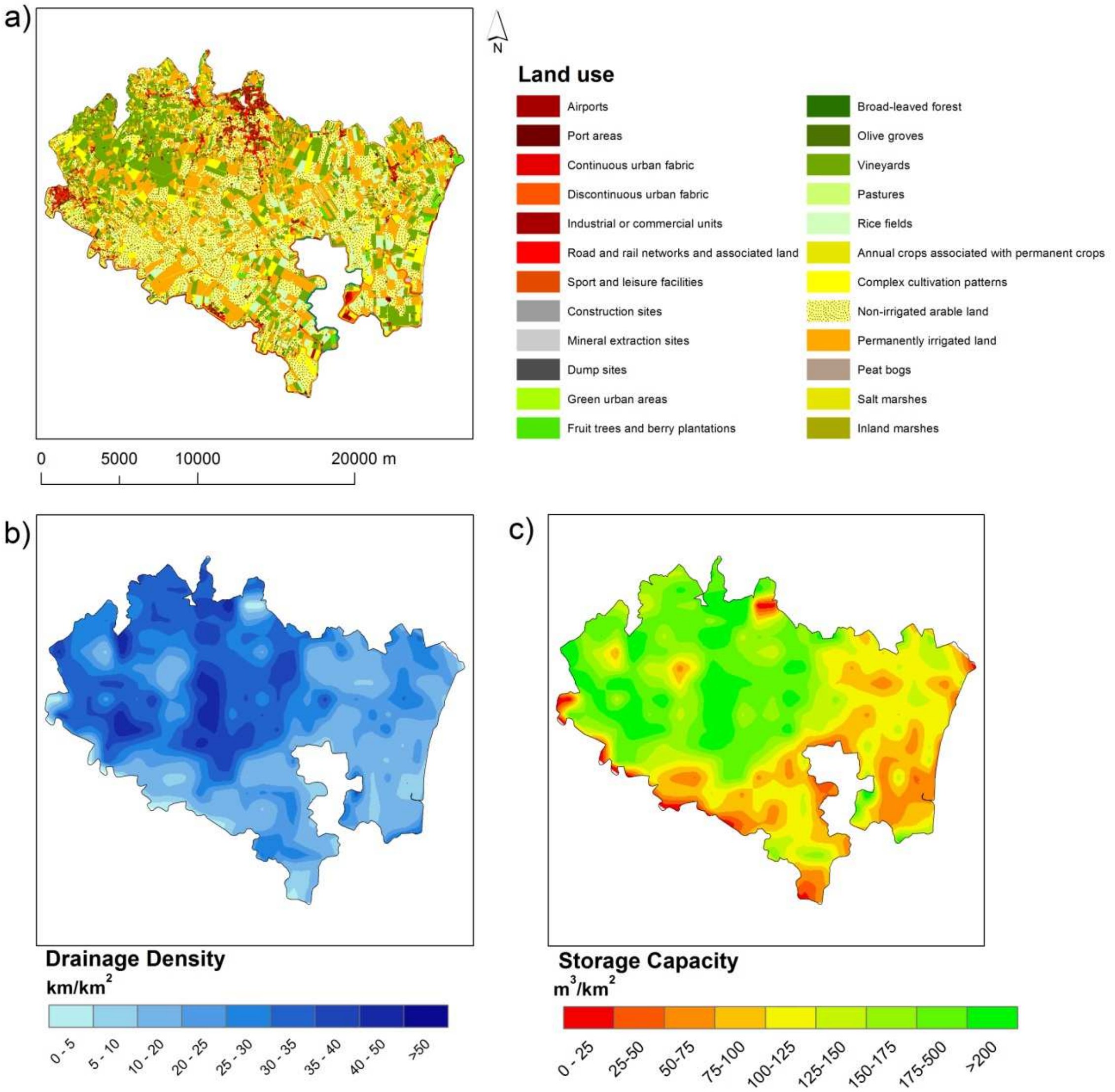

Fig. 81 Drainage density and storage capacity maps, derived for the application area. Low values of the indexes are related to specific land uses, such as urban areas or non-irrigated land.

5. Final remarks

This work analyzed different objective methodologies to extract features in mountainous and enginereed environments, through the use of topographic parameters.

The first DTA approach (Chapt. 1, Sect. *IV. DTA for feature recognition*) was carried out considering geomorphic features (landslide crowns, and bank erosion), and it considered the statistical analysis of variability of landform curvature in order to define a likely threshold for feature extraction. In the same approach, the suitability of different smoothing factors for the landscape curvature calculation has been tested, suggesting the minimal standards required for such analyses. The results of the approach reflect similar considerations as those suggested in previous works on channel network extraction through landform curvature (Tarolli and Dalla Fontana 2009; Pirotti and Tarolli 2010). The most reliable window size for curvature calculations has to be related to the morphology, and features size to be detected: a topographic parameter evaluated at scale that is not able to fully capture the features is not suitable for a good recognition, since only a limited area is investigated. Very large window sizes are not so representative as well, since the topography approximation is too smooth, and morphological features sited in place far from areas actually interested by the investigated process could be reached, providing a misinterpretation. In the considered case, a window size of 10.5 m was found to be the optimal for surface representation. However, some noises related to the complex morphology of the upper part of the study area affected the performance of the method. Automatic extraction of geomorphic features as landslide crowns and bank erosion based on thresholding operations was proven to be efficient in terms of time consumption, and valid to associate shapes and pattern derived from high resolution topography with real topographic signature of earth surface processes on the ground. The approach, anyway, presented some limits, especially in areas with complex morphology where also other surface features not related to slope instabilities have been detected. Nevertheless, this fast and preliminary interpretation could meet the requirements for emergency planning. The extraction of geomorphic features from airborne LiDAR data according to the proposed approach can be at this stage considered for modeling integration (i.e. terrain stability and erosion models) and can be used to interactively assist the interpreter/user on the task of shallow landslide and bank erosion of debris flow channel hazard mapping.

The issue of a full automatic feature extraction in area with different morphologies, and with different feature sizes was anyway still a subject research, and some open question remained, as in how to objectively select the scale of analysis, if no information about the feature size is available, and how to deal with noises derived by complex morphologies.

The second approach to DTA addressed in this work (Chapt. 2, Sect. *IV. DTA for feature recognition*) analyzed a mathematical and statistical approach to a combination of topographic attributes for an unsupervised channel network identification in complex mountainous terrains. Considering the results obtained by the previous application, the primary focus has been to develop and present a method that could describe accurately the drainage network considering objective thresholds without an a priori knowledge of the study area or of the input dataset. The methodology included two main aspect: (a) normalization of openness and minimum curvature maps according to their $QQ\text{-}plot_{thr}$ and their combination with upslope area to highlight potential surface convergences, and (b) a thresholding procedure based on standardized values of the weighted upslope area. To assess the feasible objectivity of the method, the DTA has been applied to two areas with different morphologies: a rectangular area with no reference to a complete hydrologic unit and a fully-organized basin used as a test site. The results showed at first that a joined use of two topographic parameters, a direct surface derivative and an approximation of surface relief, allowed a sort of independency of the procedure from errors in the input data. Thus, a first goal was obtained: the proposed procedure does not require a user to assess the quality of the considered map. It is true that such analysis should be always accounted for, but the most common situation faced by users, is that maps are provided with only an *RMSE*, routinely used as indicators of maps quality. However, this index might not be a good proof of the actual quality of the DTM, and assessment of the multiple factors that contribute to DTM uncertainty, and their propagation to topographic parameters is a complex process for users to be likely to spend time on it. In this study case, the skewness/kernel evaluation through the polynomial 'fitting/enforcing' approach allowed to select optimum scale of analysis without assessing the quality of the input maps, and it was able to identify kernels that had already been proven as optimal for other works carried out for the same study area. The approach based on distribution analysis also, allowed independency from assessing the morphology of the areas: skewness is statistically identified and does not imply morphological similarities of the basins, because it does not consider the spatial location and organization of concavities and convexities, but, more in general, their location among distributions. The use of statistical operators as objective indexes, results on a network correctly delineated and strongly consistent with surface morphology, without assessing the study areas. Automatic detection of network based on thresholding operations was demonstrated to be valid to associate shapes and pattern with actual topographic signature of flow processes. The proposed approach, anyway, presented again some limits. As in the DTA for geomorphic features, also in this case areas with highly complex morphology, other surface features not related to the actual process networks are detected. Network extraction carried out using openness and curvature independently shows some flaws detecting localized patterns and misleading noisy cells, which do not actually represent the features. The method, yet, can provide a quantitative and qualitative description of the network and can give an overall information about position and orientation of local convergences. The analysis of surface entropy has been proven in this case to be a useful and objective tool to assist the user on discarding doubtful extractions. The only flaw is showed by the fact that entropy has to be applied interactively to assist on the task of automatic network mapping, but noises can be objectively discarded (Entropy higher than the mean). In area with lower morphological complexity, the procedure is instead fully automatic in all its steps. The results obtained by the method on two areas with different complexity, considering morphology, network shape and also structural shape, shows promising effectiveness for practical applications.

However hydrological processes span outside the less disturbed mountainous environments, and there is nowadays an increasing interest in relating hydrological research to interpretative studies, including approaches that account for changing in watershed condition due to human disturbances. It is the case of analyses carried out in enginereed landscapes, where direct human alteration of processes is significant, and even if it is aimed toward servicing the needs of human populations, it might results also in changes of the watershed behavior that directly affect and influence the landscape. The present work, therefore, assessed DTA also for such type of environments (Chapt. 3 and 4, Sect. *IV. DTA for feature recognition*).

The use of different topographic parameters, and different approaches to account for scale have been assessed trying to answer two main question: in an environment where features assume different characteristic and shapes, what topographic parameter is more feasible for application? Does the shape of the analyzed area and its size have influence on the quality of the analyses (as it was assessed in the DTA for geomorphic features)? A further question has been assessed, as in how to improve the extractions, considering that when dealing with disturbed environments, as in mountainous ones, local morphologies due to human alteration might be present but not necessarily related to the features in analysis.

In the proposed DTA, therefore, different parameters have been considered and compared, both in terms of shape of the analyzed area and scale of analysis scale (Chapt. 3, Sect. *IV.DTA for feature recognition*). In this study case, considering that levees and banks, being artificial elements in a floodplain context, might be represented by outliers respect the elevation of the general surface, the boxplot has been considered to identify outliers and label anthropogenic features. As a final step, a filtering procedure is proposed, to improve the quality of results. As already found for mountainous environment, this analysis underlined how statistical parameters can effectively describe and characterize features starting from geomorphic maps. In line with other works, the research underlined that the effectiveness of topographic parameters to actually identify anthropogenic features is strictly related to the dimension of the investigated areas, rather than on its shape. The shape of the considered neighborhood, in fact, has just a slight importance in improving or decreasing the quality of the extractions. However, the greatest improvements are provided by the post-processing and the automatic filtering. While the effectiveness of residual topography had already been proven, the proposed DTA underlined how the use of maximum curvature or entropy can anyway provide good extractions in anthropogenic landscapes, with overall quality comparable to the one offered by residual topography. The higher sensitivity of curvature to surface convexities (highlighted also in the first two DTA for geomorphic and hydrologic feature extraction in mountainous environment) might determine a higher suitability of the parameter to identify smaller features, such as the one derived, for example, from farming activities. Entropy, as a new parameter, has been proven to be reliable for feature extractions, with the only limitation that the extracted features are slightly wider than the investigated one. Results underlined also how the proposed automatic post processing of the extractions, based on the dimension of the fragments and on a statistical threshold to discard them, can be an effective automatic tool to improve the quality of the extractions.

The final DTA (Chapt. 4, Sect. *IV.DTA for feature recognition*), presented a method for fast drainage network detection and quantification of water storage capacity and other network main statistics for agrarian landscape within floodplains. Considering the comparison between topographic parameters, the approach was based on the quantification of elevation residuals, as the main parameter to detect the network. The performance testing has demonstrated that this implementation can be efficient on gathering detailed and correct information for large datasets, thanks to the modern mapping technologies that can rapidly produce large DTMs at high resolutions. The accuracy assessment using field surveyed control values and information derived from a manually updated cartography, provided insight into the accuracy of drainage network derived through the proposed procedure. The strength of correlations between derived values and the control values in the majority of the instances suggests a promising and valuable reliability of the method, especially considering the regularity of shapes and structures of agrarian drainage network. The method is still not perfect, considering that some small inconsistencies between values exist, due to the DTM grid cell constraint that determines a slight underestimation of the derived parameters. However, the network extracted through the methodology has been proven to be more reliable than the information provided by the cartography, when updates on the maps are not available. The method, furthermore, allows the definition of indexes generally available only through time-consuming and cost-prohibitive field surveys (network geometry): it was possible to identify correctly some network characteristics over a large extent (3000 ha), and using only few control points (15), to derive information previously unknown about the storage capacity within the channels. This assessment is a crucial tool for flood management: low values of channel storage capacity can underline deficit in the network, and they can outline areas whose hydrological behavior is potentially critical during floods.

This fast processing of large DTM datasets opens their application to a new level of detail and spatial extent, for example, in rapid response operations, and they can become a useful tool in regions where available cartography needs to be updated or correct according to the land-use changes, especially in agrarian/urban contexts.

In this specific DTA, scale was accounted for through the use of the REA index, and the results suggest that the conceptually simple approach of removing large scale landscape features to extract small linear element is suitable, fast and enough accurate for anthropogenic environments. Also, even in this case, the use of the standard deviation as a threshold to detect the network has been proven to be reliable, underlining the power of statistics as an inference tool to label elements.

V. CONCLUSIONS AND FUTURE CHALLENGES

The need for developing comparative principles and tools for implementing management of land and water resources has long been recognized. Most management efforts require a broad spatio-temporal context based on a process-oriented understanding of how landscapes work in a spatially distributed context and a recognition of the spatial and temporal scales over which natural systems operate. However, the challenge of upscaling process understanding gained in smaller, experimental scales to larger scales, where management decisions are needed, requires an empirically based conceptualization of these scale processes and how they integrate to produce new processes, which emerge at larger scales. Process conceptualization and classification is therefore central, and it has been suggested that there should be a focus on the form of catchments, how and why they are geomorphologically, ecologically and pedologically structured in the way that they are. Further, there is the need to understand and quantify the ways in which this form determines how and why catchments function hydrologically and behave dynamically (Wagener *et al*., 2007). However, while the variables influencing catchment dynamics might be clear, it has been difficult to quantify and generalize them, and the approach to catchment characterization and classification, and consequent comparison, remain still a challenge (Sivapalan 2005; Wagener et al. 2007). In hydrological sciences, it has been argued that a paradigm shift is needed towards the development of unifying ideas and organizing principles that might facilitate extrapolation and prediction of processes in different provinces and across scales (e.g. McDonnell et al. 2007). In regional studies too, there is growing recognition of the need to move beyond single region case studies in order to examine the operation of similar processes across different places.

Due to the heterogeneities in landscape properties and climatic inputs, all processes are highly variable and complex at all scales. Therefore, to gain correct insight about the actual behavior of hydrologic systems it would be useful, or even necessary, to measure the relevant data at all of these scales, for a complete understanding and/or prediction of these processes. However, this is not practical nor feasible for all applications, and observations are generally carried out at one scale, either dictated by technical limits or operative choices, that does not necessarily correspond to the inherent scale of the process. As a consequence, there is the general need of understanding and/or transforming the process at the scale of interest, from the corresponding process at the observational scale. Moreover, generalization tools are needed, as analytical frameworks to provide a basis for cross-scale characterization and prediction. Such principles require the definition of indicators of similarities and attributes of spatial units characterizing the behavior of catchments and regions.

Despite considerable ongoing progress in conceptualization, there remains the need for better coordination in research and collaborative comparative studies to develop transferable tools to integrate theoretical perspectives and empirical studies. Hydrological data collection is invariably carried out for different reasons, in different regions, in different ways, over varying scales, by people with different backgrounds, biases and inevitable budget constraints (Hamilton, 2007). As a consequence, there is often a barrier between the hydrological research and the actual application of the proposed models. While high resolution topography is nowadays available not only to researchers, but also for public authorities, this is not always true for the models that derive from the application of such high-res information: they are in some cases too complex to be feasible for fast and efficient direct applications. The study by Sivakumar (2005), for example, highlighted the negative effect of the increasing emphasis on techniques that serve mostly 'the specialists,' rather than a more generalized approach that would serve everyone. Discussing the role of 'thresholds' in hydrologic systems and the various implicit forms in which they are already being adopted, for example, Sivakumar (2005) comments: "*Looking at the direction in which hydrologic research is moving, with our emphasis on specific data analysis techniques than common hydrologic problems [an opinion may not be shared by everyone], we could end up with enormous difficulties in understanding hydrologic literature [dealing with thresholds]. This is immediately evident [from the above examples], since [I suspect] not many hydrologists who are familiar with the concept of self-organized criticality are also familiar with the concept of artificial neural networks and/or nonlinear deterministic and chaos theories. It is obvious that the [above] situation would only become worse when hydrologic concepts, research activities and model success/failure need to be explained and disseminated to new and emerging hydrologists (e.g. undergraduate and graduate students), water managers and policy makers*."

Comparison of catchment behavior in different geographical areas is an obvious need that will aid meaningful classification and lead to a more systematic understanding of catchment similarities and dissimilarities in catchment form and function. Given the importance of heterogeneity at all scales, this requires the development of diagnostic classification tools that integrate measurement and consider factors such as topography to develop indices of similarity. The improvement of computational abilities and of remote sensing detection, facilitated extensive data collection (both in time and in space), formulation of sophisticated methods (including those for studying the inherent hydrologic nonlinearities and scaling), and development of models. There are no doubts that we today have a far greater ability to represent real hydrologic systems, and we possess a much better understanding and predictive ability of hydrologic phenomena than we did not long ago. From this, there is a need for simple rules and/or clear procedures to determine the dominant processes operating in different catchments, and how these reflect variations in landscape controls. Developing such tools would allow a much more systematic approach to understanding the interactions between catchment form and function in different parts of the world. Literature review showed that, in general, hydrology is facing the need for moving beyond the notion of ‘modeling everything’ to the notion of ‘capturing the essential features’. From features capturing, then, and the identification of the dominant processes, the further step is the development of models that correctly represent the investigated process. The DTA proposed in this work can be framed in the mentioned context. As main outcomes, the proposed DTA underlined that: 1) If physical processes do leave important signatures on the statistics of landscapes, and if we can quantify these signatures in detail, statistics can be used in assisting modeling, prediction and observatory design across scales and across environments; 2) since statistical properties of land-surface models are also scale dependent, studying their variation across scales can be effective in identifying ‘characteristic scales’ in the digital context, and therefore, can be a useful tool to identify the optimum scale for the desired analysis in the hydrogeomorphic realms. At the catchment scale, light detecting and ranging (LiDAR) is now becoming increasingly available and has the ability to resolve catchment land surfaces to the scale of a few centimeters in DTMs. The proposed approaches, based on statistics, are feasible for fast application and easy to be repeated. The derived hydrological features from DTM are not only accurate, but also they accelerate the processing speed of modeling of projects like water resource management and hazard modeling in different environments. At this point, some open questions still remain: Are statistically-distinct hydrological features the result of physically-distinct processes? Do differences in laws governing processes leave their signature on the statistical properties of landform geometry, and how much of the behavior of the coupled hydrologic/geomorphologic system is reflected in the statistics that we can digitally derive? Now that we can assess landforms with a high level of detail thanks to high resolution topography, some of these questions can be answered.

REFERENCES

Achard, F.; Eva, H.D.; Stibig, H.J.; Mayaux, P.; Gallego, J.; Richards, T. (2002). Determination of deforestation rates of the world's humid tropical forests. Science, 297, 999–1002.

Acharya, Y.B.; Sharma, S.; Chandra, H. (2004). Signal induced noise in PMT detection of LiDAR signals. Measurement, 35(3), 269-276.

Ackermann, F. (1999). Airborne laser scanning – present status and future expectations. ISPRN Journal of Photogrammetry and Remote Sensing, 54, 64-67.

Acreman, M.C.; Sinclair, C.D. (1986). Classification of drainage basins according to their physical characteristics; an application for flood frequency analysis in scotland. Journal of Hydrology, 84:365-380.

Adams, J.; Chandler, J. (2002). Evaluation of LiDAR and medium scale photogrammetry for detecting soft-cliff coastal change. Photogrammetric Record, v. 17, p. 405-418.

Ahlberg, S.; Söderman, U.; Elmqvist, M.; Persson, A. (2004). On modelling and visualisation of high resolution virtual environments using LiDAR data. Proceedings of 12th International Conference on Geoinformatics, Gävle, Sweden, 299-306.

Albani, M.; Klinkenberg, B.; Andison, D.W.; Kimmins, J.P. (2004). The choice of window size in approximating topographic surfaces from digital elevation models. International Journal of Geographical Information Science, 18(6), 577-593.

Alexander, D.E. (2008). A brief survey of GIS in massmovement studies, with reflections on theory and methods. Geomorphology, 94 (2008): 261-267.

Ali, T.A. (2004). On the selection of an interpolation method for creating a terrain model (TM) from LIDAR data. Proceedings of the American Congress on Surveying and Mapping (ACSM) Conference 2004, Nashville TN, U.S.A,

Anderson, M.G.; Burt, T.P. (1978a). The role of topography in controlling throughflow generation. Earth Surface Processes, 3:331-344.

Anderson, M.G.; Burt, T. P. (1978b). Toward more detailed field monitoring of variable source areas. Water Resources Research, 14:1123-1131.

Ardizzone, F.; Cardinali, M.; Galli, M.; Guzzetti, F.; Reichenbach, P. (2007). Identifcation and mapping of recent rainfall-induced landslides using elevation data collected by airborne LiDAR. Natural Hazards Earth System Science, 7(6), 637-650.

Arrell, K. , Wise, S.; Wood, J.; Donoghue, D. (2008). Spectral filtering as a method of visualising and removing striped artefacts in digital elevation data. Earth Surface Processes and Landforms, 33: 943–961.2008. doi: 10.1002/esp.1597

Bailly, J.S.; Lagacherie, P.; Millier, C.; Puech, C.; Kosuth, P. (2008). Agrarian landscapes linear features detection from LiDAR: application to artificial drainage networks. International Journal of Remote Sensing, 29(12), 3489.

Baltsavias, E.; O'Sullivan, L.; Zhang, C. (2004). Automated road extraction and updating using the Atomi system - performance comparison between aerial film, ADS40, Ikonos and Quickbird orthoimagery. International Archives of Photogrammetry, Remote Sensing and Spatial Information Sciences, 35, B2, 741-746.

Band, L.E. (1986).Topographic partition of watersheds with digital elevation models. Water Resources Research, 22(1), 15-24.

Barbarella, M.; Lenzi, V.; Zanni, M. (2004). Integration of airborne laser data and high resolution satellite images over landslides risk areas. International Archives of the Photogrammetry, Remote Sensing and Spatial Information Sciences 35(B4), 945-950.

Bartels, M.; Wei, H.; Mason, D.C. (2005). Wavelet packets and cooccurrence matrices for texture-based image segmentation. IEEE International Conference on Advanced Video and Signal-Based Surveillance, 1, 428–433.

BC-CARMS (2006). LiDAR -overview of technology, applications, market features and industry. Victoria, BC: Centre for Applied Remote Sensing, Modelling and Simulation, University of Victoria.

Bergström, H. (1952). On some expansions of stable distributions. Arkiv for Mathematik II, 375-378.

Berry, P.A.M.; Hoogerboord J.E. and Pinnock, R.A. (2000). Identification of common error signatures in global digital elevation models based on satellite altimeter reference data. Physics and Chemistry of the Earth, Part A: Solid Earth and Geodesy 25 (1), 95–99

Beven K.J.; Kirkby, M.J. (1979). A physically based, variable contributing area model of basin hydrology. Hydrol. Sci. Bull.; 24, 43–69.

Bishop, M.; Shroder, J.; Hickman, B.; Copland, L. (1998). Scale-dependent analysis of satellite imagery for characterization of glacier surfaces in the Karakoram Himalaya. Geomorphology, 21, 217–232.

Bishop,M.; Shroder, J.; Colby, J. (2003). Remote sensing and geomorphometry for studying relief production in high mountains. Geomorphology, 55, 345–361.

Blaschke, T.; Tiede, D.; Heurich, M. (2004). 3D landscape metrics to modelling forest structure and diversity based on laser scanning data. International Archives of the Photogrammetry, Remote Sensing and Spatial Information Sciences 36(8/W2), 129-132.

Blöschl, G.; Sivapalan, M. (1995). Scale Issues in Hydrological Modelling: A Review. Hydrological Processes, 9, no 3-4 (243 p.) (7 p.3/4), pp. 251-290

Bock, M.; Rossner, G.; Wissen, M.; Langanke, T.; Lang, S.; Klug, H.; Blaschke, T.; Remm, K.; Vrscaj, B. (2005). Spatial indicators for nature conservation from European to local scale. Ecological Indicators, 5, 322-338.

Bolongaro-Crevenna, A.; Torres-Rodríguez, V.; Sorani, V.; Frame, D.; Ortiz, M.A. (2004). Geomorphometric analysis for characterizing landforms in Morelos State, Mexico. Geomorphology, 67, 407–422.

Bonin,O. , F. Rousseaux. (2005). Digital terrain model computation from contour lines: how to derive quality information from artifact analysis. Geoinformatica, 9 (3), 253–268.

Bonk, R. (2002). Scale-dependent geomorphometric analysis for glacier mapping at Nanga Parbat: GRASS GIS approach. Proceedings of the Open Source GIS - GRASS Users Conference 2002, Trento, Italy, 1–4.

Booth, A.M.; Roering, J.J.; Perron, J.T. (2009). Automated landslide mapping using spectral analysis and high-resolution topographic data: Puget Sound lowlands, Washington, and Portland Hills, Oregon. Geomorphology 109, 132-147. doi:10.1016/j.geomorph.2009.02.027

Borak, S.z.; Härdle, W.; Weron, R. (2004). Stable Distributions. In P. Cizek, W. Härdle, R. Weron (eds.) Statistical Tools for Finance and Insurance, Springer.

Borga, M.; Dalla Fontana, G.; Cazorzi, F. (2002). Analysis of topographic and climatic control on rainfall-triggered shallow landsliding using a quasi-dynamic wetness index. Journal of Hydrology 268: 56-71

Brath, A.; Montanari, A.; Moretti, G. (2003). Assessing the effects on flood risk of land-use changes in the last five decades: an Italian case study. IAHS Publication, 278,. 435-441, IAHS Press, Olanda.

Brenning, A. (2008). Statistical geocomputing combining r and saga: the example of landslide susceptibility analysis with generalized additive models. In: J. Böhner, T. Blaschke and L. Montanarella (eds.) SAGA – Seconds Out, Hamburger Beiträge zur Physischen Geographie und Landschaftsökologie vol. 19, Hamburg University, Hamburg, 23–32.

Briese, C. (2004). Breakline modeling from airborne laser scanner data. Ph.D. Thesis. Institute of Photogrammetry and Remote Sensing, Vienna University of Technology.

Briese, C. (2010). Extraction of digital terrain models. In Vosselman, G.; Maas, H.G. (eds.) Airborne and terrestrial laser scanning. First ed. Whittles Publishing, UK, pp. 135-168.

Broscoe, A.J. (1959). Quantitative analysis of longitudinal stream profiles of small watersheds. Office of Naval Research, Project NR 289-042, Technical Report n.18, Department of Geologyy, Columbia University, New York.

Brown, D.G.; Bara T.J. (1994). Recognition and reduction of systematic error in elevation and derivative surfaces from 7.5 min DEMs, Photogrammetric Engineering and Remote Sensing 60 (2), 189–194-

Brunson, E.G.; Olsen, R.W. (1978). Data digital elevation model collection systems. In Proceedings of the digital terrain models (DTM) Symposium, 9–11 May, St Louis, Missouri (American Society of Photogrammetry, Falls Church, Virginia); 72–99.

Burel, F.; Baudry, J. (2005). Habitat quality and connectivity in agricultural landscapes: the role of land use systems at various scales in space and time. Ecological Indicators, 5, 305-313.

Burrough, P.A.; McDonnell, R.A. (1998). Principles of Geographic Information Systems. Oxford University Press, Oxford (GB).

Burrough.P.A. (2002). GIS and geostatistics for environmental modeling. In W. Shi, P.F. Fisher, M.F. Goodchild (eds.), Spatial data quality, Taylor and Francis, London, 18–34.

Buttle, J. (2006). Mapping first-order controls on streamflow from drainage basins: the T3 template. Hydrological Processes 20, pp. 3415–3422.

Carey, S.K.; Woo, M. (2001). Spatial variability of hillslope water balance,Wolf Creek basin, subarctic Yukon. Hydrological Processes 15(16): 3113–3132, DOI:10.1002/hyp.319.

Carluer, N.; Marsily, G.D. (2004). Assessment and modelling of the influence of man-made networks on the hydrology of a small watershed: implications for fast flow components, water quality and landscape management. Journal of Hydrology 285: 76-95.

Carrara, A. (1983). A multivariate model for landslide hazard evaluation. Mathematical Geology 15: 403-426.

Carrara, A.; Guzzetti, F. (Ed.) (1995). Geographical Information Systems in Assessing Natural Hazards. Kluwer Academic Publisher, Dordrecht, The Netherlands, 353 pp.

Carrara, A.; Cardinali, M.; Detti, R.; Guzzetti, F.; Pasqui, V.; Reichenbach, P. (1991). GIS Techniques and statistical models in evaluating landslide hazard. Earth Surface Processes and Landform 16: 427-445.

Carrara, A.; Guzzetti, F.; Cardinali, M.; Reichenbach, P. (1999). Use of GIS Technology in the Prediction and Monitoring of Landslide Hazard. Natural Hazards 20:2-3 117-135.

Carturan, L.; Cazorzi, F.; Dalla Fontana, G. (2009). Enhanced estimation of glacier mass balance in unsampled areas by means of topographic data. Annals of Glaciology, 50, 37– 56.

Cavalli, M.; Tarolli, P.; Marchi, L.; Dalla Fontana, G. (2008). The effectiveness of airborne LiDAR data in the recognition of channel bed morphology. Catena 73: 249-260. doi:10.1016/j.catena.2007.11.001.

Cavalli, M.; Tarolli, P.; Marchi, L.; Dalla Fontana, G. (2008). The effectiveness of airborne LiDAR data in the recognition of channel-bed morphology. Catena, 73(3), 249-260.

Cavalli, M.; Trevisani S.; Goldin, B.; Mion E.; Marchi, L. (2011). Derivation of channel network of an alpine region from high-resolution DTM: the example of the Autonomous Province of Trento (Italy), Geophysical Research Abstracts, 13, EGU2011-8188, eISSN: 1607-7962

Cavalli, M.; Tarolli, P. (*in press*). Application of LiDAR technology for rivers analysis, Italian Journal of Engineering Geology and Environment, ISSN 1825-663.

Cavalli, M.; Marchi, L. (2008). Characterisation of the surface morphology of an alpine alluvial fan using airborne LiDAR, Nat. Hazards Earth Syst. Sci.; 8, 323-333, doi:10.5194/nhess-8-323-2008.

Cazorzi,F.; Dalla Fontana, G.; De Luca, A.; Sofia, G.; Tarolli, P., *(in press)*. Drainage network detection and assessment of network storage capacity in agrarian landscape. Hydrological Processes.

Challis, K. (2006). Airborne laser altimetry in alluviated landscapes. Archaeological Prospection, 13(2), 103–127. DOI: 10.1002/arp.272.

Challis, K.; Howard, A.J. (2006). A review of trends within archaeological remote sensing in alluvial environments. Archaeological Prospection, 13(4), 231–240. DOI: 10.1002/arp.296.

Chambers, J.M.; Mallows, C.L.; Stuck, B.W. (1976). A method for simulating stable random variables. J. Amer. Statist. Assoc.; 71, 340–344.

Chaplot, V.; Darboux, F.; Bourennane, H.; Leguédois, S.; Silvera, N.; Phachomphon, K. (2006). Accuracy of interpolation techniques for the derivation of digital elevation models in relation to landform types and data density. Geomorphology 77(1-2), 126-141.

Charaniya, A.P.; Manduchi, R.; Lodha, S. K. (2004). Supervised parametric classification of aerial LiDAR data. Proceedings of 2004 Conference on Computer Vision and Pattern Recognition Workshop (CVPRW'04), Washington D.C, USA,

Chaubey, I.; Cotter, A.S.; Costello, T. A.; Soerens, T.S. (2005). Effect of DEM data resolution on SWAT output uncertainty. Hydrological Processes 19, 621-628.

Chigira, M.; Duan, F.J.; Yagi, H.; Furuya, T. (2004). Using an airborne laser scanner for the identification of shallow landslides and susceptibility assessment in an area of ignimbrite overlain by permeable pyroclastics. Landslides 1(3): 203-209

Chris, A.; Glasbey, R. (1997). Fast computation of moving average and related filters in octagonal windows. Pattern Recognition Letters, 555,565 .

Clerici A, Perego S, Tellini C, Vescovi P (2002). A procedure for landslide susceptibility zonation by the conditional analysis method. Geomorphology 48: 349–364.

Cobby, D.M.; Mason, D.C.; Davenport, I.J. (2001). Image processing of airborne scanning laser altimetry data for improved river flood modeling. ISPRS Journal of Photogrammetry and Remote Sensing 56(2), 121–138.

Cohen, J. (1960). A coefficient of agreement for nominal scales. Educational and Psychological Measurement, 20, 37–46.

Cooke, R.U.; Doornkamp, J.C. (1990). Geomorphology in environmental management. Oxford University Press, 2nd edition.

Coren, F.; Visintini, D.; Prearo, G. and Sterzai, P. (2005). Integrating LiDAR intensity measures and hyperspectral data for extracting of cultural heritage. Proceedings of Italy - Canada 2005

Workshop on 3D Digital Imaging and Modeling: Applications of Heritage, Industry, Medicine and Land, Padova, Italy.

Costa-Cabral, M. C.; Burges, S. J. (1994). Digital elevation model networks (DEMON): A model of flow over hillslopes for computation of contributing and dispersal areas. Water Resour. Res. 30(6), 1681–1692.

Cowen, D.J.; Jensen, J.R.; Hendrix, C.; Hodgson, M.E.; Schill, S.R. (2000). A GIS-assisted rail construction econometric model that incorporates LIDAR data. Photogramm. Eng. Rem. Sens.; 66: 1323-1328.

Crosta, G.B.; Frattini, P. (2003). Distributed modelling of shallow landslide triggered by intense rainfall. Natural Hazards and Earth System Sciences 3: 81-93.

Dagès, C.; Voltz, M.; Bsaibes, A.; Prévot, L.; Huttel, O.; Louchart, X.; Garnier, F.; Négro, S. (2009). Estimating the role of a ditch network in groundwater recharge in a Mediterranean catchment using a water balance approach. Journal of Hydrology 375: 498-512.

Dal Cin, C.; Moens, L.; Dierickx, P.; Bastin, G.; Zech, Y. (2005). An integrated approach for realtime floodmap forecasting on the Belgian Meuse river'. Natural Hazards, 36(1–2), 237–256.

Dalla Fontana, G.; Marchi, L. (2003). Slope-area relationships and sediment dynamics in two alpine streams. Hydrological Processes 17(1): 73-87.

Davies, E.R. (1984). Circularity — A new principle underlying the design of accurate edge orientation operators. Image and Vision Comput. 2, 134–142.

Davis, C.H.; Jiang, H.; Wang, X.Y. (2001). Modeling and estimation of the spatial variation of elevation error in high-resolution DEMs from stereo-image processing" IEEE Transactions on Geoscience and Remote Sensing, 39(11), 2483–2489.

DeGraff, J.V. (1985).Using isopleth maps of landslide deposits as a tool in timber sale planning. Bulletin American Association of Engineering Geologists 22:445–453.

Desmet, P.J.J.; Govers, G. (1996). Comparison of routing algorithms for digital elevation models and their implications for predicting ephemeral gullies.. Int. J. Geogr. Inf. Syst.; 10: 311–331.

Devito, K.; Creed, I.; Gan, T.; Mendoza, C.; Petrone, R.; Silins, U.; Smerdon, B. (2005). A framework for broad-scale classification of hydrologic response units on the Boreal Plain: is topography the last thing to consider? Hydrological Processes 19(8): 1705–1714, DOI:10.1002/hyp.5881.

Dietrich, E.W.; Reiss, R.; Hsu, M.L.; Montgomery, D.R. (1995). A process-based model for colluvial soil depth and shallow landsliding using digital elevation data. Hydrological Process 9: 383–400.

Dietrich, W. E.; Dunne, T. (1993). The channel head. In: Channel Network Hydrology, K. Beven and M. J. Kirkby (eds.), 175-219. Wiley, Chichester, UK.

Dikau, R. (1989). The application of a digital relief model to landform analysis in geomorphology. In Raper, J.; editor, Three dimensional application in Geographic Information Systems, pages 51-77. Taylor & Francis.

Dodds, P. S. , Rothman, D.H. (2000). Scaling, universality, and geomorphology. Annu. Rev. Earth Planet. Sci. 28, 571-610.

Doneus, M.; Briese, C. (2006). Full-waveform airborne laser scanning as a tool for archaeological reconnaissance. In: From Space to Place. 2nd International Conference on Remote Sensing in Archaeology, Campana S, Forte M (eds). BAR International Series 1568, 99–105. Archaeopress: Oxford.

Douglas, D.H (1994). Least cost path in GIS using an accumulated cost surface and slope lines. Cartographica, 31, 37-51.

Dubuisson, M-P.; Jain, A.K. (1994). A modified Hausdorff distance for object matching. Pattern Recognition, 1994. Vol. 1 - Conference A: Computer Vision & Image Processing.; *Proceedings of the 12th IAPR International Conference on* , vol.1, no.; pp.566-568 vol.1, 9-13, doi: 10.1109/ICPR.1994.576361.

Duda, R.O.; Hart, P. E. and Stork, D. G. (2001). Pattern classification. New York: Wiley.

Duke, G.; Kienzle, S.; Johnson, D.; Byrne, J. (2006). Incorporating ancillary data to refine anthropogenically modified overland flow paths. Hydrological Processes 20, 1827-1843.

Dunn, S.M.; Mackay, R. (1996). Modelling the hydrological impacts of open ditch drainage. Journal of Hydrology 179: 37-66.

Eastman, J.R. (1989). Pushbroom algorithms for calculating distances in raster grids [online]. Proceedings of the International Symposium on Computer-Assisted Cartography, Autocarto 9, 288-97.

Ellis, E.C. (2004). Long-term ecological changes in the densely populated rural landscapes of China. In: R.S. DeFries, G.P. Asner and R.A. Houghton, Editors, Ecosystems and Land Use Change, American Geophysical Union, Washington, DC, 303–320.

Ellis, E.C.; Wang, H.; Xiao, H.; Peng, K.; Liu, X.P.; Li, S.C.; Ouyang, H.; Cheng, X.; Yang, L.Z. (2006). Measuring long-term ecological changes in densely populated landscapes using current and historical high resolution imagery. Remote Sensing of Environment, 100(4), 457-473.

El-Sheimy, N.; Valeo, C. and Habib, A. (2005) Digital terrain modeling: acquisition, manipulation, and application. Boston and London: Artech House.

Endreny, T. A.; Wood, E.F. (2003). Maximizing spatial congruence of observed and DEM-delineated overland flow networks, Int. J. Geogr. Inf. Syst.; 17, 699– 713.

Erskine, R. H.; Green, T. R.; Ramirez, J. A. and MacDonald, L. H. (2006). Comparison of grid-based algorithms for computing upslope contributing area.. Water Resour. Res.; 42: W09416 doi:10.1029/2005WR004648.

Eshani, A.H.; Quiel, F. (2008). Geomorphometric feature analysis using morphometric parameterization and artificial neural networks. Geomorphology, 99, 1–12.

Evans, I.S. (1972). General geomorphology, derivatives of altitude and descriptive statistics. In: Chorley, R.J. (Ed.), Spatial Analysis in Geomorphology. Methuen & Co. Ltd, London, pp. 17-90.

Evans, I.S. (1979). An integrated system of terrain analysis and slope mapping. Final report on grant DA-ERO-591-73-G0040, University of Durham, England.

Evans, I.S. (1980). An integrated system of terrain analysis and slope mapping. Zeitschrift für Geomorphologic Suppl-Bd 36: 274-295.

Evans, I.S. (2003). Scale-specific landforms and aspects of the land surface. In Concepts and Modelling in Geomorphology: International Perspectives, eds. I. S. Evans, R.Dikau, E. Tokunaga,H.Ohmori and M. Hirano. Tokyo: Terrapub, pp. 61–84.

Fairfield, J.; Leymarie, P. (1991). Drainage networks from grid digital elevation models.. Water Resour. Res.; 27: 709–717.

Fisher, P.F. (1993). Algorithm and implementation uncertainty in viewshed analysis. International Journal Of Geographical Information Systems, 7:331--347.

Fisher, P.F.; Tate, N. J. (2006). Causes and consequences of error in digital elevation models. Progress in Physical Geography 30(4), 467-489.

Fisher, P. (1998). Improved modeling of elevation error with geostatistics. GeoInformatica, 2, 215–233.

Florinsky I.V. (1998). Accuracy of local topographic variables derived from digital elevation models. International Journal of Geographical Information Science 12(1): 47-61.

Florinsky, I.V. (2002). Errors of signal processing in digital terrain modelling, International Journal of Geographical Information Science, 15 (5), 475–501.

Florinsky I.V. (2005). Artificial Lineaments in Digital Terrain Modelling: Can Operators of Topographic Variables Cause Them?. Mathematical Geology, 37, 357-372. DOI: 10.1007/s11004-005-5953-3

Florinsky I.V.; Kuryakova, G.A. (2000). Determination of grid size for digital terrain modeling in landscape investigations - exemplified by soil moisture distribution at a micro-scale. International Journal of Geographical Information Science 14(8), 815-832.

Foley, J.A.; DeFries, R.; Asner, G.P.; Barford, C.; Bonan, G.; Carpenter, S.R. (2005). Global consequences of land use. Science, 309, 570–574.

Forlani, G.; Nardinocchi, C. (2007). Adaptive filtering of aerial laser scanning data. International Archives of Photogrammetry, Remote Sensing and Spatial Information Sciences 36(part 3/W52), 130-135.

Frankel, K.L.; Dolan, J.F. (2007). Characterizing arid-region alluvial fan surface roughness with airborne laser swath mapping digital topographic data. Journal of Geophysical Research - Earth Surface 112, F02025. doi:10.1029/2006JF000644.

Freeman, T.G. (1991). Calculating catchment area with divergent flow based on a regular grid.. Comput. Geosci.; 17: 413–422.

French, J.R. (2003). Airborne LiDAR in support of geomorphological and hydraulic modeling. Earth Surface Processes and Landforms, 28(3), 321–335. DOI: 10.1002/esp.484

Gallant, J.C.; Wilson, J.P. (2000). Primary Topographic Attributes. In: Terrain Analysis: Principles and Applications, J. P. Wilson and J. Gallant (eds.). New York: John Wiley & Sons Inc.; 51-85.

Gallart, F.; Llorens, P.; Latron, J. (1994). Studying the role of old agricultural terraces on runoff generation in a small Mediterranean mountainous basin. Journal of Hydrology, 159, 291–303.

Ganas, A.; Pavlides, S.; Karastathis, V. (2005). DEM-based morphometry of range-front escarpments in Attica, central Greece, and its relation to fault slip rates. Geomorphology, 65, 301–319.

Gandoy-Bernasconi, W.; Palacios-Velez, O. L. (1990). Automatic cascade numbering of unit elements in distributed hydrological models.. J. Hydrol.; 112: 375–393.

Garbrecht, J.; Martz, L. (1997). The assignment of drainage direction over flat surfaces in raster digital elevation models. Journal of Hydrology, 193, 204–213.

Garbrecht, J.; Starks, P. (1995). Note on the use of USGS Level 1 7.5-Minute DEM coverages for landscape drainage analysis. Photogrammetric Engineering and Remote Sensing, 61(5):519–522.

Garcia, M.; Camarasa, A. (1999). Use of geomorphological units to improve drainage network extraction from a dem : Comparison between automated extraction and photointerpretation methods in the carraixet catchment (valencia, spain). International Journal of Applied Earth Observation and Geoinformation, 1 (3-4), 187-195.

Gascuel-Odoux, C.; Aurousseau, P.; Doray, T.; Squividant, H.; Macary, F.; Uny, D.; Grimaldi, C. (2011). Incorporating landscape features to obtain an object-oriented landscape drainage network representing the connectivity of surface flow pathways over rural catchments. Hydrological Processes 25: 3625-3636.

Geneletti, D.; Gorte, B.G.H. (2003). A method for objectoriented land cover classification combining Landsat TM data and aerial photographs. International Journal of Remote Sensing, 24: 1273–1286.

Gilbert, G.K. (1909). The convexity of geology. J. Geol.; 17: 344-350.

Glenn, N.F.; Streutker, D.R.; Chadwick, D.J.; Thackray, G.D.; Dorsch, S.J. (2006). Analysis of LiDAR-derived topographic information for characterizing and differentiating landslide morphology and activity. Geomorphology 73: 131-148.

Gonçalves-Seco, L.; Miranda, D.; Crecente, F.; Farto, J. (2006). Digital terrain model generation using airborne LiDAR in a forested area Galicia, Spain. Proceedings of 7th International symposium on spatial accuracy assessment in natural resources and environmental sciences, Lisbon, Portugal, 169-180.

Gonzalez, R.C.; Woods, R.E.; Eddins, S.L. (2003). Digital Image Processing Using MATLAB, New Jersey, Prentice Hall, 2003, Chapter 11.

Goodchild, M.F. (1986). Spatial autocorrelation. Concepts and techniques in modern geography (CATMOG), 47, 1-56, 1986.

Grabs, T.; Seibert, J.; Bishop, K.; Laudon, H. (2009). Modeling spatial patterns of saturated areas: a comparison of the topographic wetness index and a dynamic distributed model. Journal of Hydrology 373: 15–23.

Grayson, R.; Blöschl G (2001). Spatial Patterns in Catchment Hydrology : Observations and Modelling, Cambridge University Press, Cambridge, U.K. ; New York.

Gregory, K. J. and Walling, D. E. (1973). Drainage basin. Form and Process. Edward Arnold.

Gritzner, M.; Marcus, A.; Aspinall, R.; Custer, S. (2001). Assessing landslide potential using GIS, soil wetness modeling and topographic attributes, Payette River, Idaho. Geomorphology, 37 , 149–165.

Guntner, A.; Seibert, J.; Uhlenbrook, S. (2004). Modeling spatial patterns of saturated areas: An evaluation of different terrain indices. Water Resour. Res.; 40, W05114, .

Gupta, V. A.; Waymire, E.; Wang, C. T. (1980). A representation of an instantaneous unit hydrograph from geomorphology. Water Resources Research, 16(5), 855-862.

Guth, P.L. (1999). Contour line “ghosts” in USGS level 2 DEMs, Photogrammetric Engineering and Remote Sensing, 65 (3), 289–296.

Guzzetti, F.; Carrara, A.; Cardinali, M.; Reichenbach, P. (1999). Landslide hazard evaluation: a review of current techniques and their application in a multi-scale study, Central Italy. Geomorphology 31: 181-216.

Habib, A.; Ghanma, M.; Morgan, M.; Al-Ruzouq, R. (2005). Photogrammetric and LiDAR data registration using linear features. Photogrammetric Engineering and Remote Sensing 71(6), 699-707.

Hamilton, S. (2007). Completing the loop: from data to decisions and back to data. Hydrological Processes 21: 3105–3106.

Hammond, C.J.; Prellwitz, R.W.; Miller, S.M. (1992). Landslides hazard assessment using Monte Carlo simulation. In: Bell DH (ed) Proceedings of 6th international symposium on landslides, Christchurch, New Zealand, Balkema, 2, 251–294.

Haneberg, W.C. (2008). Elevation errors in a LIDAR digital elevation model of West Seattle and their effects on slope-stability calculations Reviews in Engineering Geology, 20, 55-65, doi:10.1130/2008.4020(03)

Harayama, A.; Jaquet, J.M. (2004). Multi-source object-oriented classification of landcover using very high resolu-tion imagery and digital elevation model. Switzerland: UNEP.

Hassan, M. (1988). Filtering digital profile observations”. Photogrammetric Engineering and Remote Sensing 54: 1391–1394.

Hays, W. L. (1988). Statistics (4th ed.). New York: CBS College Publishing, 1988.

Heine, R. A.; Lant, C.L.; Sengupta, R.R. (2004). Development and comparison of approaches for automated mapping of stream channel networks, Ann. Assoc. Am. Geogr.; 94(3), 477–490.

Heipke, C.; Mayer, H.; Wiedemann, C.; Jamet, O. (1997). Automated reconstruction of topographic objects from aerial images using vectorized map information. International Archives of Photogrammetry and Remote Sensing 23: 47-56.

Hengl, T. (2006). Finding the right pixel size. Computer and Geosciences 32(9), 1283-1298.

Hengl, T.; Heuvelink, G.B.; van Loon, E.E. (2010). On the uncertainty of stream networks derived from elevation data: the error propagation approach. Hydrol. Earth Syst. Sci.; 14, 1153-1165, doi:10.5194/hess-14-1153-2010.

Heuvelink, G.B.; Burrough, P.; Stein, A. (2007). Developments in Analysis of Spatial Data Uncertainty Since 1989. in: Classics from IJGIS: twenty years of the International Journal of Geographical Information Science and Systems, edited by: Fisher, P.; Taylor and Francis, Boca Raton, FL, 91–95.

Heuvelink. G.B (1998).Error Propagation in Environmental Modelling with GIS. Taylor & Francis Ltd, London, England, 127 p.

Hiller, J.K.; Smith, M. (2008). Residual relief separation: digital elevation model enhancement for geomorphological mapping. Earth Surface Processes and Landforms, 33, 2266–2276. DOI: 10.1002/esp.1659.

Hodgson, M.E.; Bresnahan, P. (2004). Accuracy of airborne LiDAR-derived elevation: empirical assessment and error budget. Photogrammetric Engineering and Remote Sensing 70(3), 331-339.

Hodgson, M.E.; Jensen, J.R.; Raber, G.; Tullis, J.; Davis, B.; Thompson, G.; Schuckman, K. (2005). An Evaluation of LIDAR-Derived Elevation and Terrain Slope in Leaf-off Conditions. Photogrammetric Engineering & Remote Sensing,71(7):817–823.

Hodgson, M.E.; Jensen, J.R.; Schmidt, L.; Schill, S.; Davis, B. (2003). An evaluation of LIDAR- and IFSAR-derived digital elevation models in leaf-on conditions with USGS Level 1 and Level 2 DEMs" Rem Sens Environ 84: 295-308.

Höfle, B.; Vetter, M.; Pfeifer, N.; Mandlburger, G.; Stötter, J. (2009). Water surface mapping from airborne laser scanning using signal intensity and elevation data. Earth Surface Processes and Landforms 34 (12): 1635-1649.

Höfle, B.; Pfeifer, N. (2007). Correction of laser scanning intensity data: data and model-driven approaches. ISPRS Journal of Photogrammetry and Remote Sensing *in press*.

Hollaus, M.; Wagner, W.; Kraus, K. (2005). Airborne laser scanning and usefulness for hydrological models. Advances in Geosciences 5(1), 57-63.

Hollingworth, R.; Kovacs, G.S. (1981). Soil slumps and debris flows: prediction and protection. Bull.Assoc.Eng.Geol.; 18, 17-28.

Holmes, K.W.; Chadwick, O.A.; Kyriakidis, P. C. (2000). Error in a USGS 30-meter digital elevation model and its impact on terrain modeling. Journal of Hydrology, Vol. 233, 154–173.

Holmgren, P. (1994). Multiple flow direction algorithms for runoff modelling in grid based elevation models: an empirical evaluation. Hydrol. Processes, 8: 327–334.

Horn, B.K.P. (1981). Hill shading and the reflectance map. Proceedings of the IEEE, 69(1), 14-47.

Horton, R.E. (1945). Erosional development of streams and their drainage basins: hydrophysical approach to quantitative morphology. Geol. Soc. Am. Bull.; 56: 275–370.

Hrachowitz, M.; Soulsby, C.; Tetzlaff, D.; Dawson, J.J.C.; Malcolm, I.A. (2009). Regionalization of transit time estimates in montane catchments by integrating landscape controls. Water Resources Research 45: DOI:10.1029/2008WR00749.

Humme, A.; Lindenbergh, R.; Sueur, C. (2006). Revealing Celtic fields from LiDAR data using kriging based filtering. Proceedings of the ISPRS Commission V Symposium, Dresden, 25–27 September, Vol. XXXVI, part 5.

Hunter, G.J.; Goodchild, M.F. (1995). Dealing with error in spatial databases: A simple case study", Photogrammetric Engineering and Remote Sensing, vol. 61, pp. 529–537.

Hutchinson, M.F. (1988). Calculation of hydrologically sound digital elevation models. Proceedings, 3rd International Symposium on Spatial Data Handling, International Geographical Union, Sydney, Australia, 117-133.

Hutchinson, M.F. (1989). A new procedure for gridding elevation and streamline data with automatic removal of spurious pits. Journal of Hydrology 106 (1989), 211–232.

Iovine, G.; Di Gregorio, S.; Lupiano, V. (2003). Debris-flow susceptibility assessment through cellular automata modeling: an example from 15-16 December 1999 disaster at Cervinara and San Martino Valle Caudina (Campania, southern Italy). Natural Hazards and Earth System Sciences 3: 457-468.

James, L.A.; Watson, D.G.; Hansen, W.F. (2007). Using LIDAR data to map gullies and headwater streams under forest canopy: south carolina, USA. Catena 71(1),132-144

Jelalian, A.V.(1992). Laser Radar Systems. Artech House. Boston and London, 292 p.

Jencso, K.G.; McGlynn, B.L.; Gooseff, M.N.; Wondzell, S.M.; Bencala, K.E.; Marshall, L.A. (2009). Hydrologic connectivity between landscapes and streams: transferring reach- and plot-scale understanding to the catchment scale. Water Resources Research 45: 10, DOI:1029/2008WR007225.

Jenson, S.K.; Domingue, O.J. (1988). Extracting Topographic Structure from Digital Elevation Data for Geographic Information System Analysis, Photogrammetric Engineering and Remote Sensing. Vol. 54, No. 11, November 1988, pp. 1593-1600.

Jones, A.F.; Brewer, P.A.; Johnstone, E.; Macklin, M.G. (2007). High resolution interpretative geomorphological mappign of river valley environments using airborne LiDAR data. Earth surface processes and landform, 21, 1574-1592

Jones, K.H. (1998). A comparison of algorithms used to compute hill slope as a property of the DEM. Computers & Geosciences, vol. 24 (4), 315–323.

Jones, N.L.; Wright, S.G.; Maidment, D.R. (1990). Watershed delineation with triangle-based terrain models.. J. Hydraul. Div. ASCE, 116(10): 1232–1251.

Kachigan, S.K. (1986). Statistical analysis: An interdisciplinary introduction to univariate and multivariate methods. New York: Radius Press.

Kak, A.; Rosenfeld, A.C. (1982). Digital picture Processing, 2nd ed.; New York: Academic, 1982, 1-2, p 435+ 349 pp.

Karel W.; Kraus K. (2006). Quality parameters of digital terrain models. In Semina on Autmated Quality Control of Digital Terrain Models, EuroSDR Seminar, 18-19 August 2005, Aalborg, Denmark; available online at http://www.ipf.tuwien.ac.at/publications/2006/Karel_Kraus_QualityPar4DTM.pdf [*last access jan.; 2012*]

Karel W.; Pfeifer, N.; Briese, C. (2006). Dtm Quality Assessment. Talk: ISPRS Technical Commission Symposium, Vienna; 07-12-2006 - 07-14-2006; in: "ISPRS Technical Commission II Symposium 2006", International Archives of the ISPRS, XXXVI/2, 1682-1750; 7 – 12.

Kendall, M.; Stuart, A. (1979). The advanced theory of statistics (Vol. 2). New York: Hafner.

Kenward, T.; Lettenmaier, D.P.; Wood, E.F.; Fielding, E. (2000). Effects of digital elevation model accuracy on hydrologic predictions. Remote sensing of environment, 74(3):432-444.

Kienzle, S. (2004). The effect of DEM raster resolution on first order, second order and compound terrain derivatives. Transactions in GIS 8(1), 83-111.

Kim, S.; Lee, H. (2004). A digital elevation analysis: a spatially distributed flow apportioning algorithm. Hydrological Processes, 18(10), 1777–1794. DOI: 10.1002/hyp.1446

Kirkby, M.J.; Bracken, L.; Reaney, S. (2002). The influence of land use, soils and topography on the delivery of hillslope runoff to channels in SE Spain. Earth Surface Processes and Landforms 27: 1459–1473.

Kirkby, M.J. (1988). Hillslope runoff processes and models. Journal of Hydrology, 100:315-339.

Klemes, V. (1983). Conceptualization and Scale in Hydrology. Journal of Hydrology, 65, 1-23.

Klinkenberg, B. , Goodchild, M.F. (1992). The fractal properties of topography: a comparison of methods. Earth Surface Processes and Landforms 17: 217–234.

Kobler, A.; Pfeifer, N.; PeterOgrinc, Todorovski, L.; Oštir, K. and Džeroski, S. (2007). Repetitive interpolation: A robust algorithm for DTM generation from aerial laser scanner data in forested terrain. Remote Sensing of Environment 108, 9-23.

Korup, O. (2004). Landslide-induced river channel avulsions in mountain catchments of southwest New Zealand. Geomorphology, 63, 57–80.

Köthe, R.; Bock, M. (2009). Preprocessing of Digital Elevation Models – derived from Laser Scanning and Radar Interferometry – for Terrain Analysis in Geosciences. Proceedings of Geomorphometry, Zurich, Switzerland, 31 August - 2 September.

Kraus K.; Pfeifer, N. (1998). Determination of terrain models in wooded areas with airborne laser scanner data, ISPRS Journal of Photogrammetry and Remote Sensing, 53/4, 193–203.

Kraus, K.; Pfeifer, N. (2001). Advanced DTM generation from LIDAR data. International Archives of Photogrammetry and Remote Sensing, XXXIV-3/W4, 23-35.

Krcho, J. (1991). Georelief as a subsystem of landscape and influence of morphometric parameters of georelief on spatial differentiation of landscape-ecological processes. Ecology (CSFR) vol.10 115-157.

Krüger, T.; Meinel, G. (2008). Using Raster DTM for Dike Modelling. In: Advances in 3D Geoinformation Systems, 2008, Part II, Theme I:,101-113, DOI: 10.1007/978-3-540-72135-2_6

Kyriakidis, P.C.; Shortridge, A.M.; Goodchild, M.F. (1999). Geostatistics for conflation and accuracy assessment of digital elevation models. International Journal of Geographical Information Science, 13 (7), 677–707.

Lagacherie, P.; Diot, O.; Domange, N.; Gouy, V.; Floure, C.; Kao, C.; Moussa, R.; Robbez-Masson, J.; Szleper V. (2004). An indicator approach for describing the spatial variability of human-made stream network in regard with herbicide pollution in cultivated watersheds. Ecological indicators, 6, 265-279.

Lam, L.; Lee, S.W.; Suen, C.Y. (1992). Thinning methodologies: A comprehensive survey. IEEE Trans. Pattern Anal. Machine Intel.; 14: 869-885.

Landis, J.R.; Koch, G.G. (1977). The measurement of observer agreement for categorical data. Biometrics, 33, 159-174.

Lashermes, B.; Foufoula-Georgiou, E.; Dietrich, W.E. (2007). Channel network extraction from high resolution topography using wavelets. Geophysical Research Letters 34, L23S04. doi:10.1029/2007GL031140.

Lassueur, T.; Joost, S.; Randin, C. F. (2006). Very high resolution digital elevation models: do they improve models of plant species distribution. Ecological Modelling 198, 139-153.

Laudon, H.; Soblom, V.; Buffam, I.; Seibert, J.; Morth, C.M. (2007). The role of catchment scale and landscape characteristics for runoff generation of boreal streams. Journal of Hydrology 344: 198–209.

Lee, S.; Shan, J.; Bethel, J.S. (2003). Class-guided building extraction from Ikonos imagery. Photogrammetric Engineering and Remote Sensing 69(2): 143-150.

Lee, J.; Snyder, P.K.; Fisher, P.F. (1992). Modeling the effect of data errors on feature extraction from digital elevation models. Photogrammetric Engineering and Remote Sensing, 58, 1461-1467.

Lee, H.S. (2004). A hybrid model for DTM generation from LiDAR signatures, (PhD Thesis). Mississippi: Department of Electrical and Computer Engineering, Mississippi State University.

Lemmens, M. (2007). Airborne LiDAR Sensors. GIM International 21(2).

Lenzi, M.A. (2001). Step-pool evolution in the Rio Cordon, Northeastern italy. Earth Surfaces Processes and Landforms 26: 991-1008.

Lenzi, M.A.; Mao, L.; Comiti, F. (2003). Interannual variation of suspended sediment load and sediment yield in an Alpine catchment. Hydrological Science Journal 48(6): 899-915.

Lenzi, M.A.; Mao, L.; Comiti, F. (2004). Magnitude-frequency analysis of bed load data in Alpine boulder bed stream. Water Resources Research 40, W07201. doi:10.1029/2003WR002961

LePage, R.; Woodroofe, M.; Zinn, J. (1981). Convergence to a stable distribution via order statistics. Annals of Probability, 9, 624-632.

Levavasseur, F.; Bailly, J.S.; Lagacherie P.; Colin, F.; Rabotin, M. (2011). Simulating the effects of spatial configurations of agricultural ditch drainage networks on surface runoff from agricultural catchments. Hydrological processes, 'Accepted Article', doi: 10.1002/hyp.8422

Li, Z. (1991). Effects of check points on the reliability of DTM accuracy estimates obtained from experimental test. Photogramm. Eng. Remote Sens.; 57(10), 1333–1340.

Li, Z.; Zhu, Q.; Gold, C. (2005). Digital Terrain Modelling: Principles and Methodology. 1st Edn.; CRC Press, New York.

Li, Z. (1993). Theoretical models of the accuracy of digital terrain models: an evaluation and some observations. The Photogrammetric Record, 14(82), 651–660.

Lim, K.; Treitz, P.; Wulder, M.; St-Onge, B.; Flood, M. (2003). LiDAR Remote Sensing of Forest Structure. *Progress in Physical Geography,* 27(1):88-106.

Liu, H. Jezek, K. (1999). Investigating DEM error pattern by directional variograms and Fourier analysis. Geographical Analysis, 31(3):249-266.

Liu, J.; Liu, S.; Tieszen, L.T.; Chen, M. (2007). Estimating soil erosion using the USPED model and consecutive remotely sensed land cover observations. In Proceedings of the 2007 summer computer simulation conference (SCSC). Society for Computer Simulation International, San Diego, CA, USA, 16 , 6.

Liu, X.; Zhang, Z.; Peterson, J.; Chandra, S. (2007). LiDAR-derived high quality ground control information and DEM for image orthorectification. GeoInformatica 11(1), 37-53.

Liu, X. (2008). Airborne LiDAR for DEM generation: some critical issues. Progress in Physical Geography: an international review of geographical work in the natural and environmental sciences, 32 (1). pp. 31-49. ISSN 0309-1333

Lloyd, C.D.; Atkinson, P.M. (2002). Deriving DSMs from LiDAR data with kriging. International Journal of Remote Sensing 23(12), 2519-2524.

Lohani, B.; Mason, D.C. (2001). Application of airborne scanning laser altimetry to the study of tidal channel geomorphology. ISPRS Journal of Photogrammetry and Remote Sensing, 56(2): 100–120. DOI: 10.1016/S0924-2716(01)00041-7

Lohr, U. (1998). Digital elevation models by laser scanning. Photogrammetric Record 16, 105-109.

Lopez, C. (2000). Improving the elevation accuracy of digital elevation models: a comparison of some error detection procedures. Transactions in GIS, 4, 43–64.

Maas, C.; Olsthoorn, T. (1997). Snelle oudjes gaan MATLAB (Golden oldies go MATLAB). Stromingen 3/4, p21-42.

Mackay, D.S.; Band, L.E. (1998). Extraction and representation of nested catchment areas from digital elevation models in lake-dominated topography. Water Resour. Res.; 34: 897–901.

MacMillan, R.A.; Pettapiece, W.W. (1997). Soil Landscape Models: Automated landscape characterization and generation of soil-landscape models. Research Report No. 1E.

MacMillan, R.A.; Pettapiece, W.W.; Nolan, S.C.; Goddard, T.W. (2000). A generic procedure for automatically segmenting landforms into landform elements using DEMs, heuristic rules and fuzzy logic. Fuzzy Sets and Systems. 113 (1):81-109.

Makarovic, B. (1973). Progressive sampling for digital terrain models. ITC. J, vol. 3, pp 397–416.

Makarovic, B. (1977). Composite sampling for digital terrain models. ITC. J,vol. 3, pp 406–433.

Makarovic, B. (1980). Automatic off-line generation of digital terrain models. ITC. J, vol. 3, pp 408–419.

Makarovic, B. (1984). Structures for geo-information and their application in selective sampling for digital terrain models. ITC. J, vol. 4, pp 285–295.

Malano, H.; Hofwegen, P.V. (1999). Management of Irrigationand Drainage Systems: A Service Approach. Monography IHE 3.A.A.Balkema,Rotterdam,Netherlands.ISBN 90 5410 482 1

Mantovani, F.; Soeters, R.; Van Westen, C.J.; (1996). Remote sensing techniques for landslide studies and hazard zonation in Europe. Geomorphology, 15: 213-225.

Mardikis, M.G.; Kalivas, D.P.; Kollias, V. J. (2005). Comparison of interpolation methods for the prediction of reference evapotranspiration - an application in Greece. Water Resources Management 19(3), 251-278.

Mark, D.M. (1988). Network models in geomorphology. In Modeling Geomorphological Systems, M.G. Anderson (eds.), 73–97, John Wiley, New York.

Marks, D.; Dozier, J. Frew, J. (1984). Automated basin delineation from digital elevation data. Geo-Process.; 2: 299-311.

Marofi, S. (1999). Rôle des échanges nappes-fossés dans le fonctionnement hydrologique d'un bassin versant en milieu méditerranéen cultivé. PhD thesis, Ecole Nationale Supérieure Agronomique de Montpellier, France, 240 pp.

Marra, F.; Zanon, F.; Penna, D.; Mantese, N.; Zoccatelli, D.; Cavalli, M.; Marchi, M. (2011). Hydrometeorological and hydrological analysis for the Nov 1, 2010 flood event in North-eastern Italy. Geophysical Research Abstracts, 13, EGU2011-10727-1.

Martz, L.W.; Garbrecht, J. (1998). The treatment of flat areas and depressions in automated drainage analysis of raster digital elevation models. Hydrol. Process.; 12: 843-855.

Maune, D.F. (2001). Digital Elevation Model Technologies and Applications: The DEM Users Manual. The American Society for Photogrammetry and Remote Sensing, Bethesda, Maryland, 2001.

McClean, C.J.; Evans, I.S. (2000). Apparent fractal dimensions from continental scale digital elevation models using variogram methods. Trans. GIS, vol. 4 (4), 361–378.

McCullagh. M. (1988). Terrain and surface modelling systems: theory and practice". The Photogrammetric Record, 12(72), 747–779.

McDonnell, J.J.; Woods, R. (2004). On the Need for Catchment Classification. Journal of Hydrology(Amsterdam), 299(1), 2-3.

McDonnell, J. J.; et al. (2007), Moving beyond heterogeneity and process complexity: A new vision for watershed hydrology, Water Resour. Res.; 43, W07301, doi:10.1029/2006WR005467.

McGlynn, B.L.; McDonnell, J.J. (2003). Quantifying the relative contributions of riparian and hillslope zones to catchment runoff, Water Resour. Res.; 39(11), 1310.

Mckean, J.; Roering, J. (2004). Objective landslide detection and surface morphology mapping using high-resolution airborne laser altimetry. Geomorphology 57: 331-351. doi:10.1016/S0169-555X(03)00164-8.

Mckean, J.; Roering, J. (2003). Operational accuracy of LiDAR in mountainous terrain [abs.]: Eos (Transactions American Geophysical Union), v. 84, no. 46, Fall Meeting Supplement, Abstract G11A-0239.

McMaster, K. J. (2002). Effects of digital elevation model resolution on derived stream network positions. Water Resour. Res.; 38(4), 1042.

Mendicino, G. (1996). Analysis of the information content of environmental data using GIS procedures, In: N. B. Harmancioglu, M. N. Alpaslan, S. D. Ozkul, and V. P. Singh (eds), Integrated Approach to Environmental Data Managements Systems, NATO ASI Series, Kluwer Academic Pulishers, pp 387 400.

Meneses, A.S.; Chasco, F.R.; García, B.; Cabrejas, J.; González-Audícana, M. (3005). Quality Control in Digital Terrain Models", Journal of Surveying Engineering, 131, 4, 118-124.

Metternicht G.; Hurni L.; Gogu R. (2005). Remote sensing of landslides : An analysis of the potential contribution to geospatial systems for hazard assessment in mountainous envronments. Remote Sensing of Environment, 98: 284-303.

Miska, L.; Hjort, J. (2005). Evaluation of current statistical approaches for predictive geomorphological mapping. Geomorphology, 67, 299–315.

Mitasova, H.; Hofierka, J. (1993). Interpolation by Regularized Spline with Tension: II. Application to Terrain Modeling and Surface Geometry Analysis. Math. Geol. 25, 641-655.

Molloy I.; Stepinski, T.F. (2007). Automatic mapping of valley networks on Mars. Computers and Geosciences 33,728–738.

Montgomery, D.R.; Dietrich, W.E. (1988). Where do channels begin? Nature 336,232,234.

Montgomery, D.R.; Dietrich, W.E. (1992). Channel initiation and the problem of landscape scale. Science, 255, 826-830, 1992.

Montgomery, D.R.; Dietrich, W.E. (1994). A physically based model for the topographic control on shallow landsliding. Water Resources Research 30: 1153-1171.

Montgomery, D.R.; Wright, R.H.; Booth, T. (1991). Debris flow hazard mitigation for colluvium-filled swales. Bull Assoc Eng Geol 28:303–323.

Montgomery, D.R. (1994). Road surface drainage, channel initiation, and slope stability. Water Resources Research 30: 1925–32.

Moore, I.D.; Grayson, R.B.; Ladson, A.R. (1991). Digital terrain modelling: A review of hydrological, geomorphological, and biological applications. Hydrological Processes 5:3-30.

Moore, I.D.; Gessler, P.E.; Nielsen, G.A.; Peterson, G.A. (1993). Soil attribute prediction using digital terrain analysis. Soil Science Society of America Journal, 57:443-452.

Moussa, R.; Voltz, M.; Andrieux, P. (2002). Effects of the spatial organization of agricultural management on the hydrological behaviour of a farmed catchment during flood events. Hydrological Processes, 16(2), 393–412.

Mukai, T.; Nakamura, A.M.; Sakai, T. (2006). Asteroidal surface studies by laboratory light scattering and LIDAR on HAYABUSA. Advances in Space Research 37(1), 138-141.

Nelson, P.A.; Smith, J.A.; Miller, A.J. (2006). Evolution of channel morphology and hydrologic response in an urbanizing drainage basin. Earth Surface Processes and Landforms, 31(9), 1063–1079. DOI: 10.1002/esp.1308

Nogami, M. (1995). Geomorphometric measures for digital elevation models. Z. Geomorphologie Suppl. 101, 53–67.

Nolan, J.P. (2006). Bibliography on stable distributions, processes and related topics. Mimeo. Department of Mathematics and Statistics. American University, Washington, DC.

O' Callaghan, J.F.; Mark, D.M. (1984). The extraction of drainage networks from digital elevation data. Computer Vision, Graphics and Image Processing, 28, 323–344.

Oimoen, M.J. (2000). An effective filter for removal of production artifacts in U.S. Geological Survey 7.5-minute digital elevation models. Proceedings of the Fourteenth International Conference on Applied Geologic Remote Sensing, 06–08 November, Las Vegas, Nevada (Veridian ERIM International, Ann Arbor, Michigan), 311–319.

Oksanen, J.; Sarjakoski, T. (2005). Error propagation analysis of DEM-based drainage basin delineation. International Journal of Remote Sensing, 26 (14), 3085–3102.

Oksanen, J.; Sarjakoski, T. (2006). Uncovering the statistical and spatial characteristics of fine toposcale DEM error. Int. J. Geogr. Inf. Sci, 20, 345–369.

Olaya, V. (2009). Basic Land-Surface Parameters. In: Hengl, T. and Reuter, H.I. (Eds), Geomorphometry: Geomorphometry: Concepts, Software, Applications. Developments in Soil Science, vol. 33, Elsevier, 1-28 pp.

Openshaw, S.; Charlton, M.; Carver, S. (1991). Error Propagation: A Monte Carlo Simulation, in: Handling Geographical Information – Methodology and Potential Applications, edited by: Masser, I. and Blakemore, M.; John Wiley and Sons.

Orlandini, S.; Moretti, G. , Franchini, M.; Aldighieri, B.; Testa, B. (2003). Path-based methods for the determination of nondispersive drainage directions in grid-based digital elevation models, Water Resour. Res.; 39(6), 1144, doi: 10.1029/2002WR001639.

Orlandini, S.; Moretti, G. (2009a). Comment on "Global search algorithm for nondispersive flow path extraction" by Kyungrock Paik. J. Geophys. Res. 114(10):F04004.

Orlandini, S.; Moretti, G. (2009b). Determination of surface flow paths from gridded elevation data. Water resources research, 45(3):W03417.

Orlandini, S.; Tarolli, P.; Moretti, G.; Dalla Fontana, G. (2011). On the prediction of channel heads in a complex alpine terrain using gridded elevation data, Water Resour. Res.; 47, W02538, doi:10.1029/2010WR009648.

Pack, R.T.; Tarboton, D.G.; Goodwin, C.N. (1998). The SINMAP Approach to Terrain Stability Mapping, 8th Congress of the International Association of Engineering Geology, Vancouver, British Columbia, Canada.

Palacios-Velez, O. L.; Cuevas-Renaud, B. (1986). Automated river-course, ridge and basin delineation from digital elevation data. J. Hydrol.; 86: 299–314.

Passalacqua, P.; Do Trung, T.; Foufoula-Georgiou, E.; Sapiro, G.; Dietrich, W.E. (2010a). A geometric framework for channel network extraction from LiDAR: Nonlinear diffusion and geodesic paths. Journal of Geophysical Research 115: F01002. doi:10.1029/2009JF001254.

Passalacqua, P.; Tarolli, P.; Foufoula-Georgiou, E. (2010b). Testing space-scale methodologies for automatic geomorphic feature extraction from LiDAR in a complex mountainous landscape. Water resources research, 46, W11535. doi:10.1029/2009WR008812.

Passmore, D.G.; Macklin, M.G. (2001). Late Holocene alluvial sediment budgets in an upland gravel bed river: the River South Tyne, Northern England. In: River Basin Sediment Systems: Archives of Environmental Change, Maddy, D.; Macklin M.G.; Woodward, J. (eds). Balkema: Rotterdam; 423–444.

Peuker, T.; Douglas, D.H. (1975). Detection of surface-specific points by local parallel processing of discrete terrain-elevation data. Computer Graphics and Image Processing 4 (1975), 375–387.

Pfeifer, N.; Briese, C. (2007). Geometrical aspects of airborne laser scanning and terrestrial laser scanning. International Archives of Photogrammetry, Remote Sensing and Spatial Information Sciences 36(part 3/W52), 311-319.

Pike, J.R. (2000). Geomorphometry – diversity in quantitative surface analysis. Progress in Physical Geography vol.24. no.1 pp.1-20.

Pike, R.J.; Acevedo, W.; Thelin, G.P. (1988). Some topographic ingredients of a geographic information system, Proceedings, International Geographic Information Systems Symposium, 15-18 November, Arlington, Virginia (NASA, Washington, D.C.), 2,151-164.

Pilesjo, P.; Zhou, Q.; Harrie, L. (1998). Estimating flow distribution over digital elevation models using a form-based algorithm.. Geogr. Inf. Sci.; 4(1-2): 44–51.

Pirotti, F.; Tarolli, P. (2010). Suitability of LiDAR point density and derived landform curvature maps for channel network extraction. Hydrological Processes 24: 1187-1197. doi: 10.1002/hyp.758

Prima, O.D.A.; Echigo, A.; Yokoyama, R.; Yoshida, T. (2006). Supervised landform classification of Northeast Honshu from DEM-derived thematic maps. Geomorphology, 78, 373–386.

Prosser I.P.; Abernethy, B. (1996). preditcing the topographic limits of gully network using a digital terrain model and process thresholds. Water resources research, 32: 2289-2298.

Pullar, D.V. (2004). SimuMap: a computational system for spatial modelling. Environmental Modelling and Software, 19 3: 235-243.

Quattrocchi, D.; Goodchild, M.F. (eds). (1997). Scale in Remote Sensing and GIS. Boca Raton, Florida: CRC Press. 406 pp.

Quinn, P.; Beven, K. J.; Lamb, R. (1995). The ln(a/tanB) index: how to calculate it and how to use it within the TOPMODEL framework. Hydrol. Processes 9, 161–182.

Quinn, P.; Beven, K.; Chevallier, P.; Planchon, O. (1991). The prediction of hillslope flow paths for distributed hydrological modeling using digital terrain models, Hydrol. Processes, 5, 59-79.

Raaflaub, L.D. , Collins, M.J. (2006). The effect of error in gridded digital elevation models on the estimation of topographic parameters. Environmental Modelling & Software, vol. 21, pp. 710-732. DOI: 10.1016/j.envsoft.2005.02.003.

Raber, G.T.; Jensen, J.R.; Hodgson, M.E.; Tullis, J.A.; Davis, B.A.; Berglend, J. (2007). Imact of LiDAR nominal post-spacing on DEM accuracy and flood zone delineation. Photogrammetric Engineering and Remote Sensing 73(7), 793-804.

Ramirez, J.R. (2006). A new approach to relief representation. Surveying and Land Information Science 66(1), 19-25.

Resnikoff, H.L. (1989). The Illusion of Reality; Springer-Verlarg: New York, NY, USA.

Reutebuch, S.E.; Andersen, H.E.; McGaughey, R. J. (2005). Light detection and ranging (LIDAR): an emerging tool for multiple resource inventory. Journal of Forestry 103(6), 286-292.

Rigon, R.; Antonello, A.; Franceschi, S. (2008). JGrass: The Horton machine, Geophysical Research Abstracts, 10.

Rodríguez-Iturbe, I.; Rinaldo, A. (1997). Fractal River Basins: Chance and Self- Organization by I.; Cambridge University Press, 580 pp.

Rodríguez-Iturbe, I.; Gupta, V.K.; Wood, E.F. (1986). Scale Problems in Hydrology Runoff Generation and Basin Response. D. Reidel Pub. Co, Dordrecht, Holland.

Rodriguez-Iturbe, I.; Valdes, J.B. (1979). The geomorphologic structure of hydrologic response. Water Resources Research, 15(6):1409-1420.

Runyon, R.P.; Haber, A. (1976). Fundamentals of behavioral statistics. Reading, MA: Addison-Wesley.

Sauer, V. B.; Thomas, Jr.; W. O.; Strickler, V.; Wilson, K. (1983). Flood characteristics of urban watersheds in the united states. U.S. Geological Survey Water-Supply Paper, 2207.

Saunders, W.; Maidment, D. (1995). Grid-based watershed and stream network delineation for San Antonio-Nueces coastal basin. Texas Water, San Antonio, Texas, 14-18 August.

Schmidt, J.; Andrew, R.(2005). Multi-scale landform characterization. Area;37:341–350.

Schmidt, J.; Evans, I.S.; Brinkmann, J. (2003). Comparison of polynomial models for land surface curvature calculation. International Journal of Geographic Information Science, 17(8), 797-814.

Schoorl, J.M.; Sonneveld, M.P.W.; Veldkamp A. (2000). Threedimensional landscape process modelling: The effect of DEM resolution, Earth Surf. Processes Landforms, 25, 1025-1034.

Schrott, L.; Niederheide, A.; Hankammer, M.; Hufschmidt, G.; Dikau, R. (2002). Sediment storage in mountain catchment: geomorphic coupling and temporal variability (Reintal, Bavarian Alps, Germany). Zeitschrift für Geomorphologie (Supplement) 127, 175–196.

Schwanghart, W.; Kuhn, N.J. (2010). TopoToolbox: a set of Matlab functions for topographic analysis. Environmental Modelling & Software, 25, 770-781.

Seibert, J.; McGlynn, B. L. (2007). A new triangular multiple flow direction algorithm for computing upslope areas from gridded digital elevation models. Water Resour. Res.; 43: W04501 doi:10.1029/2006WR005128.

Shannon, C.E.; Weaver, W. (1949). The Mathematical Theory of Communication, University of Illinois Press, Urbana, Illinois.

Shary, P.A.; Sharaya, L.S.; Mitusov, A.V. (2002). Fundamental quantitative methods of land surface analysis, Geoderma, 107, 1-32.

Shary, P.A.; Sharaya, L.S.; Mitusov, A.V. (2005). The problem of scale-specific and scale-free approaches in geomorphometry. Geografia Fisica e Dinamica Quatrenaria, 28 (1), 81-101.

Sheng, Y.; Gong, P. and Biging, G. S. (2003). Orthoimage production for forested areas from large-scale aerial photographs. Photogrammetric Engineering and Remote Sensing 69(3), 259-266.

Sibson, R. (1981). A brief description of natural neighbor interpolation (Chapter 2). in V. Barnett: Interpreting Multivariate Data. Chichester: John Wiley, pp. 21-36.

Singh, V.P. (2011). Hydrologic Synthesis Using Entropy Theory: Review. J. Hydrologic Eng. 16, 421. doi:10.1061/(ASCE)HE.1943-5584.0000332

Singh, V.P.; Fiorentino, M. (1992). A historical perspective of entropy applications in water resources. In: Entropy and Energy Dissipation in water resources (ed. by W.P. Sing and M. Fiorentino), 21-61, Kluwer, Boston, Massachussets.

Sithole, G.; Vosselman, G. (2003). Report: ISPRS Comparison of Filters. The Netherlands: Department of geodesy, Faculty of Civil Engineering and Geosciences, Delft University of Technology.

Sivakumar, B. (2005), Hydrologic modeling and forecasting: role of thresholds, Environmental Modeling & Software, 20(5), 515-519

Sivakumar, B. (2008). Dominant Processes Concept, Model Simplification and Classification Framework in Catchment Hydrology. Stochastic Environmental Research and Risk Assessment, 22(6), 737-748.

Sivapalan, M. (1995). Scale Problems in Hydrology. Contributions of the Robertson Workshop. Hydrological Processes, 9(3-4).

Sivapalan, M. (2005). Pattern, process and function: elements of a unified theory of hydrology at the catchment scale. In: Anderson, M.G. (Ed.), Encyclopaedia of Hydrological Sciences, chp. 13. pp. 193–219.

Skidmore, A.K. (1989). A comparison of techniques for calculating gradient and aspect from a gridded digital elevation model. International Journal of Geographic Information Systems, 3(4), 323-334.

Slatton, K.C.; Carter, W.E.; Shrestha, R.L.; Dietrich, W.E. (2007). Airborne laser swath mapping: achieving the resolution and accuracy required for geosurficial research. Geophysical Research Letters 34: L23S10. doi:10.1029/2007GL031939.

Smith, M.J.; Rose, J.; Booth, S. (2006). Geomorphological mapping of glacial landforms from remotely sensed data: an evaluation of the principal data sources and an assessment of their quality. Geomorphology 76:148-165. doi:10.1016/j.geomorph.2005.11.001.

Smith, L. (2001). Columbia Mountain landslide: late-glacial emplacement and indications of future failure, Northwestern Montana, USA. Geomorphology, 41, 309–322.

Smith, M.J.; Rose, J.; Booth, S. (2006). Geomorphological mapping of glacial landforms from remotely sensed data: an evaluation of the principal data sources and an assessment of their quality. Geomorphology, 76, 148-165. doi:10.1016/j.geomorph.2005.11.001.

Sofia, G.; Tarolli, P.; Cazorzi, F.; Dalla Fontana, G. (2011). An objective approach for feature extraction: distribution analysis and statistical descriptors for scale choice and channel network identification. Hydrol. Earth Syst. Sci.; 15, 1387–1402. ISSN: 1027-5606,doi:10.5194/hess-15-1387-2011.

Sofia, G.; Pirotti, F.; Tarolli, P. *(under review).* Multiscale analysis of curvature distribution as an error diagnosis tool for LiDAR derived DTMs, IEEE Transactions on Geoscience and Remote Sensing.

Soille, P.; Vogt, J.V.; Colombo, R. (2003). Carving and adaptive drainage enforcement of grid digital elevation models. Water Resources Research 39(12), 1366–1379.

Soille, P.; Gratin, C. (1994). An efficient algorithm for drainage network extraction on DEMs. J. Visual Commun. Image Represent.; 5: 181-189.

Speight, J.G. (1974). A parametric approach to landform region, Progress in Geomorphology, 213-230.

Spence, C. (2007). On the relations between dynamic storage and runoff:a discussion on thresholds, efficiency and function. Water Resources Research 43: W12416, DOI:10.1029/2006WR005645.

Staley, D.M.; Wasklewicz, T.A.; Blaszczynski, J.S. (2006). Superficial patterns of debris flow deposition on alluvial fans in Death Valley, CA using airborne laser swath mapping. Geomorphology 74: 152-163

Tarboton D.G.(1997). A new method for the determination of flow directions and contributing areas in grid digital elevation models. Water Resources Research, 33, pp. 309–319.

Tarboton D.G. (2003). Terrain Analysis Using Digital Elevation Models in Hydrology, ESRI Users Conference, San Deigo, 7-11 July, 2003.

Tarboton D.G.; Bras R.L.; Rodriguez-Iturbe I. (1991). On the extraction of channel network from digital elevation data. Hydrological processes 5, 81-100.

Tarboton D.G.; Ames, D. P. (2001). Advances in the mapping of flow networks from digital elevation data. In: Proceedings of World Water and Environmental Resources Congress, Orlando, Florida.

Tarolli, P.; Tarboton, D.G. (2006). A New Method for Determination of Most Likely Landslide Initiation Points and the Evaluation of Digital Terrain Model Scale in Terrain Stability Mapping. Hydrology and Earth System Science 10: 663-677.

Tarolli, P.; Borga, M.; Dalla Fontana, G. (2008). Analyzing the infuence of upslope bedrockoutcrops on shallow landsliding. Geomorphology 93: 186-200.

Tarolli, P.; Dalla Fontana, G. (2008). High resolution LiDAR-derived DTMs: some applications for the analysis of the headwater basins’ morphology. International Archives of Photogrammetry, Remote Sensing and Spatial Information Sciences 36 (5/C55): 297-306.

Tarolli, P.; Dalla Fontana, G. (2009). Hillslope to valley transition morphology: new opportunities from high resolution DTMs. Geomorphology 113: 47-56. doi:10.1016/j.geomorph.2009.02.006.

Tarolli, P.; Arrowsmith, J.R.; Vivoni, E.R. (2009). Understanding earth surface processes from remotely sensed digital terrain models. Geomorphology 113: 1-3. doi:10.1016/j.geomorph .2009.07.005

Tarolli, P.; Dalla Fontana, G.; Moretti, G.; Orlandini, S. (2009). Cell Size Dependence of Threshold Conditions for the Delineation of Drainage Networks from Gridded Elevation Data. Geomorphometry 2009, University of Zurich.

Tarolli, P.; Sofia, G.; Dalla Fontana, G. (2010). Geomorphic features extraction from high resolution topography: landslide crowns and bank erosion, Natural Hazards, ISSN: 0921-030X, doi:10.1007/s11069-010-9695-2.

Temme, A. , Heuvelink, G.; Schoorl, J.; Claessens, L. (2008). Geostatistical simulation and error propagation in geomorphometry”, in: Geomorphometry: concepts, software, applications, edited by: Hengl, T. and Reuter, H. I.; Developments in Soil Science, Elsevier, 121–140, 770, 776, 779, 782.

Tetzlaff, D.; Soulsby, C.; Waldron, S.; Malcolm, I.A.; Bacon, P.J.; Dunn, S.M.; Lilly, A. (2007a). Conceptualisation of runoff processes using GIS and tracers in a nested mesoscale catchment. Hydrological Processes 21:1289–1307.

Tetzlaff, D.; Soulsby, C.; Bacon, P.J.; Youngson, A.F.; Gibbins, C.N.; Malcolm, I.A. (2007b). Connectivity between landscapes and riverscapes—a unifying theme in integrating hydrology and ecology in catchment science?Hydrological Processes 21: 1385–1389.

The MathWorks, Inc. 2010. Using MATLAB, Version 2010b.

Thommeret, N.; Bailly, J.S.; Puech, C. (2010). Robust extraction of thalwegs network from DTM: application on badlands. Hydrol. Earth Syst. Sci.; 14, 1527-1536, doi:10.5194/hess-14-1527- 2010.

Travis, M.R.; Elsner, G.H.; Iverson, W.D.; Johnson, C.G. (1975). VIEWIT computation of seen areas, slope and aspect for land use planning. PSW 11/1975, Pacific Southwest Forest and Range Experimental Station, Berkley, California, USA.

Trevisani, S.; Cavalli, M.; Marchi, L. (2009). Variogram maps from LiDAR data as fingerprints of surface morphology on scree slopes. Natural Hazards and Earth System Sciences 9: 129-133. doi:10.5194/nhess-9-129-2009.

Tribe, A. (1992). Automated recognition of valley lines and drainage networks from grid elevation models: a review and a new method. J. Hydrol.; 139: 263–293.

Troch, P.A.; Carrillo, G.A.; Heidbuchel, I.; Rajagopal, S.; Switanek, M.; Volkmann, T.H.M.; Yaeger, M. (2009). Dealing with landscape heterogeneity in watershed hydrology: a review of recent progress toward new hydrological theory. Geography Compass 3: 375–392.

Tucker, G.E. , Catani, F. , Rinaldo, A. (2001). Statistical analysis of drainage density from digital terrain data, Geomorphology, 36(3-4),187-202, ISSN: 0169-555X.

Tukey, J.W. (1977). Exploratory Data Analysis. Addison-Wesley, Reading, MA.

Turcotte, R.; Fortin, J.P.; Rousseau, A.; Massicotte, N.; Villeneuve, J.P. (2001). Determination of the drainage structure of a watershed using a digital elevation model and a digital river and lake network. J. Hydrol.; 240: 225-242.

U.S. Department of Agriculture, Natural Resources Conservation Service. National Soil Survey Handbook, title 430-VI. Available online at http://soils.usda.gov/technical/handbook/. [*last access jan.; 2012*]

Uchida, T.; Asano, Y.; Onda, Y.; Miyata, S. (2005). Are headwaters just the sum of hillslopes? Hydrological Processes 19: 3251–3261.

Van Niel, K. , Laffan, S.; Lees, B. (2004). Effect of error in the DEM on environmental variables for predictive vegetation modeling. J. Veg. Sci.; 15, 747–756.

Varado, N. (2004). Contribution au developpement d'une modelisation hydrologique distribuee. Application au bassin versant de la Donga au Benin. PhD thesis, Institut National Polytechnique de Grenoble, France: 320 pp.

Veregin, H. (1997). The effects of vertical error in Digital Elevation Models on the determination of flowpath direction. Cartography and GIS, 24, 67–79.

Vianello, A.; Cavalli, M.; Tarolli, P. (2009). LiDAR-derived slopes for headwater channel network analysis. Catena 76, 97-106. doi:10.1016/j.catena.2008.09.012

Vieux, B.E. (1993). DEM aggregation and smoothing effects on surface runoff modeling. J. Comput. Civil Eng.; 7(3), 310–338.

Vivoni, E.R.; Teles, V.; Ivanov, V. Y.; Bras, R. L. and Entekhabi, D. (2005a). Embedding landscape processes into triangulated terrain models. Int. J. Geogr. Inf. Sci.; 19(4): 429–457.

Vivoni, E.R.; Ivanov, V.Y.; Bras, R.L.; Entekhabi, D. (2005b). On the effects of triangulated terrain resolution on distributed hydrologic model response. Hydrol. Processes, 19(11): 2101–2122.

Vogel, H. J.; Roth, K. (2003). Moving through scales of flow and transport in soil. J. Hydrol.; 272, 95/106.

Voltz, M.; Andrieux, P.; Bouzigues, R.; Lennartz, B.; Louchart, X.; Moussa, R.; Ribolzi, O. (1998). Transport of water and matter in a farmed sedimentary soil system in the mediterranean environment. In Proceedings of the 16th International Congress of Sol Science, Montpellier; 8 pp.

Vosselman, G. (2000). Slope based filtering of laser altimetry data. International Archives of Photogrammetry, Remote Sensing and Spatial Information Sciences 33(part B3/2), 935-934.

Vosselman, G.; Maas, H.G. (2010). Airborne and Terrestrial Laser Scanning. Whittles Publishing, Dunbeath, Caithness (Scotland-United Kingdom).

Wack, R.; Wimmer, A. (2002). Digital terrain models from airborne laser scanner data - a grid based approach. International Archives of Photogrammetry, Remote Sensing and Spatial Information Sciences 34(part 3/B), 293-296.

Wagner, W.; Blöschl, G.; Pampaloni, P.; Calvet, J.C.; Bizzarri, B.; Wigneron, J.P.; Kerr, Y. (2007). Operational readiness of microwave remote sensing of soil moisture for hydrologic applications,Nordic Hydrology, 38(1), 1-20.

Wagner, W.; Ullrich, A.; Melzer, T.; Briese, C. and Kraus, K. (2004). From single-pulse to full-waveform airborne laser scanners: potential and practical challenges. International Archives of the Photogrammetry, Remote Sensing and Spatial Information Sciences 35(B3).

Wallace, J.; Morris, B.; Howarth, P. (2004). The effects of scale on fractal dimension of topography: a case study from Sudbury, Ontario, Canada. Geoscience and Remote Sensing Symposium, 2004. IGARSS '04. Proceedings. IEEE International , 5, 2845-2848, 5, 20-24 Sept. 2004 doi: 10.1109/IGARSS.2004.1370285

Walsh, S.J.; Bian, L.; McKnight, S.; Brown, D.G.; Hammer, E.S. (2003). Solifluction steps and risers, Lee Ridge, Glacier National Park, Montana, USA: a scale and pattern analysis. Geomorphology, 55, 381–398.

Warren, S.D.; Hohmann, M.G.; Auerswald, K. and Mitasova, H. (2004). An evaluation of methods to determine slope using digital elevation data. Catena, 58: 215–33.

Watkins, D. (2005). LiDAR Types and Uses: with a Case Study in Forestry. State College, PA, USA: Department of Geography, Pennsylvania State University.

Webster, T.L.; Dias, G. (2006). An automated GIS procedure for comparing GPS and proximal LiDAR elevations. Computers & Geosciences 32(6), 713-726.

Wechsler, S.P. (2000). Effect of DEM Uncertainty on Topographic Parameters, DEM Scale and Terrain Evaluation, State University of New York College of Environmental Science and Forestry, Syracuse, NY, Ph.D. Dissertation, 380.

Wechsler. S.P. (2003). Perceptions of Digital Elevation Model Uncertainty by DEM Users". URISA Journal, 15, 57-64.

Wechsler. S.P. (2007). Uncertainties associated with digital elevation models for hydrologic applications: a review. Hydrol. Earth Syst. Sci.; 11, 1481-1500, doi:10.5194/hess-11-1481-2007.

Wechsler, S.P.; Kroll, C. (2006). Quantifying DEM Uncertainty and its Effect on Topographic Parameters. Photogramm. Eng. Rem. S.; 72, 1081–1090.

Wehr, A.; Lohr, U. (1999). Airborne laser scanning - an introduction and overview. ISPRS Journal of Photogrammetry and Remote Sensing 54(4), 68-82.

Weibel, R.; Heller, M. (1991). Digital Terrain Modeling. In: Maguire, D.J.; Goodchild, M.F. and Rhind, D.W. (eds.). Geographical Information Systems: Principles and Applications. London: Longman, 269-297.

Weitkamp, C. (2005). LiDAR: Introduction. In Fujii, T. and Fukuchi, T.; editors, Laser Remote Sensing, Boca Raton, London, New York and Singapore: Taylor & Francis, 1-36.

Wemple B.C.; Jones, J.A.; Grant, G.E. (1996). Channel network extension by logging roads in two basins, wester cascades, oregon, Water resources bulletin, 32(6), 1195-1207.

Weron, R. (1996). On the Chambers-Mallows-Stuck Method for Simulating Skewed Stable Random Variables. Statistics and Probability Letters, 2, 165-171.

Wichel, G.J.; Jenson, S.K.; Baglio, J.V, Dominingue, J.O. (1992). Application of digital elevation models to delineate drainage area and compute hydrologic characteristics for sites in the James River Basin, North Dakota. United States Geological Survey (USGS), Water Supply Paper 2383.

Wieczorek, G.F.; Morrissey, M.M.; Iovine, G.; Godt, J. (1999). Rock-fall potential in the Yosemite Valley, California. USGS Open File report 99-578.

Willgoose, G.; Bras, R.L.; Rodríguez-Iturbe, I. (1991a). A coupled channel network growth and hillslope evolution model. 1. Theory. Water Resour. Res.; 27(7): 1671–1684.

Willgoose, G.; Bras, R.L.; Rodríguez-Iturbe, I. (1991a). A coupled channel network growth and hillslope evolution model. 2 Nondimensionalization and application.. Water Resour. Res.; 27(7): 1685–1696.

Wilson, J.P.; Gallant, J.C. (2000). Terrain Analysis: Principles and Applications. Hoboken, New Jersey, , USA: John Wiley.

Wilson, M.F.J.; O'Connel, B.; Brown, C.; Guinan, J.C.; Grehan, A.J. (2007). Multiscale terrain analysis of multibeam bathymetry data for habitat mapping on the continental slope. Marine Geodesy, 30, 3–35.

Wise, S. (1998). The effect of GIS interpolation errors on the use of digital elevation models in geomorphology. In: S.N. Lane, K.S. Richards and J.H. Chandler, Editors, Landform Monitoring, Modelling and Analysis, Wiley, New York, NY, 139–164.

Wise, S. (2000). Assessing the quality for hydrological applications of digital elevation models derived from contours, Hydrological Processes 14 (11–12),1909–1929.

Wise, S. (2011). Cross-validation as a means of investigating DEM interpolation error, Computers & Geosciences, In Press, Corrected Proof, Available online 20 January 2011, ISSN 0098-3004, DOI: 10.1016/j.cageo.2010.12.002.

Wolock, D.M.; McCabe, G.J. (1995). Comparison of single and multiple flow direction algorithms for computing topographic parameters, Water Resour. Res.; 31, 1315– 1324.

Wood J.D. (1996). The Geomorphological Characterisation of Digital Elevation Models. Ph.D. Thesis, University of Leicester.

Wood J.D. (2009). Chapter 14 Geomorphometry in LandSerf, In: Tomislav Hengl and Hannes I. Reuter, Editor(s), Developments in Soil Science, Elsevier, 33, Geomorphometry - Concepts, Software, Applications, ISSN 0166-2481, ISBN 9780123743459, Doi: 10.1016/S0166-2481(08)00014-7, 333-349.

Wood J.D.; Fisher, P.F. (1993). Assessing interpolation accuracy in elevation models, IEEE Computer Graphics and Applications, 13/2, 48–56, 1993.

Yokoya, N.; Levine, M.D. (1989). Range image segmentation based on differential geometry: a hybrid approach. IEEE Trans Pattern Anal Mach Intell, 2(6), 643–649.

Yokoyama, R.; Sirasawa, M.; Pike, R. (2002). Visualizing topography by openness: A new application of image processing to digital elevation models. Photogrammetric Engineering & Remote Sensing, 68 (3), 257-265.

Youfu, D.; Guoan, T.; Zhang, T. (2008). A Systematic Classification Research of Topographic Descriptive Attribute in Digital Terrain Analysis, ISPRS Congress Beijing 2008,Vol. XXXVII, B2, ISSN 1682-1750 p.357.

Yuan, X.; Hu, L.; Buckles, B.P.; Steinberg, L.; Sarma, V. (2008), An Adaptive Method for the Construction of Digital Terrain Model from LiDAR Data, the IEEE International Geoscience and Remote Sensing Symposium, Boston, MA, 6-11 July, 2008.

Zandbergen. P.A. (2008). Positional accuracy of spatial data: non-normal distributions and a critique of the national standard for spatial data accuracy", Transactions in GIS, vol. 12 (1), pp. 103–130.

Zevenbergen, L.W.; Thorne, C. (1987). Quantitative analysis of land surface topography. Earth Surface Processes and Landforms, 12, 47-56.

Zhang, K. Q.; Chen, S. C.; Whitman, D.; Shyu, M. L.; Yan, J. H. and Zhang, C. C. (2003). A progressive morphological filter for removing nonground measurements from airborne LiDAR data. IEEE Transactions on Geoscience and Remote Sensing 41(4), 872-882.

Zhang, W.; Montgomery, D. (1994). Digital elevation model grid size, landscape representation and hydrologic simulations, Water Resources Research, 30, 1019–1028, 1994.

Zhou, Q.; Liu, X. (2002). Error assessment of grid-based flow routing algorithms used in hydrological models, International Journal of Geographical Information Science 16 (8), 819–842.

Zhou, Q.; Liu, X. (2004). Analysis of errors of derived slope and aspect related to DEM data properties, Comput. Geosci.; 30, 369–378.

Ziadat, F.M. (2007). Effect of Contour Intervals and Grid Cell Size on the Accuracy of DEMs and Slop Derivatives. Transactions in GIS 11(1), 67-81.

Zimmerman, D.; Pavlik, C.; Ruggles, A.; Armstrong, M.P. (1999). An experimental comparison of ordinary and universal Kriging and inverse distance weighting. Mathematical Geology 31(4), 375-389.

APPENDIX A

Topographic parameters evaluation in Matlab®

Over the past years expertise has been built up GIS systems in diverse areas, including hydrology, ecology, process technology and distribution technology. GIS-technology has been widely used to support the integration of various fields of knowledge to develop innovative tools and concepts. GIS software are the ideal platform for Digital Terrain Analysis and spatial analysis in general, and they have been widely applied starting from the 1990s. When referring to hydrology, a classical hydrological modeling problem is initially conceived in the geographical context, and the spatial features are the first to be considered when dealing with a river system, therefore, GIS capabilities are indispensable for feeding spatial models and analyzing their results. For hydrological application, the GIS support represent the beginning and sometime the ending step of a modeling procedure: its capability to derive spatial attributes from multiple sources, such as remote sensing, sampling, interpolation and digitizing existing maps and to store them in a geographic database simplifies the collection of input for a model and analyzing model results is helped by the possibility of simultaneous graphic display of spatial attributes on the GIS itself. A further step to ease this work, implies the GIS to incorporate the additional feature of modeling: often spatial and non-spatial analyses are combined, and while GIS software provides powerful tools for spatial analysis, non-spatial analysis tools are sometimes deficient in GIS environments. On the opposite hand, usually, script softwares do not include spatial analysis capability (Pullar, 2004).

The integration of spatial and non-spatial analysis software aims at providing a combination of the most efficient and powerful tools available in both environments (Brenning, 2008). The main result is that simulations performed in a script environment can be presented as features of a GIS project, with all the advantages of geographical referencing and integration with other features typical of a GIS environment, such as Digital Picture Processing (Kak and Rosenfeld, 1982).

There are various examples where this has been accomplished using access links between different software packages. JGrass, for example, provides integration of the statistic R package into the scripting environment (Rigon et al., 2008). RSAGA provides access to SAGA GIS geoprocessing functions from within the R statistical data analysis environment (Brenning, 2008). Maas et al., (1997) were pioneers in using MATLAB software (the MathWorks) to solve simple and complex hydrological problems in their daily work. Recently contribution to the endeavor for combining powerful GIS tools for geomorphical and hydrological application with the vast functionality of Matlab® have been showed (Swhanghart et al., 2010).

The coupled use of spatial modelling tools (GIS), statistical packages and hydrologic approaches provides a powerful combination for investigating landform structure in relation to landform processes. However, basic problems within this framework are (1) storage and exchange of various data types, and (2) a missing interoperability of different methods and investigation techniques.

The ability to perform multiscale surface characterization (Wood, 1996), relies just on some softwares (LandSerf, Wood, 1996) that offers the opportunity to examine how measurements taken from a surface model are dependent on the scale at which they are taken. To evaluate multiple analysis (as the effect of kernel size on topographic attribute evaluation) and multiple statistics at once, algorithms largely based on sparse matrix algebra and image processing techniques can be used and implemented through scripts on different software supports. For the present work, to avoid issues as large efforts in data exchange between different software packages and format and to guarantee a unique tool for multiple statistical analysis, each topographic attribute function and statistical evaluation have been implemented in Matlab-code (*.m-files) that can be easily modified and adapted to specific needs.

MATLAB stands for 'MATrix LABoratory'. It handles a range of computing tasks in engineering and science, from data acquisition and analysis to application development. The MATLAB environment integrates mathematical computing, visualization, and a powerful technical language. It is used in a variety of application areas, including signal and image processing, control system design, earth and life sciences, finance and economics, and instrumentation. Because the data is stored in matrices of multiple dimensions, a quick data access in 3D and 4D is also possible.

In many ways, the evolution of MATLAB resembles the evolution of GIS, although in most application areas it has made a quicker transition from the universities to the industries. However, this does not hold true for applications in hydrology. This is due to the fact that hydrologists have built their models with the existing (numerical) modelling software. All their site-specific knowledge has been fed into these models, making them very valuable. There is an ongoing trend however to put this knowledge into GIS, so they become available to a broader group of (potential) users.

Some problems may be tackled effectively with GIS techniques whereas others are more suitable for processing with MATLAB tools (e.g.3D and 4D modelling and visualization/animation). For these purposes a lot of AML's, Avenue scripts and MATLAB m-files have been developed over the past years.

MATLAB eased the procedure proposed on this work by enabling the completing of the following tasks:

- design custom digital filters in MATLAB and apply them to DTM in order to evaluate topographic parameters at different scales (chance already offered by Landserf (Wood, 1996) but not implemented as automatically reiterative);
- Simulate errors on DTMs to test their influences on topographic parameters (Chapt. 4.3, Sect. *III.Materials and methods*)
- graphically visualize results in 2-D and 3-D plots to gain insight of the results immediately, without needing of converting files from one format to another;

- develop applications to enable the chance to execute advanced statistical analysis and tests;
- automatic measurements that are difficult to acquire manually or need to be acquired multiple times; i.e. Curvature at multiple window size in order to evaluate the optimum scale of analysis through the polynomial fitting-enforcing approach (Sofia et al. 2011) (see . Chapt. 4.2, Sect. *III.Materials and methods)*

For Digital Terrain Analysis, one must note that DTMs and topographic attributes maps themselves are most commonly represented as rectangular grids where values are assigned to each cell. Mathematically, this kind of data model is a matrix where the elements are referenced either by specifying rows and columns of each respective scalar in the matrix or by a linear, row-wise increasing index (Swhanghart et al. 2010). Their representation through MATLAB does not require a dimensioning procedure: matrices are a series of numbers, independent of the size of the pixels. All the digital terrain analysis, therefore, can be performed without requiring to manage the dimensioning of the input data: matrix are handled using pixel-oriented algorithms, treated as Boolean surfaces and performing Boolean, mathematical or statistical operations on the pixel-by-pixel basis where the geographic location of each pixel is determined according to its position within the matrix (row and column). This allows to solve technical computing problems, especially those with large matrix and vector formulations, in a very effective way. The MATLAB environment itself offers a comprehensive set of built-in functions, and many toolboxes have been developed, and are often freely available, for more specialized needs (Swanghart et al., 2010).

Scripts to measure surface parameters at different scales can be implemented using the concept of moving windows, and they can be designed to incorporate scale-based analysis into surface parameterization. Each given parameter (e.g. curvature, openness etc.) can be evaluated at once for different ranges of scale, and statistical analysis can be carried out simultaneously to identify the scale at which that parameter is most extreme (see Chapt. 4). This can be used to explore scale sensitivity of a surface. Parallel computing can also be implemented, resulting in a time consumption compared to different GIS approach.

The main advantage for the present work, is the chance of using detailed statistical analysis of the data directly on the original matrixes, thus avoiding the need of manually extract statistical values most of the time not available on common GIS package (qqplot thresholds, skewness, z-scores etc.). Another issue is related to the fact that, while different softwares packages are present that can offers all these analyses (multiscale feature parameterization, statistical analysis of data, graphical visualization of results), the outputs that they produce are sometimes not directly compatible and data have to be converted if they need to be processed and transferred from software to another.

This causes a large time consumption that can be easily avoided using a unique software for all evaluations.

The form of description investigated in this work refers to the parameterization of a surface model (DTM). For effective geomorphologic parameterization, two criteria are required. Firstly, terrain parameters should be sensitive to geomorphologic process as well as form. For example, altitude, slope and surface curvature (0, 1st and 2nd derivatives) are all affected by or influence geomorphologic processes. Secondly, a complete surface parameterization must include analysis of scale-based characteristics. The effects due to the scale of sampling and the way in which the surface model is stored should be separated from actual processes and surface scale-dependencies as far as possible. This chapter will briefly express the implementation of surface parameterization not constrained by the grid resolution of the DTM, as in Landserf (Wood,1996) as it is applied to the MATLAB environment. The theoretical background is expressed in Chapt. 2.1 sect III.Materials and methods.

Generally, the techniques for morphometric characterization of DTMs are constrained by the resolution of the model. The information derived using these techniques is relevant only to the scale implied by the resolution of the DTM. Since this scale is often arbitrarily defined and not necessarily related to the scale of characterization required, derived results may not always be appropriate. Indeed, most of the acknowledged problems of morphometric characterization result from either variation at a finer scale than the DTM ('noisy data') or variations on a coarser scale ('flat regions'). What is required are characterization techniques that are somewhat independent of the resolution of the database used to store topographic information. This process is fundamentally based on techniques using neighborhoods. The key idea is that an analysis which is performed on a pixel of a DTM, depends not only on this pixel but also on its neighboring area, and this neighborhood is defined by all those pixels that are connected to the one of interests. This kind of analysis is achieved through a so called ‘sliding neighborhood operation’.

A sliding neighborhood operation is an operation that is performed a pixel at a time, with the value of any given pixel in the output being determined by the application of an algorithm to the values of the corresponding input pixel's *neighborhood.* A pixel's neighborhood is some set of pixels, defined by their locations relative to that pixel, which is called the *center pixel*. The neighborhood is a block, and as you move from one element to the next in a matrix, the neighborhood block slides in the same direction.

The center pixel is the actual pixel in the input being processed by the operation. If the neighborhood has an odd number of rows and columns, the center pixel is actually in the center of the neighborhood.

To perform a sliding neighborhood operation, the basic steps after selecting the pixel of interest, are

1. Define the pixel's neighborhood size and shape
2. Defining a function to apply considering the values of the pixels in the neighborhood.
3. Find the pixel in the output whose position corresponds to that of the center pixel in the input. Set this output pixel to the value returned by the function.

In the following sections, these three steps will be described, and some extracts of the needed codes to evaluate topographical parameters in matlab will be provided.

1. Kernel definition

It is necessary to define the concept of connectivity as the criteria that describe how pixels within a discrete matrix form a connected group. The two most common examples of connectivity refer to:

- 4 connected neighborhood: the central pixel has only four neighboring pixels (Fig. IA);
- 8 connected neighborhood: the central pixel has eight neighboring pixels (Fig IB).

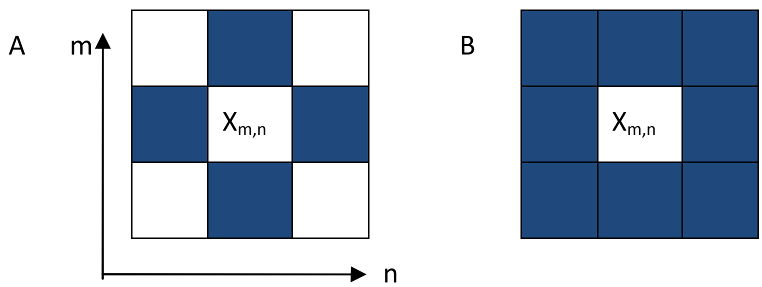

Figure I Concept of neighboring: 4- connected (A) and 8-connected (B) neighborhood.

For the present work, different shapes of moving window during the evaluation of the geomorphic parameters have been considered (Fig. 69). The tested kernels have been: rectangular, circular, and annulus shaped kernels. The basic approach is to create creates a morphological structuring element, of the type specified by *shape*. The morphological element is then passed through the input matrix, and element labeled with 1 are included in processing the neighborhood, while element labeled with 0 are excluded.

The morphological element is created through the use of the function

```
SE = strel(shape, parameters)
```

That creates a structuring element, *SE*, of the type specified by *shape*. Depending on *shape*, *strel* can take additional parameters.

To create the classical rectangular kernel, the correspondent function would be

```
kernel   = strel('arbitrary', ones(kernelsize));
```

where '*arbitrary*' impose the square shape, and *ones(kernelsize)* determine the kernel to have the desired shape and be filled with ones.

To create the circular kernel, *SE = strel('disk', RadiusSize, 0)* creates a flat, disk-shaped structuring element, where the structuring element members consist of all pixels whose centers are no greater than *RadiusSize (R)* away from the origin (i.e. Fig. II).

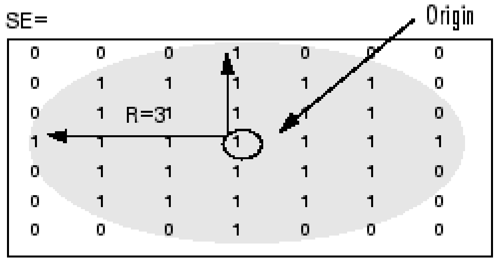

Figure II Representation of the circular kernel in Matlab®.

The creation of the annulus kernel, starts from the creation of two disks, one by setting its diameter according to the desired final inner diameter of the annulus ($2r_{in}$), the other setting its diameter according to the desired final outer diameter of the annulus ($2r_{out}$).

The difference between the two objects, creates the annulus kernel, as expressed in Fig. (III).

$2r_{out} = 5$:

$$\begin{array}{ccccc} 0 & 0 & 1 & 0 & 0 \\ 0 & 1 & 1 & 1 & 0 \\ 1 & 1 & 1 & 1 & 1 \\ 0 & 1 & 1 & 1 & 0 \\ 0 & 0 & 1 & 0 & 0 \end{array}$$

$2r_{in} = 3$:

$$\begin{array}{ccccc} 0 & 0 & 0 & 0 & 0 \\ 0 & 0 & 1 & 0 & 0 \\ 0 & 1 & 1 & 1 & 0 \\ 0 & 0 & 1 & 0 & 0 \\ 0 & 0 & 0 & 0 & 0 \end{array}$$

annulus

$$\begin{array}{ccccc} 0 & 0 & 1 & 0 & 0 \\ 0 & 1 & 0 & 1 & 0 \\ 1 & 0 & 0 & 0 & 1 \\ 0 & 1 & 0 & 1 & 0 \\ 0 & 0 & 1 & 0 & 0 \end{array}$$

Figure III Representation of the annulus kernel in Matlab®.

The creation of the kernel is implemented in a complete function, ‘*ktype.m’* that requires as input the choice of the kernel shapes, and its dimensions.

```
function kernel=ktype(size,type);
%%%%%%%%%%%%%%%%%%%%%%%%%%%%%%%%%%%%%%%%%%%%%%%
% create a kernel with different shapes: circle, rectangle or annulus
% shape.
% if type is
%           'rect' the kernel is a n x n kernel with size 'size'
%           'disk' the kernel is a circle with diameter 'size'
%           'hole' the kernel is a doughnuts shaped kernel with internal
%                  diameter size(1) and external size(2).
%%%%%%%%%%%%%%%%%%%%%%%%%%%%%%%%%%%%%%%%%%%%%%%%
switch type
  case {'rect'} % Smoothing filter
     siz = size;
     kernel   = getnhood(strel('arbitrary', ones(siz,siz)));
  case {'disk'} % Disk filter (minimum size = 5!)
     rad   = (size-1)/2;
     SE = strel('disk', rad,0);
     kernel = getnhood(SE);

  case {'hole'}  % doughnuts shaped area (minimum size 3*5)
     radint   = (size(1)-1)/2;
     radext = (size(2)-1)/2;
     SEEXt = strel('disk', radext,0);
     SEINT = strel('disk', radint,0);
     kernel= %difference between SEEXt and SEINT;
end
```

Function I ktype.m *Representation of the kernels in Matlab®.*

2. Curvature evaluation

The basic assumption of the polynomial interpolation can be found in Chapt. 2.1 Sect. *III.Materials and methods*, while curvature equations are found in Chapt. 3.1.a, Sect. *III.Materials and methods*. Curvature evaluation within matlab basically require the solution of Eq. I

$$\iota = \left(G^T G\right)^{-1} \cdot G^T z \qquad (I)$$

where z is the elevation matrix within the moving neighborhood, ι is the coefficient matrix (*a-f*) and *G* is the coordinate matrix as function of the local coordinate system within the moving window (for fuller description, refer to Chapt. 2.1, *II.Materials and methods*).

While z is directly read from the DTM, the only requirement is the creation of the matrix *G* and as a consequence, the definition of $(G^TG)^{-1}G^T$.

This is obtained by creating the coordinate matrix for each pixels as a function of the DTM grid size, and in a second step, *G* is computed.

This procedure is implemented in the function *quadFit.m*

```
function G =quadFit(KernelSize,g);
%%%%%%%%%%%%%%%%%%%%%%%%%%%%%%%%%%%%%%%%%%%%%%%%%%%%%%%%%%%%%%%%%
% evaluate coefficient to solve quadratic equation
%     Required Inputs:
%   kernelSize= kernel width (in cells)
%   g = pixel size of the input DTM
%%%%%%%%%%%%%%%%%%%%%%%%%%%%%%%%%%%%%%%%%%%%%%%%%%%%%%%%%%%%%%%%%%

padsize=(KernelSize-1)/2;
matX= g*repmat(0+(-padsize:padsize), KernelSize,1);
matY= g*repmat(reshape(0-(0+(-padsize:padsize)),[],1),1,KernelSize);
% Evaluate G to solve the bi-cubic equation
F = ones(KernelSize ^2,6);
for kk= 1: KernelSize ^2
    x=matX(kk);
    y=matY(kk);
    G_=[x^2,y^2,x*y,x,y_] ;
    G(kk,1:5)=F_;
end
end
```

Function II: quadFit.m *Representation of the matrix G in Matlab®.*

$(G^TG)^{-1}G^T$ is simply obtained then by transposing G and applying the formulation. This steps need to be evaluated just once, for the considered moving window. Curvature can then be found by considering as input the DTM (where to read the z values) and deriving *G* for the considered kernel size using the function *quadFit.m (Fun. II).*

Curvature is implemented in the function *Kfast.m.*

```
function k=kfast(z,g,G,type)
%%%%%%%%%%%%%%%%%%%%%%%%%%%%%%%%%%%%%%%%%%%%%%%%%%%%%%%%%%%%%%%%%%%%%%%%%%%
% k = curvature according to Evan’s (1979) formulation
%      Required inputs:
% z = elevation within the DTM
% g = pixel size of the input DTM
% G = coordinate matrix as function of the local coordinate system, as %
      derived by the function quadFit.m
%      type= type of desired curvature:
%             ‘min’ = minimum curvature
%             ‘max’ = maximum curvature
%             ‘mean’ = mean curvature
%%%%%%%%%%%%%%%%%%%%%%%%%%%%%%%%%%%%%%%%%%%%%%%%%%%%%%%%%%%%%%%%%%%%%%%%%%%
warning off all
ker=size(z);
%evaluate coefficient
zvalue= reshape(z',1,[])';
coefficient = zvalue*(G’*((G’*G)^(-1)));
a=coefficient(1);
b=coefficient(2);
c=coefficient(3);

switch type
case {'max'}
 k= ksize*g*(-a-b+sqrt((a-b)*(a-b) + c*c));
  case {'min'}
 k= ksize*g* (-a-b-sqrt((a-b)*(a-b) + c*c))  ;
 case {'mean'}
 Kmax= ksize*g* (-a-b+sqrt((a-b)*(a-b) + c*c))  ;
 Kmin= ksize*g* (-a-b-sqrt((a-b)*(a-b) + c*c))  ;
 k=(Kmin+Kmax)/2;
 otherwise
 error('Unknown curvature type');
end
end
```

Function III: Kfast.m *evaluation of curvature in Matlab®.*

3. Openness evaluation

The basic assumption for openness evaluation can be found in Chapt. 3.1.c Sect. *III.Materials and methods*.

Openness evaluation within matlab requires as a first step, the definition of elevation angles between each visible location within the moving window and the central pixel (Eq. 18). Therefore, at first, a matrix identifying the central pixel is created, and the distance between each pixel and the central one are automatically computed, by using the function *bwdist*.

D = bwdist(BW) computes the Euclidean distance transform of the binary image BW. For each pixel in BW, the distance transform assigns a number that is the distance between that pixel and the nearest nonzero pixel of BW. *bwdist* uses the Euclidean distance metric by default, where the Euclidean distance between two points A and B, with coordinates (x_a,y_a) and (x_b,y_b) is simply given by

$$\sqrt[2]{(x_a - x_b)^2 + (y_a - y_b)^2} \qquad (II)$$

As a second step, elevation angles are computed according to Eq. 18.

Both computation are implemented in the function *elevangle.m*

```
function Angle=ElevAngle(z,g)
%%%%%%%%%%%%%%%%%%%%%%%%%% Elevation angle for a given input matrix
%      required inputs:
%      z= matrix of elevations
%      g= pixel size of the input DTM
%%%%%%%%%%%%%%%%%%%%%%%%%%%%%%%%%%%%%%%%%%%%%%%%%%%%%%%%%%%%%%%%%

%evaluate binary matrix identifying the position of central pixel
Mat0=zeros(size(z));
Mat0(floor(size(z)/2)+1,floor(size(z)/2)+1)=1;
distances=bwdist(Mat0)*g;
Angle= atan ((z-z(floor(size(z)/2)+1,floor(size(z)/2)+1))./distances);
End
```

Function IV ElevAngle.m *evaluation of elevation angle in Matlab®.*

The second step, requires the definition of the azimuths *D* (Eq. 16, 17, 19, 20 and Fig. 23) upon which to compute the zenith and nadir angles.

This is done by the use of the morphological element, in a similar fashion as explained in the first section of this appendix for the creation of the kernel, in this case applying the option 'line' and a direction to consider.

```
SE = strel('line', length, D)
```

The basic results, is then rotated to obtain all the azimuths, as exemplified in Fig. IV

```
>> D225_45= getnhood(strel('line', kernelSize(1)+2, 45))

D225_45 =

     0     0     0     0     1
     0     0     0     1     0
     0     0     1     0     0
     0     1     0     0     0
     1     0     0     0     0
```

```
>> D135_315= flipud(D225_45)

D135_315 =

     1     0     0     0     0
     0     1     0     0     0
     0     0     1     0     0
     0     0     0     1     0
     0     0     0     0     1
```

```
>> tempM=imrotate(D225_45, 45);
>> D0_180=tempM(3:end-2,3:end-2)

D0_180 =

     0     0     1     0     0
     0     0     1     0     0
     0     0     1     0     0
     0     0     1     0     0
     0     0     1     0     0
```

```
>> D270_90=imrotate(D0_180, 90)

D270_90 =

     0     0     0     0     0
     0     0     0     0     0
     1     1     1     1     1
     0     0     0     0     0
     0     0     0     0     0
```

Figure IV Representation of azimuths, for a squared moving window, in Matlab®.

Once the azimuths are compared, the computation of openness requires the identification, among each direction, of all the visible points. Basically, considering the elevation angle, the requirement is to identify the maximum value on each direction. Once these local maxima are evaluated, openness is computed according to Eq. 16, 17, 19, 20.

Openness computation is implemented in a function '*openness.m'*.

```
function O=Openness(z,g,type)
%%%%%%%%%%%%%%%%%%%%%%%%%%%%%%%%%%%%%%%%%%%%%%%%%%%%%%%%%%%%%%%%%%%%%%%%
% O = positive or negative openness
%      Required inputs:
%      z= matrix of elevations
%      g= pixel size of the input DTM
%       type= 'neg' for negative openness or 'pos' for positive
%%%%%%%%%%%%%%%%%%%%%%%%%%%%%%%%%%%%%%%%%%%%%%%%%%%%%%%%%%%%%%%%%%%%%%%%
%evaluate distances
Angle= ElevAngle(z,g);
%matrices of directions
   % direction matrix
        D225_45= getnhood(strel('line', kernelSize(1)+2, 45));
        D135_315= flipud(D225_45);
        tempM=imrotate(D225_45, 45);
        D0_180=tempM(3:end-2,3:end-2);
        D270_90=imrotate(D0_180, 90);
    %%%%%%
switch type
case {'pos'}
        OpN = min(90-(angles for direction N)));
        OpNE = min(90-(angles for direction NE));
        OpE = min(90-(angles for direction NE));
      %… repeat for all directions
        O=mean( %openness in each direction);
  case {'neg'}
        OpN = min(90+(angles for direction N));
        OpNE = min(90+(angles for direction NE));
        OpE = min(90+(angles for direction NE));
      %… repeat for all directions
        O=mean( %openness in each direction);
end;
end
```

Function V: Openness.m *evaluation of openness in Matlab®.*

4. Implementing the moving window approach

Once the function that computes the parameter is implemented, it can be applied on the input DTM, through a moving window filter function already provided within the software (*nlfilter*). The moving window filter is included in MATLAB within the image processing toolboxes and relies on linear and nonlinear filtering procedures. Regardless of whether field this generalization procedure belongs, or what frequency ranges or timescales they work on, the mathematical theory of linear and nonlinear filters is universal, therefore it can be applied to grid DTMs, since they share with images a matrix structure.

To briefly introduce, the linear filter is an operation where at every pixel $x_{m,n}$ of a matrix, a function is evaluated on the pixel and its neighbors to compute a new pixel value $y_{m,n}$ (Fig. V).

$$y_{m,n} = \sum_{j=1}^{n}\sum_{k=1}^{m} h_{j.k}\, x_{m-j,n-k} \qquad \text{(III)}$$

where x is the input, y is the output, and h is the filter impulse response.

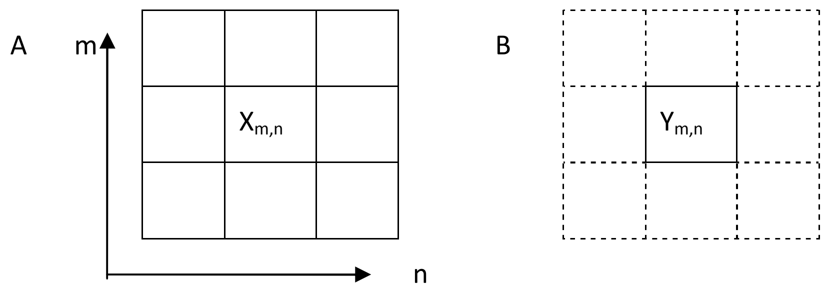

Figure V: Concept of filtering: input(A) and output (B).

The code below is an example of implementation of a general filters in matlab.

```
[M,N] = size(DTM);
Y = zeros(size(DTM));
r = (WindowSize-1)/2;     % Adjust for desired window size
for n = 1+r:N-r
    for m = 1+r:M-r
        % Extract a window of size (2r+1)x(2r+1) around (m,n)
        X = DTM(m+(-r:r),n+(-r:r));
        % ... filter equation here ...
        Y(m,n) = Filter(X);
    end
end
```

Function VI: Computational implementation of a general filter in Matlab®.

Different choices of *h* (Eq. II) lead to filters that smooth, sharpen, and detect edges, to name a few applications for image filtering applications. For the case of morphological application, the key is to build a filter that incorporates the general procedures (Eq. II) and to apply as *h* the equation representing the topographic parameters (ex. Curvature, Openness ….).

For example, if the aim is to evaluate Mimimum Curvature on a moving window of 3x3, the required information are simply the curvature function and the size of the kernel of interest.

Once the function is defined, it can be provided as an anonymous function to the Matlab filter function (*nlfilter*, see MATLAB for detailed explanations)

```
fun = @(z) Kfast(z,g,G);

Output = nlfilter(Input,[3 3],fun);
```

Chosen window size

The DTM

Starting from the top right of this syntax statement, the term *Kfast* represents the body of the function (as for example the code described in *fun. III*). This can consist of any single, valid MATLAB expression. Next is a list of input arguments to be passed to the function (for the minimum curvature, the z values, the pixel size and the coefficient matrix). The term @(z) represent the anonymous function handle (Matlab). What this code says, is to read on the input DTM a series of *nxn* values (where *n* is the size of the moving window), and to store them in a temporary matrix *z* and pass them as argument for the function *Kfast*.

5. Evaluation of the optimum scale of analysis

The basic assumption of the selection of optimum scale can be found in Chapt. 4.2 Sect. III.Materials and methods.

The procedure requires the definition of a function representing skewness of the topographic attributes as a function of the kernel size (Eq. 37). The procedure is implemented in the code *fit_enforce.m*

```
function Opt_scale =fit_enforce(dtm,g);
%%%%%%%%%%%%%%%%%%%%%%%%%%%%%%%%%%%%%%%%%%%%%%%%%%%%%%%%%%%%%%%%%%%%%%%%%%%%%%%%%%
% fitting_enforcing procedure to evaluate optimum kernel size
%     Required inputs
%     dtm = the input DTM
%     g = the pixel size
%%%%%%%%%%%%%%%%%%%%%%%%%%%%%%%%%%%%%%%%%%%%%%%%%%%%%%%%%%%%%%%%%%%%%%%%%%%%%%%%%%%%

%% beginning of routine for the polynomial fitting
count = 0;
for kernelSize=3:33;
count = count+1;
TA = % topographic attribute of interest for the defined kernelSize (i.e. curvature or openness)
% evaluate skewness of the array for the specific window size
Skew(count,1) = skewness(TA(:));
end
% evaluate polynomial, derivative and optimum kernel
% indexing initiation
n = 2; % it starts from a 2nd order polynomial
% repeat the fitting/enforcing for polynomial with different degrees (up to 50)
while isempty(optimumKernel);
n=n+1;
% fit the polynomial
p = polyfit(kernels,Skew,n);
% polynomial simulation
skewn = poly2sym(p);
% derivative
der= diff(skewn);
% solve the derivative
Khypotesis=solve(der);
% check whether there is at least one true derivative within the window size range
for j = 1:length(Khypotesis);
        solution = sym2poly(Khypotesis (j));
        if solution > 3 && solution < 33;
        optimumKernel = solution; break % break the fitting if the condition is verified and produce the optimum kernel value
        else
        end
    end
end
end
Opt_scale= optimumKernel;
End
```

Function VII: Polynomial Fitting-enforcing in Matlab®.

6. Graphical-user interface

A graphical user interface (GUI) is a pictorial interface to a program. A good GUI can make programs easier to use by providing them with a consistent appearance and with intuitive controls like pushbuttons, list boxes, sliders, menus, and so forth. The GUI should behave in an understandable and predictable manner, so that a user knows what to expect when he or she performs an action. For example, when a mouse click occurs on a pushbutton, the GUI should initiate the action described on the label of the button. This chapter introduces the basic elements of the MATLAB GUI that includes all the processes described in the previous sessions. The chapter does not contain a complete description of components or GUI features, but it provides only the basics description of the produced GUI. The advantage of such element, is that it provides the user with a familiar environment in which to work, instead of requiring the actual programming of each code. This environment contains pushbuttons, toggle buttons, lists, menus, text boxes, and so forth, all of which are already familiar to the user, so that he or she can concentrate on using the application rather than on the mechanics involved in doing things.

The Topographic parameter GUI elements are visible in Fig. VI.

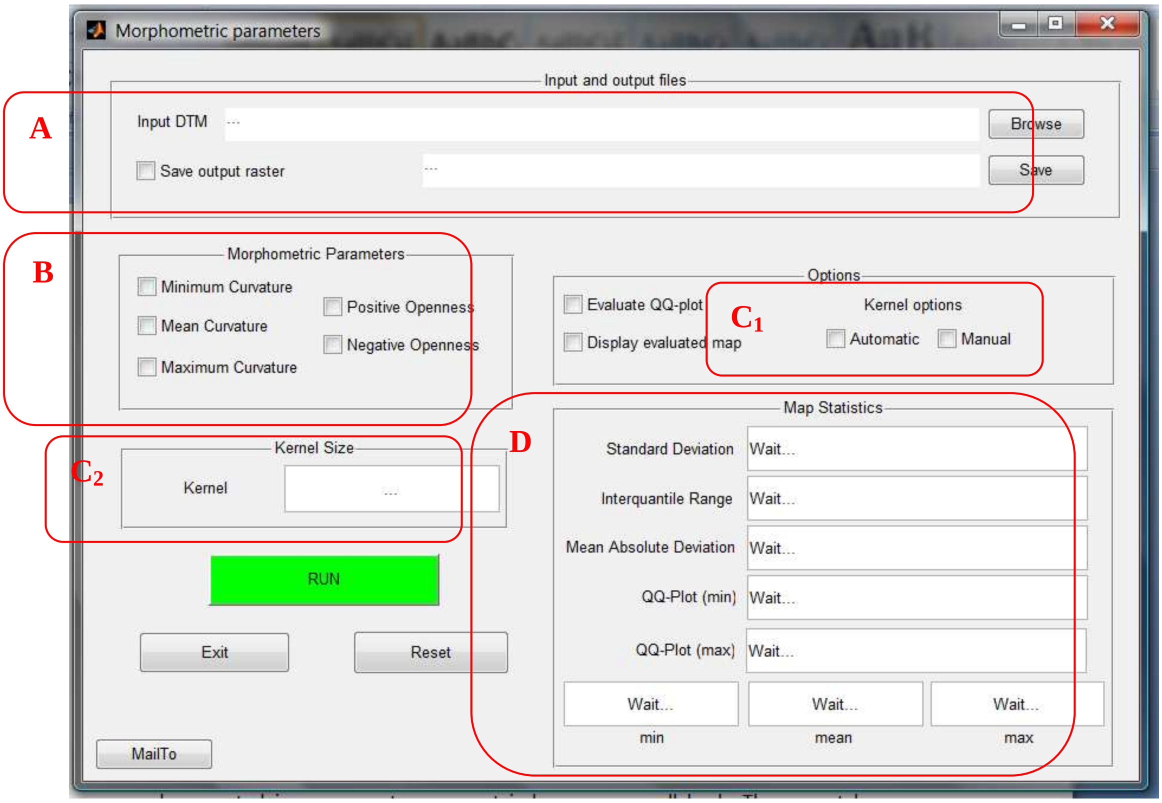

Figure VI: Topographic parameters GUI

The GUI is created in order to allow the user to select the input *DTM* (A, in Fig. VI), and to save the map of the produced topographic parameter. However, a checkbox (‘*Save output rasters*’) allows the user to decide whether to save or not the output.

Different topographic parameters (openness and curvature) can be computed (B in Fig. VI) considering a user defined kernel size (option '*manual*' in C_1), or by applying the fitting-enforcing procedure (option '*automatic*' in C_1). If the user selects the manual option, C_2 becomes active and allows to write the desired kernel size.

If the user select the *automatic* option, C_2 is not editable, but it is automatically filled by the software once the optimum kernel is computed through the *polynomial fitting-enforcing* approach.

The GUI automatically computes for the desired topographic parameter, all the statistics (*D*).

LIST OF FIGURES

Figures in Appendix A

Functions in Appendix A

LIST OF TABLES

LIST OF EQUATIONS